UNIVERSITEIT GENT

FACULTEIT GENEESKUNDE EN GEZONDHEIDSWETENSCHAPPEN

Single channel studies on the modulation of connexin hemichannels by Cx43 targeting peptides and cytoplasmic Ca^{2+} in the context of heart disease

NAN WANG

Promoter: Prof. Dr. Luc Leybaert

Thesis submitted in fulfillment of the requirements for the degree of 'Doctor of Biomedical Sciences'

Faculty of Medicine and Health Sciences

Department of Basic Medical Sciences

Physiology Group

Thesis submitted in fulfillment of the requirements for the degree of 'Doctor of Biomedical Sciences' 31 May, 2013

Promoter: Prof. Dr. Luc Leybaert
Ghent University, Belgium

Members of the Examination Committee:

Prof. Dr. Harold V.M. van Rijen
University Medical Center Utrecht, The Netherlands

Prof. Dr. Alain Labro
University of Antwerp, Belgium

Prof. Dr. Geert Bultynck
Catholic University of Leuven, Belgium

Prof. Dr. Alexander V. Panfilov
Ghent University, Belgium

Prof. Dr. Bert Vanheel
Ghent University, Belgium

Chairman: Prof. Dr. Claude Cuvelier
Ghent University, Belgium

The front cover image: Yeager et al., (2008) Curr Opin Cell Biol. 19(5): 521-8

The back cover image: Love-Heart-Beat Medical Line Backgrounds Wallpaper © 2013 SlideDesign.com

Research funded by the Interuniversity Attraction Poles Program (Belgium Science Program, Project P6/31 and P7/10)

"One of the strongest motives that lead men to art and science is escape from everyday life with its painful crudity and hopeless dreariness, from the fetters of one's own ever-shifting desires. A finely tempered nature longs to escape from the personal life into the world of objective perception and thought."

-Albert Einstein

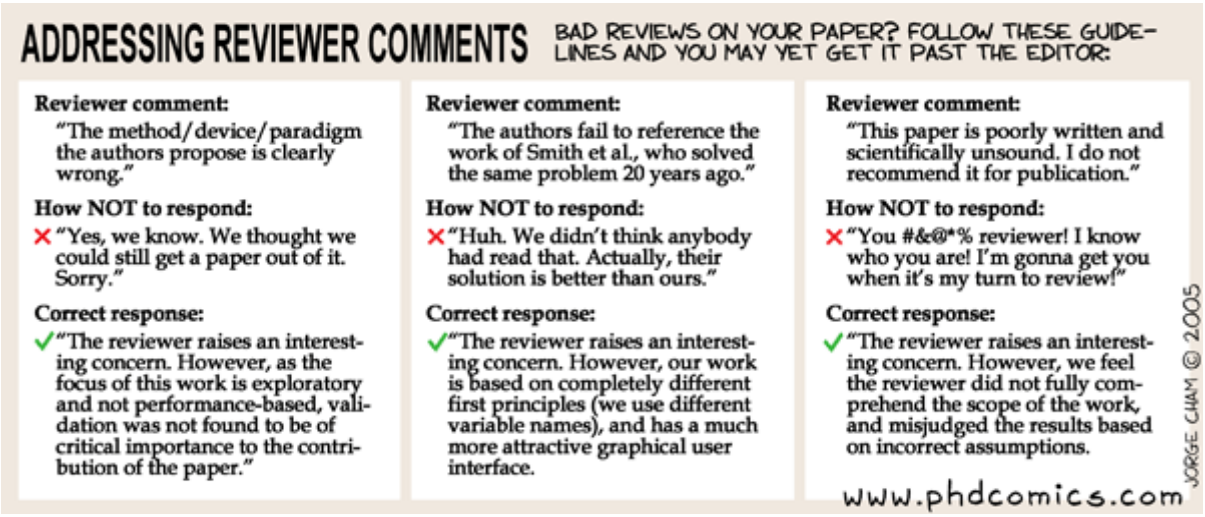

'Addressing reviewer comments' by Jorge Cham©

Acronyms

Å	Angstrom
AA	amino acid
ACE	Angiotensin converting enzyme 0
ATP	adenosine 5'-triphosphate
AFM	atomic force microscopy
AV	Atrioventricular
$[Ca^{2+}]_{o/i}$	Extracellular/intracellular Ca^{2+} concentration
CaM	Calmodulin
CaMKII	Ca^{2+}/Calmodulin kinase II
6-CF	6-carboxy fluorescein
CFDA-AM	5-carboxyfluorescein diacetate acetoxy methylester
CL	cytoplasmic loop
CMV	CytoMegalovirus
CT	carboxy-termini
Cx	connexin
CxMP	connexin mimetic peptide
DAD	delayed after depolarization
EGTA	ethylene glycol-bi(2-aminoethylether)-N,N,N',N'-tetraacetic aci
EL	extracellular loop
FBS	fetal bovine serum
FCCP	p-trifluoromethoxyphenylhydrazone
FRAP	Fluorescence recovery after photobleaching
GJ	gap junction
G_j	steady state junctional conductance

GFP	green fluorescent protein
GPCR	G-protein coupled receptor
HEPES	Hank's balanced salt solution
IAA	sodium iodoacetate
IC_{50}	half maximal inhibitory concentration
I_m	unitary membrane currents
IP_3	Inositol-1,4,5-triphosphate
I-V	current-to-voltage relation
k	Boltzmann constant
$[K^+]_e$	Extracellular K^+ concentration
K_d	equilibrium dissociation constant
KO	knock out
LAD	Left anterior descending
MAPK	mitogen-activated protein kinase
MES	2-(N-morpholino)ethanesulfonic acid
MI	metabolic inhibition
MTS	methane thiosulfonate
MW	molecular weight
NAD^+	nicotinamide adenine dinucleotide
n_H	Hill coefficient
NT	amino-termini
ODDD	Oculodentodigital dysplasia
OGD	Oxygen-glucose deprivation
Q_m	Charge transfer
Pac	puromycine N-acetyl-transferase
Panx	pannexin
PBS	Phosphate-buffered saline

PIP2	Phosphatidylinositol 4,5-biphosphate
pKa	Acid dissociation constant
PKC	protein kinase C
P_{open}	open probability
pS	picoSiemens
q	electron charge
SA	sinoatrial
SCAM	Substituted-cysteine accessibility methods
Scr	scramble
SDS-PAGE	sodium Dodecyl Sulfate Polyacrylamide Gel Electrophoresis
siRNA	small interfering ribonucleic acid
SLDT	scrape loading of dye transfer
SPR	Surface plasmon resonance
TM	transmembrane
TTC	tetrazolium chloride
Tx-100	triton X-100
V_j	transjunciton voltage
V_m	membrane potential
WT	wild type
ZO-1	zonula occludin-1
γ_o	unitary conductance of open state
γ_{sub}	unitary condutance of sub-conductance state
τ	time constant

TABLE OF CONTENTS

Part

I
INTRODUCTION

CHAPTER I. Voltage- and chemical-gating of connexin channels

This chapter is based upon:

Paracrine signaling through plasma membrane hemichannels

Nan Wang[a], Marijke De Bock[a], Elke Decrock[a], Melissa Bol[a], Ashish Gadicherla[a], Mathieu Vinken[b], Vera Rogiers[b], Feliksas F. Bukauskas[c], Geert Bultynck[d] and Luc Leybaert[a]

[a]Department of Basic Medical Sciences, Physiology Group, Faculty of Medicine and Health Sciences, Ghent University, De Pintelaan 185, 9000 Ghent, Belgium

[b]Department of Toxicology, Vrije Universiteit Brussel, Laarbeeklaan 103, 1090 Brussels, Belgium

[c]Dominick P. Purpura Department of Neuroscience, Albert Einstein College of Medicine, Bronx, NY, USA

[d]Department of Molecular Cell Biology-Laboratory of Molecular and Cellular Signalling, Faculty of Medicine, Katholieke Universiteit Leuven, Campus Gasthuisberg O/N-1 bus 802, Herestraat 49, B-3000 Leuven, Belgium

Published in Biochim Biophys Acta. 1828:35-50 (2013)

AND

Effect of Cx43 hemichannel targeting peptides on connexin hemichannel gating

Nan Wang[a], Marijke De Bock[a], Ashish Gadicherla[a], Elke Decrock[a], Melissa Bol[a], Geert Bultynck[b] and Luc Leybaert[a]

[a]Department of Basic Medical Sciences, Physiology Group, Faculty of Medicine and Health Sciences, Ghent University, De Pintelaan 185, 9000 Ghent, Belgium

[b]Department of Molecular Cell Biology-Laboratory of Molecular and Cellular Signalling, Faculty of Medicine, Katholieke Universiteit Leuven, Campus Gasthuisberg O/N-1 bus 802, Herestraat 49, B-3000 Leuven, Belgium

In preparation. Invited review for Neuropharmacology

1.1 General aspect of connexins

In multicellular systems, proper organ and tissue function is sustained by signal transduction from one cell to another that acts to coordinate cell function by intercellular communication. This cross-talk between cells can be achieved in a direct manner, by the transfer of signaling molecules through a low resistance pathway of cell-cell connecting channels, called gap junctions (Goodenough *et al.*, 1996a). The building units in vertebrates are nonglycosylated connexin proteins consisting of four membrane-spanning domains (TM1-4), two extracellular loops (EL1-2), a cytoplasmic loop (CL) and flanking N- and C-termini (NT and CT respectively) also located at the intracellular side. At present, more than 20 connexin genes have been identified in the mouse and human genome (Eiberger *et al.*, 2001). Newly synthesized connexins are oligomerized into a hexameric structure referred to as connexin hemichannels during the trafficking across the endoplasmic reticulum, the Golgi apparatus and the *trans*-Golgi network (Laird, 2006;Saez *et al.*, 2003). Following insertion into the plasma membrane, connexin hemichannels interact with their counterparts on neighboring cells in a head-to-head arrangement, forming gap junction channels that coalesce into junctional plaques which allow the direct exchange between cells of metabolic and signaling molecules with molecular weight (MW) below 1-2 kDa (Bruzzone *et al.*, 1996). Intriguingly, more than just a structural precursor to gap junctions, some connexin hemichannel may also remain unapposed in the non-junctional plasma membrane. When open, unapposed hemichannels form a transmembrane conduit, allowing the passage of ions and hydrophilic molecules with a similar size cut-off limit as for gap junction channel permeation. Cytosolic signaling molecules including adenosine triphosphate (ATP), nicotinamide adenine dinucleotide (NAD^+), glutamate, glutathione and prostaglandins thus can diffuse through the channel to reach the extracellular space, provoking a spread of the signal followed by binding to receptors on surrounding cells and activating downstream cellular responses. Pannexin (Panx) proteins are orthologues of invertebrate innexins and currently consist of 3 members: Panx1, Panx2 and Panx3 (Iglesias *et al.*, 2009;Penuela *et al.*, 2013). They share no sequence homology with connexins but have a similar structure and membrane topology (D'hondt *et al.*, 2009). Pannexins are considered to predominantly form hemichannels and not gap junctions (Penuela *et al.*, 2007a;Sosinsky *et al.*, 2011). For this reason it has been proposed to call pannexin channels just ‘channels’ and not ‘hemichannels’ (Sosinsky *et al.*, 2011). However, because there is still some discussion about the possibility that pannexins might form gap

junctions, and because this field is still in significant expansion, we chose to safely keep using the word ‘hemichannel’ for pannexins.

Nomenclature

In the literature, two nomenclature systems have been adopted to designate different connexin subtypes. The most widely applied nomenclature is based on the molecular weight predicted from the cDNA sequence (Sohl and Willecke, 2003). For example, Cx43 is named by the molecular weight of 43 kDa. A corresponding orthologe derived from a different species can possess a diverse molecular weight, such as Cx45.6, the chicken ortholgos of mouse Cx50. Alternatively, connexins could be grouped by homology of the gene sequence and length of the cytoplasmic domain into α, β, γ, δ and ε subfamilies (Cruciani and Mikalsen, 2006). In this way, a connexin protein can be denoted as ‘GJ’ for gap junction protein, followed by the gene subgroup and serially numbered in the order of its discovery. Thus Cx43 is also known as GJα1. For the sake of clarity, all connexin proteins discussed here will be named following the former nomenclature system. Based on the evolutionary relations, human Cx37, Cx40, Cx43, Cx46, Cx50, Cx58, Cx59 and Cx62 belong to α-connexins; Cx25, Cx26, Cx30, Cx30.3, Cx31, Cx31.1, Cx32 to β-connexins; Cx30.2, Cx45, Cx46.6 and Cx47 belong to the γ- subfamily, Cx31.9, Cx36 and Cx40.1 to the δ-group while Cx23 to the ε-group.

Channel structure

When a connexin hemichannel is composed of a single type of connexin protein, it is assigned to the term ‘homomeric’ (Fig. 1). A hemichannel consisting of more than one connexin isoform is classified as ‘heteromeric’ hemichannel. Accordingly, gap junction channels can be formed by two identical (homotypic) or different (heterotypic) hemichannels. Given more than 20 connexin genes in mammals, it is not surprising to find an extensive collection of divergent architectures of gap junction channels.

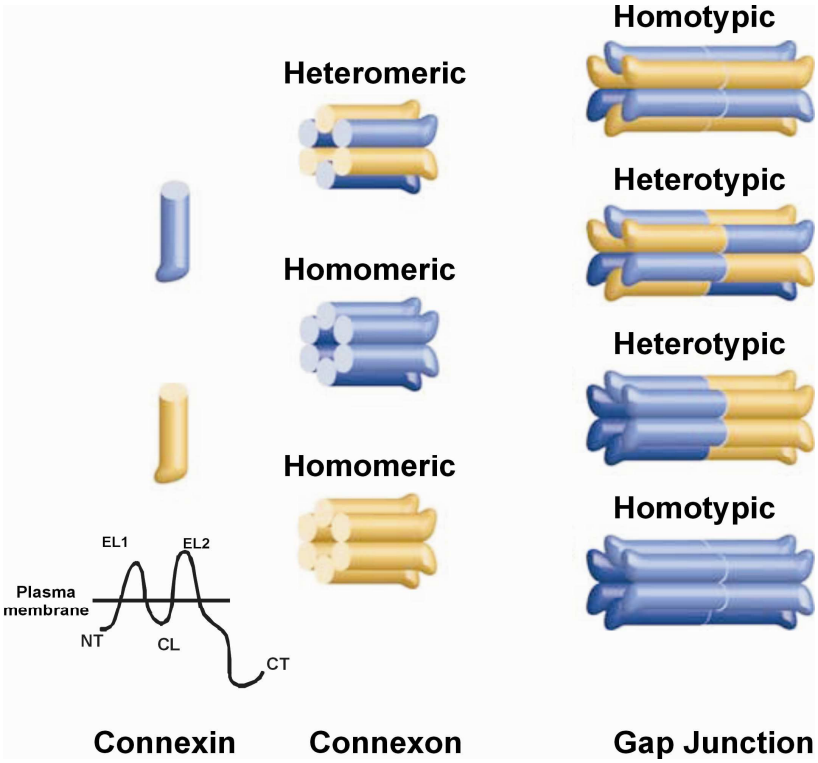

Figure 1. Molecular basis of connexin channels. Connexins are tetra-spanning transmembrane proteins with four α-helical domains spanning the plasma membrane connected by two extracellular loops (EL1 and EL2) and one cytoplasmic loop (CL). Both the N- (NT) and C-terminal region (CT) are facing the cytoplasm. Six of these connexins oligomerize into a connexon or connexin hemichannel. A connexin hemichannel at the junctional membrane readily associates with its counterpart to form a gap junction. Taken from (Mese *et al.*, 2007).

Among the various connexin isoforms, the two ELs and four α-helical TM domains share the highest level of sequence conservation whereas CT and CL regions show remarkable sequence variations. The earliest structural insight into a connexin channel was obtained from the crystal structure of a recombinant Cx43 gap junction at 7.5 Å resolution (Unger *et al.*, 1999;Yeager, 1998). General features of a junctional channel include two rings grouped by the total 24 α-helical TM domains. One of the rings lines the aqueous pore and the other exposes to the membrane lipids. To bridge the intercellular gap, EL1 and EL2 of each apposed hemichannel interact with the respective counterparts, forming an anti-parallel β-sheet stabilized by intramolecular disulfide bonds. A 30° rotational stagger between two apposing hemichannels is necessary for forming tightly-sealed intercellular gap. Cysteine mutagenesis studies were used to map the pore-lining residues but no consensus has been reached. In Cx32 gap junctions, TM3 and TM2 were identified as the primary and secondary pore-lining segments respectively (Skerrett *et al.*, 2002;Skerrett *et al.*, 2001). The pores of Cx46 and chimeric Cx32 hemichannels, on the other hand, appeared to be mostly lined by

TM1 domain (Kronengold *et al.*, 2003b;Zhou *et al.*, 1997). More recently, crystal structure of an open Cx26 gap junction at 3.5 Å resolution significantly improved our understanding of the channel organization (Maeda *et al.*, 2009). It shows that the pore of Cx26 gap junction adopts a funnel-shaped structure consisting of a wide cytoplasmic entrance, narrowing of the pore (named 'funnel') lined by NT and TM1/EL1 regions spanning through the transmembrane and again a widened extracellular cavity formed by EL1. The cut-off size of the molecules which can go through the channel is determined by the narrowed funnel.

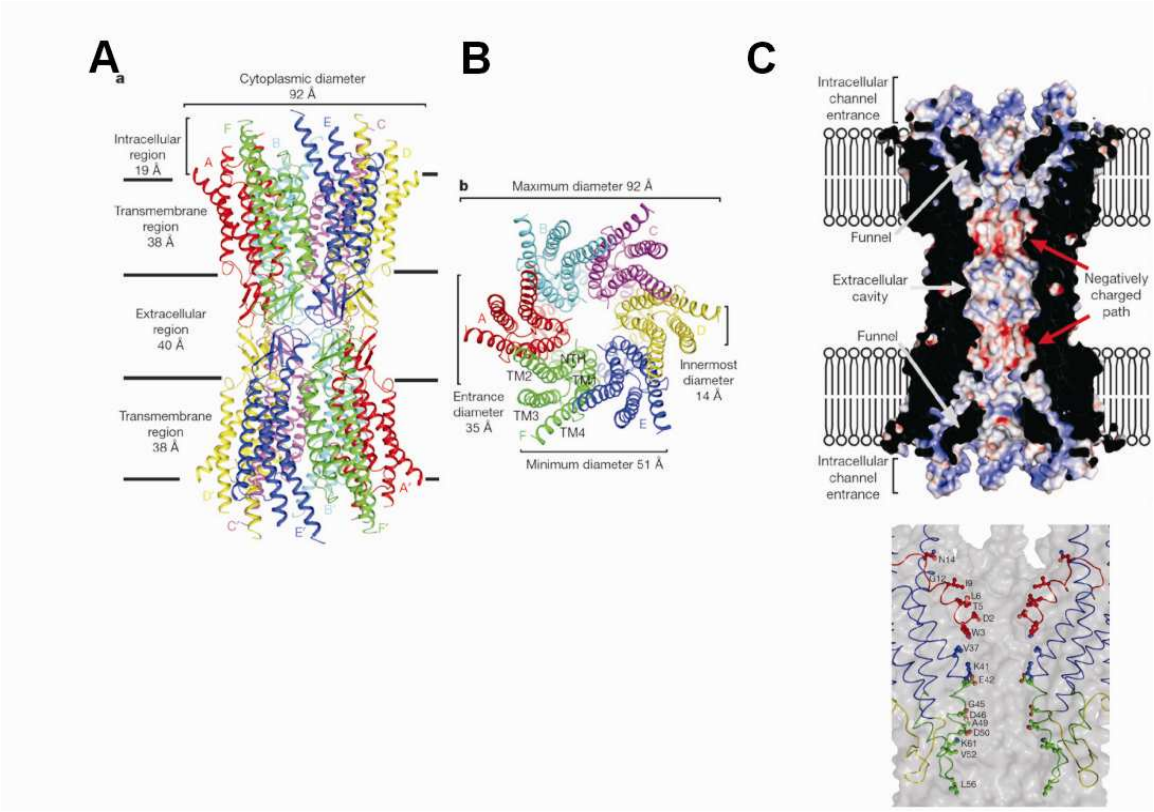

Figure 2. Overall structure of a Cx26 gap junction channel determined at 3.5 Å resolution. A. Side view of the gap junction structure. The corresponding protomers of two hemichannels are illustrated in the same color. B. Top view of the channel depicting α-helical arrangement of the transmembrane domains. C. Upper panel represents a cross-section of the junctional structure featuring a wide cytoplasmic entrance followed by a narrowing of the pore through the transmembrane domain and again a widened extracellular cavity. Lower panel illustrates the domains lining the pore funnel (color code: red, NT; blue, TM1-TM4; green, EL1; yellow, EL2). Taken from (Maeda *et al.*, 2009).

1.2 Voltage-gating of connexin channels: where are the voltage sensor and gate?

Gap junctions and unapposed hemichannels both exhibit voltage-dependent channel gating: gap junctions being mostly influenced by the transjunctional voltage (V_j, voltage difference measured between the cells sharing a gap junction) (Fig. 3A), and hemichannels by the

transmembrane voltage (V_m, membrane potential). Under normal conditions, when the V_m of the coupled cells is similar, and V_j (= $V_{m,cell\#2}$ - $V_{m,cell\#1}$) is consequently close to zero, gap junctions are open, allowing movement of ions, metabolites and signaling molecules down concentration gradients between adjacent cells. However, when the coupled cells develop different V_ms, V_j will deviate from zero (either in positive or negative direction) and the gap junction conductance (G_j, steady state junctional conductance) will start to decrease (Fig. 3B). In homotypic gap junctions, the G_j-V_j relation is typically bell-shaped with maximum G_j at 0 mV and lowering of G_j when V_j changes in positive or negative direction. Unapposed hemichannels, by contrast, are typically closed under normal resting conditions to prevent dissipative ion fluxes and loss of essential metabolites. Hemichannels can however be opened by membrane depolarization and for some connexins (f.e. Cx43), activation may only occur at positive V_m.

Voltage-gating of connexin channels is mechanistically distinct from voltage-gated Na^+, Ca^{2+} and K^+ channels, because there is no common voltage-sensing motif and it is not established whether the voltage sensor and gate are distinct entities (Horn, 2000). The argument, in general, falls into two aspects: i) connexin proteins lack the S4-like domain, a conserved membrane spanning segment rich in charged amino acids primary for other voltage-gated ion channels and ii) an essential part of connexin protein is believed to sense the voltage change and in turn, moves at least in part as a gating element to convey opening or closure of the pore.

Two gating mechanisms are identified in connexin channels (gap junction or hemichannel) based on transitions between different conductance states as well as distinct time courses (Bukauskas and Verselis, 2004a). One is referred to as ‘slow gating’ or ‘loop gating’ because of the slow transitions between the fully open and closed conductance states, which take on average 11 ms and are typically observed as multi-step transitions when two hemichannels dock to form a gap junction (Bukauskas and Weingart, 1994). In the second kind of gating, termed ‘fast gating’, the channel rapidly switches (< 1-2 ms) from the open state to one or several long-lasting subconductance states (also called residual states). It was initially proposed that V_j-sensitive gating exclusively depended on the fast gate, but it was rapidly realized that slow gating also contributes, especially in the process of channel closure. Further insight and understanding of V_j-sensitive gating needs the consideration of gating of the constituent hemichannels (apposed/junctional hemichannels). In fact, V_j gating of a gap junction is based on the intrinsic gating properties of the two constituent hemichannels

(Bukauskas *et al.*, 2002a;Srinivas *et al.*, 2005). This argument is supported by several lines of evidence: i) in homotypic gap junctions, V_j-dependence of G_j peaks at V_j=0 and decays symmetrically for both positive and negative V_j, implicating operation of one hemichannel for each of the polarities; ii) unitary conductance of a homotypic gap junction channel approximates half of that of the hemichannel component, suggesting series arrangement of hemichannels and iii) fast and slow gates have been documented in both unapposed and apposed hemichannels. The scenario becomes more complicated when considering heterotypic gap junctions. In this case, an asymmetric G_j-V_j relation is often observed, which is not always well correlated to the intrinsic parameters of the constituent hemichannels. The fast gating element of Cx43 hemichannels is for example lost when docked with Cx45 hemichannels (Elenes *et al.*, 2001a). Additionally, the gating properties of heterotypic gap junctions formed by Cx26 and Cx30 do not resemble the profiles of any of the respective homotypic channels (Yum *et al.*, 2007). Collectively, these studies propose a scenario in which the gating of a hemichannel may change upon docking, probably as a result of loop interactions and consequent conformational changes that lead to altered gating in the ensemble of apposed hemichannels that form the gap junction.

It is important to realize that the assumption of an independent operation of fast/slow gate is only valid as a first approximation. In fact, two gates of each apposed/unapposed hemichannel are more likely to be serially connected in the pore, thereby operating in a contingent manner (Bukauskas *et al.*, 2004a;Gonzalez *et al.*, 2007;Harris *et al.*, 1981). Opening/closure of each gate would redistribute the electric field inside the pore, reshaping the voltage drop across the other gates. As a consequence, operation of one gate depends on the state of the other gates as well as its own intrinsic properties including voltage sensitivity, gating polarity and unitary conductance. Taking homotypic Cx43 gap junction channels as an example (Fig. 3B), the maximal G_j at V_j = 0 experiences a multiphasic decay which is correlated with divergent gating phenotypes in response to an increasing V_j gradient (Bukauskas *et al.*, 2004a). At small V_j that is below a threshold of ±50 mV, channel closure is dominated by slow gating. As such, the slow gate must favor the closed conformation at lower V_j as compared to the fast gate. When the amplitude of V_j rises to an intermediate level between ±60 and ±80 mV, the slow gating component disappears and the G_j drops sharply mainly through fast transitions to residual states. In this case, closure of the fast gate responds to a V_j increase more rapidly because of its nature of fast kinetics, leaving limited fraction of V_j over the slow gate which is below its operation threshold. When V_j exceeds ±100 mV, an initial decay of G_j to the

residual states is followed by slow transitions that further complete channel closure, suggesting that the fraction of V_j falling over the slow gate is sufficient to close the remaining gates. Accordingly, V_j-gating in a heterotypic gap junction channel should be considered as follows: the electric field along the length of a gap junction may strongly deviate from a linear distribution (constant field approximation). Differences in unitary conductance of the two constituent hemichannels will result in an unequal voltage drop over the two hemichannels. As a result, the apposed hemichannel experiencing the largest voltage drop will have a more pronounced sensitivity to changes in V_j (Rackauskas *et al.*, 2007). Computational stochastic modeling derived from the contingent-gating theory currently can provide an accurate prediction of a heterotypic gap junction gating, when gating parameters of the respective homotypic gap junctions are given (Paulauskas *et al.*, 2012;Paulauskas *et al.*, 2009).

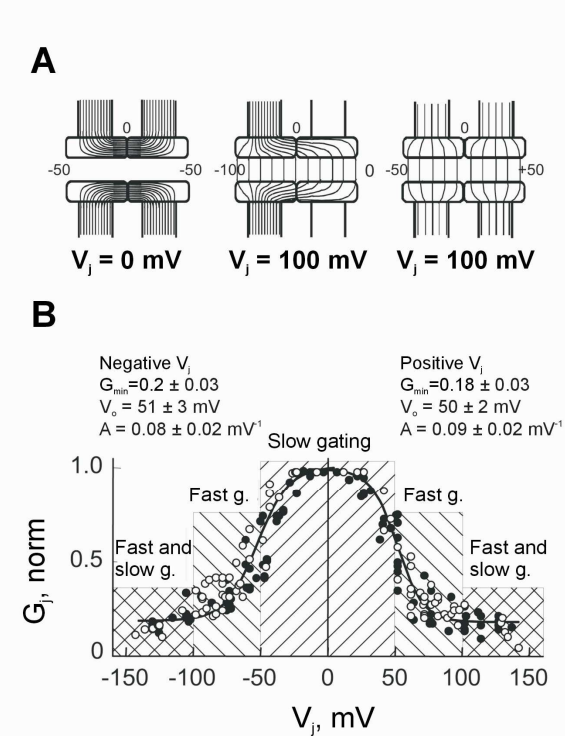

Figure 3. V_j-gating of gap junction channels. A. schematic illustration of the presumed isopotential lines distributed in the gap junction channel pore at different V_j. No V_j is established (V_j = 0 mV) when the voltage potential of the apposing cell membranes are both held at -50 mV. Hyperpolarizing one cell to -100 mV and depolarizing the other to 0 mV or holding one cell at -50 mV and depolarizing the other to +50 mV generate the same V_j (100 mV). B. Normalized steady-state G_j ($G_{j,\,norm}$) as a function of V_j for homotypic Cx43 gap junctions. The $G_{j,\,norm}$-V_j relation can be well defined by a single Boltzmann function for either polarity of V_j: $G_{j,norm} = G_{j,\min} + \frac{1-G_{j,\min}}{1+e^{A\times(V_j-V_o)}}$, where $G_{j,\,min}$ depicts the normalized residual junctional conductance, *A* reflects the V_j sensitivity ($A = \frac{zq}{kT}$; *z*, the equivalent number of electron charge *q* that moves through the transjunctional field; *k*, Boltzmann constant; *T*, absolute temperature) and V_o corresponds to the V_j at which $G_{j,\,norm}$ reaches half of its maximum value. The resulting $G_{j,\,norm} - V_j$ curve features a symmetrical bell-shaped profile. Squares filled with lines of different orientation denote the V_j range within which different gating mechanisms are dominant. Taken from (Bukauskas *et al.*, 2004a).

Regarding V_m, slow gates of all connexin hemichannels favor channel closure in response to membrane hyperpolarization and remain open at inside positive V_m (Gonzalez *et al.*, 2007). Fast gates can close for either positive or negative polarity depending on the connexin subtype. This diversity in gating polarity classifies hemichannels into two categories: unipolar and bipolar. Voltage-dependent gating of a unipolar hemichannel composed of Cx32 (Gomez-Hernandez *et al.*, 2003), Cx43 (Contreras *et al.*, 2003a) or Cx45 (Valiunas, 2002) features progressively increased channel openings with membrane polarization to positive V_m. Channel currents are sustained at positive V_m, show no apparent inactivation and deactivate upon hyperpolarization. Thus, in a given unipolar hemichannel, both fast and slow gates close at negative polarity. Typical bipolar hemichannels whose two gates operate at opposite polarities include Cx26 (Verselis *et al.*, 1994), Cx37 (Ramanan *et al.*, 1999) and Cx46 (Srinivas *et al.*, 2005;Trexler *et al.*, 1996) (Gonzalez *et al.*, 2006). Such type of hemichannels gates to the fully open state in response to membrane depolarization, having highest open probability at V_m ranging from 0 to +15 mV. Driving V_m to more positive potentials will trigger rapid closure of the channel to the residual states. Distinct from any other voltage-gated connexin hemichannels, a Cx50 hemichannel closes to its residue state when V_m either exceeds +20 mV or drops below -60 mV (Srinivas *et al.*, 2005). The question remains whether the voltage sensor of its fast gate would behave as a toggle switch in the center of the open channel pore, shutting down the gate through either direction of the movement (away or towards the cytoplasmic side of the pore) (Oh *et al.*, 2004).

1.2.1 Voltage-dependent fast gating

Involvement of the NT domain

The NT domain as an integral component of the fast-gate voltage sensor was first suggested by a gating model of heterotypic Cx26/Cx32 gap junctions. Unlike G_j-V_j relation of either homotypical gap junctions, asymmetries in V_j-dependence of Cx26/32 channels gating are characterized by a reduction in G_j only for one polarity of V_j, i.e. relative positivity on the Cx26 side. Applying a positive V_j to the Cx32 side intriguingly fails to affect the junctional coupling (Verselis *et al.*, 1994). This unexpected rectification can be explained by the opposite polarities of fast gating shared by the two apposed hemichannels: negativity for Cx32 and positivity for Cx26. Accordingly, relative positivity on the Cx26 side drives the open Cx26 hemichannel to the residual states, while the apposed Cx32 hemichannel is in favor for closed state at relative negative potential. Turning V_j of both sides to the opposite

polarity keeps both hemichannels open. Mutagenesis studies revealed that swapping of specific domains effectively manipulated the polarity of fast gating in both apposed Cx32 and Cx26 hemichannels. When a chimeric Cx26 hemichannel containing NT and TM1 domains of Cx32 docked with a wild type Cx26 hemichannel, G_j-V_j relation resembled the asymmetric profile as observed in Cx26/Cx32 gap junctions, indicating polarity reversal of the fast gate in the chimera. Conversely, docking between the chimeric hemichannel and a Cx32 hemichannel transformed the G_j-V_j relation to a symmetric pattern similar to that of the homotypic Cx32 gap junction. The region of interest was further narrowed down to the first half of the NT which is distinctly charged at the second position: negatively charged aspartic acid (D2) in Cx26 *versus* a neutral asparagine (N2) in Cx32. Mutating N2 of Cx32 to a negatively charged residue or D2 of Cx26 to an opposite charge was sufficient to reverse the polarity of each fast gates. The presence of D2 in Cx26 essentially determines the negative valence of the voltage sensor in Cx26 channel. Charge residue is absent at the same position in Cx32, but might be donated by the adjacent $^{+}NH_3$-group of methionine. The fact that fast gates of most apposed hemichannels sense V_j rather than absolute V_m embraces the idea that the voltage sensor resides within the channel pore and close to the intracellular end of the pore where the electric field of V_j is dominant over that established by absolute V_m (Harris, 2002a;Harris *et al.*, 1981). Application of positive V_j to Cx26 and negative V_j to Cx32 would electrostatically drive the movement of at least a part of the NT towards the cytoplasmic side of each apposed hemichannel.

As discussed precedingly, V_j-dependent gating of a gap junction channel may reflect biophysical properties inherent to the constituent hemichannel. Then, would an unapposed hemichannel adopt a similar gating model? Single-channel recordings of a chimeric Cx32 hemichannel having EL1 (E41-R75) replaced by that of Cx43 (E42-R76; Cx32*Cx43EL1) provided earliest evidence at unitary current level in favor of this hypothesis (Oh *et al.*, 2000). Like its WT counterpart, a chimeric Cx32*Cx43EL1 hemichannel closes to both fully closed state (slow gating) and residual states (fast gating) in response to hyperpolarization. Mutating the N2 residue to a negatively charged amino acid (N2E) converted the Cx32 chimera into a bipolar channel, with closure of the fast gate at positive V_m and slow gating from open to closed states unaffected. Remarkably, introducing a single N2E subunit into a hexameric hemichannel arrangement was adequate to initiate the polarity reversal. Deduced from the stoichiometric analysis, independent motion of each individual subunit rather than a concerted

action of all six subunits gates the channel closure to one or more residual states (Oh *et al.*, 2000).

It was further suggested that gating charges might be more dispersed through the first half of the NT (Oh *et al.*, 2004;Purnick *et al.*, 2000b). For example, introducing a negative charge at 5^{th}, 8^{th} or 10^{th} position was sufficient to switch the fast gating polarity of an apposed Cx32 hemichannel from negativity to positivity. Similar findings were reported in the context of unapposed hemichannel gating. In contrast to its intrinsic unipolar behavior, a chimeric Cx32*Cx43EL1 hemichannel containing the G5E mutation exhibits bipolar gating. Conversely, substituting the neutral residue at 5^{th} or 8^{th} position with a positive charge (G5R, T8R or T8K) maintained the original fast gating polarity of the chimeric hemichannel. As depicted by nuclear magnetic resonance (NMR) structures of Cx26 and Cx32 NT peptides (Kalmatsky *et al.*, 2009;Purnick *et al.*, 2000a), a glycine residue (G12) which is conserved among the β-connexins seems to be essential for the integrity of the channel structure, by providing a flexible hinge that folds the first half of the NT deep into the channel pore. In V_j-dependent gating, this open turn configuration proximal to the initial part of the NT (also the gating charge carrier) would therefore secure the position of the voltage sensor in the electric field for a direct capture of V_j. In the absence of a docking counterpart, the same configuration will be attained which now responds to the absolute membrane potential as the reference potential is replaced by extracellular compartment. Mutagenesis studies corroborated that substituting G12 with proline, an alternative component of molecular hinges could generate a mutant gap junction channel exhibiting gating properties similar as the wild type channel, whereas other mutant such as Cx26/32 G12S or G12Y lacking a typical hinge in the NT failed to promote junctional currents when overexpressed in pairs of *Xenopus* oocytes (Purnick *et al.*, 2000a).

Finally, electron crystallography of a mutant Cx26 gap junction (Cx26M34A) reveals a plug-like structure in the centre of the cytoplasmic vestibule at each side of the apposed hemichannel (Oshima *et al.*, 2007). The typical structural feature is correlated with the aberrant junctional coupling that is restricted to the metabolite-impermeable but ion-conductive residual states (Gassmann *et al.*, 2009;Oshima *et al.*, 2003). Deleting the first half of the NT domain (amino acid 2-7) accordingly reduced the density of the plug (Oshima *et al.*, 2008), suggesting that at least part of the NT constitutes the plug. A long-awaited crystal structure at 3.5 Å resolution has recently provided a better insight into the structural arrangement of the open Cx26 gap junction, in particular in the cytoplasmic domain (Maeda

et al., 2009). By means of *van der Waals* forces between W3 and M34 at the adjacent subunit, the initial half of the NT appears to be locked against the channel wall, thus lining the permeant pathway of the channel lumen. Collectively, structural characterization inspired a 'gating plug' model that at the fully open state, the voltage sensor dispersed along the first half of the NT protrudes into the channel pore by a flexible turn at G12 and is sequentially immobilized at the inner wall of the channel via intersubunit W3-M34 *van der Waals* forces. Increasing V_j frees the voltage sensor by destabilizing the intersubunit interaction and drives it inwardly towards the cytoplasmic entrance of the pore. It is expected that the voltage sensor would partially occlude the cytoplasmic entrance, confining the ion conductive state into the residual degree.

A question then arises as to whether all connexins adopt the same structural arrangement to confer gating charge movement. Among the three intracellular domains of all connexins, NT is the most conserved region and is thus expected to confer a comparable voltage-driven conformation in connexins other than Cx26 or Cx32 (Oshima *et al.*, 2007). Indeed, for most of the connexin channels possessing positive polarity of fast gating, such as Cx30 , Cx37, Cx46 and Cx50 channels, a negatively charged D residue is conserved at the 2^{nd} or 3^{rd} position of the NT (Gonzalez *et al.*, 2007). Neutralizing D3 of Cx50 protein, reversed fast gating polarity of Cx50 gap junction from positivity to negativity (Peracchia and Peracchia, 2005). The identical mutation also removed the intrinsic fast gating in Cx50 and Cx46 unapposed hemichannels at inside positive potentials (Srinivas *et al.*, 2005).

As appealing as the favored argument is, some doubts remain. Apposed Cx40 (Rackauskas *et al.*, 2007) and Cx43 hemichannels are unipolar yet both carry a negatively charge at position 3 (D3), making the proposed gating model difficult to reconcile exclusively with the NT sequence (Harris, 2002a). Furthermore, in most of the α-connexins, the position where conserved G12 of β-connexins would endow the hinge is occupied by glutamic acid (E). NMR studies showed that the entire NT domain of Cx37 adopts an α-helical order that by no means would fold itself into the channel pore (Kyle *et al.*, 2009). The structural discrepancy between connexin suggests that the molecular components of fast gate may vary among connexin isoforms.

Involvement of the CT domain

Earlier macroscopic recordings of gap junction currents showed that the decay of junctional currents (I_j) in response to increasing V_j is composed of a fast and slow component (Revilla *et al.*, 1999). Single-channel recordings later attributed this complex kinetics to the cooperative actions of V_j-sensitive fast gate and slow gate (Bukauskas *et al.*, 2004a). CT truncation of Cx43 gap junctions (at residue 257; Cx43Δ257) successfully abrogated the fast component of the descending I_j, providing the first evidence for a CT-constituted fast gate (Revilla *et al.*, 1999). Single-channel recording later confirmed the disappearance of the fast transitions between fully open and residual states at $V_j > \pm 60$ mV in the Cx43Δ257 gap junctions (Moreno *et al.*, 2002). Changes in biophysical parameters further included an increase in dwell open time from ~126 ms to 2450 ms and a prolonged time course of the remaining transitions, but the unitary conductance of the main open state was well preserved. Tagging a bulky molecule such as green fluorescent protein (GFP) or V5/6-His to the CT end of Cx43 can impose the same effect (Bukauskas *et al.*, 2001;Desplantez *et al.*, 2011). A similar outcome was also acknowledged in CT truncated forms of Cx40 gap junctions (at residue 248; Cx40Δ248) (Anumonwo *et al.*, 2001). Co-expressing the respective CT as a separate segment restored the fast gating events in both Cx40M248 and Cx43M257 gap junctions and more intriguingly, a fast gating behavior indifferent from that of wildtype gap junctions was also achieved by a heterodomain interaction between the Cx43CT segment and Cx40M248 (Anumonwo *et al.*, 2001;Moreno *et al.*, 2002). Multiple biophysical approaches such as resonant mirror technology, enzyme-linked sorbent assays, and NMR have identified a direct interaction between the CT and the second half of the CL domain (dubbed 'L2'; amino acid 119-144), which likely promotes the V_j-dependent gating of Cx43 gap junctions to residual states (Duffy *et al.*, 2002a;Seki *et al.*, 2004b). Histidine 142 (H142) located at the distal end of L2 is a critical constrain of the fast gate, since mutating H142 to nonpolar or negatively charged residues drastically influenced the CT-CL interaction and the fast gating profile of the channel (Shibayama *et al.*, 2006). Notably, CT serving as a molecular integral of the V_j-dependent fast gate is unique to Cx40 and Cx43 gap junctionss. CT truncated Cx50 arising from calpain cleavage at position 290 or 300 forms gap junctions whose voltage-gating profile at single-channel level is identical to the wild type channels (De Rosa *et al.*, 2006). Similarly, fast gating is not abolished in channels composed of CT truncated Cx46 (Retamal *et al.*, 2009) or Cx47 tagged by EGFP at CT end (Odermatt *et al.*, 2003).

Strikingly, Cx43 hemichannels missing most of the CT domain (Cx43Δ239 or Cx43Δ257) neither conducted ionic currents at positive V_m (Kang *et al.*, 2008a), nor mediated release of ATP in response to several potent hemichannel stimuli such as removal of extracellular Ca^{2+} or moderate increase of intracellular Ca^{2+} (De Vuyst *et al.*, 2007a;Ponsaerts *et al.*, 2010c). Intriguing evidence is now available to support a revised picture of CT-CL interaction, which differentially influences the Cx43 gap junction and hemichannels (further discussed in chapter IV).

1.2.2 Voltage-dependent slow gating

Given the fact that point mutations in the NT domain unambiguously reverse polarity of fast gating without having slow gating affected, voltage sensors of the two gates may be assigned to separate entities. In contrast to the well characterized fast gating mechanisms, little is known about the molecular determinant of the slow-gate voltage sensor. It is generally believed that the voltage sensor of the slow gate also resides within the pore, to ensure voltage sensing in both open and closed conformations (Harris, 2009;Kronengold *et al.*, 2012;Kwon *et al.*, 2012). The resemblance of the slow gating pattern in unapposed hemichannels to the step-wise appearance of I_j during *de novo* gap junction formation initially led to the idea that the two ELs serve as slow gating elements (Trexler *et al.*, 1996). The precise molecular components of slow gating have remained mysterious until recently Verselis *et al.* observed a temporal correlation between the movement of Cx50 hemichannel pore-lining residues at the TM1/EL1 border and slow gate closure (Verselis *et al.*, 2009). When subject to substituted-cysteine accessibility methods (SCAM) and single-channel recording, cysteine residues substituting phenylalanine 43 (F43), glycine 46 (G46) and aspartic acid 51 (D51) were accessible to methane thiosulfonate (MTS) reagents upon hemichannel activation, suggesting all three residues lining the open pore. One particular feature observed in the cysteine mutagenesis is that extracellular Cd^{2+} in conjunction with membrane hyperpolarization impaired slow gating of Cx50F43C or Cx50G46C hemichannels whereas the metal ions merely altered the transmembrane currents at positive V_m. Hemichannels containing a cysteine substitution at D51 were affected by extracellular Cd^{2+} to a lesser extent. If high affinity binding between Cd^{2+} and thiol groups of substituted cysteine readily form intersubunit metal bridges via S-Cd^{2+}-S bonds, it would implicate that maximum four connexin subunits could be cross linked by the arrangement of a tetradentate geometry (Bargiello *et al.*, 2012). A prerequisite to the coordination of S-Cd^{2+} metal bridges is that the cysteine side-chains of adjacent subunits move into a narrowed spatial range that is optimal

for binding to a mutual Cd^{2+} ion (~3-4 Å). Thus, the extracellular Cd^{2+}-induced hemichannel block was deduced in a way that membrane hyperpolarization, a condition which favors closure of slow gate triggers a pore constriction at the TM1/EL1 site, likely involves the movement of pore-lining residues F43, G46 and D51. When any of the three residues is replaced by cysteine, the narrowing of the pore at the site would confer a spatial organization allowing the Cd^{2+} ions retained originally in the open pore to form cross-linked metal bridges with thiol groups, thus locking-up the channels in the closed state.

Data yielded from work on undocked Cx32*Cx43EL1 hemichannels confirm the importance of TM1/EL1 in pore-lining, yet propose a slow gating mechanism slightly different from that of Cx50 hemichannels (Tang *et al.*, 2009). In this study, MTS reactivity was observed with cysteine mutagenesis at valine 38 (V38) and G45 (homologous to G46 of Cx50) when the channel resided in the open state. Strikingly, the two flanked residues A40 and A43 by no means line the open pore, but the respective cysteine substitutes could stabilize the channels in the closed state by accommodating the Cd^{2+}-coordinated metal bridges. Assuming a perfect α-helical structure sustained by the TM1/EL1 border, the inferred slow gating mechanism then differs from the set of Cx50 hemichannel data including an additional axial rotation and an inward tilt at the pore-lining region where A40 and A43, originally buried within the protein core of the open hemichannel, translocate to the narrowed extracellular vestibule.

In fact, the same lock-up phenomena could be reproduced in Cx26 hemichannels with G45C substitution, well pointing to a conserved structural rearrangement that accounts for slow gating (Sanchez *et al.*, 2010). The crystal structure of the open Cx26 channel is mostly convergent with the information obtained by the electrophysiological approach, portraying an open pore lined by TM1/EL1 domain (Maeda *et al.*, 2009). However in contrast to the SCAM studies, an important aspect of the structure, is that the span of the TM1/EL1 transition (residue E42-F51) is in fact packed into a parahelical arrangement rather than a perfect α-helix, in addition to a substantial bend angle of ~34° (Kwon *et al.*, 2011;Kwon *et al.*, 2012) initiated at or near V43. Taken together, the dramatic rotation of A40 and A43 initially predicted for the closure of Cx32*Cx43EL1 might not be necessary. Instead, the presence of a parahelix is amenable for a greater flexibility at the pore-lining region. Then, a more energetically favored conformation involving a straightened bend angle at TM1/EL1 is expected to suffice the structural need for repositioning A40 and A41 towards the narrowed extracellular entrance. A recent computational simulation based on the crystal structure has detailed the atomic interactions that stabilize the open Cx26 hemichannel (Kwon *et al.*, 2012).

In the model, two core elements were critical for maintaining the parahelical integrity and the bend angle of TM1/EL1 border: i) intrasubunit *van der Waals* forces extending from the parahelix to the intracellular side of TM1 and ii) an intra- and intersubunit electrostatic network derived from the charged residues lining the parahelix. The electrostatic network interconnecting all six subunits is in support of a concerted slow gating which requires simultaneous motions of all six subunits. Charged pore-lining residues involved in the electrostatic network are expected to dynamically change the structure of the parahelix in response to voltage, thereby positioning themselves as at least part of the voltage sensor.

1.3 Chemical gating of connexin channels

Extracellular Ca^{2+}

Hemichannel activities are potentiated by lowering the extracellular Ca^{2+} concentration ($[Ca^{2+}]_o$; normal level 1-2 mM). Under physiological conditions such as neuronal activity (Torres *et al.*, 2012), this change in $[Ca^{2+}]_o$ can take place in a form of regional and rhythmic fluctuations ranging from 200 µM to 1 mM (Brown, 1991;Quist *et al.*, 2000). More pronounced reduction down to 0.1 mM occurs upon pathological insults including hyperglycemia, ischemia and epilepsy. Over the past decade, methods varying from atomic force microscopy (AFM) imaging to single-channel measurement have collectively provided structural and mechanistic insights into the broad effect of $Ca^{2+}{}_o$ on connexin hemichannels.

The earliest report concerning structural details of hemichannel closure by $Ca^{2+}{}_o$ is dated back to an AFM imaging of Cx26 hemichannels. The hemichannels subject to the study were dissected from gap junctions making use of the AFM stylus (Muller *et al.*, 2002). Application of 0.5 mM $[Ca^{2+}]_o$ caused conformational changes at the extracellular side of the hemichannels with the diameter of the extracellular vestibule being reduced from 15Å to 6Å . The effect was reversible and could not be mimicked by up to 2 mM extracellular Mg^{2+}. Complementary to this finding, the same approach employing reconstituted hemichannels have detailed real-time transitions between closed and open conformations of Cx40 and Cx43 hemichannels as a function of $[Ca^{2+}]_o$ (Allen *et al.*, 2011;Thimm *et al.*, 2005). Interestingly, increasing $[Ca^{2+}]_o$ expanded the population of Cx43 hemichannels that adopted a constriction of the pore diameter from ~2.8 nm (open) to 1.8 nm (close). Thus, $Ca^{2+}{}_o$-mediated hemichannel closure can be marked as an all-or-none effect on the channel configuration. A hydrophobic surface detected only at the open extracellular vestibule prompts the authors to

speculate that Ca^{2+}-binding at the extracellular face refolds the ELs into a tightly packed conformation where the hydrophobic domains are buried. Comparable structural rearrangements by Ca^{2+}_o were reported for reconstituted Cx40 hemichannels, except this time, changes were also caught on the intracellular face of the channel (Allen *et al.*, 2011).

The mechanistic perspectives defined by electrophysiological data, however, slightly diverge from those by structural analysis. Unconditional hemichannel block by Ca^{2+}_o has rarely been observed in patch-clamp measurements and most of the interpretations favor a voltage-dependent block. Evident from the whole-cell recording of Cx46 hemichannels, 5 mM Ca^{2+} completely blocked the hemichannel currents at negative V_m while had little effect at positive potential (Pfahnl and Dahl, 1999). More importantly, Mg^{2+}_o ions were shown to promote Cx46 hemichannel closure in the same manner (Ebihara *et al.*, 2003). Removal of extracellular Ca^{2+} and Mg^{2+} virtually abolished the voltage gating properties of both Cx37 and Cx46 hemichannels, generating a linear relation between hemichannel currents and V_m (Ebihara *et al.*, 2003;Puljung *et al.*, 2004). The initial explanation was that divalent cations attracted by negative resting V_m enter the channel pore and bind to a channel blocking site at the cytoplasmic end (Puljung *et al.*, 2004). Channel closure was anticipated as a consequence of steric block, thereby involving no conformational change. A later study on Cx46 hemichannels however argued that Ca^{2+}_o may bind to an extracellular side of the hemichannel and lock the channel to a long-lived closed state by modulating the intrinsic slow gate (Verselis and Srinivas, 2008a). In Cx32 hemichannels, a ring of 12 Asp residues residing at the external vestibule of the channel pore has been identified as a Ca^{2+}-binding site that accounts for both steric occlusion of the lumen and modulation of the slow gate (Gomez-Hernandez *et al.*, 2003). Interestingly, replacing external Na^+ with other monovalent cations such as K^+ or Cs^+ can reduce Cx50 hemichannel sensitivity to $[Ca^{2+}]_o$, implicating binding sites for monovalent and divalent cations lying in close proximity at the extracellular side of the channel (Srinivas *et al.*, 2006).

Above all, information yielded from the two distinct approaches need to be carefully interpreted apart from each other (Bargiello *et al.*, 2012). A critical factor makes the two sets of data incoherent: voltage-dependent channel block by both extracellular Ca^{2+} and Mg^{2+} clearly contrasts to the unique roles of Ca^{2+}_o in hemichannel configuration. Perhaps structural reorganization by Ca^{2+} alone and the modulation of voltage-gating by divalent cations reflect two similar, yet not identical molecular mechanisms.

Intracellular Ca^{2+}

At rest, cytoplasmic calcium concentration ($[Ca^{2+}]_i$) is below 100 nM. An increase in $[Ca^{2+}]_i$ occurs through either Ca^{2+}-entry down the concentration gradient or via release from internal stores. The earliest evidence for regulation of gap junctions by changes in $[Ca^{2+}]_i$ came from studies of Loewenstein et al. in which electrical coupling between insect gland cells were suppressed upon microinjection of ~50 nM Ca^{2+} (Loewenstein and Rose, 1978;Rose and Loewenstein, 1976). The effect was confined to the cell junctions exposed to the local Ca^{2+} rise whereas junctions distant from the injection site were not affected. To date, inhibition of junctional coupling by a $[Ca^{2+}]_i$ increase has been confirmed in a variety of cell types including amphibian embryonic cells (Spray *et al.*, 1982), cardiac cells (De Mello, 1975;Dekker *et al.*, 1996;Firek and Weingart, 1995;Maurer and Weingart, 1987), Novikoff hepatoma cells (Lazrak and Peracchia, 1993a;Lazrak *et al.*, 1994), astrocytes, lens cells (Churchill *et al.*, 2001;Crow *et al.*, 1994;Lurtz and Louis, 2003;Lurtz and Louis, 2007), pancreatic β-cells (Mears *et al.*, 1995), cochlear supporting cells (Lagostena *et al.*, 2001) and cells stably transfected with connexin proteins (Chen *et al.*, 2011;Xu *et al.*, 2012). Despite of all these findings, there is no consensus on the effective range of $[Ca^{2+}]_i$ that blocks gap junction channels. In some ruptured and internally perfused cells, elevating $[Ca^{2+}]_i$ to 40-400 μM was necessary to uncouple gap junctions. On the other hand, sensitivity of gap junctions to physiologically relevant $[Ca^{2+}]_i$ changes was observed during non-invasive measurement or patch-clamp recording that preserved most of the intracellular integrity (Table 1). It is reasonable to speculate that perfusing ruptured cells with solutions of known Ca^{2+} concentration could significantly affect the Ca^{2+} homeostasis and dilute the intermediate messenger that may be involved in the signaling cascade. An alternative explanation for the wide range of $[Ca^{2+}]_i$ threshold necessary to block gap junctions is the efficient internal buffering equipped by the cell that slows down the Ca^{2+} diffusion in the cytosol and creates large intracellular Ca^{2+} gradients. Consistent with the idea, a local increase of $[Ca^{2+}]_i$ in cultured rat aortic smooth muscle cells via inhibition of K^+/Na^+ pump or Na^+/Ca^{2+} exchanger reduced gap junction coupling whereas global $[Ca^{2+}]_i$ change had no effect (Matchkov *et al.*, 2007). In primary human fibroblast culture, neither ionomycine-induced bulk $[Ca^{2+}]_i$ rise nor Ca^{2+}-release from internal stores by G-protein coupled receptor (GPCR) activation affected dye transfer (Dakin *et al.*, 2005). In contrast, capacitive Ca^{2+} entry through store-operated Ca^{2+} channels profoundly blocked junctional coupling, suggesting the localization of Ca^{2+} entry channels in a close proximity to gap junctions (Lurtz *et al.*, 2007). However, similar

findings could not be reproduced in cultured lens cells. Instead, Ca^{2+} elevation sustained by ionomycine and high $[Ca^{2+}]_o$ appeared to effectively block gap junction communication in these cells.

Gap Junction	Cell type	$[Ca^{2+}]_i$ threshold	Kinetics	Stimulus	Reference
Innexin	Amphibian embryonic cells	500-1000 µM	100 s	Internal perfusion,	Spray *et al.*, 1982
Cx40 Cx43	Purkinje cells	~150 µM	~ 5 min	Ca^{2+} injection	De Mello, 1975
Cx43	Ventricular cardiomyocytes	~700 nM	~2.1 min	Ionomycine and blockade of Na^+/K^+ exchanger	Dekker *et al.*, 1996
Cx43	Neonatal ventricular cardiomyocytes	~300 µM	< 4 min	Ca^{2+}-EGTA delivered to one side of a cell pair via recording pipette	Firek and Weingart, 1995
Cx43	Novikoff Heptoma cells	~890 nM	~1.6 min	Ca^{2+}-EGTA via recording pipette or arachidonic acid	Lazrak *et al.*, 1994 Lazrak and Peracchia, 1993
Cx40 Cx43	Vascular smooth muscle cells A7r5	N.A.	< 5 min	inhibition of Na^+/K^+ pump or Na^+/Ca^{2+} exchanger	Matchkov *et al.*, 2007
Cx43	Bovine lens cells	~400 nM	< 15 min	Ca^{2+}-ionophore	Crow *et al.*, 1994
Cx43	Primary human fibroblasts	~300 µM	~ 8 min	Thapsigargin-induced capacitative calcium influx	Dakin and Li *et al.*, 2006
Cx43	Sheep lens cells	~300 nM	< 5 min	ionomycine, 11.8 mM Ca^{2+}_o	Churchill et al., 2001 Lurtz and Louis, 2003
Cx43	HeLa-Cx43	~400 nM	< 5 min	ionomycine, 20.1 mM Ca^{2+}_o	Lurtz and Louis, 2007
Cx43	N2A-Cx43	400-800 nM	15 min	ionomycine, 1.8 mM Ca^{2+}_o Patch-clamp recording	Xu *et al.*, 2012
Cx50	N2A-Cx50	~400-800 nM	<3 min	ionomycine, 1.8 mM Ca^{2+}_o Patch-clamp recording	Chen *et al.*, 2011

Table 1. Overview of the effect of $[Ca^{2+}]_i$ on gap junction communication in various cell types. N.A., not applicable.

It is unlikely that intracellular Ca^{2+} affects gap junction gating via direct binding to connexin proteins. A direct effect would require clusters of negative charges residing at the cytoplasmic side of the channel. Among all connexins, there is only one conserved acidic residue, glutamic acid (E) at the TM4/CT border, giving rise to total six negative charges per hexamer. However, these are not sufficient to confer sensitivity to physiological $[Ca^{2+}]_i$ changes. In addition, electrostatic interaction would not allow the channel to recognize the cytoplamsic Ca^{2+} from Mg^{2+} whose concentration is in the range of milimolar at rest. EF-hand binding motif facing cytoplasm would be necessary for the high affinity Ca^{2+}-binding, but has not been identified in any of the connexin isoforms. Alternatively, $[Ca^{2+}]_i$ can reduce junctional

coupling via an intermediate component. Consistent with the idea, high $[Ca^{2+}]_i$-induced gap junction uncoupling can be prevented by calmodulin (CaM) inhibitors such as calmidozolium and W7 (Lurtz *et al.*, 2003;Lurtz *et al.*, 2007;Peracchia, 2004a). CaM is a ubiquitous protein consisting of a C-lobe with higher Ca^{2+}-binding affinity (K_d ~10^{-7} M) and a N-lobe with Ca^{2+}-binding affinity one order of magnitude lower (K_d ~10^{-6} M). Upon activation by Ca^{2+}, Ca^{2+}/CaM complex could inhibit the electrical coupling either by directly targeting the receptor domain of a connexin channel or through downstream signaling mediators such as Ca^{2+}/CaM dependent kinases (CaMKI-V) and phosphatase (calcineurin). For α-group connexin, a unique CaM binding site has been identified in the second half of intracellular loop regions of Cx43 (residue 136-158; K_d~100 nM), Cx44 (residue 129-150, K_d ~49 nM) and Cx50 (residue 141-166, K_d ~5 nM) (Chen *et al.*, 2011;Zhou *et al.*, 2009;Zhou *et al.*, 2007a). By delivering a peptide encompassing the sequences of CaM binding domain into the cell, the inhibitory effect of elevated $[Ca^{2+}]_i$ (400-800 μM) on Cx43 and Cx50 gap junctions was alleviated (Chen *et al.*, 2011;Xu *et al.*, 2012) whereas inhibition of CaMKII failed to exert the same effect (Lurtz *et al.*, 2007). Moreover, Cx40 gap junctions lacking a putative CaM binding site did not respond to $[Ca^{2+}]_i$ changes. These findings inspired a 'cork' type gating model, suggesting that upon binding to connexin channels, the Ca^{2+}/CaM complex either acts as a 'cork' or triggers conformational change in the CL domain that eventually obstructs the intracellular vestibule of the pore. A similar gating mechanism was also proposed for the β-group Cx32 gap junctions that contain three putative CaM binding sites per monomer: two of them reside in the NT (residue 1-22 and 18-22) and one is located at the NT-end of the CT. It is important to note that not all cell receptor activations that mobilize intracellular Ca^{2+} uncouples gap junctions in a Ca^{2+}/CaM dependent manner. Extracellular ATP can block gap junction communication through a protein kinase C (PKC)-mediated signaling pathway independent of Ca^{2+}/CaM activity (Lurtz *et al.*, 2003). In addition, a local depletion of phosphatidylinositol 4,5-bisphosphate (PIP2) from the plasma membrane can readily close Cx43 gap junctions in response to GPCR activation (van Zeijl *et al.*, 2007).

Amounting evidence is available that connexin hemichannels also respond to $[Ca^{2+}]_i$ changes. In embryonic pigment epithelial cells, Cx43 hemichannels-mediated ATP release was related to spontaneous intracellular Ca^{2+} transients (Pearson *et al.*, 2005a). Approaches that manipulate $[Ca^{2+}]_i$ such as photoactivaiton of caged inositol-1,4,5-trisphosphate (IP3) or exposing cells to Ca^{2+} ionophore or caffeine could also stimulate ATP release in cells expressing Cx32 or Cx43 (Braet *et al.*, 2003a;De Vuyst *et al.*, 2009a;DeVuyst *et al.*, 2006). A

bell-shaped profile describing both Cx32 and Cx43 hemichannel activities in function of $[Ca^{2+}]_i$ has been delicately shown by De Vusyt et al. (De Vuyst *et al.*, 2009a;DeVuyst *et al.*, 2006). The response curve consists of an activation of hemichannels by a moderate $[Ca^{2+}]_i$ (~500 nM) and disappearance of the hemichannel activity upon further $[Ca^{2+}]_i$ increase (named 'inhibition'). The activation phase is mediated by a signaling cascade involving CaM, CaMKII, p38 mitogen activated kinase and arachidonic acid. Reactive oxygen species, products of arachidonic acid metabolism, are potent Cx43 hemichannel modulators. The compounds either directly induce membrane depolarization in favor for hemichannel openings or indirectly mediate S-nitrosylation of Cx43 via activation of nitric oxide synthesis. An interesting feature is that increasing CaM activity brings Cx43 hemichannels to steady-state activation, excluding its involvement in the inhibition phase. A more recent study suggests an impaired intramolecular interaction in relation to Cx43 hemichannel closure at high $[Ca^{2+}]_i$ (Ponsaerts *et al.*, 2010c). Disruption of the Cx43 CT-CL binding at $[Ca^{2+}]_i$ of ~500 nM removed the potent effect of $[Ca^{2+}]_i$ on Cx43 hemichannel-mediated ATP release while mimicking the CT-CL interaction prevented the high $[Ca^{2+}]_i$ provoked hemichannel closure. (-)Blebbistatin, an inhibitor of the actomyosin contractility, imposed a similar effect, recovering hemichannel activities at high $[Ca^{2+}]_i$. Collectively, these findings suggest that the CT-CL interaction is essential for hemichannel opening. Activation of the actomyosine contractile system by $[Ca^{2+}]_i$ > 500 nM displaces the CT from the CL, thereby keeping Cx43 hemichannels closed.

Intracellular pH

Remarkable changes in concentration of intracellular H^+ ions can take place under pathophysioclogical conditions such as organ ischemia or epilepsy. The drastic drop in pH_i (to ~ 6.1-6.5) exerts a negative impact on virtually all gap junctions, shutting down the cell-to-cell electrical and metabolic communications. Nevertheless, the pH sensitivity varies among connexin subtypes, ranging from pKa (the pH_i at which the G_j reaches half maximal reduction) of ~6.5 for Cx32 gap junctions to pKa of ~7.2 for Cx50 gap junctions. The pH_i sensitivity of other gap junctions falling in between this range is ranked in the following orders: Cx46>Cx45>Cx26>Cx37>Cx43>Cx40 ((Stergiopoulos *et al.*, 1999); reviewed in (Peracchia, 2004a)). G_j reduces rapidly following the onset of the cytoplasmic acidification and is completely reversible shortly after insult, consistent with a direct action of pH_i changes on channel gating. Single-channel activity from cell pairs expressing Cx43 demonstrated a complete channel closure in relation to increasing $[H^+]_i$ through slow, occasionally resolvable

step-wise transitions. Therefore, pH_i and V_j seem to act on a common slow gate of gap junctions (Bukauskas *et al.*, 2004a).

A genuine effect that would be provoked by increased $[H^+]_i$ is protonation of the histidine (H) residues located at the intracellular side of connexin proteins. Replacing H95 of Cx43 which is located at the NT end of CL domain with negative (H95D) or polar uncharged residue (H95Y) drastically reduced the susceptibility of the gap junction channel to pH_i decay whereas mutation with positive charge such as lysine (H95K) further enhances the pH_i sensitivity (Ek *et al.*, 1994). Succeeding studies reported a low pH_i-tolerant junctional coupling recorded in Cx43 gap junctions lacking the CT sequence (Liu *et al.*, 1993;Morley *et al.*, 1997). Over the past decade, a significant effort has been made towards understanding of a concerted action of the CT and CL domains through which low pH_i closes the gap junctions. In a proposed 'ball-and-chain' model, binding of Cx43CT to the second half of the CL underlies the pH_i-dependent gap junction closure (Duffy *et al.*, 2002a). Several factors are critical for the this interaction: i) formation of α-helix at L2 region promoted by histidine protonations (Duffy *et al.*, 2002a) and ii) dimerization of the CT domain at low pH_i (Sorgen *et al.*, 2004b). Conceptually, analogue models may be applied to explain pH_i-gating of Cx32 gap junctions based on the finding that exchanging second half of CL of Cx32 with that of Cx38 generated a mutant gap junction with the pH_i sensitivity enhanced to that of Cx38 gap junction (Wang and Peracchia, 1996). Later studies by Peracchia and his co-worker defined 5 positively charged arginines at the initial segment of CT aiding for pH_i-sensing (Wang and Peracchia, 1997;Wang and Peracchia, 1998). Upon intracellular acidification, disrupted electrostatic interaction between all 5 arginines of CT and negatively charged CL is expected to confer the closure of Cx32 gap junctions (Peracchia and Wang, 1997).

Certainly not all gap junction channels obey the principle of particle-receptor binding to convey the pH_i-dependent channel closure. CT truncation merely affects the pH_i sensitivity of Cx37, Cx45, Cx46, and Cx50 gap junctions (De Rosa *et al.*, 2006;Stergiopoulos *et al.*, 1999;Trexler *et al.*, 1999). In fact, channel closure in response to intracellular acidification can be reflective of the pH_i-sensitivity of the voltage gate (Peracchia *et al.*, 2004;Peracchia *et al.*, 2003). Low pH_i-uncoupled Cx45 gap junctions have been associated with a right shifted G_j-V_j relation as well as reduced fractions of channels available for opening (Palacios-Prado *et al.*, 2010a). Finally, several studies have engaged in elucidating indirect effects of protons on junctional coupling, involving intracellular Ca^{2+}/CaM as an intermediate factor. Increasing cytoplasmic $[H^+]$ promotes Na^+ overload in the cell by hyperactivating Na^+/H^+ exchangers,

and in turn reverses Na^+/Ca^{2+} exchange resulting in an elevation of $[Ca^{2+}]_i$. There is evidence emerging that the synergetic action of intracellular Ca^{2+} and H^+ or intracellular Ca^{2+} alone accounts for the uncoupling process at low pH_i (Peracchia, 2004a).

What do we know about pH_i-dependent gating in connexin hemichannels? Acidifying the cytoplasmic side of Cx46 hemichannels in the absence of soluble intermediate mediators could rapidly suppress the hemichannel unitary currents (Trexler *et al.*, 1999). Thus the effect is most likely attributed to a direct titration of histidine and/or cysteine residues located at the cytoplasmic side of the channel. Just on the opposite, during whole-cell recording of HeLa-Cx43 cells, imposing MES-buffered acidic pipette solution with $[Ca^{2+}]_i$ equilibrated to 50 nM failed to induce any changes of Cx43 hemichannel currents at positive V_m, even though CO_2-induced intracellular acidification was able to completely abolish the single-channel events (Wang *et al.*, 2012b). A side effect of CO_2-induced pH_i decay is that low pH_i (6.4-6.0 in the study) would significantly reduce the affinity of EGTA in the pipette and cell, turning Ca^{2+}-EGTA complex into a Ca^{2+} releasing agent. Therefore, it is possible that Cx43 hemichannel inhibition by low pH_i is associated with a prominent increase of $[Ca^{2+}]_i > 500$ nM. Similarly, lack of a direct action of protons has been suggested for low pH_i-inhibited Cx26 hemichannels (Bevans and Harris, 1999;Tao and Harris, 2004). In this case, protonated forms of aminosulfonates that buffer the pH such as HEPES, MES and taurine are the secondary messengers involved in the pH_i-sensing. Locke et al. have delicately shown a direct binding of protonated taurine to the CL region of Cx26 hemichannels. The interaction counteracted a low pH_i-strengthened CT-CL interaction which engages in hemichannel activation. In consistent with the functional assessment, AFM imaging was able to detect a narrowed pore dimension of Cx26 hemichannels at pH < 6.5 buffered by aminosulfonates (Yu *et al.*, 2007). The response is connexin specific because Cx32 hemichannels tested in the same study was aminosulfonate resistant at low pH_i. Of note, connexin hemichannel activities are not only affected by intracellular acidification, but also by extracellular alkalinization (Schalper *et al.*, 2010a). A potent effect of increasing extracellular pH on hemichannel currents was recently identified in HeLa-Cx43 hemichannels, although the underlying mechanisms remain elusive.

CHAPTER II. Connexins in the heart

2.1 connexin channel organization and its site-specific distribution in the normal adult heart

In the normal adult heart, sarcolemmal connexins are exquisitely polarized to the intercalated discs ('nexus') of the working myocardium (Severs *et al.*, 2008a). Immunostaining of Cx43, the primary connexins in the ventricle clearly shows a plaque-like aggregation of gap junctions at the ends of cardiomyocytes and the spatial organization in relation to adherent junctions and desmosomes have been largely depicted by electron microscopy (Fig. 1A). At the periphery zone surrounding the gap junction plaques, Cx43 proteins accrete in the form of unapposed hemichannels (Fig. 1B) (Rhett *et al.*, 2011a). Within this region defined by Rhett et al. as 'Perinexus', dynamic interaction between Cx43 and the scaffolding protein zonula occludin-1 (ZO-1) tightly controls the transition of hemichannels from unapposed to apposed configurations (further discussed in section 2.3).

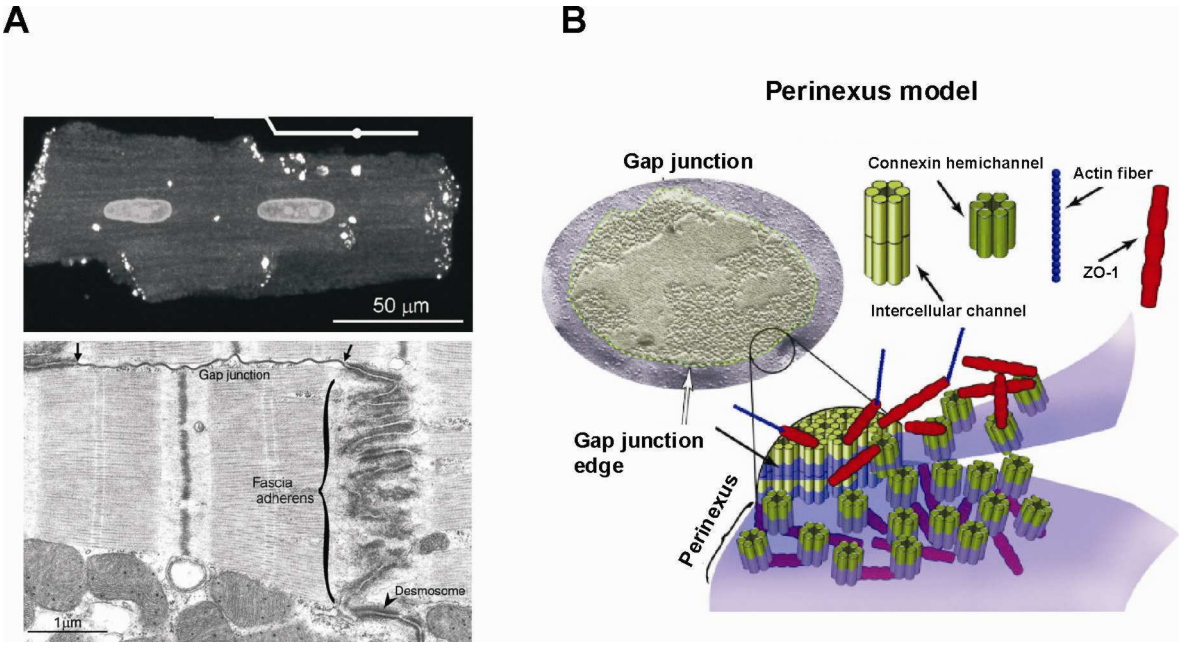

Figure 1. Connexin organization at the intercalated discs. A. Distribution of sarcolemmal Cx43 in an isolated mouse ventricular cardiomyocyte (upper panel). Gap junction organization within the intercalated disc as depicted by thin-section electron microscopy (lower panel). (Taken from (Severs *et al.*, 2008a)) B. Cx43-ZO-1 interaction extending into the periphery of gap junction plaques named 'perinexus', a region where unapposed connexin hemichannels reside. Cx43-ZO-1 complexes in the perinexus interact less with actin fibers than those in the nexus. Taken from (Rhett *et al.*, 2011a).

Up to date, the presence of three principle connexins - Cx40, Cx43 and Cx45 - has been well established in the adult mammalian heart, each characterized by a site-specific distribution pattern (Fig. 2) (Giovannone *et al.*, 2012;Jansen *et al.*, 2010a). Cx40 has been detected in the

atrial cardiomyocytes, atrioventricular (AV) node, peripheral conduction system and to a lesser extent in the sinoatrial (SA) node (Davis *et al.*, 1994;Davis *et al.*, 1995;Gros *et al.*, 1994). Cx43 is the most abundantly expressed connexin protein in the heart, mainly distributed in the atrial and ventricular working myocardium and with a scant amount restricted to the border zone between the periphery of SA node and the crista terminalis (Coppen *et al.*, 1999). Cx45 dominates the connexin expression in SA and AV nodes. His-bundles and bundle branches are also marked Cx45 positive whereas the expression level in the ventricle is tightly limited. A fourth cardiac connexin, Cx30.2, recently added up to the mouse model is mostly present in the SA and AV nodes (Kreuzberg *et al.*, 2006b). However, its human orthologue Cx31.9 was not detected in the human heart, raising a concern over species-dependent connexin expressions (Kreuzberg *et al.*, 2009).

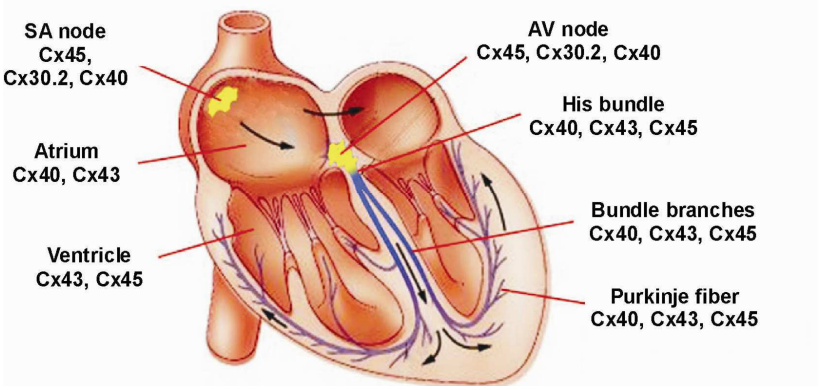

Figure 2. An overview of site-specific distribution of connexins in the mouse heart. Arrows indicate the propagation of the electrical activities in the heart. An electrical impulse initiated in the SA node is transmitted through the atria, delayed in the AV node and sequentially activates the ventricular myocardium through the specialized conduction system. Taken from (Giovannone *et al.*, 2012).

Impulse propagation in cardiac tissue is determined by multiple factors: i) cellular excitability dependent on the Na^+ and Ca^{2+} channel currents; ii) gap junctions providing intercellular pathway for cell-to-cell electrical transmission and iii) cardiac tissue architecture. The diversity of connexin expressions at least partly meets the disparate conduction profiles of the different cardiac sites (Giovannone *et al.*, 2012;Kleber, 2011). The primary role of cardiac connexins under physiological conditions is to form gap junctions, but the biophysical properties of junctional channels substantially differ among connexin isoforms. Given the presence of more than one connexin subtype expressed in each compartment, the picture is only complicated further when all possible apposed heteromeric hemichannels and heterotypic gap junctions are taken into consideration (reviewed in (Desplantez *et al.*, 2007)). To simplify the argument, unitary conductance of homotypic gap junctions alone is ranked in the following order: Cx40 (~180 pS) > Cx43 (~115 pS) > Cx45 (~40 pS) > Cx30.2 (~9 pS).

Then, it is not surprising to find a dominant distribution of Cx45 and Cx30.2 in SA and AV nodes where the conduction velocities are an order of magnitude lower than in the atria and ventricles. Low-conductance gap junctions composed of Cx45 and Cx30.2 could limit the electrical coupling between pacemaker cells to a minimum level that is still sufficient for synchronizing the pacemaker activities (Verheijck *et al.*, 1998). Similarly, activation delay between the atria and the ventricles necessitates the presence of this high-resistance coupling which would slow down the conduction through AV node. As one moves to the ventricular conduction system, the remarkable fraction of high-conductance Cx40 gap junctions is reflective of the fast conduction through His-Purkinje system which coordinates the triggering events at the ventricular myocardium (Harris *et al.*, 2012). Finally, leading gap junctions comprising Cx40 and Cx43 mediate the spread of excitation in the atria while electrical propagation over a wide range of working ventricular myocytes are best conducted by high-conductive state of Cx43 gap junctions.

Over the past decade, development of genetically modified mice has further provided an in-depth understanding towards diverse roles of connexins in impulse propagation. Cx30.2 deficient mice showed no structural abnormalities, but exhibited a shortened PQ interval (Kreuzberg *et al.*, 2006a;Kreuzberg *et al.*, 2006b). The unique pattern reflecting an accelerated impulse propagation through the AV node infers to a dominant negative influence of Cx30.2 in electrical coupling between AV nodal cells (Kreuzberg *et al.*, 2005). Germline ablation of Cx45, the other connexin abundantly present in the SA and AV nodes, gave rise to a high mortality rate of the transgenic animals at early embryonic stage. These Cx45-/- animals died of heart failure arising from endocardial cushion defects, marking a vital role of Cx45 in the early cardiac morphogenesis (Kumai *et al.*, 2000). To circumvent the developmental defects, transgenic mice were subject to cardiac-directed deletion of Cx45. Surprisingly, no prominent change of electrophysiological properties was detected in the conditional knockout (KO) except a limited restriction of AV nodal conduction (Bao *et al.*, 2011;Frank *et al.*, 2012). On the other hand, overexpression of Cx45 enhanced the susceptibility of the animals to ventricular tachycardia, by restraining the size of Cx43 gap junction plaques and electrical coupling (Betsuyaku *et al.*, 2006;Grikscheit *et al.*, 2008). Conceivably, determined by the divergent conduction pattern of each chamber, high-level expression of Cx45 can be beneficial at AV node, but detrimental for the ventricular activation. More profound consequences have been found in mice lacking cardiac Cx40 protein. The homozygous Cx40-/- mice were generally predisposed to arrhythmia and a

primary change discovered in electrocardiography includes a prolonged PR interval, mainly attributed to the impaired conduction at AV node and His-Purkinje system (Bevilacqua *et al.*, 2000;Hagendorff *et al.*, 1999;Kirchhoff *et al.*, 1998;Simon *et al.*, 1998;VanderBrink *et al.*, 2000;Verheule *et al.*, 1999). Sequentially, bundle branch block altered the temporal and spatial activation of the working ventricular myocardium, whereas the electrical coupling between ventricular myocytes was not affected by Cx40 deficiency (Simon *et al.*, 1998;Tamaddon *et al.*, 2000;van Rijen *et al.*, 2001;Verheule *et al.*, 1999). In some but not all cases, prolonged P-wave duration was detected (Bagwe *et al.*, 2005;Kirchhoff *et al.*, 1998;Schrickel *et al.*, 2009;Verheule *et al.*, 1999), in line with the reduced conduction velocity located within the right atrium. It should be borne in mind that a high incidence of developmental and congenital defects has been identified in Cx40-/- mice, including pathologic hypertrophy, common AV junction and ventricular septal defects which may by themselves cause conduction disturbances (Kirchhoff *et al.*, 2000). Homozygous germline Cx43 null mice like the Cx45-/- mice, was practically difficult to sustain because of high neonatal mortality rate associated with malformation of the right ventricular outflow tract (Reaume *et al.*, 1995). An inducible KO model by tamoxifen injection ($Cx43^{Cre\text{-}ER(T)/fl}$, one Cx43 coding region replaced by tamoxifen inducible Cre recombinase and the other flanked by two separate loxP sites) achieved up to 90% deletion of Cx43 proteins in the adult mouse heart (van Rijen *et al.*, 2004). The Langendorff-perfused heart exhibited reduced conduction velocity and increased dispersion of velocity, but no spontaneous conduction block.

2.2 Connexin remodeling in diseased myocardium

The connexin KO models may have strengthened the importance of site-dependent connexin expression, but the fact that a complete conduction block was never reached in various connexin KO models pointed to a long-standing question: are gap junctions necessary for impulse propagation in the heart? Long dated back to 1960s, Sperelakis et al. proposed an electric field effect by means of which action potential could propagate without gap junction coupling (Sperelakis, 2002;Sperelakis and Mann, Jr., 1977). The close apposition of two intercalated discs creates a narrow junctional cleft, where an electric filed can be developed by the prejunctional upstroke. The resulting negative cleft potential would induce depolarization of the postjunctional membrane which in turn activates the inward sodium currents and subsequent excitation. Several studies have recently revisited the theory arguing that sodium currents-mediated ephaptic electrical transmission can occur under the following conditions: i) junction cleft resistance is small enough and ii) the density of Na^+ channels at

the intercalated disc is high enough (Kucera *et al.*, 2002;Mori *et al.*, 2008). However, one caveat to keep in mind is that most of the theoretical models assume a uniform change in junctional coupling whereas disease myocardium is often marked with profound downregulation of connexins and heterogeneous distribution.

In overall, Cx43 remodeling consisting of altered expression, redistribution and reduced phosphorylation status is a hallmark of most cardiac diseases associated with arrhythmogenic disorders. In ischemic heart, redistribution of Cx43 from the intercalated disc to the lateral margins of the cardiomyocytes ('lateralization') occurred at 1 h post coronary occlusion and further proceeded over the course of 3h (Duffy, 2012). Immunohistochemistry showed that Cx43 proteins accreted at the intercalated discs were mostly phosphorylated while those residing at the lateral cell border were markedly dephosphorylated (Lampe *et al.*, 2006). In the healing infracted canine heart, Cx43 lateralization was identified at the epicardial infarct border zone of surviving cardiomyocytes and was spatially correlated with reentry circuits (Peters *et al.*, 1997). In canine ventricles with nonischemic dilated cardiomyopathy, Cx43 lateralization and significantly reduced phosphorylation were associated with conduction velocity slowing and enhanced susceptibility to ventricular tachycardia (Akar *et al.*, 2004). A mouse model of pressure overload hypertrophy additionally proposed a tight link of heterogeneous distribution of ventricular Cx43 to enhanced susceptibility to arrhythmogenesis (Boulaksil *et al.*, 2010). Consistently, lateralized Cx43 accompanied by reduced expression and spatial heterogeneity has been characterized in patients diagnosed with ischemic and nonishemic cardiomyopathy (Fontes *et al.*, 2012;Severs *et al.*, 2008a).

Apart from its direct contribution to reduced conduction velocity, remodeled Cx43 can exert a dominant negative effect on the intrinsic heterogeneities in Cx43 expression. Connexin expressions across the left ventricular wall do not necessarily follow a uniform pattern (Poelzing *et al.*, 2004;Poelzing and Rosenbaum, 2004;Yamada *et al.*, 2004). Several species including rodents and canine, exhibit a coherent spatial heterogeneity in Cx43 expressions with more abundant Cx43 protein content expressed in the midmyocardium and endocardium than in the epicardium. Thus, one would expect that enhanced heterogeneity in Cx43 distribution would additionally alter transmural gap junction coupling and create marked dispersion of repolarization that leads to reentrant arrhythmia.

2.3 Molecular mechanisms of connexin remodeling

The life cycle of a sarcolemmal connexin channel consists of a dynamic process balanced between forward trafficking of the newly synthesized connexins, transition from perinexus to nexus and internalization (Hesketh *et al.*, 2009;Smyth and Shaw, 2012). Disturbance at any of these phases would account for altered pools of sarcolemmal channels and/or surface redistribution.

It all starts at the beginning. Cardiac connexin proteins have a rapid turn-over rate of 1-3 hours (Beardslee *et al.*, 1998;Darrow *et al.*, 1995). In ventricular cardiomyocytes, newly oligomerized Cx43 hemichannels (*de novo* hemichannels) at the trans-Golgi network are transported to the sarcolemma in forms of vesicles. To achieve a targeted delivery towards the intercalated disc region, the vesicles are loaded onto microtubules (Giepmans *et al.*, 2001;Thomas *et al.*, 2005) whose polarized structure contains a minus-end stabilized to the centrosomal microtubule organizing center and a distal plus-end switching between the polymerization (grow) and depolymerization (catastrophe). The plus-end interacting protein EB1 stimulates and guides the growth of microtubules through docking with adherent junction proteins β-catenin and N-cadherin (Shaw *et al.*, 2007). By doing so, microtubule-based trafficking machinery accomplishes a 'highway' for targeting *de novo* Cx43 hemichannels to the discrete microdomain at the intercalated disc. Oxidative stress in ischemic human heart has been shown to dislodge the EB1 protein from the plus-end of the microtubules, limiting the growth of the microtubule (Smyth *et al.*, 2010). As a consequence, *de novo* Cx43 hemichannels are retained in the intracellular compartment, giving rise to impaired gap junction plaque formation. The succeeding studies included a second cytoskeleton component in the forward trafficking machinery and further revealed its involvement in Cx43 remodeling (Smyth *et al.*, 2012). In adult mouse ventricular cardiomyocytes, a remarkable fraction of Cx43 vesicles was associated with nonsarcomeric actin filaments which paused or slowed down Cx43 transport. Latrunculin A selectively interfering with actin polymerization perturbed the direct delivery of endogenous Cx43 to the plasma membrane. It looks likely that actin microfilament tightly controls the forward trafficking by serving as a transition hut for Cx43 vesicles on their way to the intercalated discs. Disrupted Cx43 vesicles/actin complexes were confirmed in mouse heart subject to acute ischemia, thereby being addressed as an additional contributor to the deficient Cx43 trafficking. Finally, there is evidence emerging that aberrant forward trafficking accounts for Cx43 lateralization (Chkourko *et al.*, 2012). In pressure overloaded sheep ventricles,

microtubule associated proteins EB1 and kinesin protein Kif5b were co-localized with Cx43 at the lateral membrane of the cardiomyocytes. Nevertheless, a complete understanding towards the molecular mechanism by which cellular stress impairs forward trafficking is still lacking. Little is known about how EB1 binding to plus-end of microtubule and complex formation between Cx43 vesicles and actin filaments are disrupted in diseased myocardium. Reduced phosphorylation status of remodeled Cx43 has been put forward as an additional factor affecting the forward trafficking machinery. Hypophosphorylation at Serine 325, 328, 330, CK1δ-dependent target site was associated with enriched Cx43 at the lateral side of the membrane in a mouse model of pressure overload hypertrophy (Remo *et al.*, 2011). Transgenic mice in which the three consensus sites of CK1δ were mutated to phosphomimetic glutamic residues (S3E) became resistance to Cx43 remodeling during the pathological insult, displaying normal pattern of gap junctional organization at the intercalated discs.

Being successfully delivered to the sarcolemma, Cx43 hemichannels interact directly with the PDZ-2 domain of ZO-1 and is stabilized at the 'perinexus' adjacent to the gap junction plaques (Gaietta *et al.*, 2002;Hunter *et al.*, 2005;Rhett *et al.*, 2011a). ZO-1 at the perinexus controls the transition between unapposed and apposed fractions of Cx43 hemichannels. Disturbing the Cx43-ZO-1 interaction increased the size of gap junction plaques in the exogenous system. When the same intervention was applied to the cryo-injured mouse heart, the size of gap junction plaques was restored and Cx43 redistribution was prevented. Interestingly, enhanced fractions of Cx43 bound to ZO-1 were also identified in the human ventricles with dilated or ischemic cardiomyopathy (Bruce *et al.*, 2008). This may suggest that in the failing heart, binding of ZO-1 to Cx43 is upregulated, limiting the recruitment of nonjunctional hemichannels to the nexus. Intriguingly, an interplay between Cx43 and ZO-1 imposed an opposite effect on Cx43 residing in the epicedial infarct border zone (Duffy *et al.*, 2004;Kieken *et al.*, 2009;Sorgen *et al.*, 2004a). Intracellular acidification secondary to ischemia promotes translocation of endogenous tyrosine kinase c-Src to the intercalated discs and phosphorylates the protein at tyrosine 416 (Y416). The resulting active form of c-Src leads to phosphorylation of Cx43 which closes the gap junctions and concomitantly, competes with Cx43 located at the junctional membrane for the binding site at ZO-1. Once unhooked from ZO-1, Cx43 is no longer tethered to the junctional microdomains and could freely diffuse to the lateral membrane followed by internalization. Similar mechanistic basis was proposed for aberrant Cx43 expression in transgenic mouse heart overexpressing angiotensin converting enzyme (ACE) (Sovari *et al.*, 2011). ACE cleaves decapeptide angiotensin I to

short peptide angiotensin II which in turn upregulates the c-Src activities and Cx43 remodeling. An alternative mechanism by which Cx43 is lateralized involves N^{ε}-lysine acetylation of Cx43 (Colussi *et al.*, 2011). In both mice and patients with Duchenne cardiomyopathy, lateralized Cx43 proteins were predominantly found in the N^{ε}-lysine acetylated form and co-immunoprecipitated with acetylase P300/CBP-associated factor, although the precise mechanism is yet no clear.

References

Akar FG, Spragg DD, Tunin RS, Kass DA, and Tomaselli GF (2004) Mechanisms underlying conduction slowing and arrhythmogenesis in nonischemic dilated cardiomyopathy. *Circ Res,* **95,** 717-725.

Allen MJ, Gemel J, Beyer EC, and Lal R (2011) Atomic force microscopy of Connexin40 gap junction hemichannels reveals calcium-dependent three-dimensional molecular topography and open-closed conformations of both the extracellular and cytoplasmic faces. *J Biol Chem,* **286,** 22139-22146.

Anumonwo JM, Taffet SM, Gu H, Chanson M, Moreno AP, and Delmar M (2001) The carboxyl terminal domain regulates the unitary conductance and voltage dependence of connexin40 gap junction channels. *Circ Res,* **88,** 666-673.

Bagwe S, Berenfeld O, Vaidya D, Morley GE, and Jalife J (2005) Altered right atrial excitation and propagation in connexin40 knockout mice. *Circulation,* **112,** 2245-2253.

Bao M, Kanter EM, Huang RY, Maxeiner S, Frank M, Zhang Y, Schuessler RB, Smith TW, Townsend RR, Rohrs HW, Berthoud VM, Willecke K, Laing JG, and Yamada KA (2011) Residual Cx45 and its relationship to Cx43 in murine ventricular myocardium. *Channels (Austin),* **5,** 489-499.

Bargiello TA, Tang Q, Oh S, and Kwon T (2012) Voltage-dependent conformational changes in connexin channels. *Biochim Biophys Acta,* **1818,** 1807-1822.

Beardslee MA, Laing JG, Beyer EC, and Saffitz JE (1998) Rapid turnover of connexin43 in the adult rat heart. *Circ Res,* **83,** 629-635.

Betsuyaku T, Nnebe NS, Sundset R, Patibandla S, Krueger CM, and Yamada KA (2006) Overexpression of cardiac connexin45 increases susceptibility to ventricular tachyarrhythmias in vivo. *Am J Physiol Heart Circ Physiol,* **290,** H163-H171.

Bevans CG and Harris AL (1999) Regulation of connexin channels by pH. Direct action of the protonated form of taurine and other aminosulfonates. *J Biol Chem,* **274,** 3711-3719.

Bevilacqua LM, Simon AM, Maguire CT, Gehrmann J, Wakimoto H, Paul DL, and Berul CI (2000) A targeted disruption in connexin40 leads to distinct atrioventricular conduction defects. *J Interv Card Electrophysiol,* **4,** 459-467.

Boulaksil M, Winckels SK, Engelen MA, Stein M, van Veen TA, Jansen JA, Linnenbank AC, Bierhuizen MF, Groenewegen WA, van Oosterhout MF, Kirkels JH, de JN, Varro A, Vos MA, de Bakker JM, and van Rijen HV (2010) Heterogeneous Connexin43 distribution in heart failure is associated with dispersed conduction and enhanced susceptibility to ventricular arrhythmias. *Eur J Heart Fail,* **12,** 913-921.

Braet K, Vandamme W, Martin PE, Evans WH, and Leybaert L (2003) Photoliberating inositol-1,4,5-trisphosphate triggers ATP release that is blocked by the connexin mimetic peptide gap 26. *Cell Calcium,* **33,** 37-48.

Brown EM (1991) Extracellular Ca2+ sensing, regulation of parathyroid cell function, and role of Ca2+ and other ions as extracellular (first) messengers. *Physiol Rev,* **71,** 371-411.

Bruce AF, Rothery S, Dupont E, and Severs NJ (2008) Gap junction remodelling in human heart failure is associated with increased interaction of connexin43 with ZO-1. *Cardiovasc Res,* **77,** 757-765.

Bruzzone R, White TW, and Paul DL (1996) Connections with connexins: the molecular basis of direct intercellular signaling. *Eur J Biochem,* **238,** 1-27.

Bukauskas FF, Bukauskiene A, Bennett MV, and Verselis VK (2001) Gating properties of gap junction channels assembled from connexin43 and connexin43 fused with green fluorescent protein. *Biophys J,* **81,** 137-152.

Bukauskas FF, Bukauskiene A, and Verselis VK (2002) Conductance and permeability of the residual state of connexin43 gap junction channels. *J Gen Physiol,* **119,** 171-185.

Bukauskas FF and Verselis VK (2004) Gap junction channel gating. *Biochim Biophys Acta,* **1662,** 42-60.

Bukauskas FF and Weingart R (1994) Voltage-dependent gating of single gap junction channels in an insect cell line. *Biophys J,* **67,** 613-625.

Chen Y, Zhou Y, Lin X, Wong HC, Xu Q, Jiang J, Wang S, Lurtz MM, Louis CF, Veenstra RD, and Yang JJ (2011) Molecular interaction and functional regulation of connexin50 gap junctions by calmodulin. *Biochem J,* **435,** 711-722.

Chkourko HS, Guerrero-Serna G, Lin X, Darwish N, Pohlmann JR, Cook KE, Martens JR, Rothenberg E, Musa H, and Delmar M (2012) Remodeling of mechanical junctions and of microtubule-associated proteins accompany cardiac connexin43 lateralization. *Heart Rhythm,* **9,** 1133-1140.

Churchill GC, Lurtz MM, and Louis CF (2001) Ca(2+) regulation of gap junctional coupling in lens epithelial cells. *Am J Physiol Cell Physiol,* **281,** C972-C981.

Colussi C, Rosati J, Straino S, Spallotta F, Berni R, Stilli D, Rossi S, Musso E, Macchi E, Mai A, Sbardella G, Castellano S, Chimenti C, Frustaci A, Nebbioso A, Altucci L, Capogrossi MC, and Gaetano C (2011) Nepsilon-lysine acetylation determines dissociation from GAP junctions and lateralization of connexin 43 in normal and dystrophic heart. *Proc Natl Acad Sci U S A,* **108,** 2795-2800.

Contreras JE, Saez JC, Bukauskas FF, and Bennett MV (2003) Gating and regulation of connexin 43 (Cx43) hemichannels. *Proc Natl Acad Sci U S A,* **100,** 11388-11393.

Coppen SR, Kodama I, Boyett MR, Dobrzynski H, Takagishi Y, Honjo H, Yeh HI, and Severs NJ (1999) Connexin45, a major connexin of the rabbit sinoatrial node, is co-expressed with connexin43 in a restricted zone at the nodal-crista terminalis border. *J Histochem Cytochem,* **47,** 907-918.

Crow JM, Atkinson MM, and Johnson RG (1994) Micromolar levels of intracellular calcium reduce gap junctional permeability in lens cultures. *Invest Ophthalmol Vis Sci,* **35,** 3332-3341.

Cruciani V and Mikalsen SO (2006) The vertebrate connexin family. *Cell Mol Life Sci,* **63,** 1125-1140.

D'hondt C, Ponsaerts R, De SH, Bultynck G, and Himpens B (2009) Pannexins, distant relatives of the connexin family with specific cellular functions? *Bioessays,* **31,** 953-974.

Dakin K, Zhao Y, and Li WH (2005) LAMP, a new imaging assay of gap junctional communication unveils that Ca2+ influx inhibits cell coupling. *Nat Methods,* **2,** 55-62.

Darrow BJ, Laing JG, Lampe PD, Saffitz JE, and Beyer EC (1995) Expression of multiple connexins in cultured neonatal rat ventricular myocytes. *Circ Res,* **76,** 381-387.

Davis LM, Kanter HL, Beyer EC, and Saffitz JE (1994) Distinct gap junction protein phenotypes in cardiac tissues with disparate conduction properties. *J Am Coll Cardiol,* **24,** 1124-1132.

Davis LM, Rodefeld ME, Green K, Beyer EC, and Saffitz JE (1995) Gap junction protein phenotypes of the human heart and conduction system. *J Cardiovasc Electrophysiol,* **6,** 813-822.

De Mello WC (1975) Effect of intracellular injection of calcium and strontium on cell communication in heart. *J Physiol,* **250,** 231-245.

De Rosa AM, Mui R, Srinivas M, and White TW (2006) Functional characterization of a naturally occurring Cx50 truncation. *Invest Ophthalmol Vis Sci,* **47,** 4474-4481.

De Vuyst E, Decrock E, De Bock M, Yamasaki H, Naus CC, Evans WH, and Leybaert L (2007) Connexin hemichannels and gap junction channels are differentially influenced by lipopolysaccharide and basic fibroblast growth factor. *Mol Biol Cell,* **18,** 34-46.

De Vuyst E, Wang N, Decrock E, De Bock M, Vinken M, Van Moorhem M, Lai C, Culot M, Rogiers V, Cecchelli R, Naus CC, Evans WH, and Leybaert L (2009) Ca(2+) regulation of connexin 43 hemichannels in C6 glioma and glial cells. *Cell Calcium,* **46,** 176-187.

Dekker LR, Fiolet JW, VanBavel E, Coronel R, Opthof T, Spaan JA, and Janse MJ (1996) Intracellular Ca2+, intercellular electrical coupling, and mechanical activity in ischemic rabbit papillary muscle. Effects of preconditioning and metabolic blockade. *Circ Res,* **79,** 237-246.

Desplantez T, Dupont E, Severs NJ, and Weingart R (2007) Gap junction channels and cardiac impulse propagation. *J Membr Biol,* **218,** 13-28.

Desplantez T, Halliday D, Dupont E, Severs NJ, and Weingart R (2011) Influence of v5/6-His tag on the properties of gap junction channels composed of connexin43, connexin40 or connexin45. *J Membr Biol,* **240,** 139-150.

DeVuyst E, Decrock E, Cabooter L, Dubyak GR, Naus CC, Evans WH, and Leybaert L (2006) Intracellular calcium changes trigger connexin 32 hemichannel opening. *EMBO J,* **25,** 34-44.

Duffy HS (2012) The molecular mechanisms of gap junction remodeling. *Heart Rhythm,* **9,** 1331-1334.

Duffy HS, Ashton AW, O'Donnell P, Coombs W, Taffet SM, Delmar M, and Spray DC (2004) Regulation of connexin43 protein complexes by intracellular acidification. *Circ Res,* **94,** 215-222.

Duffy HS, Sorgen PL, Girvin ME, O'Donnell P, Coombs W, Taffet SM, Delmar M, and Spray DC (2002) pH-dependent intramolecular binding and structure involving Cx43 cytoplasmic domains. *J Biol Chem,* **277,** 36706-36714.

Ebihara L, Liu X, and Pal JD (2003) Effect of external magnesium and calcium on human connexin46 hemichannels. *Biophys J,* **84,** 277-286.

Eiberger J, Degen J, Romualdi A, Deutsch U, Willecke K, and Sohl G (2001) Connexin genes in the mouse and human genome. *Cell Commun Adhes,* **8,** 163-165.

Ek JF, Delmar M, Perzova R, and Taffet SM (1994) Role of histidine 95 on pH gating of the cardiac gap junction protein connexin43. *Circ Res,* **74,** 1058-1064.

Elenes S, Martinez AD, Delmar M, Beyer EC, and Moreno AP (2001) Heterotypic docking of Cx43 and Cx45 connexons blocks fast voltage gating of Cx43. *Biophys J,* **81,** 1406-1418.

Firek L and Weingart R (1995) Modification of gap junction conductance by divalent cations and protons in neonatal rat heart cells. *J Mol Cell Cardiol,* **27,** 1633-1643.

Fontes MS, van Veen TA, de Bakker JM, and van Rijen HV (2012) Functional consequences of abnormal Cx43 expression in the heart. *Biochim Biophys Acta,* **1818,** 2020-2029.

Frank M, Wirth A, Andrie RP, Kreuzberg MM, Dobrowolski R, Seifert G, Offermanns S, Nickenig G, Willecke K, and Schrickel JW (2012) Connexin45 provides optimal atrioventricular nodal conduction in the adult mouse heart. *Circ Res,* **111,** 1528-1538.

Gaietta G, Deerinck TJ, Adams SR, Bouwer J, Tour O, Laird DW, Sosinsky GE, Tsien RY, and Ellisman MH (2002) Multicolor and electron microscopic imaging of connexin trafficking. *Science,* **296,** 503-507.

Gassmann O, Kreir M, Ambrosi C, Pranskevich J, Oshima A, Roling C, Sosinsky G, Fertig N, and Steinem C (2009) The M34A mutant of Connexin26 reveals active conductance states in pore-suspending membranes. *J Struct Biol,* **168,** 168-176.

Giepmans BN, Verlaan I, Hengeveld T, Janssen H, Calafat J, Falk MM, and Moolenaar WH (2001) Gap junction protein connexin-43 interacts directly with microtubules. *Curr Biol,* **11,** 1364-1368.

Giovannone S, Remo BF, and Fishman GI (2012) Channeling diversity: gap junction expression in the heart. *Heart Rhythm,* **9,** 1159-1162.

Gomez-Hernandez JM, de MM, Larrosa B, Gonzalez D, and Barrio LC (2003) Molecular basis of calcium regulation in connexin-32 hemichannels. *Proc Natl Acad Sci U S A,* **100,** 16030-16035.

Gonzalez D, Gomez-Hernandez JM, and Barrio LC (2006) Species specificity of mammalian connexin-26 to form open voltage-gated hemichannels. *FASEB J,* **20,** 2329-2338.

Gonzalez D, Gomez-Hernandez JM, and Barrio LC (2007) Molecular basis of voltage dependence of connexin channels: an integrative appraisal. *Prog Biophys Mol Biol,* **94,** 66-106.

Goodenough DA, Goliger JA, and Paul DL (1996) Connexins, connexons, and intercellular communication. *Annu Rev Biochem,* **65,** 475-502.

Grikscheit K, Thomas N, Bruce AF, Rothery S, Chan J, Severs NJ, and Dupont E (2008) Coexpression of connexin 45 with connexin 43 decreases gap junction size. *Cell Commun Adhes,* **15,** 185-193.

Gros D, Jarry-Guichard T, Ten V, I, de MA, van Kempen MJ, Davoust J, Briand JP, Moorman AF, and Jongsma HJ (1994) Restricted distribution of connexin40, a gap junctional protein, in mammalian heart. *Circ Res,* **74,** 839-851.

Hagendorff A, Schumacher B, Kirchhoff S, Luderitz B, and Willecke K (1999) Conduction disturbances and increased atrial vulnerability in Connexin40-deficient mice analyzed by transesophageal stimulation. *Circulation,* **99,** 1508-1515.

Harris AL (2002) Voltage-sensing and substate rectification: moving parts of connexin channels. *J Gen Physiol,* **119,** 165-169.

Harris AL (2009) Gating on the outside. *J Gen Physiol,* **133,** 549-553.

Harris AL, Spray DC, and Bennett MV (1981) Kinetic properties of a voltage-dependent junctional conductance. *J Gen Physiol,* **77,** 95-117.

Harris BS, Baicu CF, Haghshenas N, Kasiganesan H, Scholz D, Rackley MS, Miquerol L, Gros D, Mukherjee R, and O'Brien TX (2012) Remodeling of the peripheral cardiac conduction system in response to pressure overload. *Am J Physiol Heart Circ Physiol,* **302,** H1712-H1725.

Hesketh GG, Van Eyk JE, and Tomaselli GF (2009) Mechanisms of gap junction traffic in health and disease. *J Cardiovasc Pharmacol,* **54,** 263-272.

Horn R (2000) Conversation between voltage sensors and gates of ion channels. *Biochemistry,* **39,** 15653-15658.

Hunter AW, Barker RJ, Zhu C, and Gourdie RG (2005) Zonula occludens-1 alters connexin43 gap junction size and organization by influencing channel accretion. *Mol Biol Cell,* **16,** 5686-5698.

Iglesias R, Dahl G, Qiu F, Spray DC, and Scemes E (2009) Pannexin 1: the molecular substrate of astrocyte "hemichannels". *J Neurosci,* **29,** 7092-7097.

Jansen JA, van Veen TA, de Bakker JM, and van Rijen HV (2010) Cardiac connexins and impulse propagation. *J Mol Cell Cardiol,* **48,** 76-82.

Kalmatsky BD, Bhagan S, Tang Q, Bargiello TA, and Dowd TL (2009) Structural studies of the N-terminus of Connexin 32 using 1H NMR spectroscopy. *Arch Biochem Biophys,* **490,** 9-16.

Kang J, Kang N, Lovatt D, Torres A, Zhao Z, Lin J, and Nedergaard M (2008) Connexin 43 hemichannels are permeable to ATP. *J Neurosci,* **28,** 4702-4711.

Kieken F, Mutsaers N, Dolmatova E, Virgil K, Wit AL, Kellezi A, Hirst-Jensen BJ, Duffy HS, and Sorgen PL (2009) Structural and molecular mechanisms of gap junction remodeling in epicardial border zone myocytes following myocardial infarction. *Circ Res,* **104,** 1103-1112.

Kirchhoff S, Kim JS, Hagendorff A, Thonnissen E, Kruger O, Lamers WH, and Willecke K (2000) Abnormal cardiac conduction and morphogenesis in connexin40 and connexin43 double-deficient mice. *Circ Res,* **87,** 399-405.

Kirchhoff S, Nelles E, Hagendorff A, Kruger O, Traub O, and Willecke K (1998) Reduced cardiac conduction velocity and predisposition to arrhythmias in connexin40-deficient mice. *Curr Biol,* **8,** 299-302.

Kleber AG (2011) Gap junctions and conduction of cardiac excitation. *Heart Rhythm,* **8,** 1981-1984.

Kreuzberg MM, Liebermann M, Segschneider S, Dobrowolski R, Dobrzynski H, Kaba R, Rowlinson G, Dupont E, Severs NJ, and Willecke K (2009) Human connexin31.9, unlike its orthologous protein connexin30.2 in the mouse, is not detectable in the human cardiac conduction system. *J Mol Cell Cardiol,* **46,** 553-559.

Kreuzberg MM, Schrickel JW, Ghanem A, Kim JS, Degen J, Janssen-Bienhold U, Lewalter T, Tiemann K, and Willecke K (2006a) Connexin30.2 containing gap junction channels decelerate impulse propagation through the atrioventricular node. *Proc Natl Acad Sci U S A,* **103,** 5959-5964.

Kreuzberg MM, Sohl G, Kim JS, Verselis VK, Willecke K, and Bukauskas FF (2005) Functional properties of mouse connexin30.2 expressed in the conduction system of the heart. *Circ Res,* **96,** 1169-1177.

Kreuzberg MM, Willecke K, and Bukauskas FF (2006b) Connexin-mediated cardiac impulse propagation: connexin 30.2 slows atrioventricular conduction in mouse heart. *Trends Cardiovasc Med,* **16,** 266-272.

Kronengold J, Srinivas M, and Verselis VK (2012) The N-terminal half of the connexin protein contains the core elements of the pore and voltage gates. *J Membr Biol,* **245,** 453-463.

Kronengold J, Trexler EB, Bukauskas FF, Bargiello TA, and Verselis VK (2003) Single-channel SCAM identifies pore-lining residues in the first extracellular loop and first transmembrane domains of Cx46 hemichannels. *J Gen Physiol,* **122,** 389-405.

Kucera JP, Rohr S, and Rudy Y (2002) Localization of sodium channels in intercalated disks modulates cardiac conduction. *Circ Res,* **91,** 1176-1182.

Kumai M, Nishii K, Nakamura K, Takeda N, Suzuki M, and Shibata Y (2000) Loss of connexin45 causes a cushion defect in early cardiogenesis. *Development,* **127,** 3501-3512.

Kwon T, Harris AL, Rossi A, and Bargiello TA (2011) Molecular dynamics simulations of the Cx26 hemichannel: evaluation of structural models with Brownian dynamics. *J Gen Physiol,* **138,** 475-493.

Kwon T, Roux B, Jo S, Klauda JB, Harris AL, and Bargiello TA (2012) Molecular dynamics simulations of the Cx26 hemichannel: insights into voltage-dependent loop-gating. *Biophys J,* **102,** 1341-1351.

Kyle JW, Berthoud VM, Kurutz J, Minogue PJ, Greenspan M, Hanck DA, and Beyer EC (2009) The N terminus of connexin37 contains an alpha-helix that is required for channel function. *J Biol Chem,* **284,** 20418-20427.

Lagostena L, Ashmore JF, Kachar B, and Mammano F (2001) Purinergic control of intercellular communication between Hensen's cells of the guinea-pig cochlea. *J Physiol,* **531,** 693-706.

Laird DW (2006) Life cycle of connexins in health and disease. *Biochem J,* **394,** 527-543.

Lampe PD, Cooper CD, King TJ, and Burt JM (2006) Analysis of Connexin43 phosphorylated at S325, S328 and S330 in normoxic and ischemic heart. *J Cell Sci,* **119,** 3435-3442.

Lazrak A and Peracchia C (1993) Gap junction gating sensitivity to physiological internal calcium regardless of pH in Novikoff hepatoma cells. *Biophys J,* **65,** 2002-2012.

Lazrak A, Peres A, Giovannardi S, and Peracchia C (1994) Ca-mediated and independent effects of arachidonic acid on gap junctions and Ca-independent effects of oleic acid and halothane. *Biophys J,* **67,** 1052-1059.

Liu S, Taffet S, Stoner L, Delmar M, Vallano ML, and Jalife J (1993) A structural basis for the unequal sensitivity of the major cardiac and liver gap junctions to intracellular acidification: the carboxyl tail length. *Biophys J,* **64,** 1422-1433.

Loewenstein WR and Rose B (1978) Calcium in (junctional) intercellular communication and a thought on its behavior in intracellular communication. *Ann N Y Acad Sci,* **307,** 285-307.

Lurtz MM and Louis CF (2003) Calmodulin and protein kinase C regulate gap junctional coupling in lens epithelial cells. *Am J Physiol Cell Physiol,* **285,** C1475-C1482.

Lurtz MM and Louis CF (2007) Intracellular calcium regulation of connexin43. *Am J Physiol Cell Physiol,* **293,** C1806-C1813.

Maeda S, Nakagawa S, Suga M, Yamashita E, Oshima A, Fujiyoshi Y, and Tsukihara T (2009) Structure of the connexin 26 gap junction channel at 3.5 A resolution. *Nature,* **458,** 597-602.

Matchkov VV, Gustafsson H, Rahman A, Briggs Boedtkjer DM, Gorintin S, Hansen AK, Bouzinova EV, Praetorius HA, Aalkjaer C, and Nilsson H (2007) Interaction between Na+/K+-pump and Na+/Ca2+-exchanger modulates intercellular communication. *Circ Res,* **100,** 1026-1035.

Maurer P and Weingart R (1987) Cell pairs isolated from adult guinea pig and rat hearts: effects of [Ca2+]i on nexal membrane resistance. *Pflugers Arch,* **409,** 394-402.

Mears D, Sheppard NF, Jr., Atwater I, and Rojas E (1995) Magnitude and modulation of pancreatic beta-cell gap junction electrical conductance in situ. *J Membr Biol,* **146,** 163-176.

Mese G, Richard G, and White TW (2007) Gap junctions: basic structure and function. *J Invest Dermatol,* **127,** 2516-2524.

Moreno AP, Chanson M, Elenes S, Anumonwo J, Scerri I, Gu H, Taffet SM, and Delmar M (2002) Role of the carboxyl terminal of connexin43 in transjunctional fast voltage gating. *Circ Res,* **90,** 450-457.

Mori Y, Fishman GI, and Peskin CS (2008) Ephaptic conduction in a cardiac strand model with 3D electrodiffusion. *Proc Natl Acad Sci U S A,* **105,** 6463-6468.

Morley GE, Ek-Vitorin JF, Taffet SM, and Delmar M (1997) Structure of connexin43 and its regulation by pHi. *J Cardiovasc Electrophysiol,* **8,** 939-951.

Muller DJ, Hand GM, Engel A, and Sosinsky GE (2002) Conformational changes in surface structures of isolated connexin 26 gap junctions. *EMBO J,* **21,** 3598-3607.

Odermatt B, Wellershaus K, Wallraff A, Seifert G, Degen J, Euwens C, Fuss B, Bussow H, Schilling K, Steinhauser C, and Willecke K (2003) Connexin 47 (Cx47)-deficient mice with enhanced green fluorescent protein reporter gene reveal predominant oligodendrocytic expression of Cx47 and display vacuolized myelin in the CNS. *J Neurosci,* **23,** 4549-4559.

Oh S, Abrams CK, Verselis VK, and Bargiello TA (2000) Stoichiometry of transjunctional voltage-gating polarity reversal by a negative charge substitution in the amino terminus of a connexin32 chimera. *J Gen Physiol,* **116,** 13-31.

Oh S, Rivkin S, Tang Q, Verselis VK, and Bargiello TA (2004) Determinants of gating polarity of a connexin 32 hemichannel. *Biophys J,* **87,** 912-928.

Oshima A, Doi T, Mitsuoka K, Maeda S, and Fujiyoshi Y (2003) Roles of Met-34, Cys-64, and Arg-75 in the assembly of human connexin 26. Implication for key amino acid residues for channel formation and function. *J Biol Chem,* **278,** 1807-1816.

Oshima A, Tani K, Hiroaki Y, Fujiyoshi Y, and Sosinsky GE (2007) Three-dimensional structure of a human connexin26 gap junction channel reveals a plug in the vestibule. *Proc Natl Acad Sci U S A,* **104,** 10034-10039.

Oshima A, Tani K, Hiroaki Y, Fujiyoshi Y, and Sosinsky GE (2008) Projection structure of a N-terminal deletion mutant of connexin 26 channel with decreased central pore density. *Cell Commun Adhes,* **15,** 85-93.

Palacios-Prado N, Briggs SW, Skeberdis VA, Pranevicius M, Bennett MV, and Bukauskas FF (2010) pH-dependent modulation of voltage gating in connexin45 homotypic and connexin45/connexin43 heterotypic gap junctions. *Proc Natl Acad Sci U S A,* **107,** 9897-9902.

Paulauskas N, Pranevicius H, Mockus J, and Bukauskas FF (2012) Stochastic 16-state model of voltage gating of gap-junction channels enclosing fast and slow gates. *Biophys J,* **102,** 2471-2480.

Paulauskas N, Pranevicius M, Pranevicius H, and Bukauskas FF (2009) A stochastic four-state model of contingent gating of gap junction channels containing two "fast" gates sensitive to transjunctional voltage. *Biophys J,* **96,** 3936-3948.

Pearson RA, Dale N, Llaudet E, and Mobbs P (2005) ATP released via gap junction hemichannels from the pigment epithelium regulates neural retinal progenitor proliferation. *Neuron,* **46,** 731-744.

Penuela S, Bhalla R, Gong XQ, Cowan KN, Celetti SJ, Cowan BJ, Bai D, Shao Q, and Laird DW (2007) Pannexin 1 and pannexin 3 are glycoproteins that exhibit many distinct characteristics from the connexin family of gap junction proteins. *J Cell Sci,* **120,** 3772-3783.

Penuela S, Gehi R, and Laird DW (2013) The biochemistry and function of pannexin channels. *Biochim Biophys Acta,* **1828,** 15-22.

Peracchia C (2004) Chemical gating of gap junction channels; roles of calcium, pH and calmodulin. *Biochim Biophys Acta,* **1662,** 61-80.

Peracchia C, Chen JT, and Peracchia LL (2004) CO(2) sensitivity of voltage gating and gating polarity of gapjunction channels--connexin40 and its COOH-terminus-truncated mutant. *J Membr Biol,* **200,** 105-113.

Peracchia C and Peracchia LL (2005) Inversion of both gating polarity and CO2 sensitivity of voltage gating with D3N mutation of Cx50. *Am J Physiol Cell Physiol,* **288,** C1381-C1389.

Peracchia C and Wang XC (1997) Connexin domains relevant to the chemical gating of gap junction channels. *Braz J Med Biol Res,* **30,** 577-590.

Peracchia C, Young KC, Wang XG, Chen JT, and Peracchia LL (2003) The voltage gates of connexin channels are sensitive to CO(2). *Cell Commun Adhes,* **10,** 233-237.

Peters NS, Coromilas J, Severs NJ, and Wit AL (1997) Disturbed connexin43 gap junction distribution correlates with the location of reentrant circuits in the epicardial border zone of healing canine infarcts that cause ventricular tachycardia. *Circulation,* **95,** 988-996.

Pfahnl A and Dahl G (1999) Gating of cx46 gap junction hemichannels by calcium and voltage. *Pflugers Arch,* **437,** 345-353.

Poelzing S, Akar FG, Baron E, and Rosenbaum DS (2004) Heterogeneous connexin43 expression produces electrophysiological heterogeneities across ventricular wall. *Am J Physiol Heart Circ Physiol,* **286,** H2001-H2009.

Poelzing S and Rosenbaum DS (2004) Altered connexin43 expression produces arrhythmia substrate in heart failure. *Am J Physiol Heart Circ Physiol,* **287,** H1762-H1770.

Ponsaerts R, De VE, Retamal M, D'hondt C, Vermeire D, Wang N, De SH, Zimmermann P, Himpens B, Vereecke J, Leybaert L, and Bultynck G (2010) Intramolecular loop/tail interactions are essential for connexin 43-hemichannel activity. *FASEB J,* **24,** 4378-4395.

Puljung MC, Berthoud VM, Beyer EC, and Hanck DA (2004) Polyvalent cations constitute the voltage gating particle in human connexin37 hemichannels. *J Gen Physiol,* **124,** 587-603.

Purnick PE, Benjamin DC, Verselis VK, Bargiello TA, and Dowd TL (2000a) Structure of the amino terminus of a gap junction protein. *Arch Biochem Biophys,* **381,** 181-190.

Purnick PE, Oh S, Abrams CK, Verselis VK, and Bargiello TA (2000b) Reversal of the gating polarity of gap junctions by negative charge substitutions in the N-terminus of connexin 32. *Biophys J,* **79,** 2403-2415.

Quist AP, Rhee SK, Lin H, and Lal R (2000) Physiological role of gap-junctional hemichannels. Extracellular calcium-dependent isosmotic volume regulation. *J Cell Biol,* **148,** 1063-1074.

Rackauskas M, Kreuzberg MM, Pranevicius M, Willecke K, Verselis VK, and Bukauskas FF (2007) Gating properties of heterotypic gap junction channels formed of connexins 40, 43, and 45. *Biophys J,* **92,** 1952-1965.

Ramanan SV, Brink PR, Varadaraj K, Peterson E, Schirrmacher K, and Banach K (1999) A three-state model for connexin37 gating kinetics. *Biophys J,* **76,** 2520-2529.

Reaume AG, de Sousa PA, Kulkarni S, Langille BL, Zhu D, Davies TC, Juneja SC, Kidder GM, and Rossant J (1995) Cardiac malformation in neonatal mice lacking connexin43. *Science,* **267,** 1831-1834.

Remo BF, Qu J, Volpicelli FM, Giovannone S, Shin D, Lader J, Liu FY, Zhang J, Lent DS, Morley GE, and Fishman GI (2011) Phosphatase-resistant gap junctions inhibit pathological remodeling and prevent arrhythmias. *Circ Res,* **108,** 1459-1466.

Retamal MA, Yin S, Altenberg GA, and Reuss L (2009) Modulation of Cx46 hemichannels by nitric oxide. *Am J Physiol Cell Physiol,* **296,** C1356-C1363.

Revilla A, Castro C, and Barrio LC (1999) Molecular dissection of transjunctional voltage dependence in the connexin-32 and connexin-43 junctions. *Biophys J,* **77,** 1374-1383.

Rhett JM, Jourdan J, and Gourdie RG (2011) Connexin 43 connexon to gap junction transition is regulated by zonula occludens-1. *Mol Biol Cell,* **22,** 1516-1528.

Rose B and Loewenstein WR (1976) Permeability of a cell junction and the local cytoplasmic free ionized calcium concentration: a study with aequorin. *J Membr Biol,* **28,** 87-119.

Saez JC, Berthoud VM, Branes MC, Martinez AD, and Beyer EC (2003) Plasma membrane channels formed by connexins: their regulation and functions. *Physiol Rev,* **83,** 1359-1400.

Sanchez HA, Mese G, Srinivas M, White TW, and Verselis VK (2010) Differentially altered Ca2+ regulation and Ca2+ permeability in Cx26 hemichannels formed by the A40V and G45E mutations that cause keratitis ichthyosis deafness syndrome. *J Gen Physiol,* **136,** 47-62.

Schalper KA, Sanchez HA, Lee SC, Altenberg GA, Nathanson MH, and Saez JC (2010) Connexin 43 hemichannels mediate the Ca2+ influx induced by extracellular alkalinization. *Am J Physiol Cell Physiol,* **299,** C1504-C1515.

Schrickel JW, Kreuzberg MM, Ghanem A, Kim JS, Linhart M, Andrie R, Tiemann K, Nickenig G, Lewalter T, and Willecke K (2009) Normal impulse propagation in the atrioventricular conduction system of Cx30.2/Cx40 double deficient mice. *J Mol Cell Cardiol,* **46,** 644-652.

Seki A, Duffy HS, Coombs W, Spray DC, Taffet SM, and Delmar M (2004) Modifications in the biophysical properties of connexin43 channels by a peptide of the cytoplasmic loop region. *Circ Res,* **95,** e22-e28.

Severs NJ, Bruce AF, Dupont E, and Rothery S (2008) Remodelling of gap junctions and connexin expression in diseased myocardium. *Cardiovasc Res,* **80,** 9-19.

Shaw RM, Fay AJ, Puthenveedu MA, von ZM, Jan YN, and Jan LY (2007) Microtubule plus-end-tracking proteins target gap junctions directly from the cell interior to adherens junctions. *Cell,* **128,** 547-560.

Shibayama J, Gutierrez C, Gonzalez D, Kieken F, Seki A, Carrion JR, Sorgen PL, Taffet SM, Barrio LC, and Delmar M (2006) Effect of charge substitutions at residue his-142 on voltage gating of connexin43 channels. *Biophys J,* **91,** 4054-4063.

Simon AM, Goodenough DA, and Paul DL (1998) Mice lacking connexin40 have cardiac conduction abnormalities characteristic of atrioventricular block and bundle branch block. *Curr Biol,* **8,** 295-298.

Skerrett IM, Aronowitz J, Shin JH, Cymes G, Kasperek E, Cao FL, and Nicholson BJ (2002) Identification of amino acid residues lining the pore of a gap junction channel. *J Cell Biol,* **159,** 349-360.

Skerrett M, Kasperek E, Cao FL, Shin JH, Aronowitz J, Ahmed S, and Nicholson BJ (2001) Application of SCAM (substituted cysteine accessibility method) to gap junction intercellular channels. *Cell Commun Adhes,* **8,** 179-185.

Smyth JW, Hong TT, Gao D, Vogan JM, Jensen BC, Fong TS, Simpson PC, Stainier DY, Chi NC, and Shaw RM (2010) Limited forward trafficking of connexin 43 reduces cell-cell coupling in stressed human and mouse myocardium. *J Clin Invest,* **120,** 266-279.

Smyth JW and Shaw RM (2012) The gap junction life cycle. *Heart Rhythm,* **9,** 151-153.

Smyth JW, Vogan JM, Buch PJ, Zhang SS, Fong TS, Hong TT, and Shaw RM (2012) Actin cytoskeleton rest stops regulate anterograde traffic of connexin 43 vesicles to the plasma membrane. *Circ Res,* **110,** 978-989.

Sohl G and Willecke K (2003) An update on connexin genes and their nomenclature in mouse and man. *Cell Commun Adhes,* **10,** 173-180.

Sorgen PL, Duffy HS, Sahoo P, Coombs W, Delmar M, and Spray DC (2004a) Structural changes in the carboxyl terminus of the gap junction protein connexin43 indicates signaling between binding domains for c-Src and zonula occludens-1. *J Biol Chem,* **279,** 54695-54701.

Sorgen PL, Duffy HS, Spray DC, and Delmar M (2004b) pH-dependent dimerization of the carboxyl terminal domain of Cx43. *Biophys J,* **87,** 574-581.

Sosinsky GE, Boassa D, Dermietzel R, Duffy HS, Laird DW, MacVicar B, Naus CC, Penuela S, Scemes E, Spray DC, Thompson RJ, Zhao HB, and Dahl G (2011) Pannexin channels are not gap junction hemichannels. *Channels (Austin),* **5,** 193-197.

Sovari AA, Iravanian S, Dolmatova E, Jiao Z, Liu H, Zandieh S, Kumar V, Wang K, Bernstein KE, Bonini MG, Duffy HS, and Dudley SC (2011) Inhibition of c-Src tyrosine kinase prevents angiotensin II-mediated connexin-43 remodeling and sudden cardiac death. *J Am Coll Cardiol,* **58,** 2332-2339.

Sperelakis N (2002) An electric field mechanism for transmission of excitation between myocardial cells. *Circ Res,* **91,** 985-987.

Sperelakis N and Mann JE, Jr. (1977) Evaluation of electric field changes in the cleft between excitable cells. *J Theor Biol,* **64,** 71-96.

Spray DC, Stern JH, Harris AL, and Bennett MV (1982) Gap junctional conductance: comparison of sensitivities to H and Ca ions. *Proc Natl Acad Sci U S A,* **79,** 441-445.

Srinivas M, Calderon DP, Kronengold J, and Verselis VK (2006) Regulation of connexin hemichannels by monovalent cations. *J Gen Physiol,* **127,** 67-75.

Srinivas M, Kronengold J, Bukauskas FF, Bargiello TA, and Verselis VK (2005) Correlative studies of gating in Cx46 and Cx50 hemichannels and gap junction channels. *Biophys J,* **88,** 1725-1739.

Stergiopoulos K, Alvarado JL, Mastroianni M, Ek-Vitorin JF, Taffet SM, and Delmar M (1999) Hetero-domain interactions as a mechanism for the regulation of connexin channels. *Circ Res,* **84,** 1144-1155.

Tamaddon HS, Vaidya D, Simon AM, Paul DL, Jalife J, and Morley GE (2000) High-resolution optical mapping of the right bundle branch in connexin40 knockout mice reveals slow conduction in the specialized conduction system. *Circ Res,* **87,** 929-936.

Tang Q, Dowd TL, Verselis VK, and Bargiello TA (2009) Conformational changes in a pore-forming region underlie voltage-dependent "loop gating" of an unapposed connexin hemichannel. *J Gen Physiol,* **133,** 555-570.

Tao L and Harris AL (2004) Biochemical requirements for inhibition of Connexin26-containing channels by natural and synthetic taurine analogs. *J Biol Chem,* **279,** 38544-38554.

Thimm J, Mechler A, Lin H, Rhee S, and Lal R (2005) Calcium-dependent open/closed conformations and interfacial energy maps of reconstituted hemichannels. *J Biol Chem,* **280,** 10646-10654.

Thomas T, Jordan K, Simek J, Shao Q, Jedeszko C, Walton P, and Laird DW (2005) Mechanisms of Cx43 and Cx26 transport to the plasma membrane and gap junction regeneration. *J Cell Sci,* **118,** 4451-4462.

Torres A, Wang F, Xu Q, Fujita T, Dobrowolski R, Willecke K, Takano T, and Nedergaard M (2012) Extracellular Ca(2)(+) acts as a mediator of communication from neurons to glia. *Sci Signal,* **5,** ra8.

Trexler EB, Bennett MV, Bargiello TA, and Verselis VK (1996) Voltage gating and permeation in a gap junction hemichannel. *Proc Natl Acad Sci U S A,* **93,** 5836-5841.

Trexler EB, Bukauskas FF, Bennett MV, Bargiello TA, and Verselis VK (1999) Rapid and direct effects of pH on connexins revealed by the connexin46 hemichannel preparation. *J Gen Physiol,* **113,** 721-742.

Unger VM, Kumar NM, Gilula NB, and Yeager M (1999) Three-dimensional structure of a recombinant gap junction membrane channel. *Science,* **283,** 1176-1180.

Valiunas V (2002) Biophysical properties of connexin-45 gap junction hemichannels studied in vertebrate cells. *J Gen Physiol,* **119,** 147-164.

van Rijen HV, Eckardt D, Degen J, Theis M, Ott T, Willecke K, Jongsma HJ, Opthof T, and de Bakker JM (2004) Slow conduction and enhanced anisotropy increase the propensity for ventricular tachyarrhythmias in adult mice with induced deletion of connexin43. *Circulation,* **109,** 1048-1055.

van Rijen HV, van Veen TA, van Kempen MJ, Wilms-Schopman FJ, Potse M, Krueger O, Willecke K, Opthof T, Jongsma HJ, and de Bakker JM (2001) Impaired conduction in the bundle branches of mouse hearts lacking the gap junction protein connexin40. *Circulation,* **103,** 1591-1598.

van Zeijl L, Ponsioen B, Giepmans BN, Ariaens A, Postma FR, Varnai P, Balla T, Divecha N, Jalink K, and Moolenaar WH (2007) Regulation of connexin43 gap junctional communication by phosphatidylinositol 4,5-bisphosphate. *J Cell Biol,* **177,** 881-891.

VanderBrink BA, Sellitto C, Saba S, Link MS, Zhu W, Homoud MK, Estes NA, III, Paul DL, and Wang PJ (2000) Connexin40-deficient mice exhibit atrioventricular nodal and infra-Hisian conduction abnormalities. *J Cardiovasc Electrophysiol,* **11,** 1270-1276.

Verheijck EE, Wilders R, Joyner RW, Golod DA, Kumar R, Jongsma HJ, Bouman LN, and van Ginneken AC (1998) Pacemaker synchronization of electrically coupled rabbit sinoatrial node cells. *J Gen Physiol,* **111,** 95-112.

Verheule S, van Batenburg CA, Coenjaerts FE, Kirchhoff S, Willecke K, and Jongsma HJ (1999) Cardiac conduction abnormalities in mice lacking the gap junction protein connexin40. *J Cardiovasc Electrophysiol,* **10,** 1380-1389.

Verselis VK, Ginter CS, and Bargiello TA (1994) Opposite voltage gating polarities of two closely related connexins. *Nature,* **368,** 348-351.

Verselis VK and Srinivas M (2008) Divalent cations regulate connexin hemichannels by modulating intrinsic voltage-dependent gating. *J Gen Physiol,* **132,** 315-327.

Verselis VK, Trelles MP, Rubinos C, Bargiello TA, and Srinivas M (2009) Loop gating of connexin hemichannels involves movement of pore-lining residues in the first extracellular loop domain. *J Biol Chem,* **284,** 4484-4493.

Wang N, De BM, Antoons G, Gadicherla AK, Bol M, Decrock E, Evans WH, Sipido KR, Bukauskas FF, and Leybaert L (2012) Connexin mimetic peptides inhibit Cx43 hemichannel opening triggered by voltage and intracellular Ca2+ elevation. *Basic Res Cardiol,* **107,** 304.

Wang XG and Peracchia C (1996) Connexin 32/38 chimeras suggest a role for the second half of inner loop in gap junction gating by low pH. *Am J Physiol,* **271,** C1743-C1749.

Wang XG and Peracchia C (1997) Positive charges of the initial C-terminus domain of Cx32 inhibit gap junction gating sensitivity to CO2. *Biophys J,* **73,** 798-806.

Wang XG and Peracchia C (1998) Molecular dissection of a basic COOH-terminal domain of Cx32 that inhibits gap junction gating sensitivity. *Am J Physiol,* **275,** C1384-C1390.

Xu Q, Kopp RF, Chen Y, Yang JJ, Roe MW, and Veenstra RD (2012) Gating of connexin 43 gap junctions by a cytoplasmic loop calmodulin binding domain. *Am J Physiol Cell Physiol,* **302,** C1548-C1556.

Yamada KA, Kanter EM, Green KG, and Saffitz JE (2004) Transmural distribution of connexins in rodent hearts. *J Cardiovasc Electrophysiol,* **15,** 710-715.

Yeager M (1998) Structure of cardiac gap junction intercellular channels. *J Struct Biol,* **121,** 231-245.

Yu J, Bippes CA, Hand GM, Muller DJ, and Sosinsky GE (2007) Aminosulfonate modulated pH-induced conformational changes in connexin26 hemichannels. *J Biol Chem,* **282,** 8895-8904.

Yum SW, Zhang J, Valiunas V, Kanaporis G, Brink PR, White TW, and Scherer SS (2007) Human connexin26 and connexin30 form functional heteromeric and heterotypic channels. *Am J Physiol Cell Physiol,* **293,** C1032-C1048.

Zhou XW, Pfahnl A, Werner R, Hudder A, Llanes A, Luebke A, and Dahl G (1997) Identification of a pore lining segment in gap junction hemichannels. *Biophys J,* **72,** 1946-1953.

Zhou Y, Yang W, Lurtz MM, Chen Y, Jiang J, Huang Y, Louis CF, and Yang JJ (2009) Calmodulin mediates the Ca2+-dependent regulation of Cx44 gap junctions. *Biophys J,* **96,** 2832-2848.

Zhou Y, Yang W, Lurtz MM, Ye Y, Huang Y, Lee HW, Chen Y, Louis CF, and Yang JJ (2007) Identification of the calmodulin binding domain of connexin 43. *J Biol Chem,* **282,** 35005-35017.

Part

II
Aim of the study

At the start of this PhD thesis work, work from the host lab and others demonstrated that connexin-targeting peptides like Gap26 and Gap27 inhibited connexin hemichannels, in addition to their well documented inhibitory effect on gap junctions. A major problem with these data was that the hemichannel-inhibitory effect of these peptides was based on indirect measures of hemichannel function, the release of ATP via hemichannels or the uptake of hemichannel-permeable fluorescent indicators. The **first aim** of my work was to **unequivocally demonstrate that Gap26 and Gap27 inhibit connexin hemichannels**. To this purpose, I decided to approach this aim by using single channel studies on hemichannels. As there are no specific inhibitors of hemichannels available as of now, the only way to indisputably demonstrate that a certain candidate molecule inhibits these channels, single channel analysis is the only approach possible because such analysis gives information on the single channel conductance which is typical for hemichannels composed of a certain connexin type.

Electrophysiological analysis at the single channel level requires hemichannel opening to be triggered via voltage steps to positive membrane potentials. In most cases, in particular for non-excitable cells, the voltage steps necessary to activate the opening of Cx43 hemichannels, the target connexin of this PhD thesis, are very positive and strongly above potentials that can realistically be attained in such cells. Previous work from the host lab has demonstrated that increases of the cytoplasmic Ca^{2+} concentration promoted the opening of hemichannels without associated voltage changes to unrealistically positive potentials. Thus, **my second aim** was to investigate, again at the single channel level, the **effect of changes in cytoplasmic Ca^{2+} concentration on hemichannel opening**. To this purpose and as a first move, we investigated whether cytoplasmic Ca^{2+} elevation influenced single channel currents through hemichannels triggered by positive voltage steps.

Most of the work performed previously in the host lab was done on cell lines or exogenous overexpression of Cx43 in C6 glioma or HeLa cells. At the start of my PhD research work, there was accumulating evidence for a role of Cx43 hemichannels in brain astrocytes and in cardiac myocytes. I decided to further explore the case and evidence of Cx43 hemichannels in the heart, mainly because in this organ and in these cells, the plateau phase of the action potentials attains levels that come close to the voltage activation threshold of Cx43 hemichannels This is not the case for astrocytes which are electrically non-excitable cells. As a consequence, the **third aim** of my work was to **investigate whether Cx43 hemichannels do play a role in cardiomyocytes**, especially **in the context of ischemia/hypoxia** which is a

condition demonstrated by others to activate hemichannel opening. Ventricular cardiomyocytes have a particularly dominant expression of Cx43 and we therefore chose those cells for this particular analysis. Moreover, we investigated both the effect of cytoplasmic Ca^{2+} elevation and ischemia-mimicking conditions on hemichannel unitary (single channel) current events.

Last but not least, previous work from the host lab has demonstrated that L2 peptide, mimicking a domain located on the intracellular loop of Cx43 had a selective Cx43 hemichannel inhibitory effect and based on observations of theirs, this was associated with slight potent effects on gap junctions. Thus, I decided as a **fourth aim**, to investigate the effect of L2 peptide and a small peptide identical to a subdomain of the L2 region, Gap19, on single channel analysis of Cx43 hemichannels. Such analysis was performed on both expression systems and endogenously Cx43 expressing ventricular cardiomyocytes.

Work from several groups had, at the start of my investigations, demonstrated that Cx43 hemichannels open under ischemia/hypoxia conditions and consequently, I included as a **fifth aim** to determine whether selective **inhibition of Cx43 hemichannels would have beneficial effects on cardiomyocyte viability and infarct size after cardiac ischemia** applied *in vivo* in mice. The central hypothesis tested here was that blocking the putative toxic pore formed by open Cx43 hemichannels, would have a beneficial effect on cardiomyocyte viability and cardiac infarct size.

Part

III

Experimental Work

Chapter III. Connexin mimetic peptides inhibit Cx43 hemichannel opening triggered by voltage and intracellular Ca^{2+} elevation

Nan Wang[1], Marijke De Bock[1], Gudrun Antoons[2], Ashish K. Gadicherla[1], Mélissa Bol[1], Elke Decrock[1], William Howard Evans[3], Karin R. Sipido[4], Feliksas F. Bukauskas[5], Luc Leybaert[1]

[1]Department of Basic Medical Sciences, Physiology Group, Faculty of Medicine and Health Sciences, Ghent University, De Pintelaan 185, 9000 Ghent, Belgium

[2]Division of Cardiology, Medical University of Graz, Auenbruggerplatz 15, 8036 Graz, Austria

[3]Department of Medical Biochemistry and Immunology, Cardiff University School of Medicine, Heath Park, Cardiff CF14 4XN, Wales, UK

[4]Department for Experimental Cardiology, O & N1, K.U.Leuven, Herestraat 49, 3000 Leuven, Belgium

[5]Dominick P. Purpura Department of Neuroscience, Albert Einstein College of Medicine, 1300 Morris Park Ave, Bronx, NY 10461, USA

Published in Basic Res Cardiol. 107::304 (2012)

Abstract

Connexin mimetic peptides (CxMPs) like Gap26 and Gap27 are known as inhibitors of gap junction channels but evidence is accruing that these peptides also inhibit unapposed/non-junctional hemichannels (HCs) residing in the plasma membrane. We used voltage clamp studies to investigate the effect of Gap26/27 at the single channel level. Such an approach allows unequivocal identification of HC currents by their single channel conductance that is typically ~220 pS for Cx43. In HeLa cells stably transfected with Cx43 (HeLa-Cx43), Gap26/27 peptides inhibited Cx43 HC unitary currents over minutes and increased the voltage threshold for HC opening. By contrast, an elevation of intracellular calcium ($[Ca^{2+}]_i$) to 200-500 nM potentiated the unitary HC current activity and lowered the voltage threshold for HC opening. Interestingly, Gap26/27 inhibited the Ca^{2+}-potentiated HC currents and prevented lowering of the voltage threshold for HC opening. Experiments on isolated pig ventricular cardiomyocytes, which display strong endogenous Cx43 expression, demonstrated voltage-activated unitary currents with biophysical properties of Cx43 HCs that were inhibited by small interfering RNA targeting Cx43. As observed in HeLa-Cx43 cells, HC current activity in ventricular cardiomyocytes was potentiated by $[Ca^{2+}]_i$ elevation to 500 nM and was inhibited by Gap26/27. Our results indicate that under pathological conditions, when $[Ca^{2+}]_i$ is elevated, Cx43 HC opening is promoted in cardiomyocytes and CxMPs counteract this effect.

Key words: connexin 43, connexin hemichannel, mimetic peptides, cardiomyocytes, single channel

Introduction

In vertebrates, connexin (Cx)-based hemichannels (HCs) embedded in the plasma membrane interact with their counterparts on neighboring cells in a head-to-head arrangement, forming gap junction channels that coalesce into junctional plaques that allow the direct exchange of metabolic and signaling molecules with molecular weight below 1kDa between cells (Goodenough *et al.*, 1996b;Matsuyama and Kawahara, 2009;Willecke *et al.*, 2002). On the other hand, unapposed/undocked HCs present in non-junctional plasma membrane can open and form a conduit between the cell's interior and the extracellular milieu, allowing Na^+ and Ca^{2+} to enter the cell and K^+ and messengers like ATP, glutamate and others to leave the cell (Kang *et al.*, 2008b;Kondo *et al.*, 2000a;Li *et al.*, 2001;Schalper *et al.*, 2010b;Ye *et al.*, 2003). Cx HCs are typically closed under resting conditions, but may open under ischemic conditions (Clarke *et al.*, 2009a;Johansen *et al.*, 2011a;Orellana *et al.*, 2009;Shintani-Ishida *et al.*, 2007a) by alterations in the redox status (Retamal *et al.*, 2007b), the connexin phosphorylation status (Bao *et al.*, 2004;Kim *et al.*, 1999a) or by an increased presence of these channels in the plasma membrane (Retamal *et al.*, 2006a;Sanchez *et al.*, 2009a).

Cx mimetic peptides (CxMPs) are peptides identical to sequences located on one of the two extracellular loops of the Cx protein (Evans *et al.*, 1992). They were introduced in the 90's based on the hypothesis that such peptides could prevent the docking of two HCs, thereby preventing the formation of GJCs (Evans and Boitano, 2001a;Warner *et al.*, 1995a). Among them, Gap26 and Gap27, mimicking sequences on the first and second extracellular loop regions of Cx43 respectively (see Online Resource Fig. S1), have been most extensively investigated and used as gap junction blockers (Boitano and Evans, 2000;Chaytor *et al.*, 1997;Samoilova *et al.*, 2008;Wright *et al.*, 2009a). Recent evidence raised the possibility that CxMPs may also affect the function of HCs (Braet *et al.*, 2003b;Evans *et al.*, 2001a), and to date, they have become a frequently applied pharmacological tool to explore new functions of the Cx HC signaling pathway. CxMPs like Gap26 and Gap27 have been applied to establish the contribution of HCs in cell death propagation (Decrock *et al.*, 2009c). In embryonic neural retina, these peptides have been used to demonstrate an essential role of HCs as an ATP release pathway in the development of neural retina progenitor cells (Pearson *et al.*, 2005b). In the context of cardiac ischemia, targeting of Cx43 HC at the cell surface by Gap26/27 showed cardioprotective effect in both primary myocytes culture and intact heart (Hawat *et*

al., 2010a;Johansen *et al.*, 2011a;Shintani-Ishida *et al.*, 2007a). Further work with CxMPs has suggested a role of HCs in a variety of pathological insults ranging from amyloid β-mediated neuronal death to hypoxia-induced inflammation (Eltzschig *et al.*, 2006;Karpuk *et al.*, 2011;Orellana *et al.*, 2011). Intriguingly, despite the growing interest in CxMPs-based HC studies, no conclusive arguments are available to support a direct action of the peptides on HCs. Short exposure to CxMPs has been reported to inhibit indirect measures of HC function based on ATP release or dye uptake studies. Electrophysiological studies further indicated that Gap26 rapidly diminished macroscopic currents in Cx43 expressing cells (Hawat *et al.*, 2010a;Hawat *et al.*, 2012a;Romanov *et al.*, 2008a). Studies performed in the Xenopus oocyte expression system, however, failed to demonstrate clear inhibition of macroscopic currents: limited inhibition was only observed with long exposures (3 h) and appeared to depend on peptide size rather than sequence (Wang *et al.*, 2007a). Due to the lack of studies at single channel level, it remains uncertain whether CxMPs block HC openings and if so, whether this effect is sequence-specific or merely the consequence of steric occlusion.

Here, we investigated the effect of Gap26 and Gap27 at the level of unitary currents through Cx43 HCs, allowing detailed analysis at the highest resolution. In HeLa cells expressing exogenous Cx43, unitary events associated with Cx43 HC opening can be unambiguously identified by the single channel conductance that is typically ~220 pS. Our data show that HC-based unitary events are inhibited by Gap26/27 within several minutes, by shifting the voltage-dependence of Cx43 HC opening to more positive transmembrane potentials (V_m). In addition, moderate elevation of the intracellular calcium concentration ($[Ca^{2+}]_i$) to 200-500 nM shifted the V_m-dependence of HC opening to lower V_m values (shift to the left) while Gap26/27 fully prevented this shift. Interestingly, low pH induced HC inhibition was also found to depend on $[Ca^{2+}]_i$ changes, with HC closure being mediated by (strong) $[Ca^{2+}]_i$ elevation to micromolar concentrations. In isolated left ventricular cardiomyocytes of adult pig, single channel openings triggered by stepping V_m to positive potentials were abolished by short interfering RNA (siRNA) against Cx43. These unitary current activities were promoted by 500 nM $[Ca^{2+}]_i$ and inhibited by Gap26/27. We conclude that (i) functional Cx43 HCs are present in ventricular cardiomyocytes, (ii) when $[Ca^{2+}]_i$ is moderately elevated, these channels open at V_m = +40 mV, and (iii) CxMPs prevent Ca^{2+} and voltage dependent HC activation. These effects are likely to play a prominent role in the protective effect of CxMPs on cardiac ischemia.

Materials and Methods

Chemical reagents

Gap26 (VCYDKSFPISHVR) and Gap27 (SRPTEKTIFII), two connexin mimetic peptides corresponding to a sequence in the first and second extracellular loop regions of Cx43 respectively were used in the study. Two associated scrambled peptides SGap26 (PSFDSRHCIVKYV) (Pearson *et al.*, 2005b) and SGap27 (TFEPIRISITK) (Wright *et al.*, 2009a) were applied in some experiments as inactive controls (overviewed in Online Resource Table S1). All peptides were synthesized to a purity > 90 %.

Cell culture

HeLa-wild type (HeLa-WT) cells were cultured in Dulbecco's modified Eagle's medium (Invitrogen, Gent, Belgium) supplemented with 20 % fetal bovine serum (FBS), 2 mM glutamine, 10 U/ml penicillin, 10 µg/ml streptomycin, and 0.25 µg/ml fungizone (Invitrogen, Gent, Belgium). Cells stably transfected with Cx43 (Elfgang *et al.*, 1995) grown in the medium with additional 1µg/ml puromycin (Sigma-Aldrich, Bornem, Belgium). Mouse Cx43 gene was cloned into the Eco RI/Bam HI restricted cloning site of the expression vector pMJgreen. CytoMegalovirus (CMV) promoter was used. The vector also contains a puromycin N-acetyl-transferase (Pac) gene encoding region.

Calcein efflux

Subconfluent cultures of HeLa-Cx43 seeded on glass coverslips (Knittel, Novolab, Geraardsbergen, Belgium) were loaded with 10 µM calcein-acetoxymethyl ester (calcein-AM) for 1h at room temperature. Thereafter, cells were washed and left for another 30 min to allow for de-esterification. Cultures were then transferred to an inverted epifluorescence microscope (Eclipse TE300, Nikon Belux, Brussels, Belgium) equipped with a x 40 oil-immersion objective and an electron-multiplying CCD camera (Quantem 512SC, Photometrics, Tuscon, AZ, USA). Calcein was excited at 482 nm by a Lambda DG-4 filterswitch (Sutter Instrument, Novato, CA, USA). A 505 nm long-pass dichroic mirror and a 535 nm bandpass filter (35 nm bandwidth) were used to capture calcein emission light.

Fluorescent images were recorded every second and the fluorescent decay as a function of time was quantified as described in (De Bock M. *et al.*, 2011).

Cardiomyocyte isolation

Left ventricular cardiomyocytes from adult domestic pigs were enzymatically isolated as previously described (Stankovicova *et al.*, 2000b). Briefly, the left anterior descending coronary artery was cannulated, and the cells were dissociated by enzymatic tissue digestion through Langendorff perfusion at 37°C. The cells were then filtered and resuspended in a low Ca^{2+} Tyrode solution containing (in mM): 130 NaCl, 5.4 KCl, 1.2 $KHPO_4$, 1.2 $MgSO_4$, 0.18 $CaCl_2$, 6 HEPES, 10 glucose, pH 7.2. Ca^{2+}-tolerant cells were stored at room temperature and used within 8-10 h after isolation.

RNA interference

Acutely isolated cardiomyocyte suspension was centrifuged at 300 rpm for 5 min. The cell pellets containing both cardiomyocytes and fibroblasts were resuspended in Medium 199 (Sigma-Aldrich) supplemented with 10% FBS, 10 U/ml penicillin and 10 µg/ml streptomycin. After 2-h incubation at 37°C in 5% CO_2, cardiomyocytes remained suspended in the medium while fibroblasts adhered to the bottom of the polystyrene flask. The fibroblast-depleted suspension was again collected and cultured at a density of 2×10^4 cells/cm^2 in a Petri dish (9.2 cm^2; TPP Techno Plastic Products AG, Trasadingen, Switzerland) or glass coverslip (2.5 cm^2) coated in advance with natural mouse laminin (Invitrogen).

Cultured cardiomyocytes were transfected the following day with siRNA using DharmaFECT lipid reagent (Dharmacon, Thermo Fisher Scientific, Aalst, Belgium). siRNA duplex targeting the porcine Cx43 gene *gja1* (5'-GAAAGAGGAGGAACUCAAA-dTdT-3') was synthesized and annealed by Eurogentec (Luik, Belgium). Cultures transfected with scrambled sequence ($siCx43^{scr}$: 5'-AGAGAUACGAACAAGAGAG-3') or lipid reagent alone (MOCK) were used as negative controls. The transfection mixture was removed from the cultures after 24-h treatment.

Western Blot analysis

Whole cell lysates were prepared by treating confluent cell culture with RIPA buffer (25 mM Tris, 50 mM NaCl, 0.5% NP-40, 0.5% deoxycholate, 0.1% SDS, 5.5% β-glycerophosphate, 1 mM dithiothreitol, 10 µL/mL protease inhibitor cocktail (Sigma-Aldrich), 30 µL/mL phosphatase inhibitor cocktail (Sigma-Aldrich), and 20 µL/mL mini EDTA-free protease inhibitor cocktail. Proteins were resolved by 10% SDS-poly-acrylamide (SDS-PAGE) gel and transferred to a nitrocellulose membrane (Amersham, Buckinghamshire, United Kingdom). Blots were probed with a rabbit polyclonal anti-Cx43 antibody (Sigma-Aldrich) or a rabbit anti-Panx1 (a gift kindly provided by Dr. Dale W. Laird, University of Western Ontario, Canada) followed by alkaline phosphatase-conjugated goat anti-rabbit IgG antibody (Sigma-Aldrich). The blots were then developed with nitro blue tetrazolium/5-bromo-4-chloro-3-indolyl-phosphate reagent (Zymed, Invitrogen). Total protein stains by SYPRO® Ruby (Invitrogen) prior to antibody staining or detection with a rabbit anti-β-tubulin antibody (Abcam, Cambridge, United Kingdom) was used as a loading control.

Triton X-100 (Tx-100) insoluble fraction was obtained by harvesting cells in 1% Trixton X-100 supplemented with 50 mM NaF, 1 mM Na_3VO_4, 10 µL/mL protease inhibitor cocktail, 30 µL/mL phosphatase inhibitor cocktail. Samples were centrifuged at 16,000 g for 10 min and the Triton X-100 insoluble pellets were resuspended in 1 x Laemmli buffer (10% glycerol, 2.3% SDS and 125 mM Tris pH 6.8).

Detection of the fraction of unapposed Cx43 in the plasma membrane was achieved by biotin-labeling of surface protein with the Pierce cell surface protein isolation kit (Thermo Scientific, Erembodegem, Belgium). Confluent cultures were incubated with 0.25 mg/ml sulfosuccinimidyl-2-(biotinamido)ethyl-1,3-dithiopropionate (Sulfo-NHS-SS-Biotin) phosphate-buffered saline for 2h at 4 °C. This membrane-impermeable, thiol-cleavable and amine-reactive reagent labels free surface membrane proteins including unapposed Cx43 HCs that have their extracellular domains unoccupied. By contrast, HCs incorporated into gap junctions have no accessible extracellular domains and the amine-reactive sites are effectively sealed. Unreacted biotin was quenched by glycine-based solution and the cells were lysed immediately. Cell extracts were then mixed with Neutravidine™ agarose for purification of biotin-labeled proteins. Biotinylated proteins containing the pool of unapposed HCs were

subsequently eluted from the Neutravidine™ agarose and separated by a 10% SDS-PAGE gel for further immunoblotting with Cx43 antibody (Sigma-Aldrich).

Electrophysiological recording

Hela-Cx43 cells were bathed in a recording chamber filled with a modified Krebs-Ringer solution consisting of (in mM): 150 NaCl, 6 CsCl, 2 $CaCl_2$, 2 $MgCl_2$, 1 $BaCl_2$, 2 pyruvate, 5 glucose, 5 HEPES and pH adjusted to 7.4. The standard whole-cell recording pipette solution was composed of (in mM): 130 CsCl, 10 Na-aspartate, 0.26 $CaCl_2$, 1 $MgCl_2$, 2 EGTA, 5 tetraethylammonium (TEA)-Cl and 5 HEPES; pH was adjusted to 7.2 and [Ca^{2+}] was 50 nM as calculated with Webmax Standard software application: http://www.stanford.edu/~cpatton/webmaxcS.htm. Estimations of attained $[Ca^{2+}]_i$ mentioned in the text were also calculated using this software. Intracellular acidification was applied via the patch pipette; to this purpose, HEPES was replaced by MES (5 mM) and pH was adjusted to 6.4 or 6.0 (Lewandowski *et al.*, 2008).Pipette resistance was 1-3 MΩ. A 3 M KCl agar bridge connected the recording chamber to a grounding compartment.

For the experiments on cardiomyocytes, cells were initially perfused with the standard Tyrode solution (in mM): 137 NaCl, 5.4 KCl, 1.8 $CaCl_2$, 0.5 $MgCl_2$, 10 glucose, 11.8 HEPES and pH adjusted to 7.4. When recording unitary HC currents, the solution was switched to a solution with the same composition but with all K^+ replaced by Cs^+. In addition, 1 mM $BaCl_2$ was added to the external solution to further inhibit K^+ currents. The pipette solution was composed of (in mM): 120 CsCl, 5 NaCl, 10 TEACl, 1 $CaCl_2$, 1 $MgCl_2$, 2 MgATP, 10 EGTA, 10 HEPES and pH adjusted to 7.2.

Single channel recordings were performed by making use of an EPC 7 PLUS patch-clamp amplifier (HEKA Elektronik, Lambrecht/Pfalz, Germany). Data were acquired at 4 kHz using a NI USB-6221 data acquisition device from National Instruments (Austin, TX) and Clampex 10.2 acquisition software (Axon instruments). All currents in whole-cell configuration were filtered at 1 kHz (7-pole Besselfilter). Liquid junction potentials were measured in current mode by placing pipette solution or bath solution in the recording pipette and the other in the bath. Membrane potentials were corrected for the liquid junction potentials.

For single-channel analysis, holding currents were substracted from the recorded current traces, giving traces that only contained unitary current events. Unitary conductances were calculated from the elementary current transitions Δi as: $\gamma = \frac{\Delta i}{Vm}$. From these data, we constructed all-point conductance histograms that displayed one or more gaussian distributions. These were fit by a probability density function assuming independent channel opening (Ramanan and Brink, 1993;Wang *et al.*, 2001). Channel activity was quantified from the charge transfer Q_m associated with unitary currents; this was done by integrating the unitary current traces (*i.e.*, a function of time) over the duration of the voltage step as: $Q_m = \int i dt$.

Statistical analysis

Data are expressed as mean ± S.E.M. with n denoting the number of independent experiments. Multiple groups were compared by one-way ANOVA with Bonferroni post-test, Two groups were compared with an unpaired student's t-test and two-tail p value.

Results

Single channel unitary currents in HeLa cells stably transfected with Cx43

Previous studies revealed that unitary Cx43 HCs events appeared upon depolarizing the membrane potential (V_m) to > +50 mV (Contreras *et al.*, 2003b). Fig. 1a illustrates single channel openings observed with whole-cell patch clamp recording from a solitary Hela-Cx43 cell upon stepping V_m from -30mV to +70 mV. Recordings were performed in the presence of extracellular Ca^{2+} and Mg^{2+} and under conditions of K^+-channel blockade with Cs^+, Ba^{2+} and TEA^+ (see Materials and Methods). Transitions between the closed and fully open state were characterized by a unitary conductance (γ_o) of ~ 220 pS (Fig. 1a). Transitions from the open state occasionally occurred to a sub-conductance state characterized by a unitary conductance (γ_{sub}) of ~58 pS (Fig. 1b), as reported by Contreras et al. (Contreras *et al.*, 2003b). Such transitions were not frequent and event histograms obtained from recordings of 30 s typically did not show a resolvable subconductance peak under control conditions. The typical 220 pS opening activity was not observed in single HeLa-WT cells (Online Resource Fig. S2a). In HeLa-Cx43 cells, unitary current activity induced by V_m = +70 mV rapidly disappeared following application of carbenoxolone (100 µM), a gap junction and HC blocker (Online Resource Fig. S3).

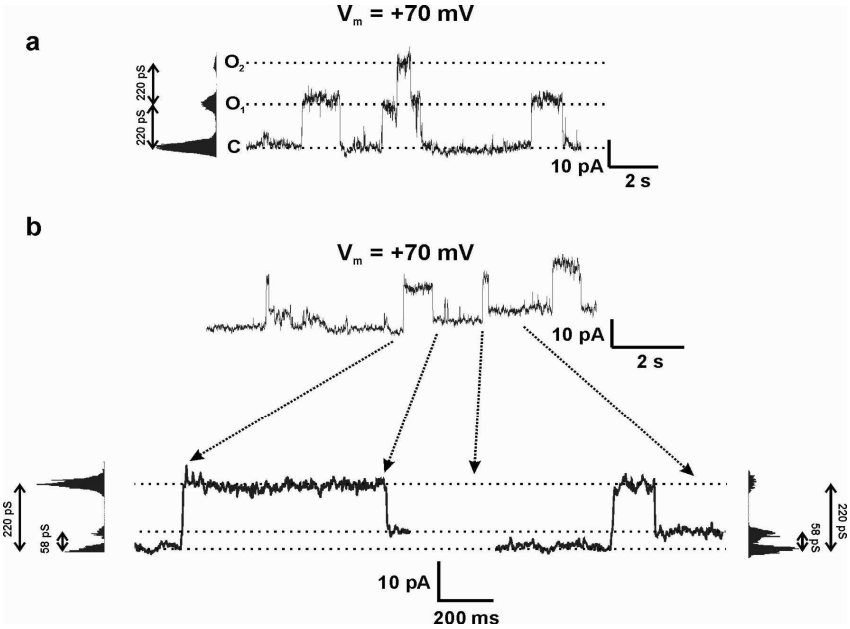

Figure 1. Unitary currents recorded in HeLa-Cx43 cells. (**a**) Single-channel events were activated by stepping V_m from -30 mV to +70 mV. The vertical graph at the left represents an all-point histogram illustrating the ~220 pS unitary conductance of a fully open channel. (**b**) Illustration of two fully open channels closing to a substate of ~58 pS as shown in the expanded traces.

Gap26 and Gap27 inhibit Cx43 hemichannel unitary currents

We tested whether Gap26 and Gap27 inhibited unitary current events recorded in HeLa-Cx43 cells at concentrations commonly used to inhibit gap junctions. Pre-incubation of cells for 30 min with Gap26 (160 µM) or Gap27 (200 µM) reduced unitary events typically observed at V_m = +70 mV (Fig. 2a and 2b). The conductance of the remaining events showed a peak at ~220 pS, indicating that Gap26/27 did not influence the γ_o. Experiments with scrambled versions of Gap26 and Gap27 (SGap26 and SGap27 respectively) did not reveal any inhibition of HC-mediated unitary events (Fig. 2a and 2c). Unitary current activities were quantified by integrating the current traces (holding current subtracted) over the time of V_m step, giving the charge transfer (Q_m) via open HCs. Fig. 2c shows a more than 3-fold decrease in Q_m by Gap26/27, whereas Q_m recorded in cells exposed to SGap26/27 was not different from control. Western blot analysis of Cx43 expression demonstrated that the density of membrane-located biotin-labeled Cx43 HCs relative to the total membrane Cx43 pool (Triton X-100 insoluble fraction) was not influenced by Gap26 treatment (Fig. 2d), in line with the findings reported by others (Martin *et al.*, 2005).

Figure 2. Cx43 HC unitary current events are inhibited by Gap26 and Gap27 in HeLa-Cx43 cells. (**a**) Example traces depicting unitary current activities induced by stepping V_m to +70 mV (30 s) in control and after addition of Gap26/27 or scrambled sequences. (**b**) All-point histograms determined from the corresponding traces in panel a. Dashed vertical lines through the peaks are each separated by ~220 pS. (**c**) Summary data of Q_m, illustrating significant inhibition by Gap26/27 but not by the scrambled sequences. **p<0.01 *vs* Control; ##p<0.01 *vs* scrambled peptides. (**d**) Biotin-labeling studies illustrating that Gap26 has no effect on the fraction of unapposed HCs. For assessment of unapposed HC fraction present in the plasma membrane, the biotin-labeled fraction was normalized to the total protein stained by SYPRO® Ruby. Membrane-associated Cx43 was

estimated by the Tx-100 insoluble fraction proportional to the total lysate. Treatment with Gap26 (160 µM, 30 min) did not influence the biotin-labeled Cx43 protein fraction, indicating that the number of HCs in the plasma membrane is not altered (n = 4).

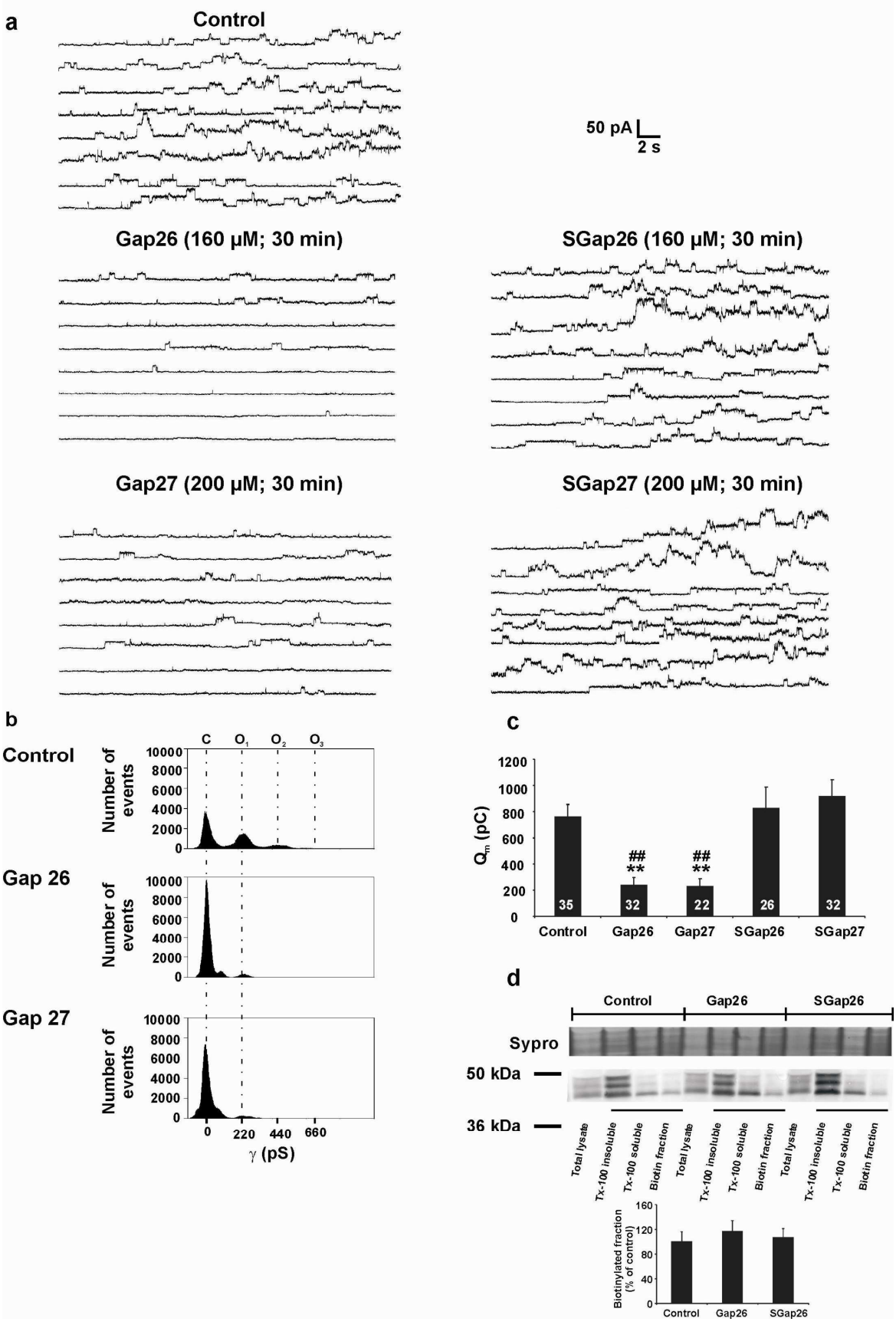

Gap26/27 inhibition of Cx43 HC unitary currents is concentration-dependent and occurs within minutes

We examined the kinetics of Gap26/27 inhibition of unitary current activity. In this experiment, we applied repeated (every 40 s) V_m steps from -30 to +70 mV (30 s) over a time period of 10 min and calculated the Q_m at different time points. Fig. 3a illustrates an example recording, showing a decrease of Q_m with time after addition of Gap26 (250 µM). There was some inherent variability in these recordings, related to shot noise associated with low probability events (Kang *et al.*, 2008b). Fig. 3b represents changes of current under control conditions and 240 s after exposure to Gap26. Fig. 3c shows averaged Q_m changes in experiments similar to the one illustrated in Fig. 3a. After addition of Gap26, Q_m progressively decreased with a time constant (τ) of 148 s (determined by fitting the data points to a mono-exponentially decaying function). At steady-state conditions, Q_m was reduced to ~35 %. In contrast, SGap26 did not cause any Q_m decay. We further examined the concentration-dependence of Gap26 inhibition (148 s exposure time) and found an IC_{50} of ~81 µM and a Hill coefficient (n_H) = 2 (Fig. 3d). SGap26 did not exhibit inhibitory effects over the concentration range at which Gap26displayed inhibition. Only when the concentration of SGap26 was increased to 1 mM,

Strong inhibition was observed (Fig. 3e). Fig. 4 illustrates a similar set of experiments performed with Gap27 (300 µM). Inhibition was somewhat slower (τ = 223 s) while the steady-state reduction of Q_m was stronger (reduction to ~15 %) compared to Gap26 (Fig. 4c). Concentration-dependent inhibition of Q_m (223 s exposure time) was characterized by an IC_{50} of ~161 µM and n_H = 2 (Fig. 4d). As expected, SGap27 did not affect Q_m unless it was applied at 1 mM concentration (Fig. 4e). The abrupt kink in the Q_m curve at 1 mM with both scrambled peptides (SGap26 and SGap27) indicates the appearance of steric occlusion of the channel pore.

We tested whether Gap27 could also inhibit the passage of larger molecules through Cx43 HCs. To that purpose, we used calcein (MW 623 Da) as a HC-permeable fluorescent reporter dye (Anselmi *et al.*, 2008) and quantified the loss of fluorescence from preloaded HeLa-Cx43 cells, as previously done (De Bock M. *et al.*, 2011). The calcein efflux rate increased upon exposure to nominal divalent free (NDF, no Ca^{2+} or Mg^{2+} added) solution and the efflux rate-increase was inhibited by Gap27 (300 µM) (Fig. 4f). Fig. 4g illustrates the effect of NDF and

NDF + Gap27 on unitary HC currents, demonstrating comparable effects as observed in the calcein experiments. Thus, Gap27 has comparable effects on calcein passage and current flow through Cx43 HCs.

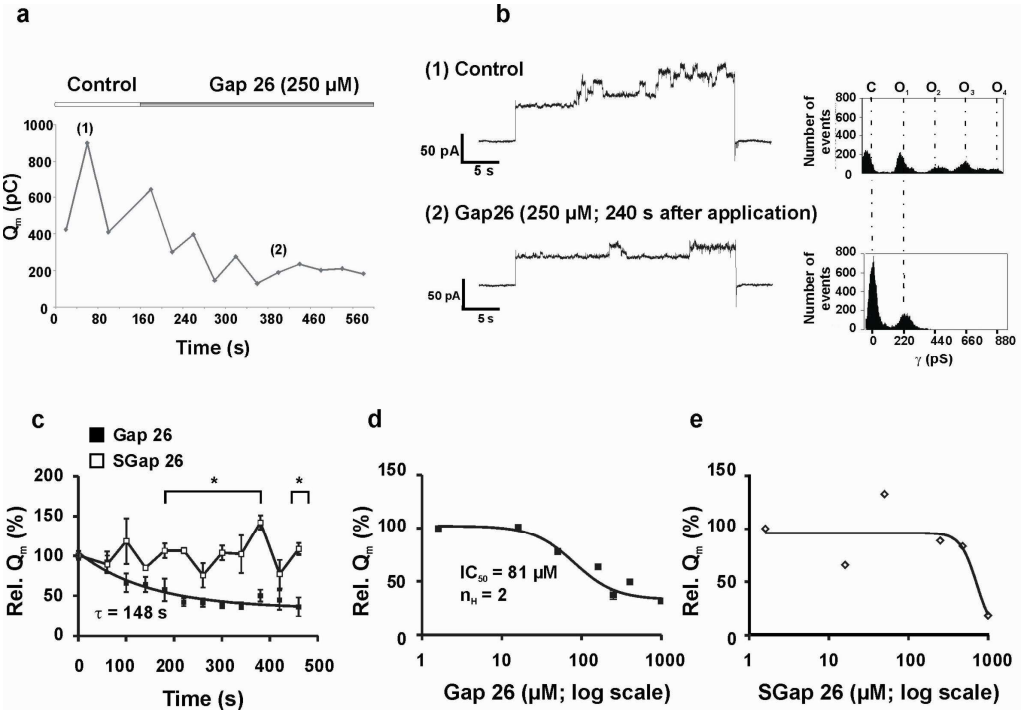

Figure 3. Gap26 inhibition occurs within minutes and is concentration-dependent. (**a**) Q_m for repeated V_m steps to +70 mV before and after application of Gap 26 (250 µM) in HeLa-Cx43 cells. (**b**) Example traces and all-point histograms before and after addition of Gap26 (points indicated as 1 and 2 respectively in panel a). (**c**) Average data illustrating the kinetics of Gap26 inhibition (n = 5). For SGap26, the curve remained fluctuating around 100 % (n = 3). Q_m was expressed as a percentage normalized to the averaged measurement before Gap26 addition. *p<0.05 Gap26 *vs* SGap26. (**d**) Concentration-dependence of Gap26 inhibition; Q_m was normalized to data values obtained without peptide. (**e**) Experiment as in panel d but with the scrambled sequence.

Gap26 and Gap27 increase the V_m necessary to open HCs

Gap26 and Gap27 had no effect on γ_o, therefore, we examined whether they exerted their effect through a change in the voltage gating. Fig. 5a shows an I-V plot obtained by applying voltage ramps from -40 to +80 mV (1.8 mV/s). Unitary current events started to appear from V_m = +50 mV while after addition of Gap26/27, unitary events appeared at more positive potentials. A similar influence was observed on I-V plots derived from slower voltage ramps (0.5 mV/s; Online Resource Fig. S4). By applying V_m steps from -30 mV to voltages in the range of +40 to +80 mV, we observed that Gap26 and Gap27 (for concentrations and exposure times see Fig. 5b) significantly shifted the V_m dependence of HC opening to the right over ~15 mV, i.e. they increased the V_m for HC activation (Fig. 5c).

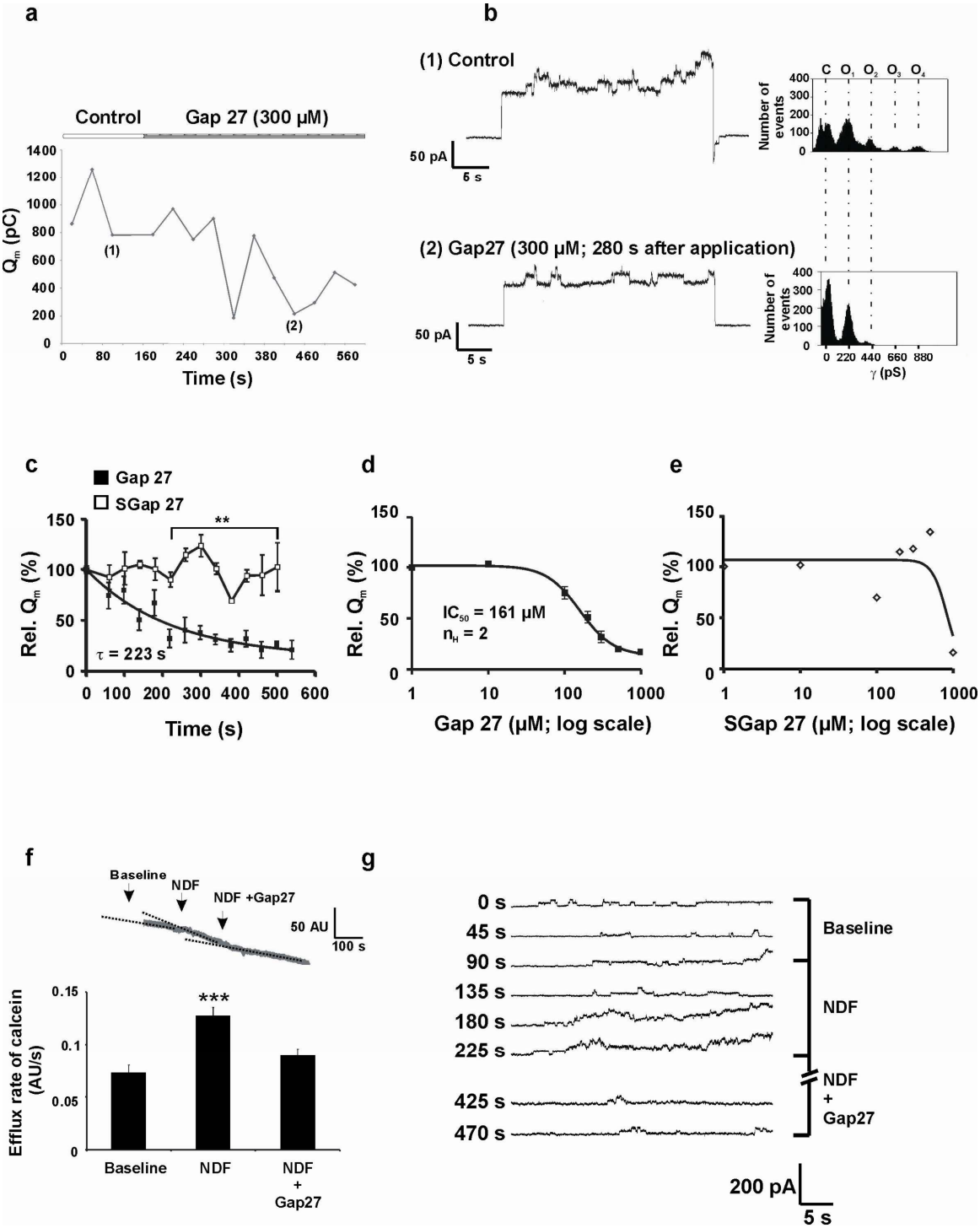

Figure 4. Gap27 inhibition occurs within minutes and is concentration-dependent. (**a**) Q_m for repeated V_m steps to +70 mV before and after application of Gap 27 (300 µM). (**b**) Example traces and all-point histograms before and after addition of Gap27 (points indicated as 1 and 2 respectively in panel a). (**c**) Average data illustrating the kinetics of Gap27 inhibition (n = 5). For SGap27, the curve remained fluctuating around 100 % (n = 3). Q_m was expressed as a percentage normalized to the averaged measurement before Gap27 addition. **p<0.01 Gap27 *vs* SGap27. (**d**) Concentration-dependence of Gap27 inhibition; Q_m was normalized to data values obtained without the peptide. (**e**) Experiment as in panel d but with the scrambled sequence. (**f**) Gap27 inhibits dye transfer triggered by exposure to nominally divalent-free (NDF) solution. NDF triggered the efflux of calcein preloaded in HeLa-Cx43 cells and this was inhibited by Gap27 (300 µM; n = 31 cells from 5 experients). *** p<0.001 NDF *vs* baseline. (**g**) Gap27 inhibits NDF-promoted HC currents in HeLa-Cx43 cells. Traces show unitary current activity upon stepping from -30 to +60 mV (40 s) that was strongly promoted by NDF conditions. Gap27 (300 µM, added just after the 225 s trace) inhibited NDF-potentiated currents (300 µM).

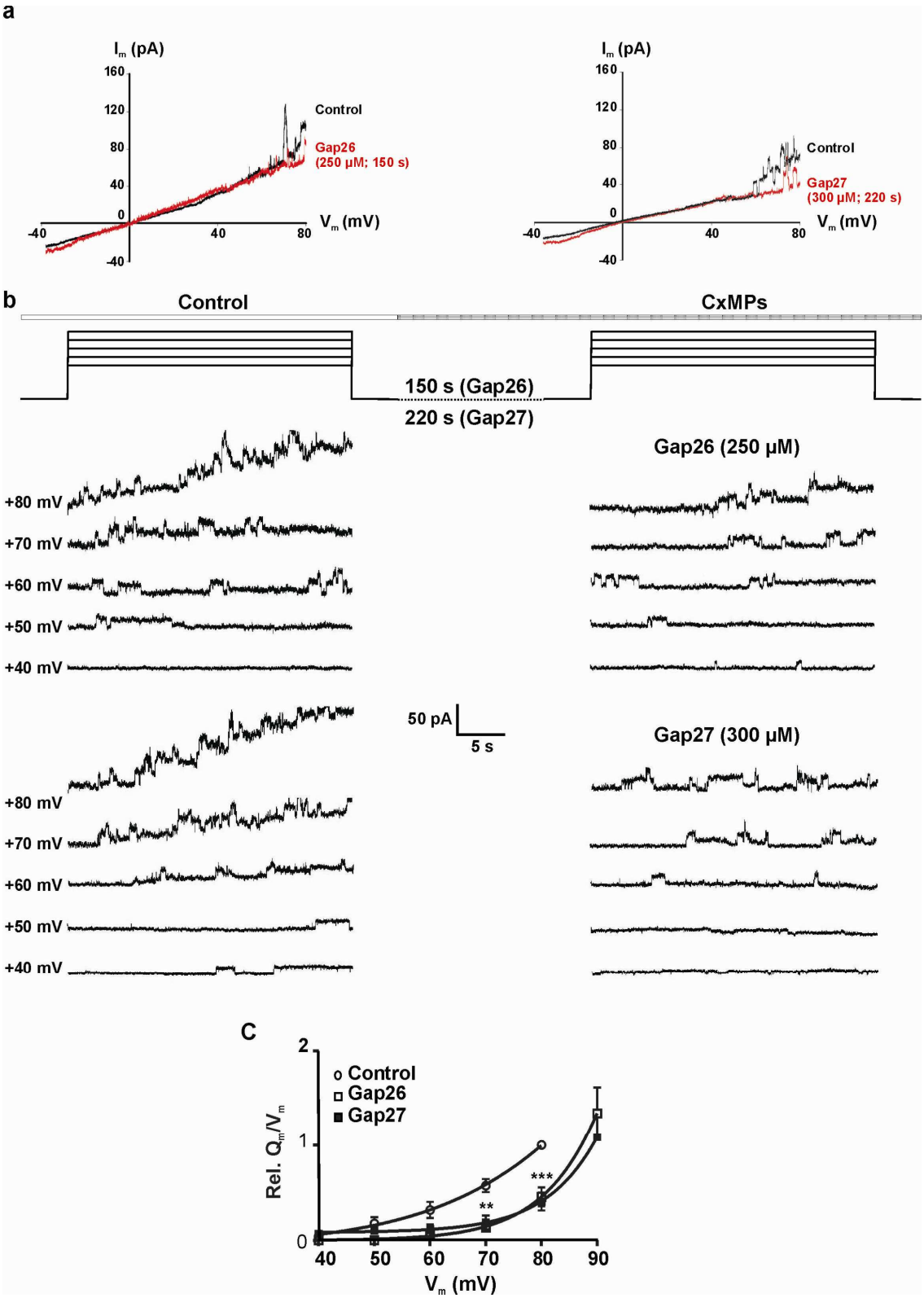

Figure 5. Gap26/27 increases the V_m required for hemichannel activation in HeLa-Cx43 cells. (**a**) Voltage ramp I-V plot illustrating that unitary current activation occurs at more positive V_m after exposure to Gap26/27. (**b**) Voltage-dependent activation studies performed by V_m steps in the range of +40 to +80 mV in 10 mV increments (30 s). (**c**) Voltage activation curve, obtained by normalizing the Q_m/V_m data to the control value at +80 mV as a relative measure of HC openings (n = 5). **p<0.01 and ***p<0.001 Gap26 and Gap27 *vs* Control

$[Ca^{2+}]_i$-dependent modulation of Cx43 HC unitary currents under control/normal conditions and in the presence of Gap26/27

Unitary Cx43 HC currents appear only at strong positive V_m as reported earlier (Contreras *et al.*, 2003b;Kang *et al.*, 2008b) and confirmed here. Previous studies demonstrated that an elevation of $[Ca^{2+}]_i$ stimulates HC-mediated ATP release and dye uptake (De Vuyst E. *et al.*, 2006;De Vuyst *et al.*, 2009b;Ponsaerts *et al.*, 2010a;Schalper *et al.*, 2008). We investigated whether $[Ca^{2+}]_i$ elevation alters the properties of unitary HC currents in HeLa-Cx43 cells. For this purpose, the pipette solutions used for whole-cell recordings were buffered to different $[Ca^{2+}]$ of 50 (standard pipette solution), 200, 500, and 1000 nM. Fig. 6a demonstrates that unitary current activity measured at V_m = +60 mV was clearly potentiated at moderately elevated $[Ca^{2+}]_i$ levels of 200 and 500 nM, while the effect disappeared with further elevation to 1 µM. Fig. 6b shows the corresponding all-point histograms, demonstrating an increased frequency of ~220 pS openings and less activity in the closed state. Average data of such experiments are shown in Fig. 6c, illustrating a significant increase of Q_m at 200 and 500 nM (compared to 50 nM) while this potentiation disappeared at 1 µM. HeLa-WT cells exhibited no unitary current activities upon $[Ca^{2+}]_i$ elevation to 500 nM (Online Resources Fig. S2b). The bell-shaped profile of these responses in HeLa-Cx43 cells is very similar to previously reported results that were based on indirect measurements of HC activity (De Vuyst E. *et al.*, 2006;De Vuyst *et al.*, 2009b). Moreover, we found that $[Ca^{2+}]_i$ elevation from 50 to 200 and 500 nM significantly altered the V_m dependence of HC opening by shifting it ~15 mV leftwards, i.e. 200-500 nM $[Ca^{2+}]_i$ decreased the V_m for HC opening (Fig. 6d). The effect of $[Ca^{2+}]_i$ elevation to 200 nM was stronger than for 500 nM. $[Ca^{2+}]_i$ elevation had no effect on the reversal potential of the unitary current recordings (0 mV; Online Resource Fig. S5). Interestingly, Gap26 (250 µM) and Gap27 (300 µM) inhibited the Q_m increase mediated by $[Ca^{2+}]_i$ elevation to 200/500 nM (Fig. 6c) and completely prevented changes of V_m dependence induced by $[Ca^{2+}]_i$ increase (Fig. 6d).

Figure 6. Effect of $[Ca^{2+}]_i$ elevation on Cx43 HC unitary currents recorded in HeLa-Cx43 cells. (**a**) Representative current traces obtained by voltage steps stepping V_m to +60 mV (30 s). 10 consecutive runs were recorded and the beginning of each 30-s example trace was separated by 40 s. The various $[Ca^{2+}]_i$ depicted were applied via the whole-cell recording pipette. (**b**) All-point histograms of each set of recordings depicted in panel a. $[Ca^{2+}]_i$ elevation to 200 and 500 nM increased the number of peaks and reduced the frequency of the closed state while elevation to 1 µM had no effect. (**c**) Summary data illustrating the effect of various $[Ca^{2+}]_i$ levels on Q_m (n = 8). Gap26 (250 µM) significantly attenuated the Ca^{2+}-promoted Q_m (n =5); Gap27 had similar effects (data not shown). **p<0.01 *vs* 50 nM $[Ca^{2+}]_i$. #p< 0.05 *vs* 200 or 500 nM $[Ca^{2+}]_i$. (**d**) Effect of $[Ca^{2+}]_i$ elevation to 200 and 500 nM on the V_m dependence of HC activation (Q_m/V_m normalized to control value at +90 mV). The curve was left-shifted and this was completely prevented by Gap26 (250 µM, 150 s) and Gap27 (300 µM, 220 s) (n = 5). *p<0.05, **p<0.01 and ***p<0.001 for 200 or 500 nM $[Ca^{2+}]_i$ *vs* 50 nM $[Ca^{2+}]_i$.

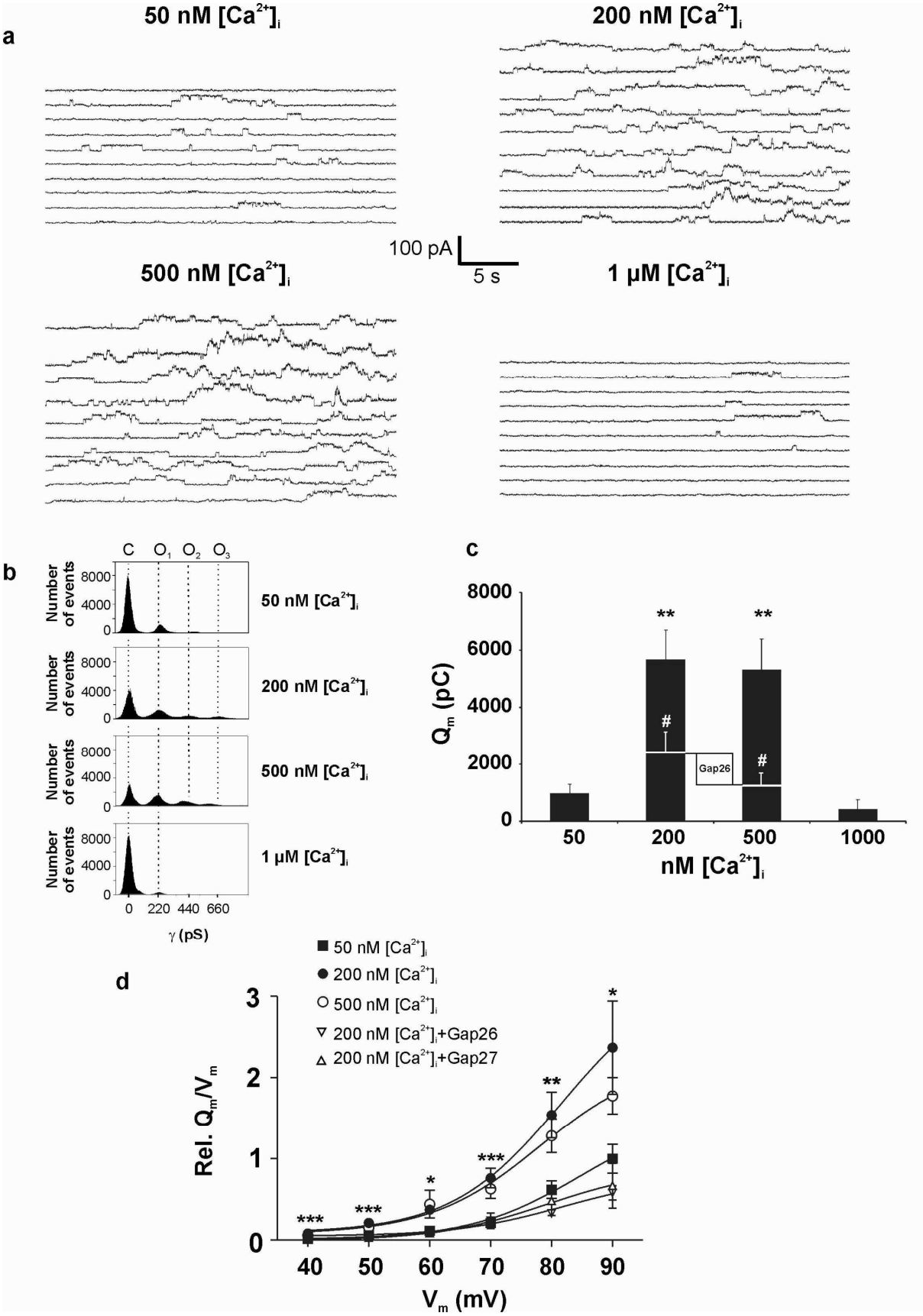
a
50 nM [Ca2+]i
200 nM [Ca2+]i
100 pA
5 s
500 nM [Ca2+]i
1 µM [Ca2+]i
b
C O1 O2 O3
Number of events
8000
4000
0
50 nM [Ca2+]i
200 nM [Ca2+]i
6000
500 nM [Ca2+]i
1 µM [Ca2+]i
0 220 440 660
γ (pS)
c
Qm (pC)
8000
6000
4000
2000
0
**
**
#
#
Gap26
50
200
500
1000
nM [Ca2+]i
d
50 nM [Ca2+]i
200 nM [Ca2+]i
500 nM [Ca2+]i
200 nM [Ca2+]i+Gap26
200 nM [Ca2+]i+Gap27
Rel. Qm/Vm
3
2
1
0
***
***
*
***
**
*
40
50
60
70
80
90
Vm (mV)

$[Ca^{2+}]_i$-dependent modulation is involved in acidification-induced Cx43 HC closure

Acidification is known to inhibit gap junction channels (Bukauskas and Verselis, 2004b;Palacios-Prado *et al.*, 2010b) and it has been suggested that this effect depends on a $[Ca^{2+}]_i$ elevation (Cotrina *et al.*, 1998;Lazrak and Peracchia, 1993b;Peracchia, 2004b). We further tested whether HCs close with pH lowering and whether a $[Ca^{2+}]_i$ increase is involved in this. Intracellular acidification from pH 7.2 to 6.4 induced by 2% CO_2 (Palacios-Prado *et al.*, 2010b) rapidly inhibited Cx43 HC unitary currents (Fig. 7a and b). Because pH_i lowering decreases the affinity of EGTA present in the pipette and cell, it is possible that inhibition is partly caused by an associated and prominent (> 500 nM) $[Ca^{2+}]_i$ elevation. Calculation of the expected $[Ca^{2+}]_i$ increase (making use of the Webmax program – see M&M) indeed indicated a micromolar increase of $[Ca^{2+}]_i$ in response to CO_2-induced pH lowering to 6.4. We therefore performed experiments with MES-buffered acidic pipette solutions with defined $[Ca^{2+}]$. When $[Ca^{2+}]_i$ was 50 nM, pH_i lowering to 6.4 or 6.0 did not inhibit HC currents (traces shown in Fig. 7c; summary data given in Fig. 7d). However, when $[Ca^{2+}]_i$ was set to 6 µM, HC currents were strongly inhibited by the pH 6.0 condition as they were at pH 7.2 (Fig. 7d). Thus, large $[Ca^{2+}]_i$ elevations can be involved in the low pH closure of Cx43 HCs. Of notice, Fig. 6c indicates that HC activity at 1 µM $[Ca^{2+}]_i$ is slightly lower than at 50 nM while Fig. 7d (first two bars) shows that HC activity is significantly depressed by further elevating $[Ca^{2+}]_i$ to 6 µM.

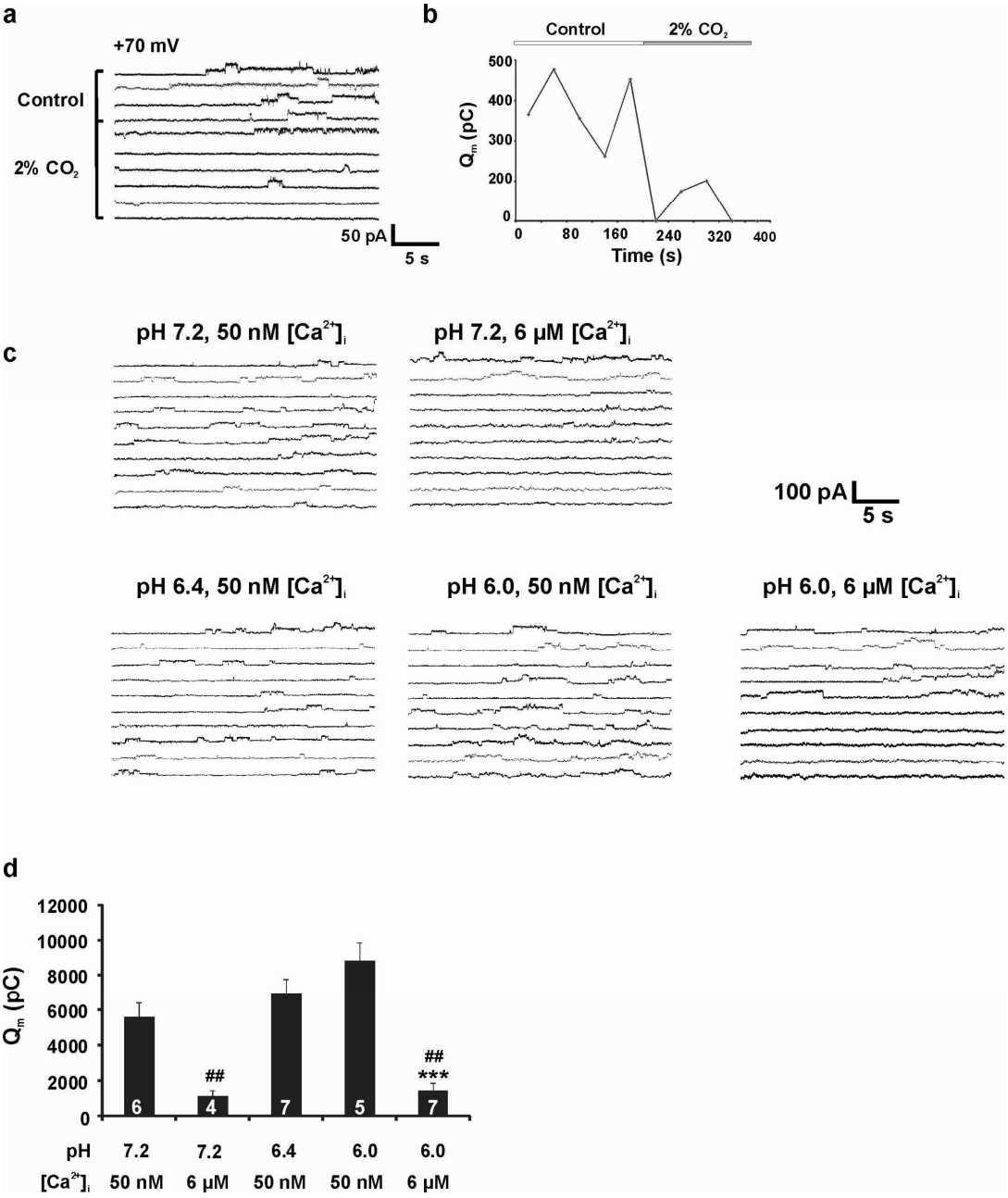

Figure 7. Role of $[Ca^{2+}]_i$ in acidification-induced Cx43 HC closure. (**a**) Intracellular acidification triggered by 2% CO_2 abolished HC unitary current activities in HeLa-Cx43. (**b**) Corresponding time evolution of single-channel activities of the experiment demonstrated in panel a. (**c**) Example unitary current traces recorded in HeLa-Cx43 cells under various pH_i $[Ca^{2+}]_i$ conditions as indicated. Voltage steps to +70 mV (30 s) were applied. Top-down current traces consist of 10 consecutive runs, each separated by 40 s. (**d**) Summary data of experiments as in panel c. At pH 7.2, 6 µM $[Ca^{2+}]_i$ strongly inhibited HC unitary activity compared to 50 nM $[Ca^{2+}]_i$. Acidosis (pH 6.4 and 6.0) did not significantly influence HC currents when $[Ca^{2+}]_i$ was 50 nM. However, pH 6.0 combined with 6 µM 50 nM strongly suppressed the currents. *** $p<0.01$ $[Ca^{2+}]_i$ = 6 µM (pH 6.0) *vs* $[Ca^{2+}]_i$ = 50 nM (pH 6.0). ## $p< 0.01$ $[Ca^{2+}]_i$ = 6 µM (pH 7.2 and 6.0) *vs* $[Ca^{2+}]_i$ = 50 nM (pH 7.2).

Gap26/27 inhibits $[Ca^{2+}]_i$-dependent modulation of Cx43 HC unitary currents in ventricular cardiomyocytes

In a next step, we examined whether we could reproduce the modulation of Cx43 HC opening by $[Ca^{2+}]_i$ and Gap26/27 measured in HeLa transfectants with those obtained from primary cardiomyocytes, acutely isolated from the left ventricle of pigs. In these experiments, perfusion conditions were similar to those used for HeLa-Cx43 cells. Stepping the V_m from -70 mV to +80 mV demonstrated the appearance of unitary current events characterized by a γ_o of ~200 pS (Fig. 8a, left panel). These unitary current events were not influenced by a low concentration of carbenoxolone (20 µM) that is known to block Panx1 HCs but not Cx43 HCs (Bruzzone *et al.*, 2005) (Fig. 8a middle panel). Carbenoxolone at higher concentration (100 µM) acted inhibitory, as expected for Cx43 HCs (Fig. 8a, right panel). Western blot analysis (Online Resource Fig. S6) showed no Panx1 signal in ventricular cardiomyocytes, in line with a recent report by Penuela et al. (Penuela *et al.*, 2009a). Thus, the ~200 pS opening events are likely to be mediated by Cx43 HCs. To further confirm this, we used an siRNA approach to silence Cx43 expression: this led to ~50 % knockdown of Cx43 expression in cultured pig ventricular cardiomyocytes (Fig. 8b). Unitary current activities were present in MOCK-treated cultured cardiomyocytes (Fig. 8c), although the activities were less frequent compared to those in acutely isolated cells. Histogram analysis indicated a γ_o of ~220 pS, which suggests that culturing of cardiomyocytes slightly increases the γ_o to the levels recorded in cultured HeLa-Cx43 cells. The bar chart in Fig. 8c summarizes average Q_m data, demonstrating that current activity was significantly inhibited by siRNA directed against Cx43 (siCx43) while scrambled siRNA ($siCx43^{scr}$) had no effect. We next tested the effect of $[Ca^{2+}]_i$ elevation and Gap26/27 on unitary HC current activity in freshly isolated cardiomyocytes. Fig. 8d shows that a $[Ca^{2+}]_i$ increase from 50 to 500 nM reduced the voltage threshold for HC opening from +60 mV to +40 mV. Furthermore, we found that Gap26 (160 µM, 5 min) reduced the Ca^{2+}-mediated enhancement of unitary current activity in a similar fashion as it was observed in HeLa-Cx43 cells (Fig. 8e). Average Q_m data (Fig. 8f) obtained from such cardiomyocyte recordings, demonstrated strong inhibition of Ca^{2+}-potentiated Cx43 HC activity by Gap26 (160 µM, 5 min) and Gap27 (200 µM, 5 min).

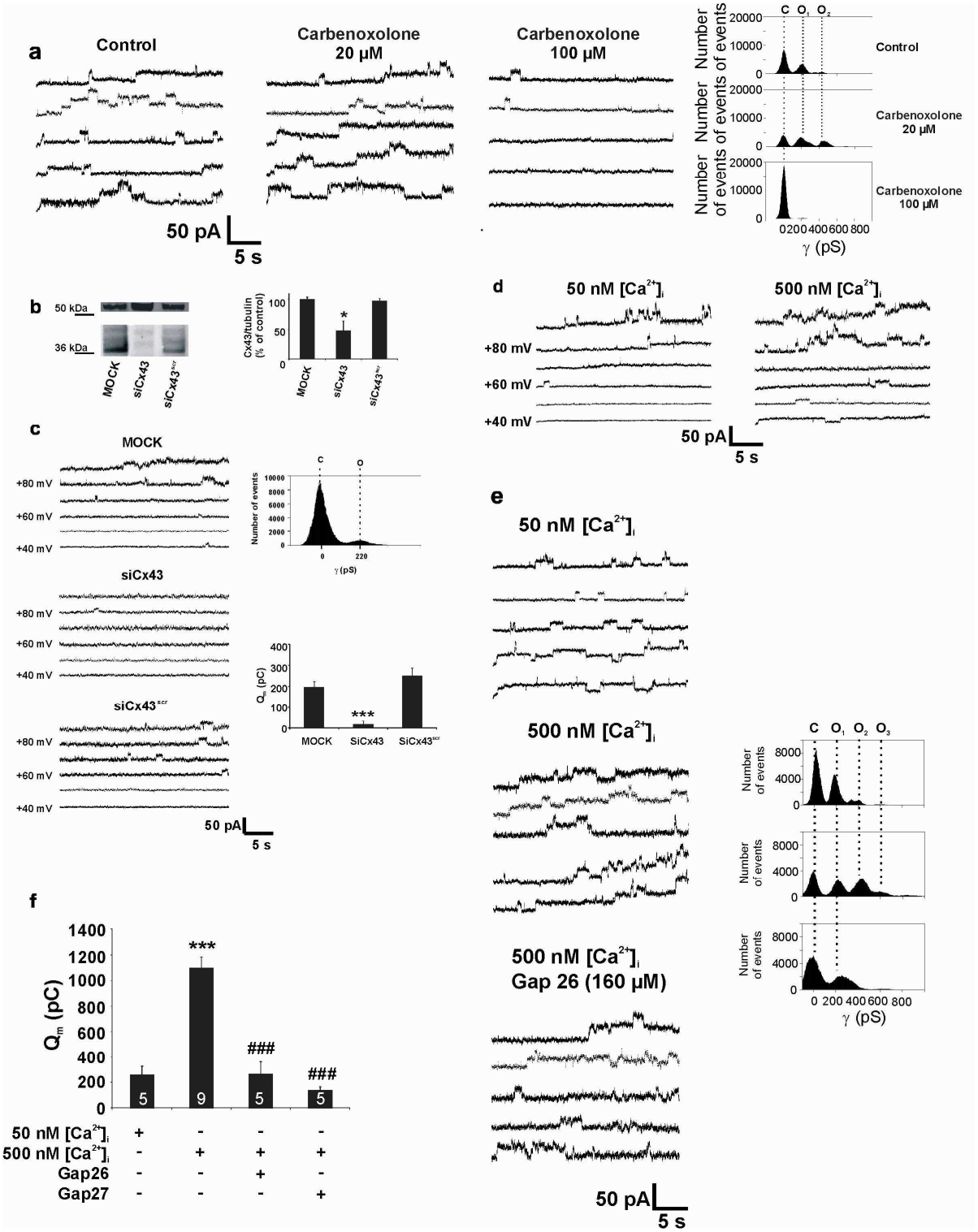
a
Control
Carbenoxolone 20 µM
Carbenoxolone 100 µM
50 pA
5 s
C O1 O2
Number of events
Control
Carbenoxolone 20 µM
Carbenoxolone 100 µM
γ (pS)
b
50 kDa
36 kDa
MOCK
siCx43
siCx43scr
Cx43/tubulin (% of control)
c
MOCK
siCx43
siCx43scr
+80 mV
+60 mV
+40 mV
Number of events
γ (pS)
Qm (pC)
MOCK
SiCx43
SiCx43scr
d
50 nM [Ca2+]i
500 nM [Ca2+]i
e
50 nM [Ca2+]i
500 nM [Ca2+]i
500 nM [Ca2+]i
Gap 26 (160 µM)
C O1 O2 O3
f
Qm (pC)
50 nM [Ca2+]i
500 nM [Ca2+]i
Gap26
Gap27

Figure 8. Effect of $[Ca^{2+}]_i$ elevation and Gap26/27 on unitary current activities in isolated pig ventricular cardiomyocytes. (**a**) Representative traces illustrating single-channel events triggered by stepping V_m to +80 mV. The all-point histograms at the right illustrate that the distribution peaks are separated by a γ_o of ~200 pS. Carbenoxolone had no effect when applied at 20 µM but clearly inhibited the currents at 100 µM. (**b**) Treatment of cultured ventricular cardiomyocytes with siRNA directed against Cx43 (siCx43) brought down Cx43 expression to 50 % of control (MOCK) while scrambled siRNA ($siCx43^{scr}$) had no effect. *p<0.05 siCx43 *vs* $siCx43^{scr}$ and MOCK. (**c**) Example traces depicting unitary currents recorded in MOCK-, siCx43- and $siCx43^{scr}$-treated cells. The bar chart summarizes average data for Cx43 HC currents activated at +70 mV (MOCK: n = 3; siCx43: n =9; $siCx43^{scr}$: n =6). All-point histogram depicting the γ_o of the unitary current activities recorded in cultured cardiomyocytes treated with siCx43scr and MOCK, *** p< 0.001 siCx43 vs MOCK and $siCx43^{scr}$ (**d**) Elevating $[Ca^{2+}]_i$ to 500 nM resulted in increased activity and a lowered V_m for channel activation. (**e**) Unitary current events triggered by V_m steps to +60 mV (30 s) were potentiated by 500 nM $[Ca^{2+}]_i$ and the increased activity was inhibited by Gap26 (160 µM, 5 min). The beginning of each trace is separated by 35 s. The all-point histograms at the right illustrate the effect on conductance distributions. (**f**) Average data of $[Ca^{2+}]_i$ and Gap26/27 effects on Q_m. $[Ca^{2+}]_i$ elevation to 500 nM strongly and significantly increased Q_m and this effect was completely prevented by Gap26 (160 µM, 5 min) and Gap27 (200 µM, 5 min). ***p<0.001 *vs* 50 nM $[Ca^{2+}]_i$; ###p<0.001 *vs* 500 nM $[Ca^{2+}]_i$ without peptides.

Discussion

Gap26/27 and related peptides, have been reported to inhibit HC-related ATP and dye uptake (Braet *et al.*, 2003b;Pollok *et al.*, 2011;Robertson *et al.*, 2010;Shintani-Ishida *et al.*, 2007a) and have been frequently applied to interfere with HC function under various conditions (De Bock M. *et al.*, 2011;Eltzschig *et al.*, 2006;O'Carroll *et al.*, 2008;Oviedo-Orta *et al.*, 2010;Pearson *et al.*, 2005b;Verma *et al.*, 2009). Macroscopic current studies have been inconclusive, with some reports showing inhibition by Gap26/27 (Hawat *et al.*, 2010a;Romanov *et al.*, 2008a) and others claiming that inhibition is related to non-specific pore block (Wang *et al.*, 2007a). Here, we demonstrate at single channel level that these peptides inhibit function of Cx43 HCs and that this effect is sequence specific. Moreover, we show that the peptides also inhibit Cx43 HC openings in acutely isolated ventricular cardiomyocytes, including HC currents promoted by moderate ($\leq$ 500 nM) $[Ca^{2+}]_i$ elevation. Interestingly, the Ca^{2+}-mediated potentiation of HC function indicates that Cx43 HCs can be opened at physiologically relevant V_m (+40 mV) and Gap26/27 antagonizes this Ca^{2+}-promoted HC opening.

Inhibition of HC currents by Gap26/27 occurring over a time span of minutes was incomplete and not associated with alterations in single channel conductance or number of unapposed HCs in the plasma membrane. Currently, the mechanisms as to how CxMPs inhibit the function of HCs are not known. We assume that Gap26/27 peptides bind to as yet undefined domains in the extracellular loops of Cx43 resulting in HC inhibition (Berthoud *et al.*, 2000).

For Gap26, evidence is available that this peptide indeed interacts with the extracellular Cx43 domains (Liu *et al.*, 2006a). If CxMPs inhibit HCs by interacting with freely accessible, unoccupied extracellular domains of Cx43, then the inhibition kinetics in duration of minutes appears to be slow. In fact, this suggests that the interaction site is less accessible than hypothesized, either as a consequence of being located deeper in the channel pore or being only accessible when the channel is open. We demonstrate that Gap26/27 reduces HC opening by shifting the V_m dependence of opening to more positive voltages (right-shift). This may be mediated by the shielding of a charged amino acid residue, as a consequence of the interaction, that changes the local electrical field sensed by the voltage-sensor and alters the activation threshold, as has been suggested for the shift in voltage-dependence of Na^+ and K^+ channels by a variety of stimuli (Thibault *et al.*, 1993;Zhang *et al.*, 1999).

Millimolar extracellular Ca^{2+} concentrations normally keep Cx43 HCs closed but when extracellular Ca^{2+} decreases, for example during ischemia (Silver and Erecinska, 1990), HCs open and HC currents at positive V_m are promoted (Contreras *et al.*, 2003b). It has been proposed that divalent cations such as Ca^{2+} and Mg^{2+} influence the intrinsic voltage-gating and lock the channel in the closed state by interacting with the extracellular side of the channel (Verselis and Srinivas, 2008b). We found that Gap27 inhibited the passage of the fluorescent dye calcein triggered by exposure to nominally Ca^{2+}- and Mg^{2+}-free extracellular conditions. Thus, CxMPs inhibit currents equally well as the passage of larger molecules through Cx43 HCs.

In addition to extracellular Ca^{2+} also intracellular Ca^{2+} modulates Cx43 HC function. Here, we show that a moderate increase of $[Ca^{2+}]_i$ promotes HC unitary current activity while this effect disappears upon further elevation to 1 µM (Fig. 6c), as reported in previous studies based on dye transfer or ATP release (De Vuyst *et al.*, 2006;Ponsaerts *et al.*, 2010a). These indirect measurements of HC opening have suggested that increased HC opening with moderate $[Ca^{2+}]_i$ elevation is dependent on Ca^{2+}-calmodulin signaling (De Vuyst *et al.*, 2009b); Cx43 contains several putative calmodulin binding sites located on the amino terminus and cytoplasmic loop (Torok *et al.*, 1997;Zhou *et al.*, 2007b). We further demonstrate here that increasing $[Ca^{2+}]_i$ to micromolar concentrations not only removes the $[Ca^{2+}]_i$-promotion effect (1 µM) but also actively inhibits HC opening at 6 µM (Fig. 7d). Apparently, this inhibitory effect also plays a role in the low pH closure of HCs. It is very much likely that the transient nature of hemichannel opening reported in *in vitro* simulated

ischemia, is caused by the dual effects (stimulation *versus* inhibition) of $[Ca^{2+}]_i$ on Cx43 HC opening (Shintani-Ishida *et al.*, 2007a). Interestingly, the HC-stimulation by moderate $[Ca^{2+}]_i$ elevation was related to a left-shift of the V_m dependence and this shift along the voltage axis was completely reversed by Gap26/27. Thus, Gap26/27 peptides inhibit HC function by interacting with extracellular domains of Cx43, while $[Ca^{2+}]_i$ potentiates HC function by interacting with intracellular Cx43 domains, both influences possibly acting on a common target that is the voltage sensor (Bukauskas *et al.*, 2002b;Harris, 2002b). While HCs are activated from +40 mV on in the presence of a moderate $[Ca^{2+}]_i$ increase, Online Resource Fig. S7 clearly demonstrates that unitary currents appear at +30 mV upon exposure to chemical ischemia conditions applied by metabolic inhibition. These potentials can realistically be attained during the plateau phase of the cardiac action potential.

In the heart, Cx43, predominantly expressed in ventricular cardiomyocytes, is an important determinant of myocardial ischemic injury (Ruiz-Meana *et al.*, 2008). Cx43 proteins form gap junction channels that are clustered in the nexus, which is one of major components of the intercalated disks. Non-junctional (unapposed) Cx43 HCs reside in the zone surrounding the junctional nexus area, called the perinexus (Rhett *et al.*, 2011b). As discussed above, Cx43 HC opening may be triggered under ischemic conditions (Contreras *et al.*, 2002a;Schulz *et al.*, 2003;Shintani-Ishida *et al.*, 2007a), and this has been associated with cardiomyocyte cell swelling in response to simulated ischemia (Schulz *et al.*, 2007a). When exposed to metabolic inhibition, rabbit ventricular myocytes have also been reported to display a $[Ca^{2+}]_i$-dependent non-selective current which may be attributed to Cx43 HC opening (Kondo *et al.*, 2000a). Here, we demonstrate, for the first time, unitary currents in acutely isolated left ventricular cardiomyocytes from pig, that are characterized by an activation threshold ≥ +50 mV and a single channel conductance of ~200 pS. These biophysical properties are similar to those of mouse Cx43 HCs observed in HeLa transfectants (≥ +50 mV, ~220 pS). Moreover, the unitary current activity was also promoted by moderate $[Ca^{2+}]_i$ elevation and was inhibited by Gap26 and Gap27. A recent study has proposed Panx1 HCs as the conductance pathway exhibiting large unitary conductance and $[Ca^{2+}]_i$-dependent currents in cultured atrial cardiomyocytes from rat (Kienitz *et al.*, 2011a). Panx1 HCs can, however, be ruled out based on the following arguments: i) Panx1 proteins could not be detected in acutely isolated pig left ventricular cardiomyocytes, ii) the recorded unitary currents were not affected by 20 µM carbenoxolone which is known to inhibit Panx1 HCs and iii) a specific siRNA targeting Cx43 abolished the single channel activities. An absence of Panx1 expression and therefore of

Panx1 HC function in cardiomyocytes used in our studies may be related to differences in cell preparation (acutely isolated cells *versus* cultured cells), differences in tissue types (ventricles *versus* atrium) and species (pig *versus* rat).

In summary, our data show that Cx43 HCs in ventricular cardiomyocytes can be activated by positive V_m ($\geq$ +30 mV) and $[Ca^{2+}]_i$ elevation (~500 nM). As a consequence, this may cause a leakage of ions and metabolites that may reduce excitability, safety of signal transfer between the cardiomyocytes and contribute to arrhythmogenesis. Gap26 and Gap27 inhibit these V_m/Ca^{2+}-mediated HC currents and thus open a new pathway for novel therapeutic approaches in treating cardiac arrhythmia.

Acknowledgements

We express our gratitude to Dr. R. Ponsaerts for designing the siRNA duplex. This work was supported by the Interuniversity Attraction Poles Program (Belgian Science Policy Project P6/31 to L. Leybaert), the Fund for Scientific Research Flanders (FWO grant numbers G.0140.08, 3G.0134.09 and G.0298.11 to L. Leybaert) and supported by NIH Grants (R01NS072238 and RO1HL084464 to F.F. Bukauskas).

References

Anselmi F, Hernandez VH, Crispino G, Seydel A, Ortolano S, Roper SD, Kessaris N, Richardson W, Rickheit G, Filippov MA, Monyer H, Mammano F (2008) ATP release through connexin hemichannels and gap junction transfer of second messengers propagate Ca2+ signals across the inner ear. *Proc Natl Acad Sci U S A,* **105**, 18770-18775.

Bao X, Altenberg GA, Reuss L (2004) Mechanism of regulation of the gap junction protein connexin 43 by protein kinase C-mediated phosphorylation. *Am J Physiol Cell Physiol*, **286**, C647-C654.

Berthoud VM, Beyer EC, Seul KH (2000) Peptide inhibitors of intercellular communication. *Am J Physiol Lung Cell Mol Physiol*, **279**, L619-L622.

Boitano S, Evans WH (2000) Connexin mimetic peptides reversibly inhibit Ca(2+) signaling through gap junctions in airway cells. *Am J Physiol Lung Cell Mol Physiol*, **279**, L623-L630.

Braet K, Vandamme W, Martin PE, Evans WH, Leybaert L (2003) Photoliberating inositol-1,4,5-trisphosphate triggers ATP release that is blocked by the connexin mimetic peptide gap 26. *Cell Calcium,* **33**, 37-48.

Bruzzone R, Barbe MT, Jakob NJ, Monyer H (2005) Pharmacological properties of homomeric and heteromeric pannexin hemichannels expressed in Xenopus oocytes. *J Neurochem*, **92**, 1033-1043.

Bukauskas FF, Bukauskiene A, Verselis VK (2002) Conductance and permeability of the residual state of connexin43 gap junction channels. *J Gen Physiol*, **119**, 171-185.

Bukauskas FF, Verselis VK (2004) Gap junction channel gating. *Biochim Biophys Acta,* **1662**, 42-60.

Chaytor AT, Evans WH, Griffith TM (1997) Peptides homologous to extracellular loop motifs of connexin 43 reversibly abolish rhythmic contractile activity in rabbit arteries. *J Physiol,* **503** (Pt 1), 99-110.

Clarke TC, Williams OJ, Martin PE, Evans WH (2009) ATP release by cardiac myocytes in a simulated ischaemia model: inhibition by a connexin mimetic and enhancement by an antiarrhythmic peptide. *Eur J Pharmacol*, **605**, 9-14.

Contreras JE, Saez JC, Bukauskas FF, Bennett MV (2003) Gating and regulation of connexin 43 (Cx43) hemichannels. *Proc Natl Acad Sci U S A,* **100**, 11388-11393.

Contreras JE, Sanchez HA, Eugenin EA, Speidel D, Theis M, Willecke K, Bukauskas FF, Bennett MV, Saez JC (2002) Metabolic inhibition induces opening of unapposed connexin 43 gap junction hemichannels and reduces gap junctional communication in cortical astrocytes in culture. *Proc Natl Acad Sci U S A,* **99**, 495-500.

Cotrina ML, Kang J, Lin JH, Bueno E, Hansen TW, He L, Liu Y, Nedergaard M (1998) Astrocytic gap junctions remain open during ischemic conditions. *J Neurosci*, **18**, 2520-2537.

De Bock M., Culot M, Wang N, Bol M, Decrock E, De Vuyst E., da Costa A, Dauwe I, Vinken M, Simon AM, Rogiers V, De LG, Evans WH, Bultynck G, Dupont G, Cecchelli R, Leybaert L (2011) Connexin channels provide a target to manipulate brain endothelial calcium dynamics and blood-brain barrier permeability. *J Cereb Blood Flow Metab,* **31**, 1942-1957.

De Vuyst E., Decrock E, Cabooter L, Dubyak GR, Naus CC, Evans WH, Leybaert L (2006) Intracellular calcium changes trigger connexin 32 hemichannel opening. *EMBO J*, **25**, 34-44.

De Vuyst E, Wang N, Decrock E, De Bock M, Vinken M, Van Moorhem M, Lai C, Culot M, Rogiers V, Cecchelli R, Naus CC, Evans WH, Leybaert L (2009) Ca(2+) regulation of connexin 43 hemichannels in C6 glioma and glial cells. *Cell Calcium*, **46**, 176-187.

Decrock E, DeVuyst E, Vinken M, Van Moorhem M, Vranckx K, Wang N, Van Laeken L, De Bock M, D'Herde K, Lai CP, Rogiers V, Evans WH, Naus CC, Leybaert L (2009) Connexin 43 hemichannels contribute to the propagation of apoptotic cell death in a rat C6 glioma cell model. *Cell Death Differ*, **16**, 151-163.

Elfgang C, Eckert R, Lichtenberg-Frate H, Butterweck A, Traub O, Klein RA, Hulser DF, Willecke K (1995) Specific permeability and selective formation of gap junction channels in connexin-transfected HeLa cells. *J Cell Biol*, **129**, 805-817.

Eltzschig HK, Eckle T, Mager A, Kuper N, Karcher C, Weissmuller T, Boengler K, Schulz R, Robson SC, Colgan SP (2006) ATP release from activated neutrophils occurs via connexin 43 and modulates adenosine-dependent endothelial cell function. *Circ Res*, **99**, 1100-1108.

Evans WH, Boitano S (2001) Connexin mimetic peptides: specific inhibitors of gap-junctional intercellular communication. *Biochem Soc Trans*, **29**, 606-612.

Evans WH, Carlile G, Rahman S, Torok K (1992) Gap junction communication channel: peptides and anti-peptide antibodies as structural probes. *Biochem Soc Trans*, **20**, 856-861.

Goodenough DA, Goliger JA, Paul DL (1996) Connexins, connexons, and intercellular communication. *Annu Rev Biochem*, **65**, 475-502.

Harris AL (2002) Voltage-sensing and substate rectification: moving parts of connexin channels. *J Gen Physiol*, **119**, 165-169.

Hawat G, Benderdour M, Rousseau G, Baroudi G (2010) Connexin 43 mimetic peptide Gap26 confers protection to intact heart against myocardial ischemia injury. *Pflugers Arch*, **460**, 583-592.

Hawat G, Helie P, Baroudi G (2012) Single intravenous low-dose injections of connexin 43 mimetic peptides protect ischemic heart in vivo against myocardial infarction. *J Mol Cell Cardiol*, **53**, 559-566.

Johansen D, Cruciani V, Sundset R, Ytrehus K, Mikalsen SO (2011) Ischemia Induces Closure of Gap Junctional Channels and Opening of Hemichannels in Heart-derived Cells and Tissue. *Cell Physiol Biochem*, **28**, 103-114.

Kang J, Kang N, Lovatt D, Torres A, Zhao Z, Lin J, Nedergaard M (2008) Connexin 43 hemichannels are permeable to ATP. *J Neurosci,* **28**, 4702-4711.

Karpuk N, Burkovetskaya M, Fritz T, Angle A, Kielian T (2011) Neuroinflammation leads to region-dependent alterations in astrocyte gap junction communication and hemichannel activity. *J Neurosci,* **31**, 414-425.

Kienitz MC, Bender K, Dermietzel R, Pott L, Zoidl G (2011) Pannexin 1 constitutes the large conductance cation channel of cardiac myocytes. *J Biol Chem*, **286**, 290-298.

Kim DY, Kam Y, Koo SK, Joe CO (1999) Gating connexin 43 channels reconstituted in lipid vesicles by mitogen-activated protein kinase phosphorylation. *J Biol Chem*, **274**, 5581-5587.

Kondo RP, Wang SY, John SA, Weiss JN, Goldhaber JI (2000) Metabolic inhibition activates a non-selective current through connexin hemichannels in isolated ventricular myocytes. *J Mol Cell Cardiol,* **32**, 1859-1872.

Lazrak A, Peracchia C (1993) Gap junction gating sensitivity to physiological internal calcium regardless of pH in Novikoff hepatoma cells. *Biophys J*, **65**, 2002-2012.

Lewandowski R, Procida K, Vaidyanathan R, Coombs W, Jalife J, Nielsen MS, Taffet SM, Delmar M (2008) RXP-E: a connexin43-binding peptide that prevents action potential propagation block. *Circ Res*, **103**, 519-526.

Li F, Sugishita K, Su Z, Ueda I, Barry WH (2001) Activation of connexin-43 hemichannels can elevate [Ca(2+)]i and [Na(+)]i in rabbit ventricular myocytes during metabolic inhibition. *J Mol Cell Cardiol,* **33**, 2145-2155.

Liu F, Arce FT, Ramachandran S, Lal R (2006) Nanomechanics of hemichannel conformations: connexin flexibility underlying channel opening and closing. *J Biol Chem*, **281**, 23207-23217.

Martin PE, Wall C, Griffith TM (2005) Effects of connexin-mimetic peptides on gap junction functionality and connexin expression in cultured vascular cells. *Br J Pharmacol*, **144**, 617-627.

Matsuyama D, Kawahara K (2009) Proliferation of neonatal cardiomyocytes by connexin43 knockdown via synergistic inactivation of p38 MAPK and increased expression of FGF1. *Basic Res Cardiol*, **104**, 631-642.

O'Carroll SJ, Alkadhi M, Nicholson LF, Green CR (2008) Connexin 43 mimetic peptides reduce swelling, astrogliosis, and neuronal cell death after spinal cord injury. *Cell Commun Adhes*, **15**, 27-42.

Orellana JA, Saez PJ, Shoji KF, Schalper KA, Palacios-Prado N, Velarde V, Giaume C, Bennett MV, Saez JC (2009) Modulation of brain hemichannels and gap junction channels by pro-inflammatory agents and their possible role in neurodegeneration. *Antioxid Redox Signal*, **11**, 369-399.

Orellana JA, Shoji KF, Abudara V, Ezan P, Amigou E, Saez PJ, Jiang JX, Naus CC, Saez JC, Giaume C (2011) Amyloid beta-induced death in neurons involves glial and neuronal hemichannels. *J Neurosci,* **31**, 4962-4977.

Oviedo-Orta E, Perreau M, Evans WH, Potolicchio I (2010) Control of the proliferation of activated CD4+ T cells by connexins. *J Leukoc Biol*, **88**, 79-86.

Palacios-Prado N, Briggs SW, Skeberdis VA, Pranevicius M, Bennett MV, Bukauskas FF (2010) pH-dependent modulation of voltage gating in connexin45 homotypic and connexin45/connexin43 heterotypic gap junctions. *Proc Natl Acad Sci U S A*, **107**, 9897-9902.

Pearson RA, Dale N, Llaudet E, Mobbs P (2005) ATP released via gap junction hemichannels from the pigment epithelium regulates neural retinal progenitor proliferation. *Neuron*, **46**, 731-744.

Penuela S, Bhalla R, Nag K, Laird DW (2009) Glycosylation regulates pannexin intermixing and cellular localization. *Mol Biol Cell*, **20**, 4313-4323.

Peracchia C (2004) Chemical gating of gap junction channels; roles of calcium, pH and calmodulin. *Biochim Biophys Acta*, **1662**, 61-80.

Pollok S, Pfeiffer AC, Lobmann R, Wright CS, Moll I, Martin PE, Brandner JM (2011) Connexin 43 mimetic peptide Gap27 reveals potential differences in the role of Cx43 in wound repair between diabetic and non-diabetic cells. *J Cell Mol Med*, **15**, 861-873.

Ponsaerts R, De Vuyst E, Retamal M, D'hondt C, Vermeire D, Wang N, De Smedt H, Zimmermann P, Himpens B, Vereecke J, Leybaert L, Bultynck G (2010) Intramolecular loop/tail interactions are essential for connexin 43-hemichannel activity. *FASEB J*, **24**, 4378-4395.

Ramanan SV, Brink PR (1993) Multichannel recordings from membranes which contain gap junctions. II. Substates and conductance shifts. *Biophys J*, **65**, 1387-1395.

Retamal MA, Cortes CJ, Reuss L, Bennett MV, Saez JC (2006) S-nitrosylation and permeation through connexin 43 hemichannels in astrocytes: induction by oxidant stress and reversal by reducing agents. *Proc Natl Acad Sci U S A,* **103**, 4475-4480.

Retamal MA, Schalper KA, Shoji KF, Bennett MV, Saez JC (2007) Opening of connexin 43 hemichannels is increased by lowering intracellular redox potential. *Proc Natl Acad Sci U S A*, **104**, 8322-8327.

Rhett JM, Jourdan J, Gourdie RG (2011) Connexin 43 connexon to gap junction transition is regulated by zonula occludens-1. *Mol Biol Cell*, **22**, 1516-1528.

Robertson J, Lang S, Lambert PA, Martin PE (2010) Peptidoglycan derived from Staphylococcus epidermidis induces Connexin43 hemichannel activity with consequences on the innate immune response in endothelial cells. *Biochem J*, **432**, 133-143.

Romanov RA, Rogachevskaja OA, Khokhlov AA, Kolesnikov SS (2008) Voltage dependence of ATP secretion in mammalian taste cells. *J Gen Physiol*, **132**, 731-744.

Ruiz-Meana M, Rodriguez-Sinovas A, Cabestrero A, Boengler K, Heusch G, Garcia-Dorado D (2008) Mitochondrial connexin43 as a new player in the pathophysiology of myocardial ischaemia-reperfusion injury. *Cardiovasc Res*, **77**, 325-333.

Samoilova M, Wentlandt K, Adamchik Y, Velumian AA, Carlen PL (2008) Connexin 43 mimetic peptides inhibit spontaneous epileptiform activity in organotypic hippocampal slice cultures. *Exp Neurol*, **210**, 762-775.

Sanchez HA, Orellana JA, Verselis VK, Saez JC (2009) Metabolic inhibition increases activity of connexin-32 hemichannels permeable to Ca2+ in transfected HeLa cells. *Am J Physiol Cell Physiol,* **297**, C665-C678.

Schalper KA, Palacios-Prado N, Retamal MA, Shoji KF, Martinez AD, Saez JC (2008) Connexin hemichannel composition determines the FGF-1-induced membrane permeability and free [Ca2+]i responses. *Mol Biol Cell*, **19**, 3501-3513.

Schalper KA, Sanchez HA, Lee SC, Altenberg GA, Nathanson MH, Saez JC (2010) Connexin 43 hemichannels mediate the Ca2+ influx induced by extracellular alkalinization. *Am J Physiol Cell Physiol*, **299**, C1504-C1515.

Schulz R, Boengler K, Totzeck A, Luo Y, Garcia-Dorado D, Heusch G (2007) Connexin 43 in ischemic pre- and postconditioning. *Heart Fail Rev*, **12**, 261-266.

Schulz R, Gres P, Skyschally A, Duschin A, Belosjorow S, Konietzka I, Heusch G (2003) Ischemic preconditioning preserves connexin 43 phosphorylation during sustained ischemia in pig hearts in vivo. *FASEB J*, **17**, 1355-1357.

Shintani-Ishida K, Uemura K, Yoshida K (2007) Hemichannels in cardiomyocytes open transiently during ischemia and contribute to reperfusion injury following brief ischemia. *Am J Physiol Heart Circ Physiol*, **293**, H1714-H1720.

Silver IA, Erecinska M (1990) Intracellular and extracellular changes of [Ca2+] in hypoxia and ischemia in rat brain in vivo. *J Gen Physiol*, **95**, 837-866.

Stankovicova T, Szilard M, De S, I, Sipido KR (2000) M cells and transmural heterogeneity of action potential configuration in myocytes from the left ventricular wall of the pig heart. *Cardiovasc Res*, **45**, 952-960.

Thibault O, Porter NM, Landfield PW (1993) Low Ba2+ and Ca2+ induce a sustained high probability of repolarization openings of L-type Ca2+ channels in hippocampal neurons: physiological implications. *Proc Natl Acad Sci U S A*, **90**, 11792-11796.

Torok K, Stauffer K, Evans WH (1997) Connexin 32 of gap junctions contains two cytoplasmic calmodulin-binding domains. *Biochem J*, **326** (Pt 2), 479-483.

Verma V, Hallett MB, Leybaert L, Martin PE, Evans WH (2009) Perturbing plasma membrane hemichannels attenuates calcium signalling in cardiac cells and HeLa cells expressing connexins. *Eur J Cell Biol*, **88**, 79-90.

Verselis VK, Srinivas M (2008) Divalent cations regulate connexin hemichannels by modulating intrinsic voltage-dependent gating. *J Gen Physiol,* **132,** 315-327

Wang HZ, Day N, Valcic M, Hsieh K, Serels S, Brink PR, Christ GJ (2001) Intercellular communication in cultured human vascular smooth muscle cells. *Am J Physiol Cell Physiol*, **281**, C75-C88.

Wang J, Ma M, Locovei S, Keane RW, Dahl G (2007) Modulation of membrane channel currents by gap junction protein mimetic peptides: size matters. *Am J Physiol Cell Physiol, **293***, C1112-C1119.

Warner A, Clements DK, Parikh S, Evans WH, DeHaan RL (1995) Specific motifs in the external loops of connexin proteins can determine gap junction formation between chick heart myocytes. J Physiol 488 (Pt 3): 721-728.

Willecke K, Eiberger J, Degen J, Eckardt D, Romualdi A, Guldenagel M, Deutsch U, Sohl G (2002) Structural and functional diversity of connexin genes in the mouse and human genome. *Biol Chem,* **383**, 725-737.

Wright CS, van Steensel MA, Hodgins MB, Martin PE (2009) Connexin mimetic peptides improve cell migration rates of human epidermal keratinocytes and dermal fibroblasts in vitro. *Wound Repair Regen*, **17**, 240-249.

Ye ZC, Wyeth MS, Baltan-Tekkok S, Ransom BR (2003) Functional hemichannels in astrocytes: a novel mechanism of glutamate release. *J Neurosci*, **23**, 3588-3596.

Zhang Y, Hartmann HA, Satin J (1999) Glycosylation influences voltage-dependent gating of cardiac and skeletal muscle sodium channels. *J Membr Biol*, **171**, 195-207.

Zhou Y, Yang W, Lurtz MM, Ye Y, Huang Y, Lee HW, Chen Y, Louis CF, Yang JJ (2007) Identification of the calmodulin binding domain of connexin 43. *J Biol Chem,* **282**, 35005-35017

Supporting Information

Table S1. Overview of the peptides tested in the study.

Peptide	Sequence
Gap 26	VCYDKSFPISHVR
Gap27	SRPTEKTIFII
Scrambled Gap26	PSFDSRHCIVKYV
Scrambled Gap27	TFEPIRISITK

Fig. S1

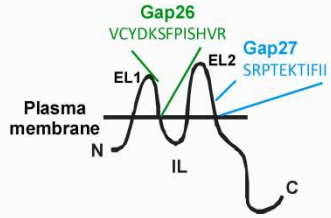

Fig. S2

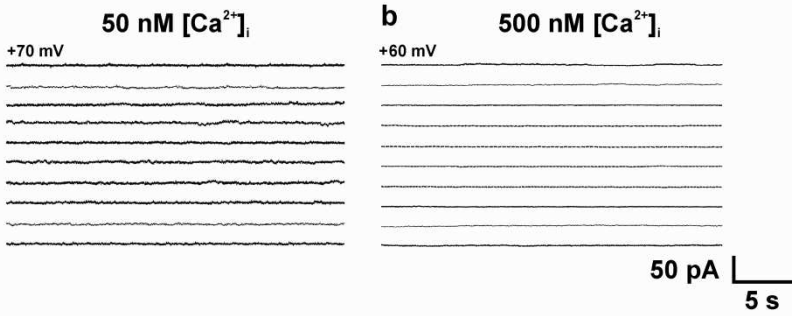

Fig. S3

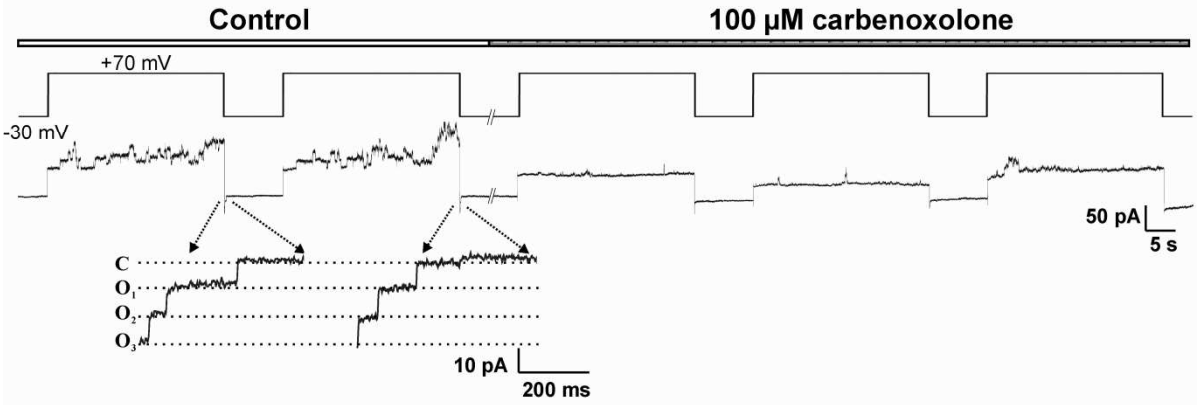

Fig. S4

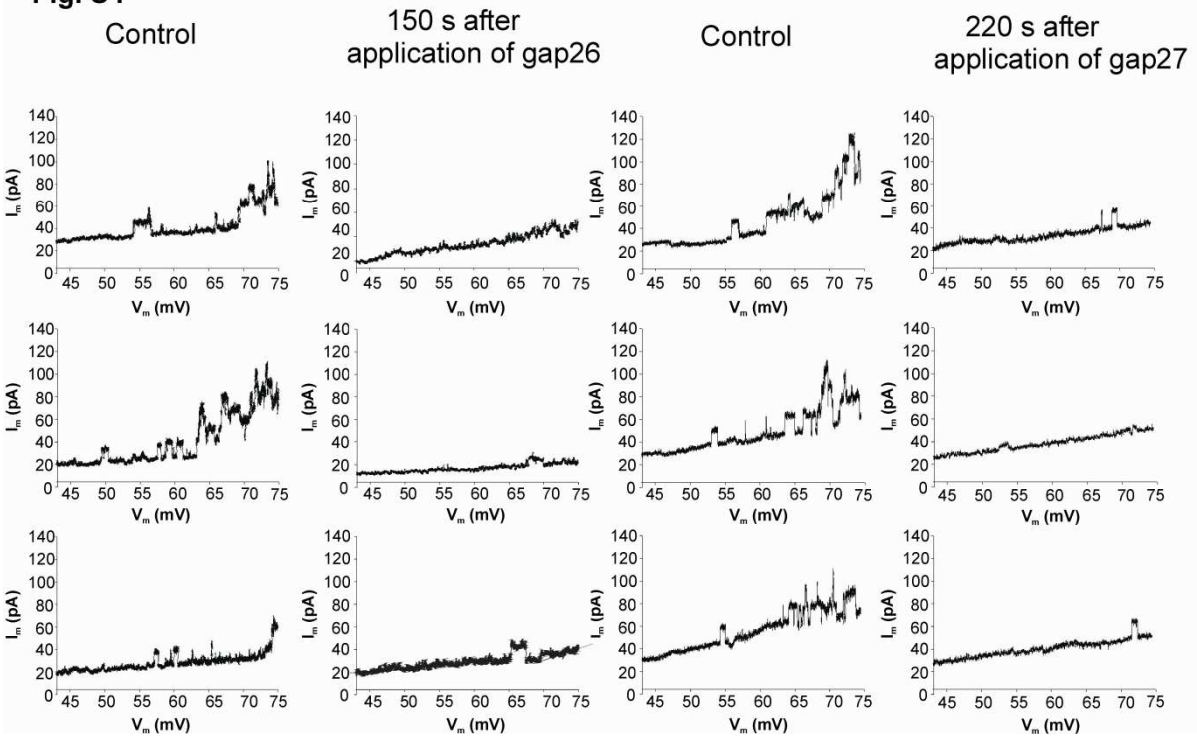

Fig. S5

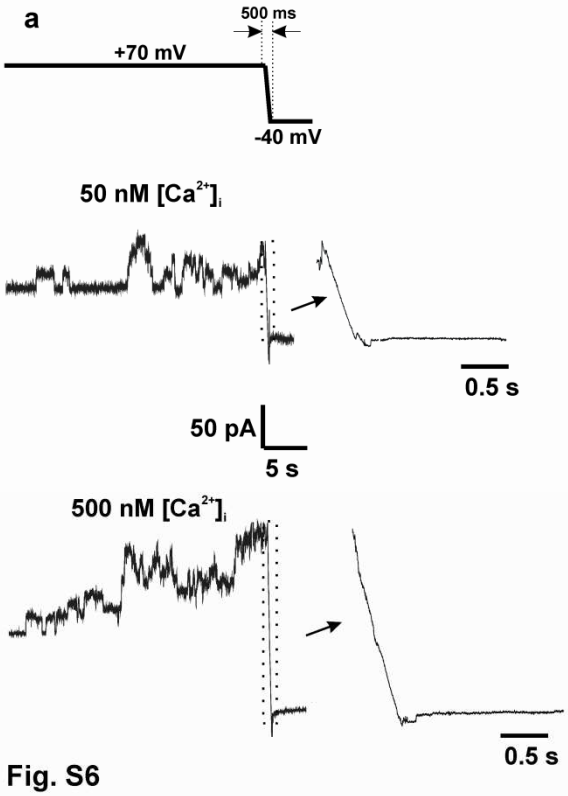

Fig. S6

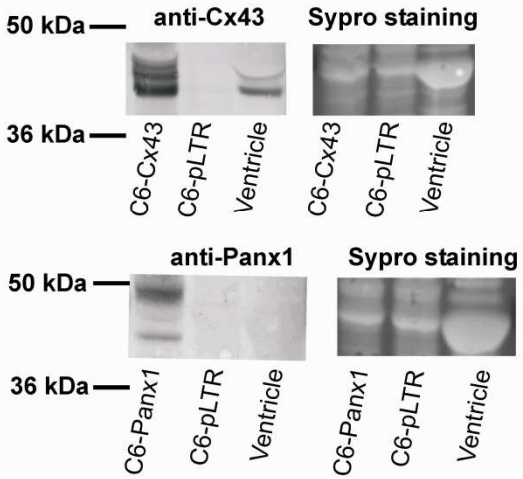

Fig. S7

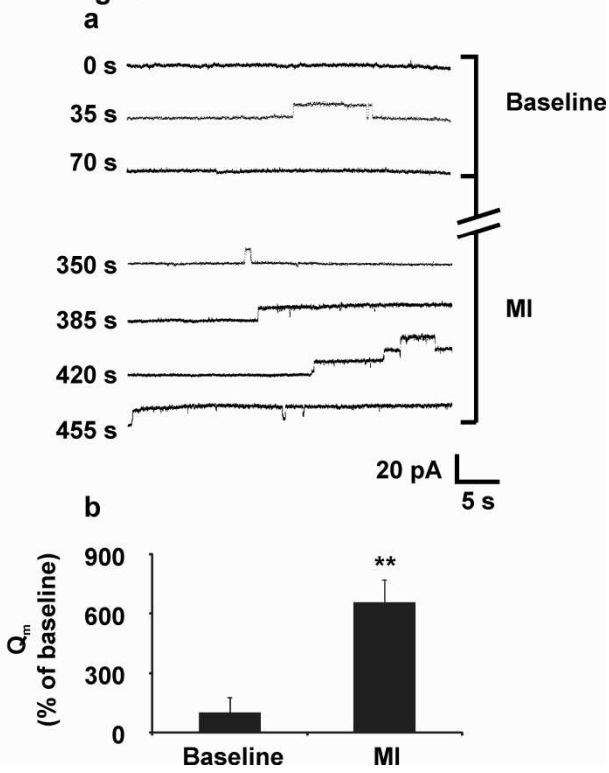

Figure S1. Topology of Cx43 protein showing the N-terminal (NT), the first and second extracellular loops (EL1 and EL2), intracellular loop (IL) and the C-terminal region (CT). Sequences of the Gap26/27 and the domains of Cx43 to which they correspond are also indicated.

Figure S2. HeLa-WT cells do not display unitary current activity. (**a)** Stepping V_m to +70 mV (30 s) did not induce any single channel openings when $[Ca^{2+}]_i$ was 50 nM. (**b**) No single channel openings were observed when $[Ca^{2+}]_i$ was 500 nM (V_m steps to +60 mV).

Figure S3. Example traces showing unitary current events triggered in HeLa-Cx43 cells by stepping V_m to +70 mV (30 s). The expanded traces below show closing of the channels upon switching back to -30 mV. The gap junction blocker carbenoxolone suppressed the unitary current activity.

Figure S4. Voltage ramp I-V plots in HeLa-Cx43 cells, illustrating that Gap26/27 inhibit unitary current activities, with the first unitary events appearing at +65 mV and above.

Figure S5. $[Ca^{2+}]_i$ changes had no influence on the reversal potential of hemichannels currents in HeLa-Cx43 cells. (**a**) V_m was stepped to +70 mV (30 s) to activate currents. This was followed by a fast ramp, repolarizing to -40 mV, applied to investigate the reversal potential of open HCs. Expanded traces show the region of the recording demarcated by dotted lines, illustrating current evolution during the fast ramp. (**b**) I-V plot of the fast repolarization currents, indicating a reversal potential of approximately zero mV for both 50 and 500 nM $[Ca^{2+}]_i$.

Figure S6. Western blot analysis illustrating Cx43 protein expression in pig ventricular cardiomyocytes. C6 glioma cells stably transfected with Cx43 (C6-Cx43) and cells transfected with empty vector alone (C6-pLTR) were used as positive and negative controls respectively. Panx1 protein was not detected in these cells. C6 glioma cells stably transfected with Panx1 (C6-Panx1) were used as a positive control condition.

Figure S7. Metabolic inhibition (MI) augments Cx43 HC unitary current activity in ventricular cardiomyocytes. (**a**) Typical traces recorded in a cardiomyocyte before and after exposure to mitochondrial uncoupler carbonyl cyanide p-trifluoromethoxyphenylhydrazone (5 µM) combined with the glycolysis inhibitor sodium iodoacetate (1 mM) (‘chemical ischemia). V_m was stepped from -70 to +30 mV for 30 s. Whole-cell currents at positive V_m were substantially increased in MI-treated cardiomyocytes. **(b**) Summary bar chart illustrating charge transfer (Q_m) before and 350 s after MI treatment (n =4). ** $p<0.01$ MI *vs* baseline.

Chapter IV. Selective inhibition of Cx43 hemichannels by Gap19 and its impact on myocardial ischemia/reperfusion injury

Nan Wang[1#], Elke De Vuyst[1#], Raf Ponsaerts[2#], Kerstin Boengler[3], Nicolás Palacios-Prado[4], Joris Wauman[5], Charles P. Lai[6], Marijke De Bock[1], Elke Decrock[1], Melissa Bol[1], Mathieu Vinken[7], Vera Rogiers[7], Jan Tavernier[5], W. Howard Evans[8], Christian C. Naus[9], Feliksas F. Bukauskas[4], Karin R. Sipido[10], Gerd Heusch[11], Rainer Schulz[3], Geert Bultynck[2$], and Luc Leybaert[1$]

[1]Department of Basic Medical Sciences - Physiology group, Faculty of Medicine and Health Sciences, Ghent University, Ghent, Belgium
[2]Laboratory of Molecular and Cellular Signaling - Department of Cellular and Molecular Medicine, Campus Gasthuisberg O/N-1 bus 802, K.U. Leuven, Leuven, Belgium
[3] Physiologisches Institut, Justus-Liebig Universität Giessen, Giessen, Germany
[4]Dominick P. Purpura Department of Neuroscience Department of Neuroscience, Albert Einstein College of Medicine, Bronx, NY, USA
[5]VIB Department of Medical Protein Research - Cytokine Receptor Laboratory, Faculty of Medicine and Health Sciences, Ghent University, Ghent, Belgium
[6]Departments of Neurology and Radiology, Massachusetts General Hospital, and Neuroscience Program, Harvard Medical School, Charlestown, MA, USA
[7]Department of Toxicology, Faculty of Medicine and Pharmacy, Vrije Universiteit Brussel, Brussels, Belgium
[8]Department of Medical Biochemistry and Immunology, Cardiff University School of Medicine, Cardiff, United Kingdom
[9]Department of Cellular and Physiological Sciences, Life Sciences Institute, Faculty of Medicine, University of British Columbia, Vancouver, BC, Canada
[10] Division of Experimental Cardiology, Department of Cardiovascular Diseases, Katholieke Universiteit Leuven, Belgium
[11] Institute for Pathophysiology, Universitätsklinikum Essen, Essen, Germany

[#]These authors contributed equally

[$]These authors share senior authorship

Published in Basic Res Cardiol. 108:309 (2013)

ABSTRACT

Connexin-43 (Cx43), a predominant cardiac connexin, forms gap junctions (GJs) that facilitate electrical cell-cell coupling and unapposed/nonjunctional hemichannels that provide a pathway for the exchange of ions and metabolites between cytoplasm and extracellular milieu. Uncontrolled opening of hemichannels in the plasma membrane may be deleterious for the myocardium and blocking hemichannels may confer cardioprotection by preventing ionic imbalance, cell swelling and loss of critical metabolites. Currently, all known hemichannel inhibitors also block GJ channels, thereby disturbing electrical cell-cell communication. Here, we aimed to characterize a nonapeptide, called Gap19, derived from the cytoplasmic loop (CL) of Cx43 as a hemichannel blocker and examined its effect on hemichannel currents in cardiomyocytes and its influence in cardiac outcome after ischemia/reperfusion. We report that Gap 19 inhibits Cx43 hemichannels without blocking GJ channels or Cx40/pannexin-1 hemichannels. Hemichannel inhibition is due to the binding of Gap19 to the C-terminus (CT) thereby preventing intramolecular CT-CL interactions. The peptide inhibited Cx43 hemichannel unitary currents in both HeLa cells exogenously expressing Cx43 and acutely isolated pig ventricular cardiomyocytes. Treatment with Gap19 prevented metabolic inhibition-enhanced hemichannel openings, protected cardiomyocytes against volume overload and cell death following ischemia/reperfusion *in vitro* and decreased the infarct size after myocardial ischemia/reperfusion in mice *in vivo*. In conclusion, preventing Cx43 hemichannel opening with Gap19 confers protective effects against myocardial ischemia/reperfusion injury.

Key word: connexin, hemichannel, gap junction, single channel, myocardial injury

INTRODUCTION

Gap junction (GJ) channels are essential for the function of the heart and blood vessels by providing electrical coupling and direct cell-cell transfer of chemical/metabolic signals (de Wit and Griffith, 2010;Jansen *et al.*, 2010b;Miura *et al.*, 2010;Veenstra and DeHaan, 1986). They are composed of two docked hemichannels (connexons) oligomerized from six connexin molecules. The 43-kDa connexin protein (Cx43) is a major connexin in the heart and is especially abundant in ventricular cardiomyocytes (Danik *et al.*, 2004). Aging and cardiac disease are associated with alterations in Cx43 expression, its localization and its phosphorylation status, and changes of GJ properties that, collectively, are thought to contribute to myocardial infarction injury and arrhythmogenesis (Kalcheva *et al.*, 2007a;Severs *et al.*, 2008b;Tribulova *et al.*, 2009). Beyond GJs, emerging evidence has suggested novel roles of Cx43 hemichannels in the diseased myocardium. These unapposed/nonjunctional hemichannels reside in the zone surrounding the GJ nexus area, called the perinexus (Rhett *et al.*, 2011c). They are typically closed under normal conditions, but may open in response to ischemic insults resulting in ATP leakage, excessive entry of Na^+ and Ca^{2+} and the loss of essential metabolites from the cells (Saez *et al.*, 2010). Uncontrolled activation of hemichannels may potentially introduce significant changes in cardiamyocyte homeostasis that are expected to cause dysfunction and finally irreversible injury. Currently, there are no tools available that allow selective targeting of hemichannels as all known pharmacological blockers inhibit both GJs and hemichannels (Evans *et al.*, 2006;Harris, 2001;Spray *et al.*, 2006). Furthermore, connexin knockout (KO) technology abolishes hemichannels as well as GJ channels, making this approach inappropriate to determine the role of hemichannels in cardiovascular disease.

Connexins are tetraspan membrane proteins that have two extracellular loops and one intracellular loop (CL). Synthetic peptides like Gap26 and Gap27 that mimic a short stretch of amino acids (AAs) on the extracellular loops have been introduced more than 15 years ago to inhibit GJs (Warner *et al.*, 1995b). These peptides are thought to interact with yet undefined sequence on the extracellular loops of the connexin protein, thereby preventing the docking of two hemichannels (Evans and Boitano, 2001b). Gap26 and Gap27 peptides also inhibit unapposed hemichannels (Wang *et al.*, 2012a); because the extracellular loops of unapposed hemichannels are unoccupied and freely available for interactions with these peptides, hemichannel inhibition often occurs before inhibition of GJs. Here, we report on a peptide,

called Gap19, that is identical to a short sequence present on the intracellular (cytoplasmic) loop of Cx43. Peptides mimicking cytoplasmic loop (CL) sequences have been used in the past as control peptides that do not inhibit GJs (Oviedo-Orta *et al.*, 2002a). In agreement, we found that Gap19 did not reduce GJ coupling as measured with dual whole-cell voltage-clamp and dye transfer assays. Surprisingly, Gap19 strongly inhibited plasma membrane Cx43 hemichannels as exemplified by ATP release/dye uptake studies and unitary hemichannel current measurements. Surface plasmon resonance experiments demonstrated that Gap19 interacts with the Cx43 C-terminus (CT) and hemichannel inhibition was counteracted by a peptide identical to the last 10 AAs of the CT, indicating that Gap19 inhibition of hemichannels is caused by preventing intramolecular interactions of the CT with the CL, which are essential for Cx43 hemichannel activities (Ponsaerts *et al.*, 2010b;Ponsaerts *et al.*, 2012). Moreover, Gap19 inhibited the potentiation of unitary hemichannel currents in acutely isolated ventricular cardiomyocytes exposed to metabolic inhibition. In line with this finding, the peptide protected against myocardial cell swelling and cell death in *in vitro* cardiac ischemia/reperfusion studies and modestly limited the infarct size in *in vivo* cardiac ischemia/reperfusion in mice. Importantly, Gap19 had no effect on pannexin-1 (Panx1) or Cx40 hemichannels. Thus, Gap19 emerges as a novel tool to specifically block Cx43 hemichannels without inhibiting GJs, allowing *in vitro* and *in vivo* work aimed at determining the role of hemichannels in cardiac disease models as well as in other tissues and organs that display a prominent Cx43 expression.

METHODS

An expanded Methods section is provided in the Online Resource.

GJ coupling studies

GJ coupling was investigated by dye coupling and electrophysiological studies. Dye coupling was assessed by fluorescence recovery after bleaching (FRAP) and scrape loading of dye transfer (SLDT) (Decrock *et al.*, 2009b). For FRAP, confluent cell cultures were loaded with 5-carboxyfluorescein diacetate acetoxy methylester (CFDA-AM, 20 μM). Fluorescence within a single cell was photobleached by spot exposure to 488 nm Argon laser light. The fluorescent intensity in the bleached cell was followed over a 5 min period and quantified at the end of this period as the percentage of recovery relative to the starting level before

bleaching. SLDT was performed by making a linear scratch across a confluent monolayer of cells in the presence of 6-carboxy fluorescein (6-CF, 0.4 mM). A fluorescence diffusion profile perpendicular to the scratch was recorded and the spatial constant of mono-exponential fluorescence decrease was determined as a measure of GJ coupling. The junctional electrical conductance between cells was measured as described .

Hemichannel studies

Hemichannel opening was investigated by ATP release studies and electrophysiological measurements of unitary hemichannel activity. ATP release was detected using a luciferin/luciferase assay kit (product no. FL-AA; Sigma) as previously described (De Vuyst *et al.*, 2006b). Hemichannel unitary currents were measured as described . For measurements in cardiomyocytes, KCl in the pipette solution was replaced by CsCl (Kondo *et al.*, 2000b).

Preparation of cardiomyocytes

Cardiomyocytes for patch-clamp experiments were isolated from left ventricles of domestic pigs (14-17 weeks) by enzymatic digestion (Stankovicova *et al.*, 2000c). The mouse cardiomyocytes used for *in vitro* ischemia/reperfusion studies were isolated by excising C57/BL6 mice (<3 months) hearts followed by cardiomyocyte isolation as described in ref. 41.

In vitro cardiomyocyte ischemia/reperfusion

Primary cardiomyocytes were isolated from mice as described by (Li *et al.*, 2004). Cells were dispersed in isolation solution (0.025 mM Ca^{2+}) by gentle agitation. Ca^{2+} in the solution was then gradually increased in small steps to 1 mM. Cardiomyocytes, sedimented to the bottom of a 10 ml tube, were exposed during 120 min to hypoxic (N_2-gassed), glucose-deprived acidic (pH 6.5) solution (oxygen-glucose deprivation [OGD]/acidosis solution) on top of which a layer of mineral oil was added. Reperfusion consisted of removing the mineral oil and replacing the OGD/acidosis solution by a normoxic solution (pH 7.4) for 3 min. After normoxia or OGD/acidosis, a 10 µl cell sample was taken and resuspended for 5 min in control solution with 0.5 % trypan blue. Images of cell morphology were obtained at x100 magnification on a Leica DMLB microscope (Leica, Bensheim, Germany). Cell viability was

quantified as the percentage of rod-shaped, unstained cells over the total cell population by an examiner blinded to the different conditions. A total of at least 1000 cells were counted per group.

For volume measurements, the cardiomyocytes were loaded with 2 µM calcein-AM in normoxic solution (15 min, 35° C) and were then scanned with a confocal microscope (Zeiss axiovert 100M, Jena, Germany) at x40 magnification and Z-stacks were taken every 2 µm in 15 cells per group. The cell volume was expressed relative to the cell volume under normoxic conditions. Exposure to OGD/acidosis was 60 min and the normoxia/reperfusion condition was applied 15 min in these experiments.

In vivo mouse model

The experiments were approved by the regional ethical committee. C57/BL6 mice were subject to 30 min ischemia and 120 min reperfusion (Boengler *et al.*, 2008a). The area at risk was determined by Evans Blue and the ischemic zone was visualized by 2,3,5-triphenyl tetrazolium chloride staining. Gap19 (MW 1161.44 Da) was intravenously administered at a concentration of 25 mg/kg, which corresponds to ~250 µM, assuming distribution in the blood volume that is approximately 8% of the body weight (blood volume values were in the 1.6-2 mL range). The 250 µM concentration gives an expected 97 % inhibition based on the data presented in Fig. 1D.

Data analysis and statistics

The data are expressed as mean ± s.e.m., with 'n' denoting the number of independent experiments. In the *in vitro* and *in vivo* ischemia experiments ‘n’ corresponds to the number of animals. Comparisons between two groups were done with a two-tailed unpaired t-test; comparison of more than two groups was done with one-way ANOVA and a Bonferroni post-hoc test; in the *in vivo* ischemia experiments a Fisher's Least Significant Difference test was used. A p value < 0.05 was considered as indicating statistical significance. In the graphs, statistical significance is indicated with a single symbol (* or #) for $p<0.05$, two symbols for $p<0.01$ and three symbols in case of $p<0.001$.

RESULTS

Gap19 inhibits Cx43 hemichannel activity but not GJ coupling

Gap19 is a synthetic nonapeptide corresponding to AAs 128-136 in the second half of the CL of Cx43 and is part of the so-called L2 region (Seki *et al.*, 2004a) (Fig. 1a and Online Resource Table S1). Furthermore, AAs 130-136 are part of a sequence (AAs 130-139) that is important for CL interactions with the CT tail of Cx43 (Bouvier *et al.*, 2009a;Duffy *et al.*, 2002b;Hirst-Jensen *et al.*, 2007a). Gap19 contains the KKFK sequence that is a known cell-membrane translocation motif that facilitates plasma membrane permeability (Carrigan and Imperiali, 2005). This may explain the higher uptake of Gap19 tagged with fluorescein isothiocyanate (FITC) in C6 glioma cells stably transfected with Cx43 (C6-Cx43) compared to fluorescein alone (Fig. 1b). We determined the effect of Gap19 on ATP release triggered by an elevation of the cytoplasmic Ca^{2+} concentration ($[Ca^{2+}]_i$) caused by exposing C6-Cx43 cells (plated at low density) to the Ca^{2+} ionophore A23187 (2.2 µM, 5 min, Fig. 1c, left bars), which, as reported, results in transient elevation of $[Ca^{2+}]_i$ to ~500 nM (De Vuyst *et al.*, 2009c;Ponsaerts *et al.*, 2010b). $[Ca^{2+}]_i$-triggered ATP release in C6-Cx43 cells depends on Cx43 hemichannels because Cx43 knock down (De Vuyst *et al.*, 2009c) or transfection of C6 cells with the empty vector (pLTR) do not display these responses (Fig. 1c, middle bar). Online Resource Fig. S1A shows Cx43 expression in C6-pLTR and C6-Cx43 cells. Gap19 inhibited $[Ca^{2+}]_i$-triggered ATP release (Fig. 1c, right bars) in a concentration-dependent manner with a half-maximal effect (IC_{50}) of ~47 µM (Hill coefficient = 2) (Fig. 1d). Gap19 (400 µM applied via the pipette solution) did not inhibit the junctional conductance determined in Novikoff cell pairs (endogenously expressing Cx43) making use of dual-cell voltage-clamp (Fig. 1e). Cell-to-cell dye transfer studies with fluorescence recovery after photobleaching (FRAP) in C6-Cx43 cells confirmed that 30 min exposure to Gap19 (200 µM) had no effect on dye coupling (Fig. 1f and g). We verified higher Gap19 concentrations in FRAP experiments and found that 1 h exposure to concentrations of 10 µM to 1 mM Gap19 had no effect on dye coupling (Online Resource Fig. S1B). In fact, 24 to 48 h exposure to 200 µM Gap19 was found to promote dye coupling in FRAP studies (Fig. 1g). ATP release was still completely blocked following 24 h incubation with 200 µM Gap19 (inset to Fig. 1g). Gap19 did not inhibit ATP release triggered by exposure of C6 cells stably transfected with pannexin-1 (C6-Panx1) to high extracellular potassium concentration ($[K^+]_e$ = 143 mM) (Fig. 1h). High $[K^+]_e$ is a known stimulus for Panx1 hemichannel opening[27] and control experiments confirmed that the triggered ATP release was suppressed by low concentrations

of carbenoxolone (10 µM, 30 min) and ^{10}Panx1 peptide (200 µM, 30 min), two blockers of Panx1 hemichannels (Locovei *et al.*, 2006;Pelegrin and Surprenant, 2006), but not by scrambled ^{10}Panx1 (Scr^{10}Panx1) (Thompson *et al.*, 2008;Wang *et al.*, 2007b) (Fig. 1h). Exposure of C6 wild type (WT) cells to high $[K^+]_e$ did not trigger ATP release above baseline (Fig. 1h – Online Resource Fig. S1A illustrates Panx1 expression in the cells used). Furthermore, Gap19 did not influence $[Ca^{2+}]_i$-triggered ATP release in HeLa cells expressing Cx40 (Fig. 1i), a major Cx expressed in the atrium and cardiac conducting system (Severs *et al.*, 2008b).

Figure 1. Gap19 inhibits $[Ca^{2+}]_i$-triggered ATP release in C6-Cx43 cells. (**a)** Topology of Cx43 and location of Gap19 in the L2 domain, part of the CL. The underlined sequence is a putative membrane translocation motif and the greyed zone is crucial for CT-CL interactions. (**b)** Confocal micrographs of C6-Cx43 cells, counterstained for F-actin (red fluorescence), illustrating cellular uptake of fluorescein-labeled (green) Gap19 (FITC-Gap19), Gap19I^{130A} (FITC-Gap19^{130A}) and fluorescein only (Fluo). Scale bar is 20 µm. The bar chart below reports fluorescence intensities (A.U., arbitrary units) measured in the cells. Uptake of fluorescein-labeled peptides was significantly stronger as compared to fluorescein only (n = 4). Stars indicate significance compared to Fluo. (**c)** Inducing $[Ca^{2+}]_i$ changes with the Ca^{2+} ionophore A23187 (inset shows experimental approach) triggered significant ATP release in C6-Cx43 but not in C6 cells stably transfected with the empty vector (C6-pLTR) (n = 12). Gap19 (200 µM, 30 min) strongly inhibited $[Ca^{2+}]_i$-triggered ATP release. (**d)** Gap19-inhibition of triggered ATP release was concentration-dependent (n = 6). (**e)** Junctional conductance (G_j) measurements in Cx43 expressing Novikoff cell pairs at different time points in the absence or presence of Gap19 (400 µM) in the recording pipette solution. G_j was normalized to the corresponding values at the beginning of the experiment. Gap19 had no effect on G_j (n = 4-16). (**f)** Representative images of a FRAP experiment in C6-Cx43 cells preloaded with CFDA. Images were acquired before photobleaching (pre-bleach), just after photobleaching the cell marked with the dotted line (bleach) and 5 min later to assess fluorescence recovery in the bleached cell. (**g)** Quantification of the fluorescence recovery 5 min after photobleaching: 30 min Gap19 (200 µM) had no influence while 24-48 h incubations promoted dye transfer (n = 5). Inset above illustrates that 24 h incubation with Gap19 inhibited ATP release equally strong as 30 min incubation (n = 12). (**h)** Exposure of C6-Panx1 cells to 143 mM $[K^+]_e$ triggered ATP release that was blocked by carbenoxolone (Cbx, 10 µM, 30 min) or ^{10}Panx1 (200 µM, 30 min), and absent in C6-WT cells. Gap19 or scr ^{10}Panx1 had no effect on high $[K^+]_e$-triggered ATP release (n = 12). (**i)** Gap19 (200 µM, 30 min) did not inhibit $[Ca^{2+}]_i$-triggered ATP release (brought about by 2 µM A23187 applied during 5 min) in HeLa-Cx40 cells (n = 6). Stars indicate statistical significance compared to the neighboring grey baseline bar (except in b); number signs mark comparisons to the black control bar; one symbol $p < 0.05$, two symbols $p < 0.01$, three symbols $p < 0.001$.

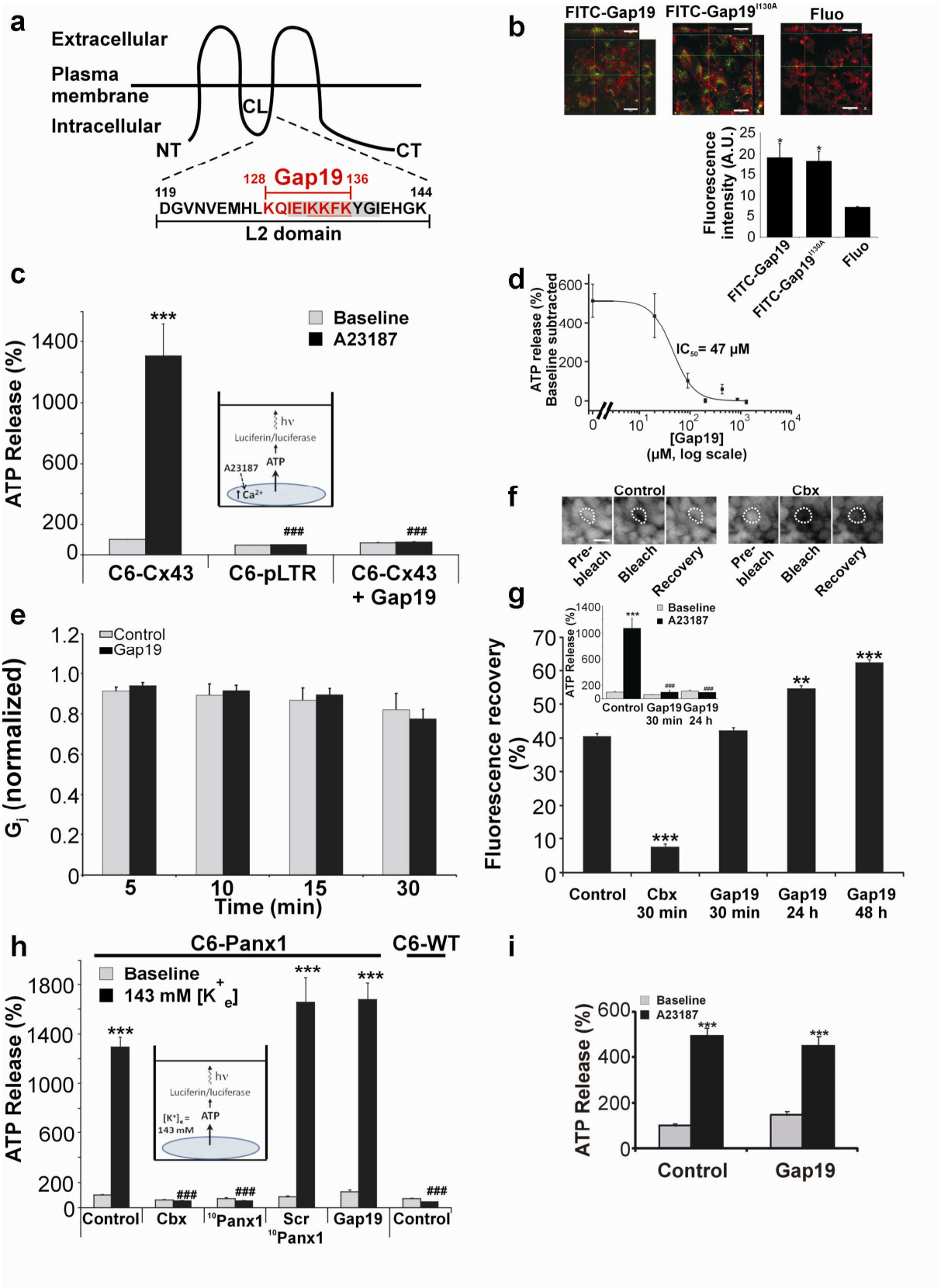
a
Extracellular
Plasma membrane
Intracellular
CL
NT
CT
128 Gap19 136
119
144
DGVNVEMHLKQIEIKKFKYGIEHGK
L2 domain
b
FITC-Gap19
FITC-Gap19I130A
Fluo
Fluorescence intensity (A.U.)
c
ATP Release (%)
Baseline
A23187
hν
Luciferin/luciferase
ATP
A23187
↑Ca2+
C6-Cx43
C6-pLTR
C6-Cx43 + Gap19
d
ATP release (%) Baseline subtracted
IC50= 47 µM
[Gap19] (µM, log scale)
e
Gj (normalized)
Control
Gap19
Time (min)
f
Control
Cbx
Pre-bleach
Bleach
Recovery
g
Fluorescence recovery (%)
Control
Cbx 30 min
Gap19 30 min
Gap19 24 h
Gap19 48 h
h
C6-Panx1
C6-WT
Baseline
143 mM [K+e]
[K+]e = 143 mM
Control
Cbx
10Panx1
Scr 10Panx1
Gap19
i
Baseline
A23187
Control
Gap19

Amino acids I130 and K134 are important for Gap19 activity

Gap19 contains two AAs known to be mutated in certain types of oculodentodigital dysplasia (ODDD), a Cx43-linked genetic disease (Seki *et al.*, 2004a;Shibayama *et al.*, 2005). I130T mutation is linked to neurological abnormalities and associated with decreased GJ dye transfer and non-functional hemichannels (Lai *et al.*, 2006a;Shibayama *et al.*, 2005). Moreover, I130 is involved in the formation of hydrogen bonds (Duffy *et al.*, 2002b), indicating that this AA might be important for Gap19 activity. K134E mutation decreases the single channel conductance of GJ channels and interferes with normal GJ plaque formation (Seki *et al.*, 2004a;Shibayama *et al.*, 2005). We found that Gap19 containing the I130A modification ($Gap19^{I130A}$, concentrations as for Gap19) failed to inhibit $[Ca^{2+}]_i$-triggered ATP release (Fig. 2a). The cellular uptake of FITC-$Gap19^{I130A}$ was comparable to the uptake of FITC-Gap19 as illustrated in Fig. 1b. To determine the importance of neighboring AAs, we measured the effect of $Gap19^{E131A}$ and found it equally active as Gap19 (Fig. 2a). Since mutations of K134 may alter the membrane permeability of Gap19, we constructed a plasmid encoding Gap19 coupled via its N-terminus to a FLAG-tag (pFLAG-Gap19). In contrast to C6-Cx43 cells expressing pcDNA5/FRT-eGFP (empty vector), C6-Cx43 cells expressing pFLAG-Gap19 displayed no significant $[Ca^{2+}]_i$-triggered ATP release (Fig. 2b) and maintained normal GJ coupling measured with SLDT (Fig. 2c and d), similar to the results obtained with exogenously applied Gap19 peptide. In line with the results obtained with $Gap19^{I130A}$ (Fig. 2a), pFLAG-$Gap19^{I130A}$ failed to suppress ATP release (Fig. 2e). pFLAG-$Gap19^{Q129A}$ inhibited ATP release like pFLAG-Gap19, further supporting the notion that AAs neighboring I130 are not essential for hemichannel inhibition (Fig. 2e). Finally, pFLAG-$Gap19^{K134A}$ was ineffective as an inhibitor of ATP release (Fig. 2e). Thus, I130 and K134 are important AAs in the inhibitory effect of Gap19 on ATP release.

Figure 2. Gap19 activity depends on AA 130 & 134 and is counteracted by adding CT10 peptide. (a) $Gap19^{I130A}$ (200 µM, 30 min) had no effect on $[Ca^{2+}]_i$-triggered ATP release in C6-Cx43 while $Gap19^{E131A}$ acted as Gap19. Combining the I130A/E131A modifications gave results as for $Gap19^{I130A}$ (n = 12). (**b)** Amino acid substitutions in the putative membrane translocation motif of Gap19 were tested using the pFLAG-Gap19 plasmid. $[Ca^{2+}]_i$-triggered ATP release was absent in C6-Cx43 cells transiently transfected with pFLAG-Gap19 (n = 12). (**c)** Example traces of SLDT dye (6-CF) spread experiments in C6-Cx43 cells (empty vector) and C6-Cx43 cells transfected with pFLAG-Gap19. (**d)** Quantification of the spatial constant of dye spread from SLDT experiments, demonstrating no effect of pFLAG-Gap19 on dye spread (n = 3; p = 0.6337). (**e)** pFLAG-$Gap19^{I130A}$ acted as $Gap19^{I130A}$ and did not inhibit $[Ca^{2+}]_i$-triggered ATP release while pFLAG-$Gap19^{Q129A}$ acted inhibitory. pFLAG-$Gap19^{K134A}$ did not inhibit $[Ca^{2+}]_i$-triggered ATP release; the combined I130A/K134A mutant acted as the single mutants (n = 12). (**f)** CT10 peptide counteracts Gap19 effects. In C6-Cx43 cells pre-incubated with TAT-CT10 (100 µM, 30 min), Gap19 (200 µM, 30 min together with TAT-CT10) did not inhibit ATP release while TAT-$CT10^{reverse}$ had no effect. The two aspartate and two proline residues in CT10 are crucial for this effect (n = 12). Stars compare to the neighboring grey baseline bar; number signs compare to the black control bar in a and f, and to the black empty vector bar in b and e.

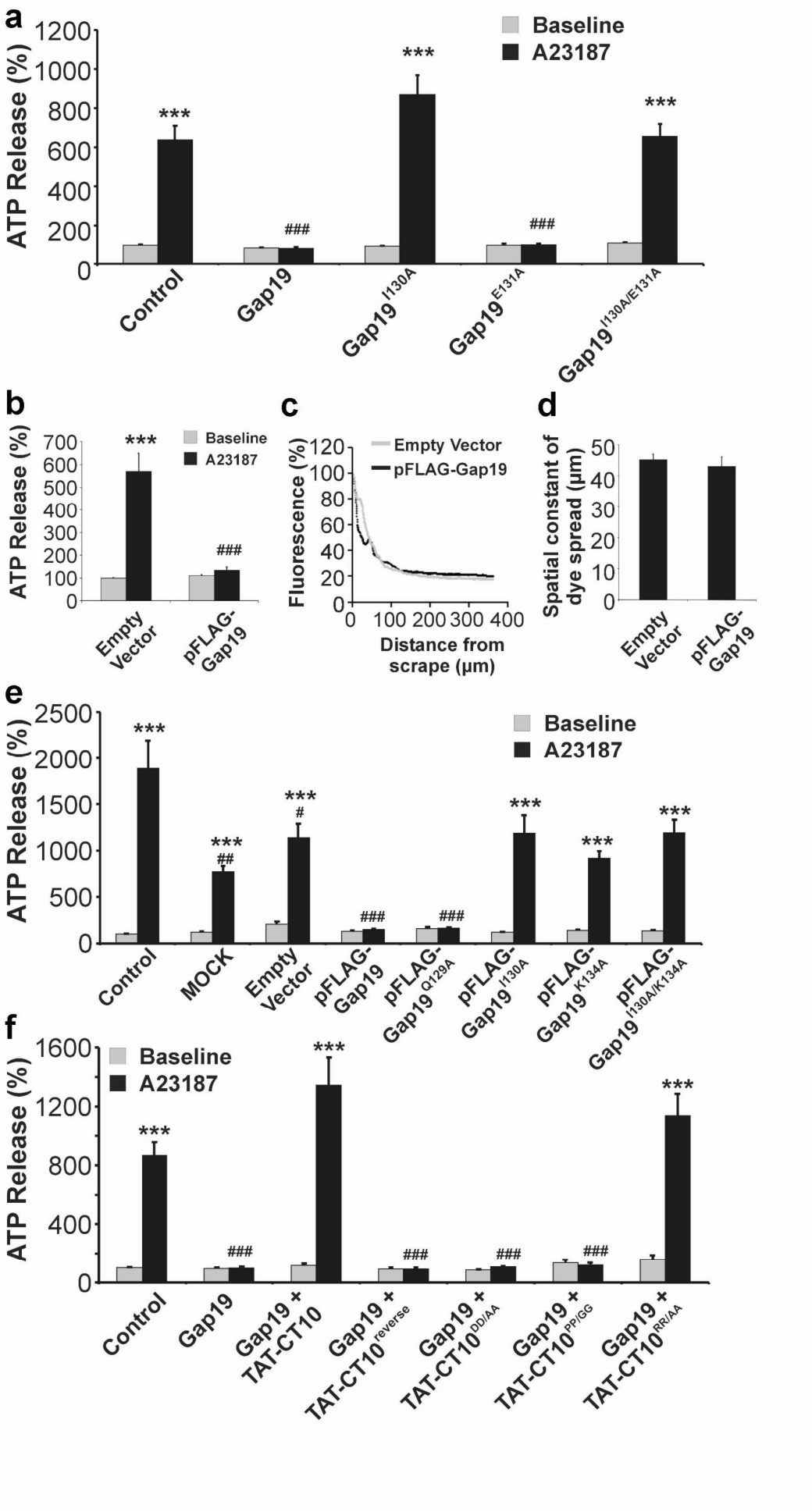
a
ATP Release (%)
Baseline
A23187
Control
Gap19
Gap19 I130A
Gap19 E131A
Gap19 I130A/E131A
b
ATP Release (%)
Empty Vector
pFLAG-Gap19
c
Fluorescence (%)
Empty Vector
pFLAG-Gap19
Distance from scrape (µm)
d
Spatial constant of dye spread (µm)
e
ATP Release (%)
MOCK
pFLAG-Gap19 Q129A
pFLAG-Gap19 I130A
pFLAG-Gap19 K134A
pFLAG-Gap19 I130A/K134A
f
ATP Release (%)
Gap19 + TAT-CT10
Gap19 + TAT-CT10 reverse
Gap19 + TAT-CT10 DD/AA
Gap19 + TAT-CT10 PP/GG
Gap19 + TAT-CT10 RR/AA

Gap19 inhibition of hemichannels involves direct interactions with the CT tail

Since intramolecular interactions of the last ten AAs of the CT with the CL are important for Cx43 hemichannel function (Ponsaerts *et al.*, 2010b) and AAs 130-136 in the CL are involved in CT binding, we investigated whether Gap19 (AAs 128-136) blocks hemichannels by binding to the CT, thereby preventing CT-CL interaction. Pre-incubating C6-Cx43 cells with membrane-permeable TAT-CT10 (100 µM, 30 min), a peptide corresponding to the last ten AAs of the Cx43 CT (Online Resource Table S1), followed by co-incubation with Gap19, completely abolished Gap19 inhibition of $[Ca^{2+}]_i$-triggered ATP release, while the peptide with reversed CT10 sequence (TAT-$CT10^{reverse}$) did not (Fig. 2f). Mutant versions of TAT-CT10 were designed to determine the residues critical for neutralizing Gap19 activity. The choice for particular mutants was based on the data of Hirst-Jensen et al. (Hirst-Jensen *et al.*, 2007a) pointing to the importance of residues in the 376-379 domain for CT-CL interactions. Modifying D378 and D379 to alanine residues (TAT-$CT10^{DD/AA}$) or P375 and P377 to glycine residues (TAT-$CT10^{PP/GG}$) resulted in peptides that failed to abolish Gap19 activity, while modifying R374 and R376 to alanine residues (TAT-$CT10^{RR/AA}$) had no effect (Fig. 2f). Similar results were obtained with pFLAG-Gap19 expression studies instead of exogenously applied Gap19 peptide (Online Resource Fig. S2). These results indicate that the two aspartate and two proline residues present in the last 10 AA-stretch of the CT are critical for Gap19-inhibitory actions.

It is known that the L2 region of the CL, in which sequence of Gap19 is located, is important for interactions with the CT (Duffy *et al.*, 2002b;Hirst-Jensen *et al.*, 2007a;Ponsaerts *et al.*, 2010b). We further explored Gap19-CT interactions with surface plasmon resonance (SPR) and monitored the association of purified Cx43 CT tail (AAs 255-382) with biotin-Gap19 immobilized to a streptavidin-coated sensor chip. Immobilized biotin-L2 (AAs 119-144) and its reversed sequence version were used as positive and negative controls respectively. These experiments displayed a clear association of the CT tail with Gap19 and L2. Interestingly, the binding of the CT tail to Gap19 seemed stronger as compared to L2 (Fig. 3a and b). The CT-Gap19 association signal increased at higher concentrations of the CT tail, indicating a bona fide specific interaction. From these results, an estimated K_D of ~2.5 µM was obtained (Fig. 3c and d).

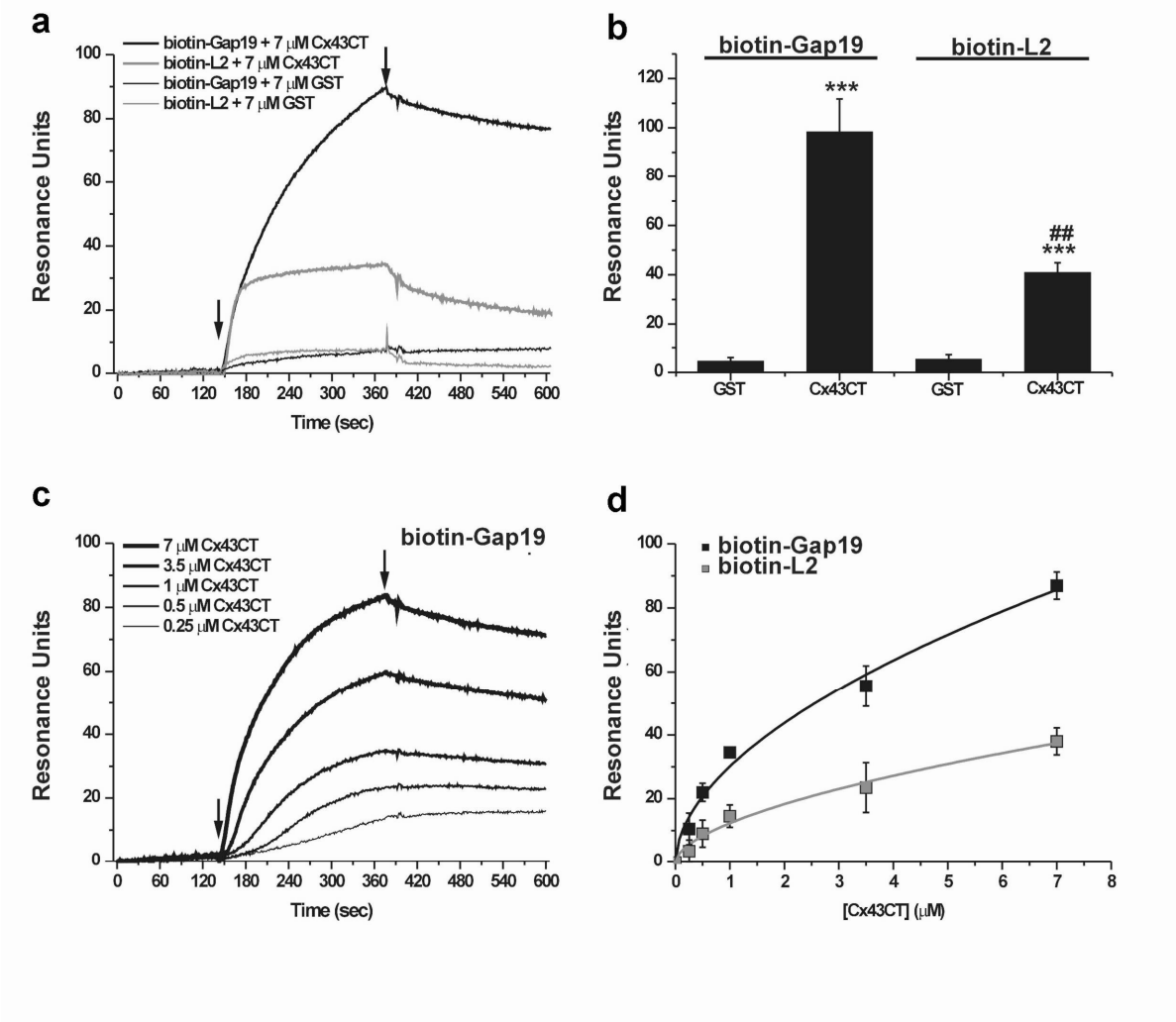

Figure 3. SPR experiments demonstrating Cx43 CT tail binding to biotin-Gap19 immobilized to a streptavidin-coated sensor chip. (a) Typical sensorgrams showing the association (first arrow) and dissociation (second arrow) between purified CT tail (Cx43CT, 7 μM) or purified GST (7 μM) and biotin-Gap19 or biotin-L2 immobilized to the streptavidin-coated sensor chip. The ordinate is calibrated in resonance units after correction for background binding to the control peptide (L2-reverse). (**b)** Summarized average data of experiments shown in a measured at maximal response (second arrow) (n = 3), demonstrating significantly stronger association between Cx43CT and Gap19 as compared to GST-Gap19. Cx43CT-Gap19 association was also stronger than for Cx43CT-L2. (**c)** Sensorgrams for Cx43CT-Gap19 and Cx43CT-L2 association at different concentrations of purified Cx43CT. (**d)** Summary of data shown in C, demonstrating a concentration-dependent increase in the association signal with half-maximal effect at ~2.5 μM for both Gap19 and L2 (n = 3).

Gap19 inhibits hemichannel unitary current activity in Cx43 expressing HeLa cells

We used HeLa cells stably transfected with Cx43 (HeLa-Cx43) to determine whether Gap19 inhibits unitary currents through hemichannels in voltage-clamp experiments (Contreras *et al.*, 2003c), performed on solitary non-coupled cells, in the presence of extracellular Ca^{2+} and Mg^{2+}, and under conditions of K^{+}-channel blockade (Fig. 4a). Application of voltage ramps showed that hemichannel currents appeared at potentials above +50 mV (Fig. 4b) and we chose +70 mV as a command voltage for subsequent experiments. Applying a depolarizing

voltage step from -30 mV to +70 mV triggered unitary current events characterized by a conductance of ~220 pS (Fig. 4c and d), which corresponds to the single channel conductance of Cx43 hemichannels (Contreras *et al.*, 2003c). The activity of unitary events was reduced when Gap19 (400 µM) was present in the pipette solution, while Gap19^{I130A} had no effect (Fig. 4c). Unitary event activity often displayed multiple superimposed stepwise channel openings, which were less frequent with Gap19. Fig. 4d (graphs in left column) illustrates that Gap19 decreased the number of peaks in the conductance histograms and increased the frequency of the closed state. Fig. 4d (graphs in right column) demonstrates that Gap19 did not influence the time constant of open dwell-time distributions while clearly decreasing the number of channel openings. Integration of the current versus time traces, which yields the membrane charge transfer (Q_m) associated with unitary current activity, showed that Gap19 significantly suppressed Q_m to ~25 % of the control level, whereas Gap19^{I130A} had no effect (Fig. 4e). Online Resource Fig. S3A illustrates that the effect of Gap19 was rapid, within 1 min. Gap19 inhibited Q_m in a concentration-dependent manner with an IC_{50} of ~6.5 µM (Hill coefficient = 2) (Fig. 4f). By contrast, Gap19^{I130A} had no effect unless applied at 1 mM concentration at which point the flat Q_m curve displayed a sharp decrease, presumably as a result of steric block of the channel pore (Fig. 4g). A separate set of experiments was performed in cell-attached patch mode, in order to determine the effect of Gap19 on the open probability (P_{open}) of single hemichannels. The P_{open} was 0.01 ± 0.0004 for control recordings (V_m steps to +70 mV) and 0.0009 ± 0.0003 with Gap19 present in the bath (200 µM, 30 min pre-incubation) demonstrating a significant ~10-fold reduction by Gap19 ($p<0.0001$, $n = 5$).

Figure 4. Gap19 inhibits unitary hemichannel currents in HeLa-Cx43 cells. (**a)** Whole cell voltage-clamp recording conditions. (**b)** I_m-V_m plot illustrating voltage ramp experiments (-40 to +80 mV, 70 s). Unitary current activity started to appear at +50 mV (control) and was enhanced by further increasing V_m. Experiments with Gap19 or Gap19^{I130A} in the pipette solution (400 µM) are also shown. (**c)** Typical traces of unitary currents activated by stepping V_m from -30 mV to +70 mV for 30 s. Ten consecutive runs (traces) were recorded over 7 min under control conditions (top) and when the pipette solution contained Gap19 (middle) or Gap19^{I130A} (bottom). (**d)** Left: All-points histograms determined from each set of recordings depicted in c. Dashed vertical lines mark peaks in the histograms separated by ~220 pS. Gap19 reduced hemichannel activity as can be appreciated from the decreased number of peaks and increased frequency of the closed state. Right: Open dwell-time histograms determined from the recordings in c. Gap19 decreased the frequency of openings but had no effect on the time constant (τ) of the mono-exponential distribution of open dwell-times. Distributions with Gap19^{I130A} were as observed in control. Data in c and d are representative for 3 different experiments. (**e)** Bar chart summarizing the results of integrating the current traces over time, giving the membrane charge transfer (Q_m), for the different conditions applied. Gap19 significantly suppressed Q_m to ~¼ of control while Gap19^{I130A} had no effect ($n = 6$ for control, 8 for Gap19 and 6 for Gap19^{I130A}). (**f)** Gap19 inhibited Q_m in a concentration-dependent manner. (**g)** Q_m was not influenced by Gap19^{I130A} unless it was applied at 1 mM concentration.

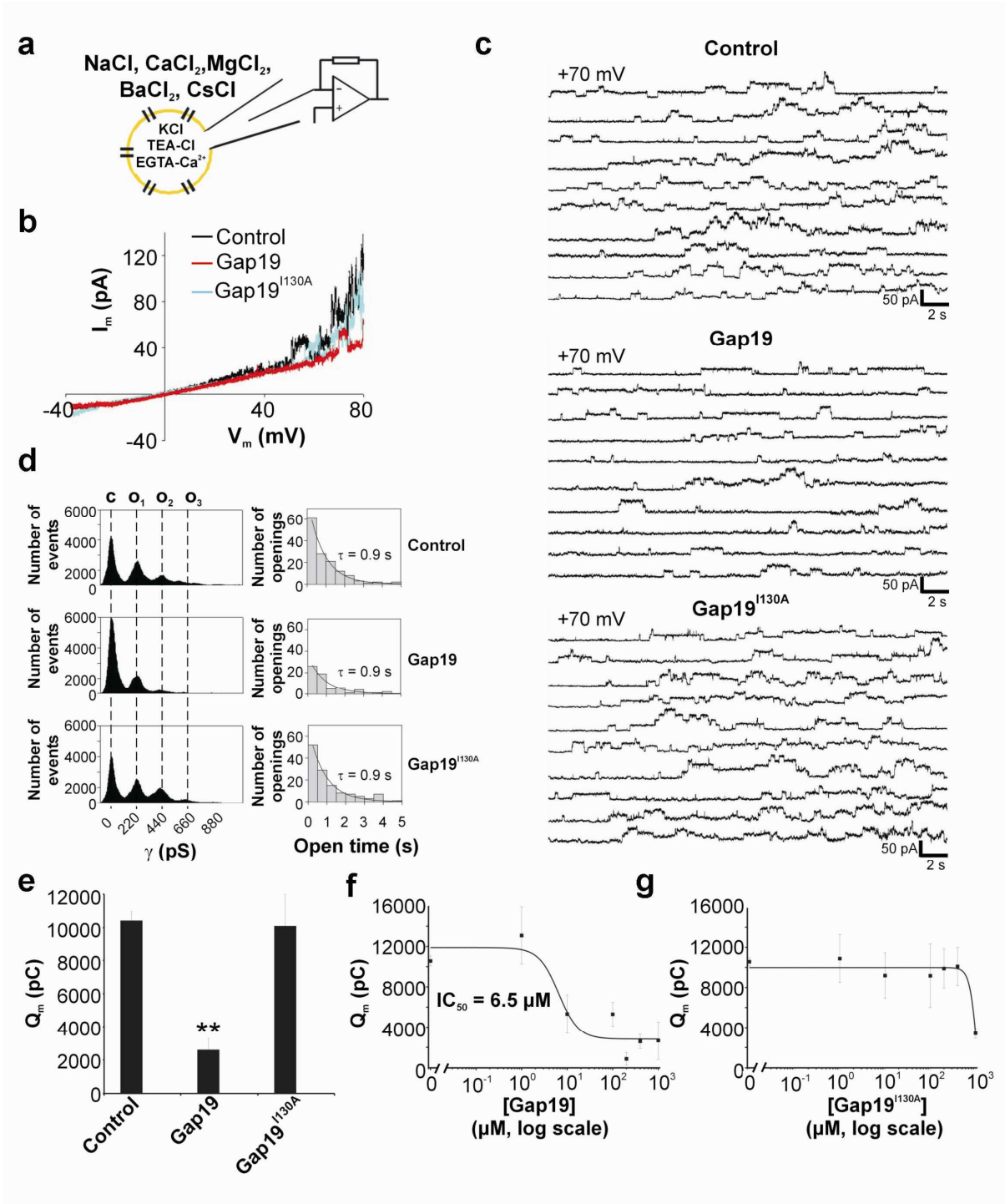

Gap19 inhibits hemichannel unitary currents in ventricular cardiomyocytes

We sought to identify single-channel Cx43 hemichannel activity in ventricular cardiomyocytes acutely isolated from adult pig heart, under recording conditions as applied in the experiments on HeLa-Cx43 cells but with CsCl instead of KCl as the main pipette salt. Voltage steps from -70 mV to V_m in the range of +10 to +100 mV triggered single-channel

current activity from V_m = +30 mV on, with a single-channel conductance of ~200 pS as judged from conductance histograms (Fig. 5a). When Gap19 was added to the recording pipette (100 µM), unitary current activity was strongly decreased and voltage steps to more positive V_m were necessary to observe unitary events (Fig. 5a). Fig. 5b illustrates that, under control conditions without Gap19, stepping back from positive V_m (applied 30 s) to -70 mV caused clearly discernible single-channel activity that was present during 100-200 ms; all-point histogram analysis indicated a ~200 pS unitary conductance (Fig. 5b). The recordings of single-channel activity at positive (during the V_m step) and negative (tail currents) voltages allowed to construct a plot of unitary membrane current (I_m) as a function of V_m (Fig. 5c). This open hemichannel I_m-V_m plot demonstrated a linear relation characterized by a reversal potential of ~0 mV and a single-channel slope conductance of 196 ± 3.8 pS (n = 7) (Fig. 5c). We analyzed the voltage-dependence of unitary current activation under control and in the presence of Gap19 (100 µM) and found that the activation curve was shifted to the right by ~30 mV (Fig. 5d). Gap19 thus significantly increased the V_m threshold for hemichannel activation. Although the unitary activity was strongly depressed by Gap19, sufficient data (at strong positive V_m and in the tails at negative V_m) were available to construct an I_m-V_m plot (Fig. 5e). This analysis revealed a reversal potential of ~0 mV and a single-channel slope conductance that were very similar to the ones obtained from control conditions (204 ± 10.4 pS; n = 6). Thus, Gap19 inhibits unitary currents by shifting the voltage-dependence of hemichannel opening without affecting the open channel properties. Hemichannel inhibition by Gap19 in cardiomyocytes was slower as compared to recordings obtained in HeLa-Cx43 and it took several minutes to attain maximal effect (Online Resource Fig. S3B). This is likely caused by the lower concentration of Gap19 (100 µM *versus* 400 µM for Hela Cx43), the larger cell size of cardiomyocytes and a possibly more restricted intracellular diffusion.

Metabolic inhibition (MI) with mitochondrial uncoupler carbonyl cyanide p-trifluoromethoxyphenylhydrazone (FCCP) combined with the glycolysis inhibitor sodium iodoacetate (IAA) ('chemical ischemia') activates hemichannel-related macroscopic currents and dye uptake in various cell types endogenously expressing Cx43 (Contreras *et al.*, 2002b;John *et al.*, 1999;Kondo *et al.*, 2000b;Retamal *et al.*, 2006b). We applied FCCP/IAA (5 µM and 1 mM respectively) and found it to strongly augment the unitary current activity recorded with V_m steps to +40 mV (Fig. 5f). Most notably, when Gap19 was added in the pipette (100 µM), unitary activity was completely absent. Fig. 5g summarizes average data from such experiments and shows that unitary current progressively increased upon prolonged

exposure to MI while intracellular application of Gap19 abolished single channel events throughout the recording.

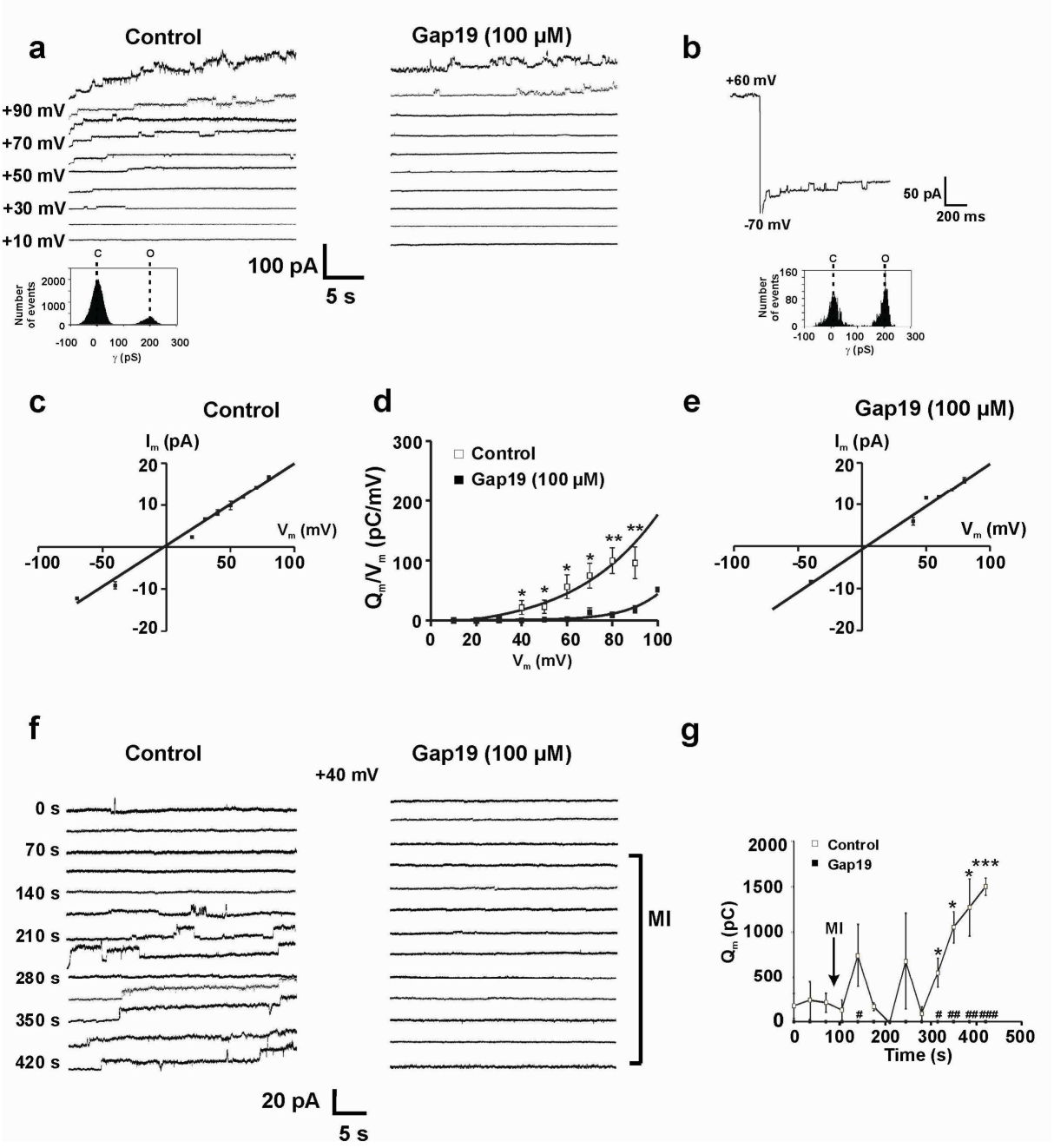

Figure 5. Gap19 inhibits hemichannel unitary currents in ventricular cardiomyocytes. (a) Whole cell recording performed in acutely isolated ventricular cardiomyocytes revealed a V_m dependent activation of Cx43 hemichannels (30 s voltage steps - traces representative for 7 similar recordings). The all-point histogram illustration below the traces indicates a ~200 pS unitary conductance at V_m = +30 mV. In the presence of Gap19 (100 µM in the pipette), V_m steps to more positive potentials were necessary (traces representative for 6 similar recordings). (**b)** Example traces illustrating that unitary current activities was still present after repolarizing to -70 mV. The all-point histogram below indicates a ~200 pS unitary conductance of the unitary tail current events. (**c)** I_m-V_m plot of open hemichannels demonstrating a reversal potential of ~0 mV and a single channel slope conductance of ~196 pS. (**d)** Voltage dependent activation of hemichannels, demonstrating that Gap19 (100 µM) shifted the activation curve to more positive potentials. The quantity Q_m/V_m was calculated by dividing the integrated unitary current activity by the corresponding V_m, and represents the integrated single channel conductance over the 30 s voltage steps (n=6). (**e)** Gap19 inhibition of unitary events did not influence the open hemichannel I_m-V_m plot (~0 mV reversal potential and 204 pS single channel slope conductance, not different from control). (**f)** Example traces recorded in a cardiomyocyte before and after exposure MI (5 µM FCCP and 1 mM IAA). Voltage steps from -70 mV (5 s) to +40 mV (30 s) were repetitively applied. Unitary current activity was completely absent with Gap19 in the recording pipette. (**g)** Summary graph illustrating progressively increasing unitary current activity after application of MI (n = 4). Stars indicate statistical significance compared to baseline before MI induction. Recordings with Gap19 in the pipette were flat, lacking any unitary activity, also after MI induction (filled squares on the abcis). Gap19 completely suppressed MI-promoted hemichannel activity. Number signs indicate statistical significance compared to the corresponding open squares recorded without Gap19 in the pipette.

Gap19 protects against myocardial ischemia/reperfusion injury in vitro and in vivo

It has been reported that ischemic conditions trigger Cx43 hemichannel opening, possibly mediated by changes in the phosphorylation status of Cx43 and the generation of reactive oxygen and nitrogen species (Hawat *et al.*, 2010b;Ramachandran *et al.*, 2007;Retamal *et al.*, 2007e;Shintani-Ishida *et al.*, 2007b). We explored whether Gap19 could prevent possible deleterious effects of uncontrolled opening of hemichannels, thereby reducing ischemia/reperfusion damage to the myocardium in *in vitro* and *in vivo* studies. Exposing isolated cardiomyocytes to 120 min oxygen-glucose deprivation (OGD) and acidosis (pH 6.5) followed by a switch to control/normoxic solution (3 min) to simulate reperfusion, resulted in extensive cell death (example image shown in Online Resource Fig. S4) with 10.9 % of the cardiomyocytes remaining viable (Fig. 6a). Cardiomyocytes exposed to normoxic solution over the same time period as OGD/acidosis showed no decline in survival (Fig. 6a). Pre-treatment of the cells with Gap19 (250 µM, 30 min) followed by OGD/acidosis (with Gap19 present) and reperfusion (normoxia) increased the viability to 14.6 %, thus enhancing the viability by approximately one third compared to treatment with vehicle-only (Fig. 6a). Exposing isolated cardiomyocytes to OGD/acidosis (60 min) followed by reperfusion (15 min) resulted in significant cell swelling that was counteracted by Gap19 (treatment as in the viability assays) (Fig. 6b). Gap19 did not affect the cell volume under normoxic conditions (99.1 ± 1.8 % compared to 100 ± 2.2 % in control, n= 5). $Gap19^{I130A}$ exhibited some protective effect against cell death and cell swelling but the effect of Gap19 was significantly stronger (Fig. 6a and b). We performed myocardial ischemia/reperfusion experiments in mice

in vivo, by applying a 30 min ligation of the left anterior descending (LAD) coronary artery followed by reperfusion (120 min). Gap19 was intravenously injected 10 min before ligation at a dose of 25 mg/kg, corresponding to an estimated 250 µM concentration when distributed in the blood volume. This significantly reduced the infarct size to 51.2 %, compared to 63.8 % infarct size in vehicle-treated control animals, i.e. a reduction by approximately one fifth. Gap19^{I130A} had no significant effect compared to control (Fig. 6c).

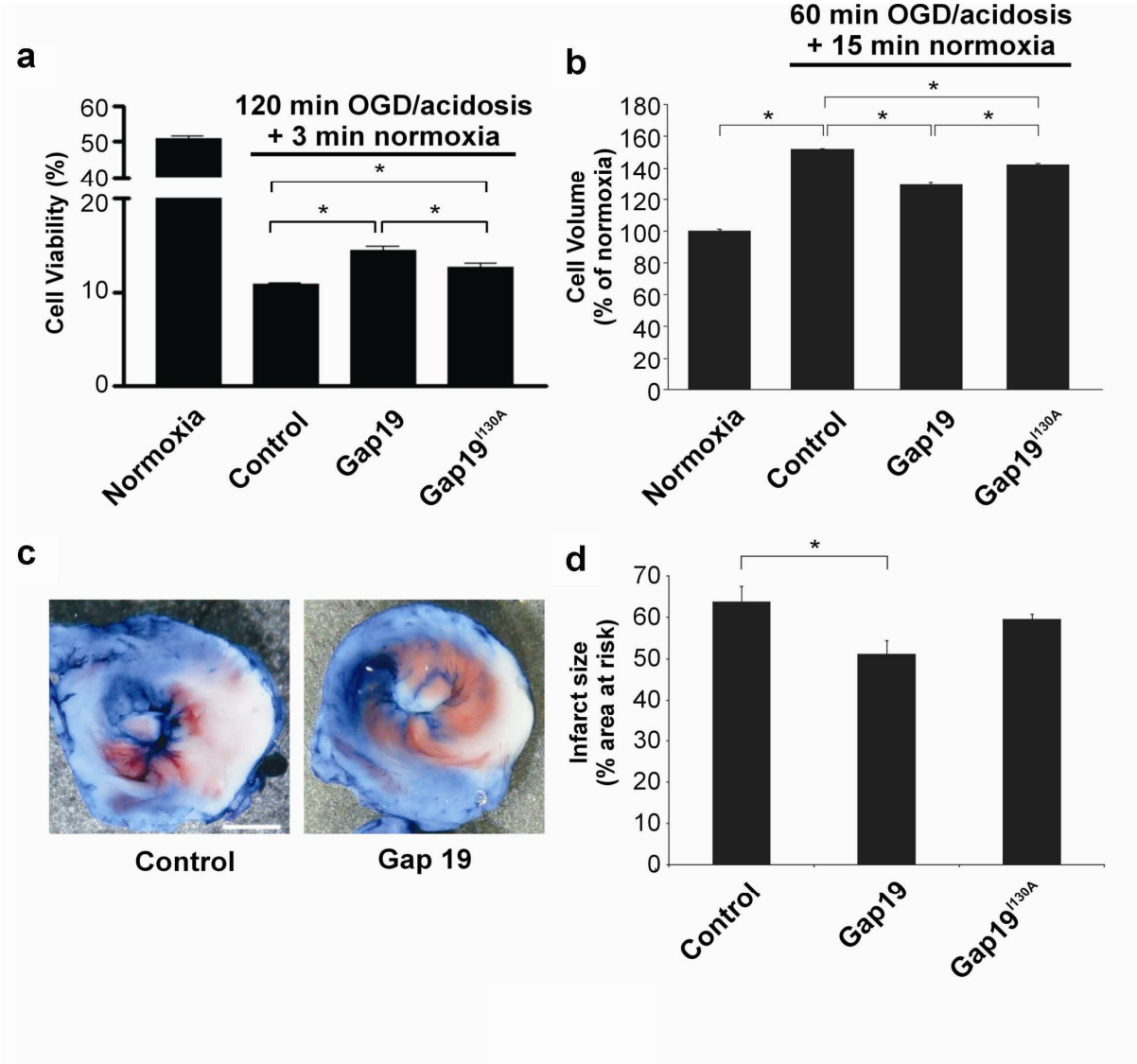

Figure 6. Gap19 improves cardiomyocyte viability following ischemia/reperfusion *in vitro* and *in vivo*. (**a).** *In vitro* simulated ischemia/reperfusion of isolated cardiomyocytes. Gap19 (250 µM, 30 min pre-incubation and present during OGD/acidosis) improved cardiomyocyte viability after 120 min OGD/acidosis (ischemia) followed by 3 min normoxia (reperfusion) compared to control cells treated with vehicle only; Gap19^{I130A} had less effect (n = 6). (**b)** OGD/acidosis + normoxia caused significant swelling of cardiomyocytes compared to normoxia. Pre-incubation of cardiomyocytes with Gap19 reduced the degree of cell swelling while Gap19^{I130A} had less effect (250 µM, 30 min) (n = 7). (**c)** *In vivo* experiments in mice with LAD ligation for 30 min followed by 120 min reperfusion. Images of a representative experiment, illustrating a reduction of the infarct area marked white (TTC staining). Red color indicates viable tissue and blue represents perfused tissue. Red and white zones together form the area at risk. Scale bar is 1 mm. (**d)** Summary data of experiments illustrated in c. The infarct size, relative to the area at risk, was reduced by Gap19 injected intravenously (25 mg/kg) 10 min prior to the ligation, while Gap19^{I130A} had no significant effect (n = 11 for control, 5 for Gap19 and 8 for Gap19^{I130A}).

DISCUSSION

Our data show that Gap19 blocks Cx43 hemichannels without inhibiting GJs, at micromolar concentrations (IC_{50} of 6.5 µM) when applied intracellulary. This corresponds well to the ~2.5 µM K_D value for interaction of Gap19 with its intracellular target, which is the Cx43 CT tail. The IC_{50} of extracellulary applied Gap19 is higher, presumably because of incomplete permeation through the plasma membrane. Online Resource Fig. S5 shows that the IC_{50} of Gap19 linked to the TAT translocation motif, to further improve its membrane permeability, is ~7 µM. Thus, micromolar intracellular Gap19 concentrations interact with the CT and inhibit hemichannels. Hemichannel inhibition is not caused by steric block of the channel pore by the peptide, because (i) the mutant peptide $Gap19^{I130A}$ had no effect unless applied at 1 mM concentration, (ii) CT peptide (TAT-CT10) removed Gap19 inhibition, (iii) the single hemichannel conductance was not altered by Gap19, and (iv) Cx43-based GJs were unaffected. The effect of Gap19 was selective as it had no effect on hemichannels composed of Cx40 or Panx1. Cx40 is a major Cx in the atria, with a long CT as Cx43 and a slightly lower MW; Panx1 hemichannels have also been reported to be expressed in atrial cardiomyocytes (Kienitz *et al.*, 2011b). The selectivity of Gap19 probably relates to the fact that the intracellular domains of the Cx protein are the least conserved region in contrast to the extracellular domains (Abascal and Zardoya, 2012).

The molecular basis of the differential effect of Gap19 on hemichannels and GJs is related to the binding of this peptide to the CT tail, which prevents CT-CL interaction. Disrupting CT-CL interaction results in reduced hemichannel openings and ATP release as demonstrated here, while avoiding closure of GJ channels as reported by others (Seki *et al.*, 2004a) and confirmed in the present experiments. The mechanisms underlying this differential regulation of hemichannels and GJs by CT-CL interactions are still unclear. However, it is important to notice that disrupting CT-CL interactions by CT-truncation of Cx43 has similar consequences: GJs remain functional (Maass *et al.*, 2007), while hemichannels become resistant to activation (De Vuyst *et al.*, 2007b;Ponsaerts *et al.*, 2010b). We anticipate that nonjunctional hemichannels (closed) may adopt different conformations as compared to those incorporated into GJs (open) (Unwin and Ennis, 1983;Unwin and Zampighi, 1980). Interactions between subunits during docking of two hemichannels are indeed likely to result in conformational changes of the Cx protein and thereby alter gating (Chen-Izu *et al.*, 2001;Elenes *et al.*, 2001b). Another element that may contribute is the fact that hemichannels and GJ channels are differentially distributed over plasma membrane domains with slightly

different properties, for example lipid rafts (Barth *et al.*, 2005;Locke *et al.*, 2005a). Alternatively, Gap19 treatment may result in a reduction of the hemichannel population in the nonjunctional plasma membrane, e.g. due to accelerated incorporation into GJs or internalization. However, we found that the density of unapposed/nonjunctional hemichannels rather increased upon ectopic expression of pFLAG-Gap19 in C6-Cx43 cells (Online Resource Fig. S6). This figure also demonstrates increased phosphorylation of the hemichannel population with pFLAG-Gap19, which may well contribute to hemichannel inhibition[54] and may counteract decreased phosphorylation associated with ischemia (John *et al.*, 1999;Kondo *et al.*, 2000b;Shintani-Ishida *et al.*, 2007b).

Limited data are currently available demonstrating that non-junctional membrane hemichannels in cardiomyocytes can open under certain conditions. The observation of a $[Ca^{2+}]_i$-dependent non-selective, macroscopic membrane current in rabbit ventricular myocytes in response to MI initially suggested Cx43 hemichannel opening in the heart (John *et al.*, 1999;Kondo *et al.*, 2000b). More recent findings report a marked increase of cell permeability based on ATP release and dye uptake associated with activated hemichannels in simulated ischemia of neonatal cardiomyocytes (Clarke *et al.*, 2009b;Johansen *et al.*, 2011b;Shintani-Ishida *et al.*, 2007b). Here, we demonstrate in ventricular cardiomyocytes single channel plasma membrane currents with a unitary conductance of ~200 pS in response to stepping V_m to +30 mV and above. The biophysical properties of the observed unitary activity point to Cx43 hemichannels: (i) the single-channel conductance determined from histogram analysis or I_m-V_m plot measurements was similar as observed in Hela cells overexpressing Cx43 and corresponds to approximately twice the single-channel conductance of Cx43 GJ channels; (ii) currents reverse around 0 mV, indicating a non-selective ion channel; iii) unitary currents are inhibited by Gap19 as in HeLa-Cx43 cells. Interestingly, unitary hemichannel activity was also present in the tail currents during repolarization from positive voltage steps which may be caused by increased $[Ca^{2+}]_i$ that is known to potentiate hemichannel opening if < 500 nM (De Vuyst *et al.*, 2009c) or slow deactivation kinetics. Gap19 inhibited unitary hemichannel opening events and this was mainly related to an increased (more positive) voltage threshold for hemichannel opening and not the consequence of channel pore block (no change in the single channel conductance). Thus, Gap19 appears to alter the voltage-sensitivity of Cx43 hemichannel gating as a consequence of disrupted CT-CL interactions.

Of note, Gap19 inhibition of ATP release was complete (Fig. 1d) while inhibition of unitary hemichannel currents was incomplete at high concentrations (Fig. 4f). This may point to a more pronounced inhibitory effect on the passage of large MW substances as compared to ions. Such differences in the potency of inhibition have been reported by others: PKC phosphorylation of Cx43 hemichannels limits the passage of sucrose (MW 342 Da – MW of ATP is 507 Da) but not of the smaller ethyleneglycol (MW 62) (Bao *et al.*, 2007). An alternative explanation is that ATP release may behave in a non-linear manner (for example by Ca^{2+}-or ATP-induced ATP release) as suggested by previous studies demonstrating complete inhibition of ATP release with only a 50 % reduction in Cx43 expression (De Vuyst *et al.*, 2009c).

The unitary hemichannel currents were strongly potentiated by imposing MI. Earlier observations in a variety of primary cells endogenously expressing Cx43 have suggested elevated hemichannel activities during chemical ischemia (Contreras *et al.*, 2002b;Retamal *et al.*, 2006b;Vergara *et al.*, 2003). These studies are however less conclusive as the evidence was based on hemichannel-permeable dye uptake studies (<1 KDa) or macroscopic current measurements. Here, we provide detailed analysis at the highest resolution in intact ventricular cardiomyocytes, demonstrating activation of hemichannel unitary currents under MI. Interestingly, our data demonstrate stimulated unitary Cx43 hemichannel activity at +30 mV and above, which is in the range of the +30-40 mV attained during the plateau phase of the cardiac action potential. Several molecular mechanisms have been put forward to underlie increased hemichannel activity: (i) ATP depletion in metabolically inhibited cells affects the phosphatase/kinase balance, leading to Cx43 dephosphorylation which favors an open channel conformation (Bao *et al.*, 2007;Kim *et al.*, 1999b); (ii) S-nitrosylation may contribute to enhanced channel activities (Retamal *et al.*, 2006b;Retamal *et al.*, 2007c) and (iii) an increased fraction of hemichannels at the cell surface as observed for both Cx32 and Cx43 hemichannels within minutes after MI could also account for stimulated unitary current activities (Retamal *et al.*, 2007c;Sanchez *et al.*, 2009b). Most notably, the unitary hemichannel currents activated by depolarization to +40 mV and promoted by MI were completely blocked by Gap19. This complete block is likely the result of a Gap19-induced increase in activation potential for hemichannel opening, which is shifted ~30 mV in the positive direction and therefore results in complete disappearance of current activity at +40 mV. Thus, ischemic conditions and depolarization activate hemichannels and this is inhibited by Gap19. The *in vitro* and *in vivo* cardiac ischemia/reperfusion experiments demonstrated

that Gap19 significantly counteracted cell swelling, cell death and development of myocardial infarction. Taking together the facts that excessive opening of hemichannels may accelerate cell death (Contreras *et al.*, 2004;Saez *et al.*, 2010) and that Gap19 counteracts hemichannel opening in cardiomyocytes, suggests that the improved outcome after ischemia/reperfusion is related to inhibition of Cx43 hemichannels present in the sarcolemma.

Not only Cx43 proteins embedded in the sarcolemma, but also those reported in mitochondria have been proposed to contribute to the cardioprotective effect of ischemic preconditioning (Heinzel *et al.*, 2005;Schwanke *et al.*, 2002a), a procedure of repeated exposure to sub-lethal ischemic conditions (Miura *et al.*, 2004;Rodriguez-Sinovas *et al.*, 2011;Schulz *et al.*, 2007b;Yang *et al.*, 2010). Located in the inner mitochondrial membrane (Boengler *et al.*, 2005;Boengler *et al.*, 2009;Miro-Casas *et al.*, 2009;Rodriguez-Sinovas *et al.*, 2006), these proteins influence mitochondrial K^+ fluxes in a process that is modulated by connexin channel blockers and linked to cardioprotection (Miro-Casas *et al.*, 2009). It is important to realize that involvement of mitochondria Cx43 in protection has only been demonstrated after ischemic preconditioning (Schulz *et al.*, 2007b). It is unlikely that mitochondria Cx43-mediated K^+ influx would be affected by a single episode of ischemia/reperfusion as applied here. It remains to be determined whether preserving GJ coupling and promoting mitochondria Cx43-associated K^+ uptake, in combination with inhibition of plasma membrane hemichannels would confer additional cardioprotection.

Considering all the evidence, the present data strongly point to the inhibition of plasma membrane hemichannel opening by Gap19 as the mechanism responsible for its protective effects against cardiac ischemia/reperfusion injury. The degree of protection, however, appears to be modest as opposed to recent evidence indicating a drastic effect of two extracellular loop mimetic peptides, Gap26 and Gap27 (Hawat *et al.*, 2010b;Hawat *et al.*, 2012b). These peptides target Cx43 channels but may also influence those composed of Cx37 and Cx40 (De Bock *et al.*, 2011a;Evans *et al.*, 2012a;Wright *et al.*, 2009b). The lesser degree of specificity towards different connexins is related to the fact that the extracellular loop sequence they mimic is highly conserved among different connexins. Thus, Gap26/27 peptides may have targets other than Cx43 hemichannels that confer additional protective potential. Alternatively, Gap19 may affect mitochondria Cx43 hereby counteracting endogenous protection mechanisms activated by ischemic preconditioning. In any case, Gap19 does not inhibit GJs and thereby circumvents potential pro-arrhythmogenic effects of

decreased GJ coupling during ischemia/reperfusion (Jansen *et al.*, 2010b;Sanchez *et al.*, 2011).

The distinctive effects of Gap19 on GJs and hemichannels are of fundamental importance: GJs and hemichannels are composed of the same Cx subunits and KO animal technology influences both channel types equally. Here, given the limited feasibility in *in vivo* recording of Cx43 hemichannel currents due to the low open probability, we report Gap19 as an alternative and novel tool allowing selective studies on the role of Cx43 hemichannels in normal and diseased heart. In addition, blocking of hemichannels with Gap19 opens an avenue for therapeutic applications, limiting cellular injuries during ischemia/reperfusion while preserving electrical and metabolic cell-cell communication that are vital for the normal function of the myocardium.

ACKNOWLEDGEMENTS

Special thanks to K. Leurs, K. Vermeulen and K. Welkenhuyzen for superb technical support. We express our gratitude to Dr. B. Himpens for support, to Dr. P. Zimmermann for the use of the Biacore 2000, to Dr. P. Sorgen for providing the pGEX6p2-Cx43CT plasmid, to Dr. G. Antoons for support with experiments on pig myocytes, and to Dr. D. Laird and Dr. S. Penuela for providing the anti-Panx1 antibody. We are very grateful to A. Gadicherla and Dr. B. Nilius for critically reading and commenting the manuscript. Research supported by the Fund for Scientific Research Flanders, Belgium (FWO, grant nos. G.0354.07, G.0140.08, 3G.0134.09 and G.0298.11 N to L.L. and G.0545.08 to G.B.), the Interuniversity Attraction Poles Program (Belgian Science Policy, project P6/31 and P7/10 to K.R.S and L.L., and P7 to J.T. and G.B.), the Concerted Actions program at KULeuven (grant no. GOA/09/012 to G.B.), the German Research Foundation (Schu 843/7-2 to R.S.), the BFH grant (grant no. PG/01/1298 to W.H.E), the Heart & Stroke Foundation of BC & Yukon and the Canadian Institutes of Health Research to C.C.N. and NIH grants (HL084464 and NS072238 to F.F.B.).

Conflict of interest

None.

DISCLOSURE

None.

References

Abascal F, Zardoya R (2013) Evolutionary analyses of gap junction protein families. *Biochim Biophys Acta*, **1828**, 4-14.

Bao X, Lee SC, Reuss L, Altenberg GA (2007) Change in permeant size selectivity by phosphorylation of connexin 43 gap-junctional hemichannels by PKC. *Proc Natl Acad Sci U S A,* **104**, 4919-4924.

Barth K, Gentsch M, Blasche R, Pfuller A, Parshyna I, Koslowski R, Barth G, Kasper M (2005) Distribution of caveolin-1 and connexin43 in normal and injured alveolar epithelial R3/1 cells. *Histochem Cell Biol*, **123**, 239-247.

Boengler K, Buechert A, Heinen Y, Roeskes C, Hilfiker-Kleiner D, Heusch G, Schulz R (2008) Cardioprotection by ischemic postconditioning is lost in aged and STAT3-deficient mice. *Circ Res*, **102**, 131-135.

Boengler K, Dodoni G, Rodriguez-Sinovas A, Cabestrero A, Ruiz-Meana M, Gres P, Konietzka I, Lopez-Iglesias C, Garcia-Dorado D, Di LF, Heusch G, Schulz R (2005) Connexin 43 in cardiomyocyte mitochondria and its increase by ischemic preconditioning. *Cardiovasc Res*, **67**, 234-244.

Boengler K, Stahlhofen S, van de Sand A, Gres P, Ruiz-Meana M, Garcia-Dorado D, Heusch G, Schulz R (2009) Presence of connexin 43 in subsarcolemmal, but not in interfibrillar cardiomyocyte mitochondria. *Basic Res Cardiol*, **104**, 141-147.

Bouvier D, Spagnol G, Chenavas S, Kieken F, Vitrac H, Brownell S, Kellezi A, Forge V, Sorgen PL (2009) Characterization of the structure and intermolecular interactions between the connexin40 and connexin43 carboxyl-terminal and cytoplasmic loop domains. *J Biol Chem*, **284**, 34257-34271.

Bukauskas FF, Kreuzberg MM, Rackauskas M, Bukauskiene A, Bennett MV, Verselis VK, Willecke K (2006) Properties of mouse connexin 30.2 and human connexin 31.9 hemichannels: implications for atrioventricular conduction in the heart. *Proc Natl Acad Sci U S A,* **103**, 9726-9731.

Carrigan CN, Imperiali B (2005) The engineering of membrane-permeable peptides. *Anal Biochem*, **341**, 290-298.

Chen-Izu Y, Moreno AP, Spangler RA (2001) Opposing gates model for voltage gating of gap junction channels. *Am J Physiol Cell Physiol*, **281**, C1604-C1613.

Clarke TC, Williams OJ, Martin PE, Evans WH (2009) ATP release by cardiac myocytes in a simulated ischaemia model: inhibition by a connexin mimetic and enhancement by an antiarrhythmic peptide. *Eur J Pharmacol*, **605**, 9-14.

Contreras JE, Saez JC, Bukauskas FF, Bennett MV (2003) Gating and regulation of connexin 43 (Cx43) hemichannels. *Proc Natl Acad Sci U S A*, **100**, 11388-11393.

Contreras JE, Sanchez HA, Eugenin EA, Speidel D, Theis M, Willecke K, Bukauskas FF, Bennett MV, Saez JC (2002) Metabolic inhibition induces opening of unapposed connexin 43 gap junction hemichannels and reduces gap junctional communication in cortical astrocytes in culture. *Proc Natl Acad Sci U S A*, **99**, 495-500.

Contreras JE, Sanchez HA, Veliz LP, Bukauskas FF, Bennett MV, Saez JC (2004) Role of connexin-based gap junction channels and hemichannels in ischemia-induced cell death in nervous tissue. *Brain Res Brain Res Rev*, **47**, 290-303.

Danik SB, Liu F, Zhang J, Suk HJ, Morley GE, Fishman GI, Gutstein DE (2004) Modulation of cardiac gap junction expression and arrhythmic susceptibility. *Circ Res*, **95**, 1035-1041.

De Bock M, Culot M, Wang N, Bol M, Decrock E, De Vuyst E, da Costa A, Dauwe I, Vinken M, Simon AM, Rogiers V, De Ley G, Evans WH, Bultynck G, Dupont G, Cecchelli R, Leybaert L (2011) Connexin channels provide a target to manipulate brain endothelial calcium dynamics and blood-brain barrier permeability. *J Cereb Blood Flow Metab*, **31**, 1942-1957.

De Vuyst E, Decrock E, Cabooter L, Dubyak GR, Naus CC, Evans WH, Leybaert L (2006) Intracellular calcium changes trigger connexin 32 hemichannel opening. *EMBO J*, **25**, 34-44.

De Vuyst E, Decrock E, De Bock M, Yamasaki H, Naus CC, Evans WH, Leybaert L (2007) Connexin hemichannels and gap junction channels are differentially influenced by lipopolysaccharide and basic fibroblast growth factor. *Mol Biol Cell*, **18**, 34-46.

De Vuyst E, Wang N, Decrock E, De Bock M, Vinken M, Van Moorhem M, Lai C, Culot M, Rogiers V, Cecchelli R, Naus CC, Evans WH, Leybaert L (2009) Ca(2+) regulation of connexin 43 hemichannels in C6 glioma and glial cells. *Cell Calcium*, **46**, 176-187.

de Wit C, Griffith TM (2010) Connexins and gap junctions in the EDHF phenomenon and conducted vasomotor responses. *Pflugers Arch*, **459**, 897-914.

Decrock E, De Vuyst E, Vinken M, Van Moorhem M, Vranckx K, Wang N, Van LL, De Bock M, D'Herde K, Lai CP, Rogiers V, Evans WH, Naus CC, Leybaert L (2009) Connexin 43 hemichannels contribute to the propagation of apoptotic cell death in a rat C6 glioma cell model. *Cell Death Differ*, **16**, 151-163.

Duffy HS, Sorgen PL, Girvin ME, O'Donnell P, Coombs W, Taffet SM, Delmar M, Spray DC (2002) pH-dependent intramolecular binding and structure involving Cx43 cytoplasmic domains. *J Biol Chem,* **277**, 36706-36714.

Elenes S, Martinez AD, Delmar M, Beyer EC, Moreno AP (2001) Heterotypic docking of Cx43 and Cx45 connexons blocks fast voltage gating of Cx43. *Biophys J*, **81**, 1406-1418.

Evans WH, Boitano S (2001) Connexin mimetic peptides: specific inhibitors of gap-junctional intercellular communication. *Biochem Soc Trans,* **29**, 606-612.

Evans WH, Bultynck G, Leybaert L (2012) Manipulating connexin communication channels: use of peptidomimetics and the translational outputs. *J Membr Biol*, **245**, 437-449.

Evans WH, De VE, Leybaert L (2006) The gap junction cellular internet: connexin hemichannels enter the signalling limelight. *Biochem J*, **397**, 1-14.

Harris AL (2001) Emerging issues of connexin channels: biophysics fills the gap. *Q Rev Biophys*, **34**, 325-472.

Hawat G, Benderdour M, Rousseau G, Baroudi G (2010) Connexin 43 mimetic peptide Gap26 confers protection to intact heart against myocardial ischemia injury. *Pflugers Arch*, **460**, 583-592.

Hawat G, Helie P, Baroudi G (2012) Single intravenous low-dose injections of connexin 43 mimetic peptides protect ischemic heart in vivo against myocardial infarction. *J Mol Cell Cardiol*, **53**, 559-566.

Heinzel FR, Luo Y, Li X, Boengler K, Buechert A, Garcia-Dorado D, Di LF, Schulz R, Heusch G (2005) Impairment of diazoxide-induced formation of reactive oxygen species and loss of cardioprotection in connexin 43 deficient mice. *Circ Res*, **97**, 583-586.

Hirst-Jensen BJ, Sahoo P, Kieken F, Delmar M, Sorgen PL (2007) Characterization of the pH-dependent interaction between the gap junction protein connexin43 carboxyl terminus and cytoplasmic loop domains. *J Biol Chem*, **282**, 5801-5813.

Jansen JA, van Veen TA, de Bakker JM, van Rijen HV (2010) Cardiac connexins and impulse propagation. *J Mol Cell Cardiol*, **48**, 76-82.

Johansen D, Cruciani V, Sundset R, Ytrehus K, Mikalsen SO (2011) Ischemia induces closure of gap junctional channels and opening of hemichannels in heart-derived cells and tissue. *Cell Physiol Biochem*, **28**, 103-114.

John SA, Kondo R, Wang SY, Goldhaber JI, Weiss JN (1999) Connexin-43 hemichannels opened by metabolic inhibition. *J Biol Chem*, **274**, 236-240.

Kalcheva N, Qu J, Sandeep N, Garcia L, Zhang J, Wang Z, Lampe PD, Suadicani SO, Spray DC, Fishman GI (2007) Gap junction remodeling and cardiac arrhythmogenesis in a murine model of oculodentodigital dysplasia. *Proc Natl Acad Sci U S A*, **104**, 20512-20516.

Kienitz MC, Bender K, Dermietzel R, Pott L, Zoidl G (2011) Pannexin 1 constitutes the large conductance cation channel of cardiac myocytes. *J Biol Chem*, **286**, 290-298.

Kim DY, Kam Y, Koo SK, Joe CO (1999) Gating connexin 43 channels reconstituted in lipid vesicles by mitogen-activated protein kinase phosphorylation. *J Biol Chem*, **274**, 5581-5587.

Kondo RP, Wang SY, John SA, Weiss JN, Goldhaber JI (2000) Metabolic inhibition activates a non-selective current through connexin hemichannels in isolated ventricular myocytes. *J Mol Cell Cardiol,* **32**, 1859-1872.

Lai A, Le DN, Paznekas WA, Gifford WD, Jabs EW, Charles AC (2006) Oculodentodigital dysplasia connexin43 mutations result in non-functional connexin hemichannels and gap junctions in C6 glioma cells. *J Cell Sci*, **119**, 532-541.

Li X, Heinzel FR, Boengler K, Schulz R, Heusch G (2004) Role of connexin 43 in ischemic preconditioning does not involve intercellular communication through gap junctions. *J Mol Cell Cardiol*, **36**, 161-163.

Locke D, Liu J, Harris AL (2005) Lipid rafts prepared by different methods contain different connexin channels, but gap junctions are not lipid rafts. *Biochemistry*, **44**, 13027-13042.

Locovei S, Bao L, Dahl G (2006) Pannexin 1 in erythrocytes: function without a gap. *Proc Natl Acad Sci U S A*, **103**, 7655-7659.

Maass K, Shibayama J, Chase SE, Willecke K, Delmar M (2007) C-terminal truncation of connexin43 changes number, size, and localization of cardiac gap junction plaques. *Circ Res*, **101**, 1283-1291.

Miro-Casas E, Ruiz-Meana M, Agullo E, Stahlhofen S, Rodriguez-Sinovas A, Cabestrero A, Jorge I, Torre I, Vazquez J, Boengler K, Schulz R, Heusch G, Garcia-Dorado D (2009) Connexin43 in cardiomyocyte mitochondria contributes to mitochondrial potassium uptake. *Cardiovasc Res*, **83**, 747-756.

Miura T, Miki T, Yano T (2010) Role of the gap junction in ischemic preconditioning in the heart. *Am J Physiol Heart Circ Physiol*, **298**, H1115-H1125.

Miura T, Ohnuma Y, Kuno A, Tanno M, Ichikawa Y, Nakamura Y, Yano T, Miki T, Sakamoto J, Shimamoto K (2004) Protective role of gap junctions in preconditioning against myocardial infarction. *Am J Physiol Heart Circ Physiol*, **286**, H214-H221.

Oviedo-Orta E, Errington RJ, Evans WH (2002) Gap junction intercellular communication during lymphocyte transendothelial migration. *Cell Biol Int*, **26**, 253-263.

Pelegrin P, Surprenant A (2006) Pannexin-1 mediates large pore formation and interleukin-1beta release by the ATP-gated P2X7 receptor. *EMBO J*, **25**, 5071-5082.

Ponsaerts R, De Vuyst E, Retamal M, D'hondt C, Vermeire D, Wang N, De Smedt H, Zimmermann P, Himpens B, Vereecke J, Leybaert L, Bultynck G (2010) Intramolecular loop/tail interactions are essential for connexin 43-hemichannel activity. *FASEB J*, **24**, 4378-4395.

Ponsaerts R, Wang N, Himpens B, Leybaert L, Bultynck G (2012) The contractile system as a negative regulator of the connexin 43 hemichannel. *Biol Cell*, **104**, 367-377.

Ramachandran S, Xie LH, John SA, Subramaniam S, Lal R (2007) A novel role for connexin hemichannel in oxidative stress and smoking-induced cell injury. *PLoS One,***2**, e712.

Retamal MA, Cortes CJ, Reuss L, Bennett MV, Saez JC (2006) S-nitrosylation and permeation through connexin 43 hemichannels in astrocytes: induction by oxidant stress and reversal by reducing agents. *Proc Natl Acad Sci U S A,* **103**, 4475-4480.

Retamal MA, Schalper KA, Shoji KF, Bennett MV, Saez JC (2007) Opening of connexin 43 hemichannels is increased by lowering intracellular redox potential. *Proc Natl Acad Sci U S A*, **104**, 8322-8327.

Retamal MA, Schalper KA, Shoji KF, Orellana JA, Bennett MV, Saez JC (2007) Possible involvement of different connexin43 domains in plasma membrane permeabilization induced by ischemia-reperfusion. *J Membr Biol*, **218**, 49-63.

Rhett JM, Jourdan J, Gourdie RG (2011) Connexin 43 connexon to gap junction transition is regulated by zonula occludens-1. *Mol Biol Cell*, **22**, 1516-1528.

Rodriguez-Sinovas A, Boengler K, Cabestrero A, Gres P, Morente M, Ruiz-Meana M, Konietzka I, Miro E, Totzeck A, Heusch G, Schulz R, Garcia-Dorado D (2006) Translocation of connexin 43 to the inner mitochondrial membrane of cardiomyocytes through the heat shock protein 90-dependent TOM pathway and its importance for cardioprotection. *Circ Res*, **99**, 93-101.

Rodriguez-Sinovas A, Sanchez JA, Fernandez-Sanz C, Ruiz-Meana M, Garcia-Dorado D (2011) Connexin and pannexin as modulators of myocardial injury. *Biochim Biophys Acta*, **1818**, 1962-1970.

Saez JC, Schalper KA, Retamal MA, Orellana JA, Shoji KF, Bennett MV (2010) Cell membrane permeabilization via connexin hemichannels in living and dying cells. *Exp Cell Res*, **316**, 2377-2389.

Sanchez HA, Orellana JA, Verselis VK, Saez JC (2009) Metabolic inhibition increases activity of connexin-32 hemichannels permeable to Ca2+ in transfected HeLa cells. *Am J Physiol Cell Physiol,* **297**, C665-C678.

Sanchez JA, Rodriguez-Sinovas A, Fernandez-Sanz C, Ruiz-Meana M, Garcia-Dorado D (2011) Effects of a reduction in the number of gap junction channels or in their conductance on ischemia-reperfusion arrhythmias in isolated mouse hearts. *Am J Physiol Heart Circ Physiol*, **301**, H2442-H2453.

Schulz R, Boengler K, Totzeck A, Luo Y, Garcia-Dorado D, Heusch G (2007) Connexin 43 in ischemic pre- and postconditioning. *Heart Fail Rev*, **12**, 261-266.

Schwanke U, Konietzka I, Duschin A, Li X, Schulz R, Heusch G (2002) No ischemic preconditioning in heterozygous connexin43-deficient mice. *Am J Physiol Heart Circ Physiol*, **283**, H1740-H1742.

Seki A, Coombs W, Taffet SM, Delmar M (2004) Loss of electrical communication, but not plaque formation, after mutations in the cytoplasmic loop of connexin43. *Heart Rhythm*, **1**, 227-233.

Severs NJ, Bruce AF, Dupont E, Rothery S (2008) Remodelling of gap junctions and connexin expression in diseased myocardium. *Cardiovasc Res*, **80**, 9-19.

Shibayama J, Paznekas W, Seki A, Taffet S, Jabs EW, Delmar M, Musa H (2005) Functional characterization of connexin43 mutations found in patients with oculodentodigital dysplasia. *Circ Res,* **96**, e83-e91.

Shintani-Ishida K, Uemura K, Yoshida K (2007) Hemichannels in cardiomyocytes open transiently during ischemia and contribute to reperfusion injury following brief ischemia. *Am J Physiol Heart Circ Physiol,* **293**, H1714-H1720.

Spray DC, Ye ZC, Ransom BR (2006) Functional connexin "hemichannels": a critical appraisal. *Glia*, **54**, 758-773.

Stankovicova T, Szilard M, De S, I, Sipido KR (2000) M cells and transmural heterogeneity of action potential configuration in myocytes from the left ventricular wall of the pig heart. *Cardiovasc Res*, **45**, 952-960.

Thompson RJ, Jackson MF, Olah ME, Rungta RL, Hines DJ, Beazely MA, MacDonald JF, MacVicar BA (2008) Activation of pannexin-1 hemichannels augments aberrant bursting in the hippocampus. *Science*, **322**, 1555-1559.

Tribulova N, Seki S, Radosinska J, Kaplan P, Babusikova E, Knezl V, Mochizuki S (2009) Myocardial Ca2+ handling and cell-to-cell coupling, key factors in prevention of sudden cardiac death. *Can J Physiol Pharmacol*, **87**, 1120-1129.

Unwin PN, Ennis PD (1983) Calcium-mediated changes in gap junction structure: evidence from the low angle X-ray pattern. *J Cell Biol*, **97**, 1459-1466.

Unwin PN, Zampighi G (1980) Structure of the junction between communicating cells. *Nature*, **283**, 545-549.

Veenstra RD, DeHaan RL (1986) Measurement of single channel currents from cardiac gap junctions. *Science*, **233**, 972-974.

Vergara L, Bao X, Bello-Reuss E, Reuss L (2003) Do connexin 43 gap-junctional hemichannels activate and cause cell damage during ATP depletion of renal-tubule cells? *Acta Physiol Scand*, **179**, 33-38

Wang J, Ma M, Locovei S, Keane RW, Dahl G (2007) Modulation of membrane channel currents by gap junction protein mimetic peptides: size matters. *Am J Physiol Cell Physiol*, **293**, C1112-C1119.

Wang N, De Bock M, Antoons G, Gadicherla AK, Bol M., Decrock E, Evans WH, Sipido KR, Bukauskas FF, Leybaert L (2012) Connexin mimetic peptides inhibit Cx43 hemichannel opening triggered by voltage and intracellular Ca2+ elevation. *Basic Res Cardiol*, **107**, 304.

Warner A, Clements DK, Parikh S, Evans WH, DeHaan RL (1995) Specific motifs in the external loops of connexin proteins can determine gap junction formation between chick heart myocytes. *J Physiol,* **488** (Pt 3), 721-728.

Wright CS, van Steensel MA, Hodgins MB, Martin PE (2009) Connexin mimetic peptides improve cell migration rates of human epidermal keratinocytes and dermal fibroblasts in vitro. *Wound Repair Regen*, **17**, 240-249

Yang XM, Liu Y, Liu Y, Tandon N, Kambayashi J, Downey JM, Cohen MV (2010) Attenuation of infarction in cynomolgus monkeys: preconditioning and postconditioning. *Basic Res Cardiol*, **105**, 119-128

Supplementary Material

Online Fig. S1

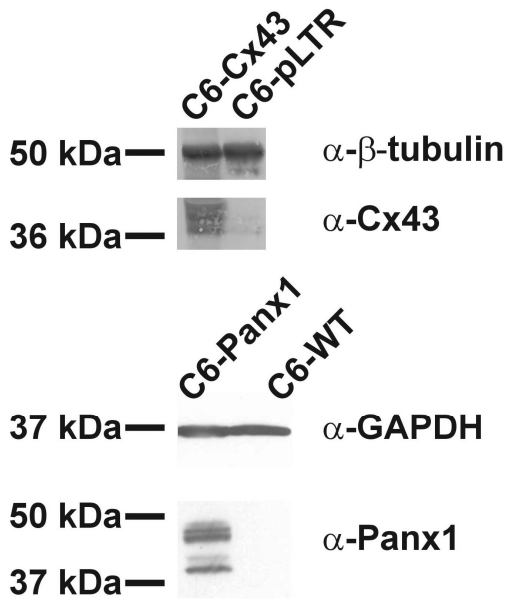

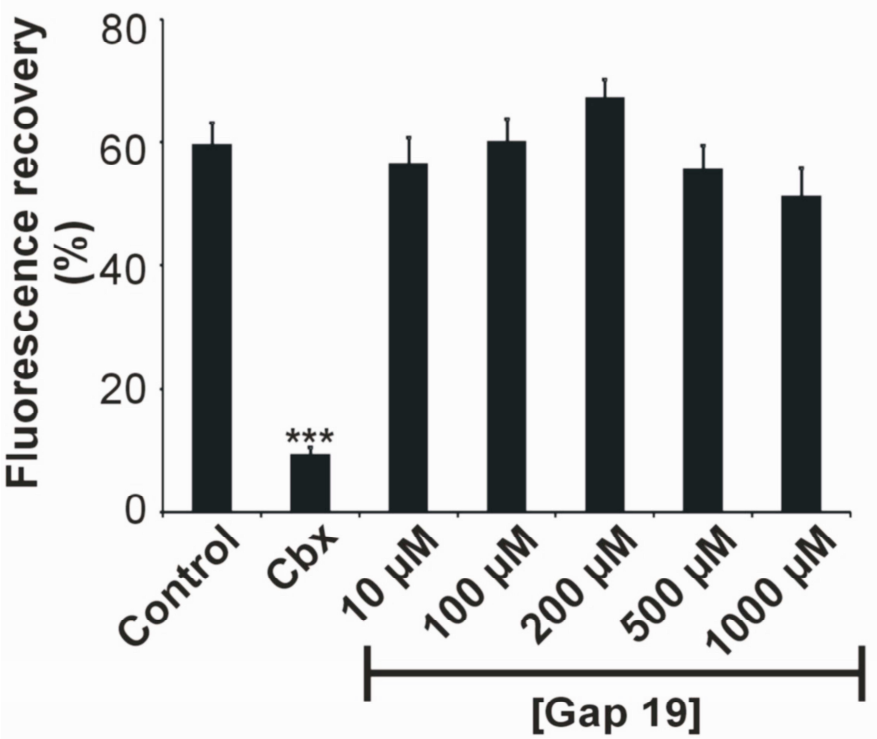

Online Figure S1. A. Western blotting demonstrating Cx43 and Panx1 expression in the C6 cell lines used. β-tubulin was the loading control for Cx43 and GADPH for Panx1. **B. Gap19 does not inhibit dye coupling in C6-Cx43 cells.** Exposing C6-Cx43 cells to different concentrations of Gap19 (10-1000 µM) during 1 h had no effect on dye coupling measured with FRAP. The GJ blocker carbenoxolone (Cbx, 25 µM, 1 h) was used as a positive control (n = 5). *** indicates significantly different from control with $p < 0.001$.

Online Fig. S2

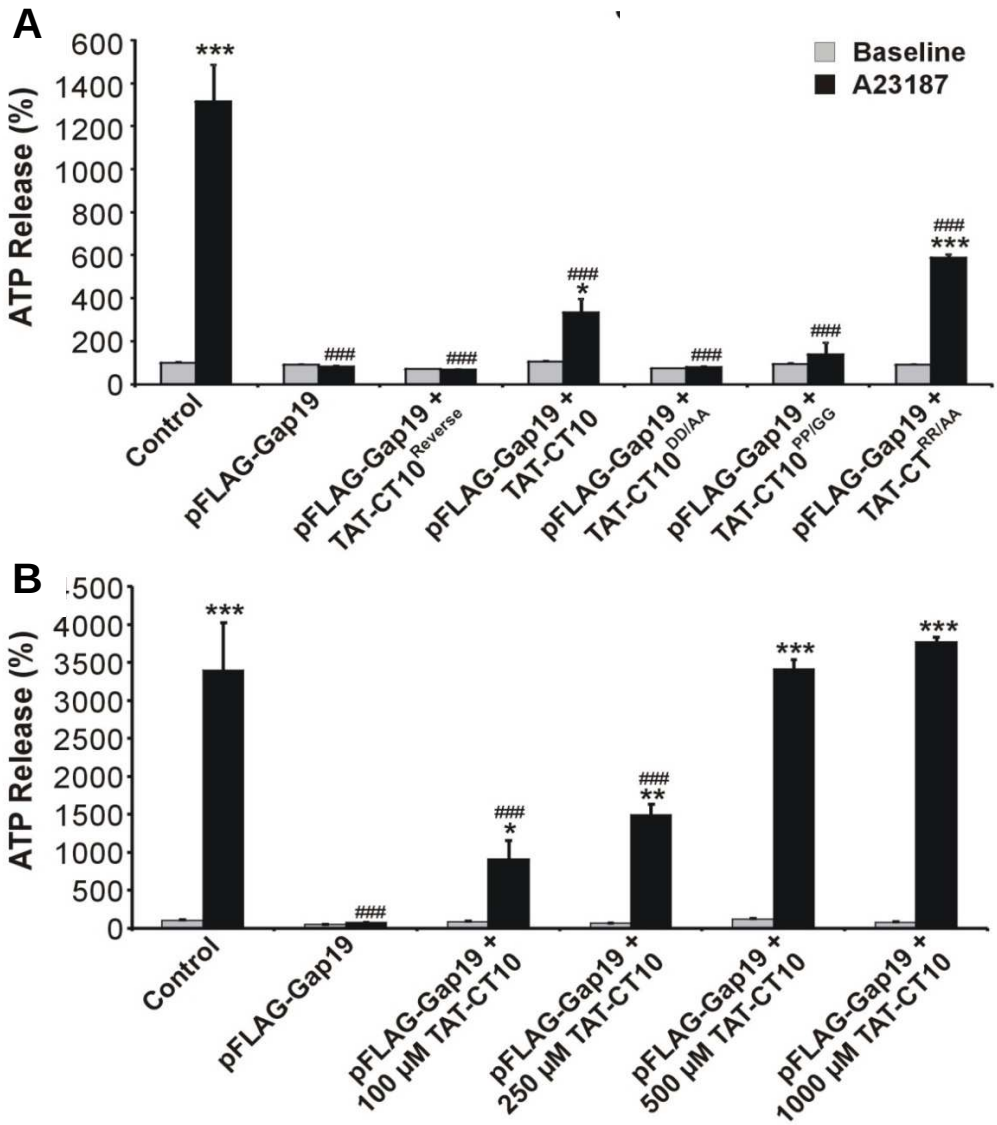

Online Figure S2. The effect of pFLAG-Gap19 is reversed by the CT10 peptide. A. Transiently transfecting C6-Cx43 cells with pFLAG-Gap19 completely abolished $[Ca^{2+}]_i$-triggered ATP release. CT10 peptide (100 µM, 30 min) partially reversed the pFLAG-Gap19 inhibitory effect, while $CT10^{reverse}$ had no effect. The two aspartate and the two proline residues are crucial for the CT10 effect (n = 12). **B.** The partial reversal of pFLAG-Gap19 inhibitory effects by TAT-CT10 becomes complete with higher concentrations of TAT-CT10 (n = 12). The fact that higher concentrations were necessary to obtain complete reversal (compared to Fig. 2F) indicates that the plasmid expression system generates higher Gap19 concentrations in the cell as compared to extracellulary added Gap19. Star signs indicate significantly different from baseline, number signs indicate significantly different from control.

Fig. S3

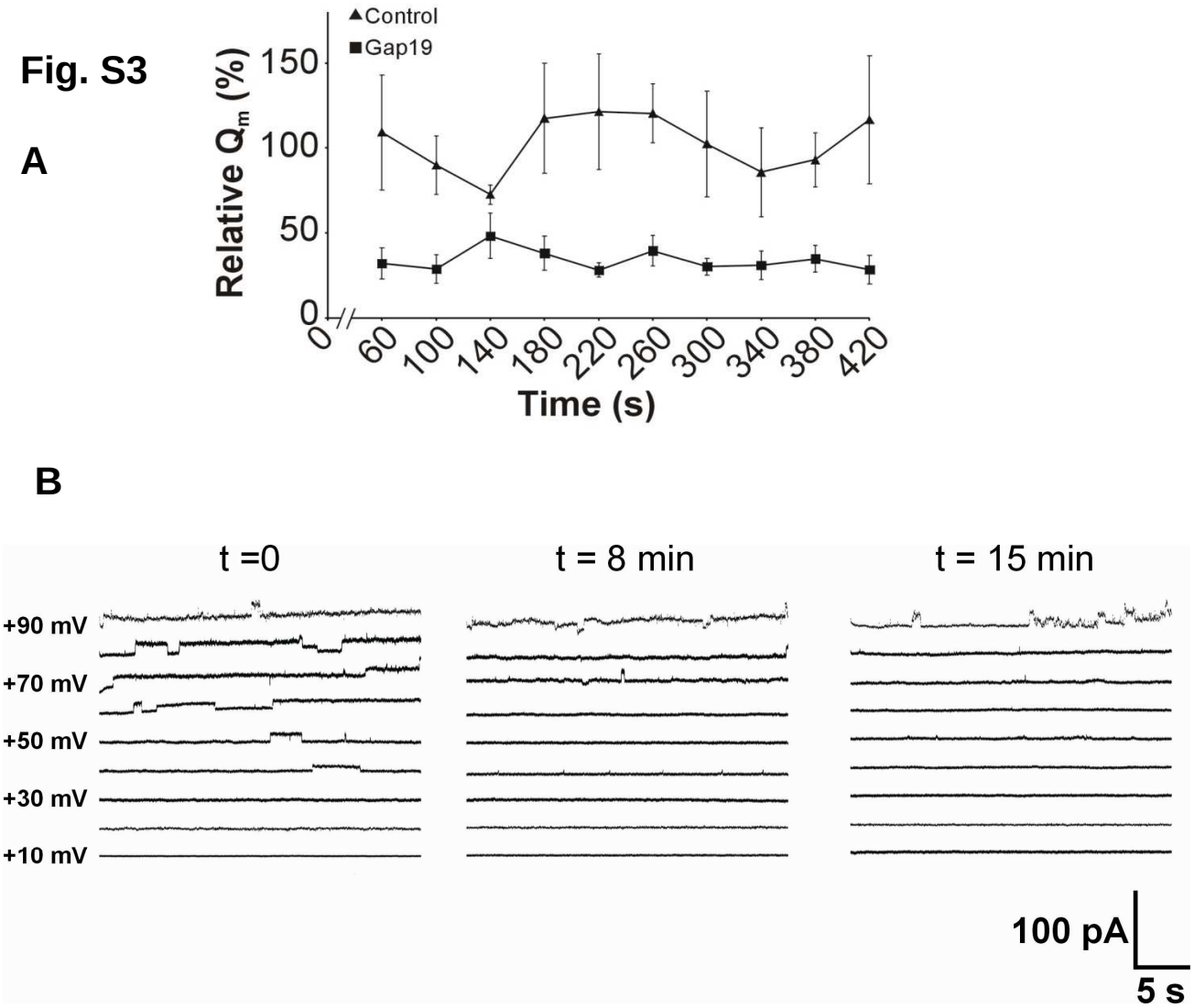

Online Figure S3. Unitary current activities as a function of time. A. Data from C6-Cx43 cells. Graph depicting Q_m as a function of time in voltage-clamp experiments. Q_m was normalized to the average value recorded in control. After formation of a gigaseal, the membrane was disrupted giving access to the cell (time zero). Depolarizing voltage steps to +70 mV (30 s) were repeatedly applied over a total recording period of 360 s and the corresponding Q_m was quantified. The effect of Gap19 (400 µM, present in the pipette) was apparent from the start of the recording (1 min after rupturing the plasma membrane in whole-cell recording) and the Q_m trace remained stable over the entire recording period, demonstrating ~75 % inhibition of the control Q_m trace. Taken together, this suggests that Gap19 acts within 1 min. The lower variability of the currents with Gap19 is related to inhibition of unitary event activity that lies at the basis of the noise observed in the control recording (n = 6 for control and 8 for Gap19). **B.** Data from acutely isolated pig ventricular myocytes. Example traces recorded at different points in time with Gap19 (100 µM) in the recording pipette. Isolated cardiomyocytes were stepped to positive V_m ranging from +10 mV to +90 mV (30 s) in 10 mV increments. Time 0 indicates onset of recording just after patch break. Effect of Gap19 on voltage-dependence of hemichannel openings was progressively enhanced over time and reached steady-state within 8 min.

Fig. S4

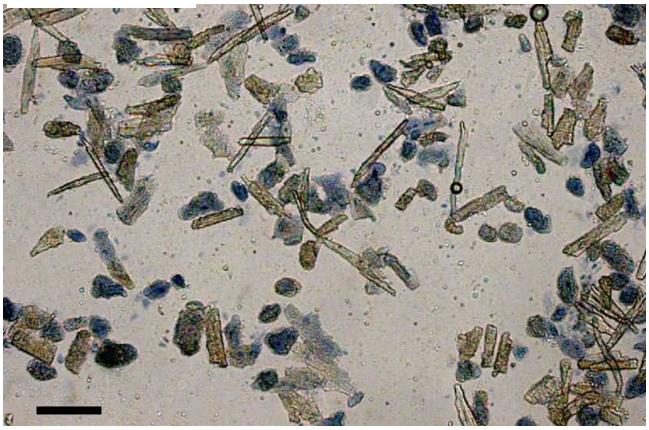

Online Figure S4. Example image illustrating a typical trypan blue cell viability staining. After exposure to *in vitro* ischemia/reperfusion, rounded cardiomyocytes were stained by trypan blue while rod-shaped healthy cells were trypan blue negative. Bar = 100 µm.

Fig. S5

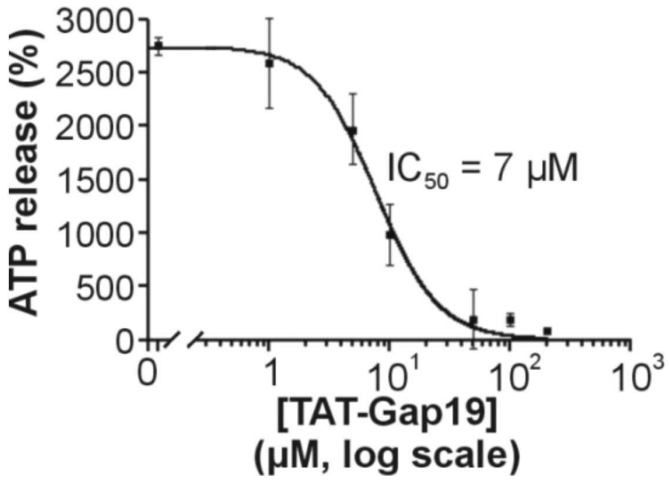

Online Figure S5. Concentration-dependent inhibition of hemichannel activities by TAT-conjugated Gap19. Inhibition of $[Ca^{2+}]_i$-triggered ATP release by TAT-Gap19 was characterized by an IC_{50} of ~7 µM (Hill coefficient = 2). ATP release in ordinate expresses baseline-subtracted measurements; data obtained in C6-Cx43 cell cultures (n = 5). Compare to Fig . 1d.

Fig. S6

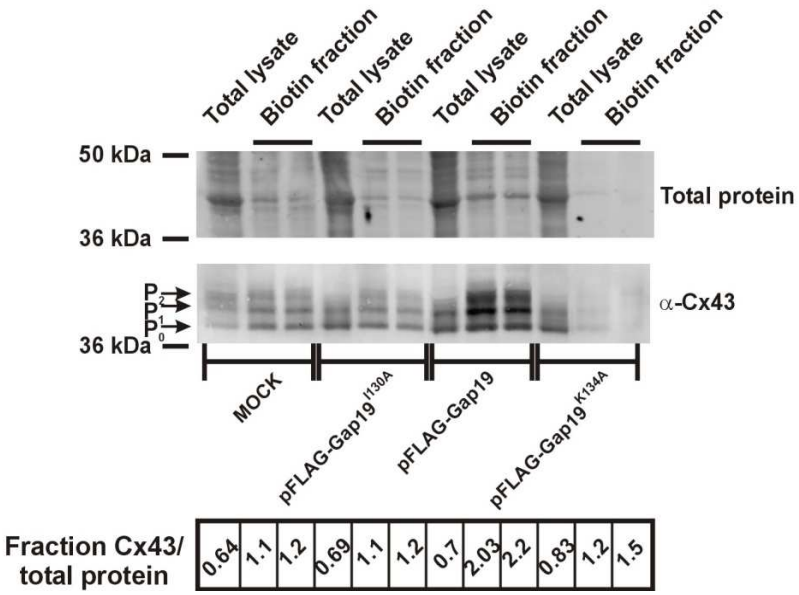

Online Figure S6. pFLAG-Gap19 increases the hemichannel fraction. Transient transfection of C6-Cx43 cells with pFLAG-Gap19 increased the hemichannel fraction (Biotin fraction) present at the plasma membrane, while the inactive mutants pFLAG-Gap19^{I130A} and pFLAG-Gap^{K134A} had no effect (data shown representative of 3 different experiments). The Biotin fraction showed clearly increased phosphorylation, especially at the P1 band.

TABLES

Table S1. Overview of the different peptides used in this study.

Peptide	Sequence
Gap19	^{128}KQIEIKKFK^{136}
Gap19^{I130A}	KQAEIKKFK
Gap19^{E131A}	KQIAIKKFK
Gap19$^{I130A/E131A}$	KQAAIKKFK
FLAG-Gap19	DYKDDDDK-GGSGGS-^{128}KQIEIKKFK^{136}
TAT-Gap19	YGRKKRRQRRR-^{128}KQIEIKKFK^{136}
TAT-CT10	YGRKKRRQRRR-^{373}SRPRPDDLEI^{382}
TAT-CT10^{reverse}	YGRKKRRQRRR-IELDDPRPRS
TAT-CT10$^{DD/AA}$	YGRKKRRQRRR-SRPRPAALEI
TAT-CT10$^{PP/GG}$	YGRKKRRQRRR-SRGRGDDLEI
TAT-CT10$^{RR/AA}$	YGRKKRRQRRR-SAPAPDDLEI
^{10}Panx1	^{74}WRQAAFVDSY^{83}
Scr^{10}Panx1	FSVYWAQADR

Table S2. DNA sequences cloned in the pcDNA5/FRT-EGFP vector.

Mutation	Forward primer	Reverse primer
Q129A	5’-GGCTCGGGCGGCTCCAAGGCG ATCGAGATA-3’	5’-CTTGAACTTCTTTATCTCGATC GCCTTGGA-3’
I130A	5’-AAGGCGGCTCGGGCGGATCCA AGCAGGCAGAGATA-3’	5’-TCTCTGCCTGCTTGGATCCGCC CGAGCCGCCTTTG-3’
K134A	5’-CCAAGCAGATAGAGATAAAGG CCTTCAAGT-3’	5’-GACTCGAGTTACTTGAAGGCC TTTATCTCT-3’
I130A/ K134A	5’-GGCTCCAAGCAGGCAGAGATA AAGGCCTTCAAGTA-3’	5’-AGTTACTTGAAGGCCTTTATCT CTGCCTGCTTGGA

SUPPLEMENTAL MATERIALS AND METHODS

An expanded methods section

Synthetic peptides,

Synthetic peptides used in this study were all obtained from Lifetein (Edison, New Jersey, USA). The identity of the peptides was confirmed by mass spectrometry and purity was ≥ 90 %.

Gap19 coding plasmids

The DNA sequence encoding Gap 19, separated from an N-terminal FLAG-tag by a double Gly-Gly-Ser linker, was cloned in a dual expression vector, pcDNA5/FRT-eGFP, which was modified with a second expression cassette allowing integration (*BamH*I-*Xho*I) of annealed oligos encoding FLAG-2x(GGS)-Gap19 under control of a second CMV promoter; 5'-GATCCACCATGGACTACAAAGACGACGACGACAAAGGCGGCTCGGGCGGCTCCA AGCAGATAGAGATAAAGAAGTTCAAGTAAC-3' and 5'-TCGAGTTACTTGAACTTC TTTATCTCTATCTGCTTGGAGCCGCCCGAGCCGCCTTTGTCGTCGTCGTCTTTGTA GTCCATGGTG-3'. Several mutated versions of this pFLAG-Gap 19 construct were generated using the Quikchange Site-directed mutagenesis kit ® (Stratagene, La Jolla, California, USA). The primer sequences used to generate the mutations are shown in Online Resource Table S2. All primers contained extra restriction sites to check the quality of the mutagenesis (Q129A: *Pvu*I; I130A: *BamH*I; K134A: *Stu*I and I130A/K134A: *Stu*I). All constructs were verified by DNA sequence analysis. Transfection with the Transfectin® reagent (Biorad) was done 6 h after seeding the cells at a density of 50000 cells/cm^2. The transfection efficiency was about 70 %. ATP release measurements were performed 24 h after transfection and SLDT 48 h after transfection.

Uptake studies of labeled Gap19 peptide

Peptide uptake studies were performed on C6 glioma cells stably transfected with Cx43 (C6-Cx43) (Zhu *et al.*, 1991). The cells were incubated with 200 µM fluorescein isothiocyanate (FITC) coupled Gap19, FITC-coupled Gap19I130A or fluorescein alone for 30 min at 37 °C. Subsequently, cells were washed extensively with PBSD to remove excessive fluorescence

and fixed with 4 % paraformaldehyde (in PBSD; 20 min at room temperature). After fixation the cells were exposed to phalloidin coupled to Alexa 546 (0.165 µM, 20 min at room temperature; Invitrogen, Merelbeke, Belgium) to label F-actin. After washing, the cells were mounted with Vectashield (Vector Laboratories, Labconsult, Brussels, Belgium) and imaged with a confocal microscope (LSM510, Carl Zeiss, Zaventem, Belgium) equipped with a x63 objective using 488 nm (fluorescein) or 543 nm (phalloidin) excitation lasers. Z-stacks were taken every 100 nm and the average intensity projection (the projection of the 3D Z-stacks on a 2D image) was calculated with ImageJ software (ImageJ 1.44; NIH, Bethesda, Maryland, USA; http://rsb.info.nih.gov/ij). In this image, the regions of interest (ROI) were defined in the cytoplasm of each cell, based on the phalloidin staining, making use of ImageJ software. All cell ROI had the same surface area.

ATP release experiments

ATP release experiments were performed on C6-Cx43 cells (Zhu *et al.*, 1991), C6-Panx1 cells (Lai *et al.*, 2007) and HeLa cells (Traub *et al.*, 1994). C6-Cx43 and C6-Panx1 cells were maintained in DMEM:Ham's F12 (1:1 - Invitrogen, Merelbeke, Belgium) and HeLa-Cx40 cells were grown in DMEM, all supplemented with 10% fetal bovine serum, 2 mM glutamine, 10 U/ml penicillin, 10 µg/ml streptomycin and 0.25 µg/ml fungizone. Cells were seeded at a density of 50000 cells/cm² and used for experiments the next day (non-confluent low density cultures).

ATP release was measured directly in the medium above the cells using luciferin-luciferase and luminometric measurements with a plate reader protocol as previously described in (De Vuyst *et al.*, 2006c). Baseline measurements were carried out on separate cultures with HBSS-HEPES (Hanks' balanced salt solution - pH 7.4) vehicle only. All applied agents were added to the medium of the cell cultures in the CO_2 incubator at 37 °C, for the times indicated in the text, and were not present during stimulation and measurement to avoid interference with luminometry.

Junctional conductance measurements

Experiments were performed on a Novikoff rat hepatoma cell line that endogenously expresses wild-type Cx43. These cells were grown in Swim's S-77 medium supplemented with 4 mM glutamine, 20 % horse serum and 5 % fetal bovine serum. Junctional conductance

was measured in cell pairs (cell-1 and -2) using dual whole-cell patch-clamp. Each cell was voltage clamped with separate amplifiers (EPC-8, HEKA Instruments, Bellmore, NY, USA) and data were digitized and acquired with a BNC-2090 A/D converter (National Instruments, Austin, TX, USA). Analysis was performed with custom-developed software (Trexler Technologies). Cells were grown onto glass coverslips and placed on an experimental chamber mounted on the stage of an Olympus IX70 inverted microscope (Olympus America, Center Valley, PA, USA). Cells were continuously perfused (at room temperature) with modified Krebs-Ringer solution that contained (in mM): NaCl, 140; KCl, 4; $CaCl_2$, 2; $MgCl_2$, 1; glucose, 5; pyruvate, 2; Hepes, 5 (pH 7.4). Pipette solution, with or without 400 μM of Gap19, contained (in mM): KCl, 140; NaAsp, 10; K_2ATP, 3; $MgCl_2$, 1; $CaCl_2$, 0.2; EGTA, 2; Hepes, 5 (pH 7.2). Transjunctional voltage (V_j) was applied by varying the voltage in cell-1 with repeated ramps of ±10 mV in amplitude and 600 ms in duration, and keeping the voltage constant in cell-2. Junctional current (I_j) was measured as the change in current in cell-2 (ΔI_2), and because I_j has the same orientation as V_j a negative sign is used, thus $I_j = -\Delta I_2$. Junctional conductance (G_j) was calculated as $G_j = I_j/V_j$. Octanol (5 mM) was perfused at the end of every experiment to completely block G_j and rule out the presence of cytoplasmic bridges.

Gap junction dye transfer

GJ dye transfer was investigated with FRAP (fluorescent recovery after photobleaching) and SLDT (scrape loading and dye transfer) methods. For FRAP, confluent C6-Cx43 cultures grown on plastic Petri dishes (Becton Dickinson, Erembodegem, Belgium) were loaded with 5-carboxyfluorescein diacetate acetoxy methylester (CFDA-AM, 20 μM) in HBSS-HEPES for 1 h at room temperature, followed by 30 min de-esterification. Fluorescence within a single cell was photobleached by spot exposure to the 488 nm line of an Argon laser (10 s). Fluorescence imaging (at 488 nm excitation) was performed using a custom-made video-rate confocal laser scanning microscope with a x40 water immersion objective (CFI Plan Fluor, NA 1.4, Nikon Benelux, Brussels, Belgium) and fluorescence recovery was measured over a 5 min time period after photobleaching.

For SLDT, confluent monolayer cultures were washed with nominally Ca^{2+}-free HBSS-HEPES and then incubated for 1 min in this solution containing 0.4 mM 6-carboxy fluorescein (6-CF). A linear scratch was made across the culture using a syringe needle and the cells were left for another minute in the same solution. Cultures were then washed 4 times with HBSS-HEPES, left for 15 min at room temperature and images were taken with a Nikon

TE300 inverted microscope with FITC excitation/emission settings, a x10 objective and a Nikon DS-5M camera (Analis, Namur, Belgium). A fluorescence diffusion profile was extracted from the images, fitted to a mono-exponential decaying function and a spatial constant of intercellular dye spread was determined.

Unitary current hemichannel measurements

Hela-Cx43 cells were placed in a recording chamber containing a bath solution composed of (in mM) 150 NaCl, 4 KCl, 2 $MgCl_2$, 5 glucose, 5 HEPES, 2 pyruvate, 2 $CaCl_2$, 2 CsCl, 1 $BaCl_2$ (pH = 7.4). Recording pipettes contained (in mM): 130 KCl, 10 Na-aspartate, 0.26 $CaCl_2$, 5 HEPES, 2 EGTA, 5 TEACl, 1 $MgCl_2$ (pH = 7.2). The free Ca^{2+} concentration of the pipette solution was estimated to be ~50 nM as calculated with WEBMAX (http://www.stanford.edu/~cpatton/webmaxcS.htm)

For the experiments on pig cardiomyocytes, left ventricular cardiomyocytes from adult domestic pigs were enzymatically isolated (Stankovicova *et al.*, 2000a). Briefly, the left anterior descending coronary artery was cannulated, and the cells were dissociated by enzymatic tissue digestion throughout Langendorff perfusion at 37°C. During the recording, isolated cells were initially perfused with the standard Tyrode solution (in mM): 137 NaCl, 5.4 KCl, 1.8 $CaCl_2$, 0.5 $MgCl_2$, 10 glucose, 11.8 HEPES and pH adjusted to 7.4. When recording unitary hemichannel currents, the solution was switched to one with the same composition but with all K^+ replaced by Cs^+ and additional 1 mM Ba^{2+}. During the 30s depolarization steps, the time dependent currents such as Na^+ and Ca^{2+} did not contaminate the observation of connexin hemichannel opening. The standard pipette solution was composed of (in mM): 120 CsCl, 5 NaCl, 10 TEACl, 1 $CaCl_2$, 1 $MgCl_2$, 2 MgATP, 10 EGTA, 10 HEPES and pH adjusted to 7.2. The free Ca^{2+} concentration of the pipette solution was estimated to be ~50 nM as calculated with WEBMAX. During metabolic inhibition, myocytes were dialyzed by pipette solution with slight modifications: 120 CsCl, 3 NaCl, 10 TEACl, 1 $CaCl_2$, 2 $MgCl_2$, 2 MgATP, 1 NaH_2PO_4, 5 sodium pyruvate, 1 NaADP, 10 HEPES, 10 EGTA, pH 7.2. Pyruvate, P_i, Mg and ADP that are metabolic substrates for oxidative phosphorylation in control were included to allow ATP depletion during metabolic inhibition.

Single channel recordings in Hela cells and cardiomyocytes were performed as previously described (Contreras *et al.*, 2003d), making use of an EPC 7 PLUS patch-clamp amplifier (HEKA Elektronik, Germany) and Axon Axopatch 200B (Axon Instruments/Molecular Devices, USA) respectively. Data were acquired at 4 kHz using a NI USB-6221 data

acquisition device from National Instruments (Austin, TX) and Clampex 10.2 acquisition software (Axon instruments/Moleuclar Devices, USA). All currents in whole-cell configuration were filtered at 1 kHz (7-pole Besselfilter). Membrane potentials were corrected for the liquid junction potentials.

Surface plasmon resonance (SPR)

SPR experiments were performed using a Biacore 2000 system. Equal amounts of > 95 % pure biotinylated peptides (biotin-gap19, biotin-L2 and biotin-L2-reverse) were immobilized on flow cells of a streptavidin-coated sensor chip (BR-1000-32, Biacore AB, Uppsala Sweden) using HEPES buffer (in mM: 10 HEPES, 1 EDTA, 100 NaCl) with 0.005 % P-20 at pH 7.4. Measurements with analyte were done at a flow rate of 30 µl/min in HEPES running buffer at pH 6.8. Binding of analyte was verified at different concentrations, in random order (injection volume 120 µl). The chip-surface was regenerated by injection of 10 µl of alkalic buffer (50 mM NaOH, 1 M NaCl) at 10 µl/min. The CT tail of Cx43 was used as analyte and measured in analytically prepared buffers. Background signals obtained from the reference flow cell, containing immobilized L2-reverse peptide, were subtracted to generate response curves. For quantification of resonance signal of repeated measurements, the resonance unit value recoded at 1 second before the stop of injection was taken for each sensorgram (acquisition at 1 Hz), corresponding to the last resonance unit value in the association phase of the sensorgram.

Purification of the CT tail of Cx43

The complete CT tail of Cx43 was recombinantly expressed in BL21(DE3) and purified as GST-fusion protein. Briefly, the pGEX6p2-Cx43CT cDNA (AA 255-382) plasmid construct, obtained from P. Sorgen (Hirst-Jensen *et al.*, 2007b), was transformed into BL21(DE3) bacteria. Protein expression was induced by 0.1 mM IPTG at 28 °C for 4 h in diluted overnight-grown bacterial cultures when the OD600 reached 0.6 to 0.8. Bacterial cells were lysed using sonication and the soluble fraction was collected by centrifugation for further purification on glutathione Sepharose 4B. GST was removed from the immobilized GST-Cx43CT protein by using 40 U PreScission protease for 4 h (GE Healthcare, Buckinghamshire, United Kingdom) and the soluble fraction containing the purified CT tail was collected, dialysed against PBS using Slide-A-Lyzer (cutoff: 3 kDa) and stored at -80 °C

awaiting further analysis. Protein concentration was determined using the BCA method. Protein purity and cleavage efficiency was analyzed using SDS-PAGE, followed by total protein staining using Gelcode Blue^{TM} stain reagent (Thermo Scientific). All samples contained at least 10 µM of the complete CT tail protein with a purity of > 90 %.

In vivo cardiac ischemia/reperfusion

Eight to 10 week old C57/Bl6 mice were subjected to 30 min ischemia by LAD coronary artery ligation followed by release of the ligature and 120 min reperfusion (Boengler *et al.*, 2008b;Schwanke *et al.*, 2002b). The area at risk was measured by Evans Blue intracardially injected after ischemia/reperfusion and the size of the ischemic zone was determined by 2,3,3-triphenyl tetrazolium chloride (TTC) staining. Gap19 or Gap19^{I130A} were injected in the jugular vein 10 min prior to ischemia dissolved in 0.9 % NaCl solution. All procedures were approved by the Bioethical Committee of the district of Düsseldorf, Germany, and conformed to the Guide for the Care and Use of Laboratory Animals (NIH publication No. 85-23, revised 1996).

Western blotting

Cell lysates were extracted by treatment of confluent cultures with RIPA buffer (25 mM Tris, 50 mM NaCl, 0.5 % NP-40, 0.5 % deoxycholate, 0.1 % SDS, 5.5 % β-glycerophosphate, 1 mM dithiothreitol, 2 % phosphatase inhibitor cocktail, and 2 % mini EDTA-free protease inhibitor cocktail) and sonicated by three 10 s pulses. Protein concentration was determined with a Biorad DC protein assay kit, and absorbance was measured with a 590 nm long-pass filter. Proteins were separated by electrophoresis on a 10 % SDS-poly-acrylamide gel and transferred to a nitrocellulose membrane (GE Healthcare). Blots were probed with a rabbit polyclonal anti-rat Cx43 antibody (1/10000; Sigma) or a rabbit polyclonal anti-rat Panx1 (Penuela *et al.*, 2007b) (1/1000) followed by alkaline phosphatase conjugated goat anti-rabbit IgG (1/8000, Sigma) and detection was done with nitro blue tetrazolium/5-bromo-4-chloro-3-indolyl phosphate reagent (Zymed, Invitrogen). Multiple bands on the Panx1 blots are probably the consequence of different glycosylated forms (Penuela *et al.*, 2009b).

Isolation of the Cx43 hemichannel fraction

The Cx43 hemichannel fraction was isolated from a confluent monolayer of C6-Cx43 cells with the Pierce cell surface protein isolation kit (Thermo Scientific, Erembodegem, Belgium) according to the manufacturer's instructions. Briefly, a monolayer of C6-Cx43 cells was exposed to PBS containing 0.25 mg/ml sulfo-NHS-SS-biotin for 2h at 4 °C. The biotinylation reaction was stopped by adding quenching solution and incubated for 5 min at room temperature. Subsequently, the cells were scraped and lysed with the provided lysis buffer, mixed with Neutravidine^{TM} agarose and incubated overnight at 4 °C with end-over-end mixing. The biotinylated proteins were eluted from the Neutravidine^{TM} agarose through heating of the mixture in SDS-PAGE sample buffer. Separation of the biotinylated proteins was done on a 10 % SDS-PAGE, followed by Western blotting and detection of Cx43.

References

Boengler K, Buechert A, Heinen Y, Roeskes C, Hilfiker-Kleiner D, Heusch G, Schulz R (2008) Cardioprotection by ischemic postconditioning is lost in aged and STAT3-deficient mice. *Circ Res*, **102**, 131-135.

Contreras JE, Saez JC, Bukauskas FF, Bennett MV (2003) Gating and regulation of connexin 43 (Cx43) hemichannels. *Proc Natl Acad Sci U S A*, **100**, 11388-11393.

De Vuyst E, Decrock E, Cabooter L, Dubyak GR, Naus CC, Evans WH, Leybaert L (2006) Intracellular calcium changes trigger connexin 32 hemichannel opening. *EMBO J*, **25**, 34-44.

Hirst-Jensen BJ, Sahoo P, Kieken F, Delmar M, Sorgen PL (2007) Characterization of the pH-dependent interaction between the gap junction protein connexin43 carboxyl terminus and cytoplasmic loop domains. *J Biol Chem*, **282**, 5801-5813.

Lai CP, Bechberger JF, Thompson RJ, MacVicar BA, Bruzzone R, Naus CC (2007) Tumor-suppressive effects of pannexin 1 in C6 glioma cells. *Cancer Res*, **67**, 1545-1554.

Penuela S, Bhalla R, Gong XQ, Cowan KN, Celetti SJ, Cowan BJ, Bai D, Shao Q, Laird DW (2007) Pannexin 1 and pannexin 3 are glycoproteins that exhibit many distinct characteristics from the connexin family of gap junction proteins. *J Cell Sci,* **120**, 3772-3783.

Penuela S, Bhalla R, Nag K, Laird DW (2009) Glycosylation regulates pannexin intermixing and cellular localization. *Mol Biol Cell*, **20**, 4313-4323.

Schwanke U, Konietzka I, Duschin A, Li X, Schulz R, Heusch G (2002) No ischemic preconditioning in heterozygous connexin43-deficient mice. *Am J Physiol Heart Circ Physiol,* **283**, H1740-H1742.

Stankovicova T, Szilard M, De Scheerder I, Sipido KR (2000) M cells and transmural heterogeneity of action potential configuration in myocytes from the left ventricular wall of the pig heart. *Cardiovasc Res,* **45**, 952-960.

Traub O, Eckert R, Lichtenberg-Frate H, Elfgang C, Bastide B, Scheidtmann KH, Hulser DF, Willecke K (1994) Immunochemical and electrophysiological characterization of murine connexin40 and -43 in mouse tissues and transfected human cells. *Eur J Cell Biol*, **64**, 101-112.

Zhu D, Caveney S, Kidder GM, Naus CC (1991) Transfection of C6 glioma cells with connexin 43 cDNA: analysis of expression, intercellular coupling, and cell proliferation. *Proc Natl Acad Sci U S A*, **88**, 1883-1887.

Part

IV
General discussion
&
Future perspectives

4.1. Gap26/27 locks Cx43 hemichannels into the closed state

Suppression of specific connexin isoform expression making use of small interfering RNA technology or knock out (KO) animals are crucial to help distinguishing hemichannels from other molecular uptake/release pathways. However, a critical limitation of these genetic tools is that such approaches deplete both gap junction channel and hemichannel populations, challenging the validity of the conclusions drawn from such experiments. Further work with more refined models making use of inducible knock in technology to switch on the expression of mutant connexins that lack the extracellular loop cysteines and therefore are unable to pair up as gap junctions may be an interesting approach. Pharmacological interventions making use of peptides targeting connexin hemichannels is another approach (reviewed in (Evans *et al.*, 2012)). The peptides most frequently in use include ^{43}Gap26 (VCYDKSFPISHVR) and ^{43}Gap27 (SRPTEKTIFII) which are derived from highly conserved regions located respectively on the first and second extracellular loops of Cx43. *In vitro,* Gap26/27 assisted to determine the involvement of connexin hemichannels in a variety of cellular processes including dynamic Ca^{2+} signals (Ca^{2+} waves and Ca^{2+} oscillations) (Braet *et al.*, 2003;De Bock *et al.*, 2011), release of neurotransmitters (Romanov *et al.*, 2007) as well as propagation of cell death (Decrock *et al.*, 2009). In *vivo*, these peptides, by targeting Cx43 hemichannels, conferred cardioprotection against ischemia/reperfusion, reduced tissue damage secondary to spinal cord injury and rescued vascular permeability following retinal ischemia (Danesh-Meyer *et al.*, 2012;Hawat *et al.*, 2012;O'Carroll *et al.*, 2013). Intriguingly, despite the growing interest and wide use of Gap26/27 in hemichannel studies, no conclusive data and arguments are available to support a direct action of these substances on hemichannels. Initial studies of our group reporting hemichannel block by Gap26/27 were based on ATP release/dye uptake measurements. This work is complemented by electrophysiology studies in Cx43 expressing taste bud cells (Romanov *et al.*, 2008), but contrasts to other findings performed in *Xenopus* oocyte claiming little effect of Gap26 on macroscopic hemichannels currents (Wang *et al.*, 2007).

To address the controversy, we investigated the effect of Gap26/27 at single-channel level which allows an unequivocal identification of Cx43 hemichannels by a typical unitary conductance of ~220 pS and conductance-voltage profile. In HeLa cells expressing Cx43, Gap26/27 inhibited the unitary current activities at positive membrane potential (+70 mV) within 4 min. The effect was Gap26/27 sequence specific when applied at hundreds of micromolar concentrations. A striking finding consists of a right-shifted voltage dependence

of Cx43 hemichannels by Gap26/27. However, if the inhibition is merely a result of an elevated voltage threshold for hemichannel activation, it simply could not reconcile with the Gap26/27 effect previously observed in electrically non-excitable cells or when stimuli other than voltage were used. In C6 glioma cells overexpressing Cx43, Gap26/27 abolished the potent effect of increased intracellular Ca^{2+} concentration ($[Ca^{2+}]_i$) on hemichannel responses. In cytokine treated astrocytes, enhanced dye permeability through open hemichannels was prevented by Gap26/27 (Retamal *et al.*, 2007a). A similar effect of Gap26 was captured in astrocytes treated with dithiothreitol that lowered the intracellular redox potential (Retamal *et al.*, 2007b). In retinal pigment epithelial cells, ATP release through Cx43 hemichannels was stimulated by spontaneous elevation of $[Ca^{2+}]_i$, but disappeared in the presence of Gap26 (Pearson *et al.*, 2005). Up to now, most of the evidence supports Gap26/27-mediated hemichannel inhibition without documented voltage changes.

Of note, Gap26/27 in our work, prohibited the fully-opening events of Cx43 hemichannels without affecting subconductance states (60.3 ± 2.4 in control *versus* 60.3 ± 2.1 pS with Gap26/27 (n = 15)). Thus, Gap26/27 is likely to block the fully open hemichannels, leaving the residual state unaffected. Owing to the reduction of opening events in Gap26/27 treated cells, the subconductance events became more apparent in the all-point histogram (Chapter III, Fig. 2b). Conceivably, reduced open probability rather than unitary conductance is the primary cause of Gap26/27-suppressed charge transfer through Cx43 hemichannels (Chapter III, Fig. 2). Currently, little is known about the precise domains of Cx43 to which the peptides bind. For Gap26, imaging with atomic force microscopy detected a specific interaction with the extracellular side of a Cx43 hemichannel (Liu *et al.*, 2006). Because the blocking kinetics over a time span of minutes seem relatively slow for a direct binding, we had initially proposed a limited accessibility of the target site either as a consequence of being only reached while a channel is open (open channel block) or being buried deep in the external channel structure. Open channel block accounts for actions of many local anesthetics and quaternary ammonium derivatives on K^+ channels. The typical feature of ionic block at the channel open state has guided the identification of pore-lining residues of Cx46, Cx50 and chimeric Cx32*Cx43EL1 hemichannels (Kronengold *et al.*, 2003a;Kronengold *et al.*, 2003b;Tang *et al.*, 2009;Verselis *et al.*, 2009). Nevertheless, there are at least three lines of evidence arguing against the hypothesis. First of all, typical features of open channel block include flickering open channels and reduced unitary conductance (Hurst *et al.*, 1995), which was not detected in any single-channel traces after Gap26/27 application. Secondly, the

peptides carry net positive charges. If the binding site resided within the open channel, Gap26/27 would need to traverse the electrical field in the pore upon binding, resulting in a voltage-dependent block (Jackson, 2010). The hemichannel activity in function of V_m was right-shifted by Gap26/27, but did not show any 'kink' at high V_m which would implicate electrical repulsion. Thirdly, exposing typically closed Cx43 hemichannels at resting V_m to extracellular Gap26/27 for 30 min, readily achieved a maximal inhibition of hemichannel currents by 70% in the following V_m steps to +70 mV. Taken together, Gap26/27 is expected to interact with closed hemichannels that expose the binding site outside the permeation pathway. Peptide binding would favor channel residency in the closed configuration, locking any Gap26/27-bound hemichannels in the original closed state. This so called 'state-dependent lock of closed channels' was originally introduced to resolve the slow gating mechanism of Cx32*Cx43EL1 hemichannels (see section 1.2.2) and is similar to the modification of voltage-gated K^+ channels by many peptide toxins (Swartz, 2007). The proposed model may explain the effect of Gap26/27 in the variety of tissue and organ systems, particularly those electrically non-excitable cells. In this case, Gap26/27 would bind to closed hemichannels under resting condition and in its turn keep the channel resistant to the diverse stimuli ranging from increasing $[Ca^{2+}]_i$ to reduced redox potential.

Two key findings may shed light on the peptide-binding site: i) the inhibition of the fully open hemichannels is a consequence of impaired slow gating; and ii) the peptides shift the voltage-dependence of hemichannel activation to more positive V_m (Chapter III, Fig. 4). As such, the peptide targeting site facing the extracellular compartment would lie within or near the voltage sensing domain of the slow gate. In Cx26, residues R75 and R784 are components of the electrostatic network which stabilizes the open conformation of the slow gate (Kwon *et al.*, 2012). As inferred by the molecular dynamic simulation, these residues form inter- and intrasubunit salt bridges with residue E42 and E47 at the TM1/EL1 domain of Cx26 hemichannel. Location of E42 and E47 at the pore-lining parahelix region underlines a critical role of the electrostatic network in both voltage-sensing and gating (see section 1.2.2). Of note, TM1/EL1 region also accounts for the slow gating element of chimeric Cx32*Cx43EL1 and Cx50 hemichannels (Tang *et al.*, 2009;Verselis *et al.*, 2009). Because the gating polarity of slow gate is unique among connexins (closure for negativity), conserved E47, R75 and R184 residues (Fig. 1) may constitute a common voltage sensor and gate shared by different connexin channels. Likewise, a recent attempt to neutralize R75 of Cx32 caused a right-shift in voltage-dependence of the mutant Cx32 channel, largely due to the disturbed interaction

between E47 and R75 (Abrams *et al.*, 2013). In Cx43, homologues residues to the Cx26 R75 and R184 (R76 and R202 respectively) are covered by Gap26 and Gap27 regions. Taken together, these findings prompt us to speculate that R76/R202 in Gap26/27 respectively guides the peptide binding towards TM1/EL1 region of Cx43 predominantly through an electrostatic interaction with E48 (homologous to Cx26 E47), and on its turn, hinder the movement of the voltage sensor for establishment of the electrostatic network. Lack of effect by scrambled peptides suggests a highly sequence-dependent cross-linking between Gap26/27 and Cx43. In fact, Gap26/27 does block connexin channels formed other than Cx43 (De Bock *et al.*, 2011;Evans *et al.*, 2012;Wright *et al.*, 2009), exhibiting a non-specificity that may be related to both conserved sequences of the peptides and target sites. To verify the potential binding site, follow-up studies will be necessary to determine whether Gap26/27 peptide interacts with the TM1/EL1 sequence by means of surface plasmon resonance. Mutant Gap26/27 peptides containing neutral or negatively charged amino acids at position R76/R202 will be included.

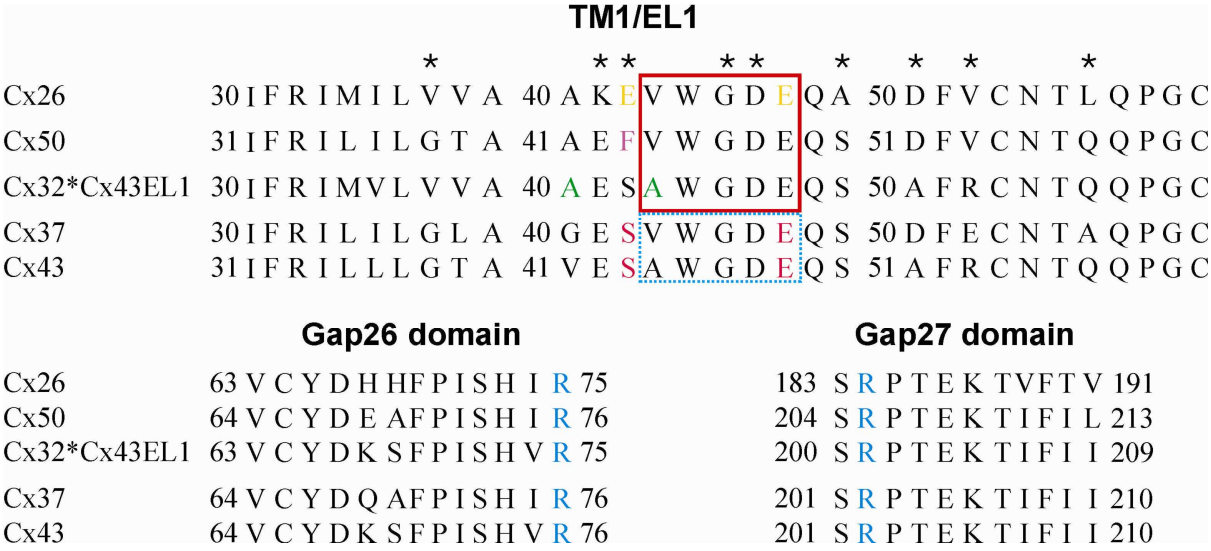

Figure 1. Sequence alignment of mouse Cxs in the TM1/EL1 region and extracellular loop domains containing sequences of Gap26 and Gap27. Of note, Cx37 hemichannels can also be inhibited by Gap27 peptide. *Asterisks* indicate pore-lining residues in the crystal structure of Cx26 channel. Box: parahelix proposed as slow gating element. Green: residues forming an electrostatic network with arginines located in the Gap26/27 domain (blue). Identical residues have been shown to stabilize the open conformation of Cx26 hemichannels. Red: residues predicted for cross-linking with Gap26/27 domains via electrostatic and *van der Waal* forces.

4.2 Gap19 selectively inhibits Cx43 hemichannels by preventing CT-CL interaction

A selective hemichannel blocker should comply with two requirements: i) only hemichannels composed of a designated connexin are inhibited and ii) junctional coupling remains unaffected. Since Gap26/27 are not complying with this last requirement, a next challenge for our study was to characterize a potential tool for selective hemichannel interference consisting of a nonapeptide, Gap19 (KQIEIKKFK) that corresponds to the CL domain of Cx43. In the past, peptides containing sequences of the CL domain were used as controls that do not inhibit gap junctions (Evans *et al.*, 2012;Oviedo-Orta *et al.*, 2002). From our work which included ATP release and dye uptake in conjunction with measurement of unitary hemichannel currents and gap junctional coupling, Gap19 emerged as the first pharmacological approach available to specifically block Cx43 hemichannels without downregulating gap junction coupling. As exemplified from the surface plasmon resonance experiments, the selective effect is due to direct binding of Gap19 to the last 10 amino acids of the CT thereby preventing an intramolecular CT-CL interaction. It was later identified that the I130 and K134 residues located in the Gap19 sequence form ionic bonds with D378 and D379 in the CT tail while prolines at position 375 and 377 coordinate the binding (D'hondt *et al.*, 2013). The notion that CT-CL interaction could differentially affect hemichannels and gap junctions was originated from the observation that binding of the CT to the second half of CL (further called 'L2 domain') in which the Gap19 sequence is located, underlies the intracellular acidification-induced gap junction closure (Fig. 2) (Duffy *et al.*, 2002). The Cx43 CT domain has been proposed to host at least two L2-binding sites at low intracellular pH (Bouvier *et al.*, 2009;Ek-Vitorin *et al.*, 1996;Hirst-Jensen *et al.*, 2007). One site is contiguous to the TM4, comprising amino acids 261-300 while the other resides in the CT end (376-379). Later studies with a peptide containing the L2 sequence have discovered that CT-CL interaction might also be essential for V_j-dependent fast gating. L2 peptide, when delivered into N2A-Cx43 cell pairs via a whole-cell recording pipette, abolished fast gating transitions between the open and residual state at high $V_j = \pm 60$ mV, while also slightly increasing the mean open time (Seki *et al.*, 2004). Over the past decade, a 'ball-and-chain' model has been proposed to explain the pH_i-sensitive chemical gating (reviewed in (Delmar *et al.*, 2004)) as well as V_j-dependent fast gating. The idea involves movement of the Cx43 CT, as a freely mobile particle towards a receptor site at L2 domain. Following the CT-CL interaction, a change in channel geometry is expected to take place, which in turn keeps the Cx43 gap junctions in the 'closed' configuration. Beyond its importance in channel function, the L2 domain seems to

preserve the integrity of the Cx43 gap junction structure. Partial deletion of the L2 sequence (I130-K134 or I139-G143) attained normal gap junction assembly, but gave rise to impaired electrical coupling (Seki *et al.*, 2004). Our collaborative work with the Bultynck and Retamal groups has recently demonstrated an apparently differential effect of L2 peptide on hemichannels. When linked to the TAT membrane-translocation sequence, L2 peptide inhibited Cx43-related ATP release and dye uptake in response to elevation of $[Ca^{2+}]_i$ (Ponsaerts *et al.*, 2010). The surface plasmon resonance approach showed a direct interaction between a peptide corresponding to the last 10 amino acids of the CT (CT10) and the biotin-labeled L2 peptide, in compliance with the previously predicted L2-binding site. TAT-CT10 successfully alleviated the inhibition of L2 peptide on Cx43 hemichannels, and rescued the opening of a mutant hemichannel whose function was silenced by CT truncation (Cx43Δ239) (Kang *et al.*, 2008). These findings collectively underpinned an essential need of CT-CL binding for Cx43 hemichannel activation and established the theoretical basis for our present work.

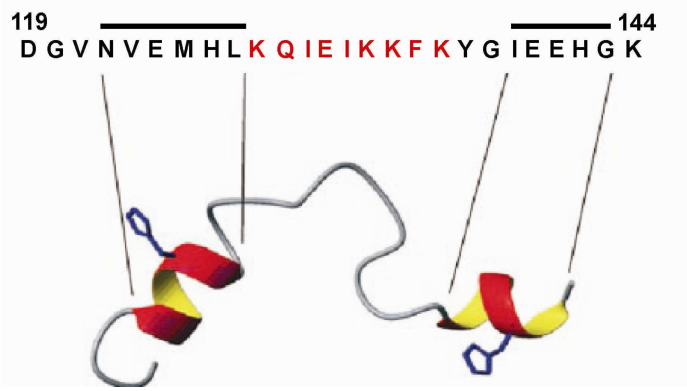

Figure 2. Structure of the L2 peptide determined in phosphate buffered solution (pH 5.8) by nuclear magnetic resonance. Red, Gap19 domain linking the two α-helixes. Taken from (Duffy *et al.*, 2002).

Knowledge on the connexin channel gating mediated by CT-CL binding is limited because of undefined positions of connexin the CT and CL relative to the channel pore. Both domains are extremely flexible (Bennett, 2011;Liu *et al.*, 2006), thereby remaining elusive in the crystal structure (Maeda *et al.*, 2009). One interesting observation in our previous work and others is that although TAT-CT10 peptide restored the response of Cx43Δ257 hemichannels to elevation of $[Ca^{2+}]_i$, it did not acutely affect the basal activity of wild type hemichannels (Ponsaerts *et al.*, 2010;Rhett *et al.*, 2011). It may suggest that in a closed channel configuration, the L2 domain either is located outside the intracellular vestibule or conforms to a less ordered structure, so that the CT-binding locus cannot be accessed. Of note, decreasing neutral pH to 5.8 promotes a structural change of the L2 peptide from a random

coil to two α-helixes linked by a less defined central region in which Gap19 sequence is encompassed (Fig. 2) (Duffy *et al.*, 2002;Seki *et al.*, 2004). The organized secondary structure increases the binding affinity of Cx43 CL to L2 residues I130-I139 (Bouvier *et al.*, 2009;Duffy *et al.*, 2002). A stronger interaction between Gap19 peptide and CT tail detected at normal pH comes along to support the hypothesis that Gap19 sequence when embedded in a random coiled L2 region is less accessible by Cx43CT (Chapter IV, Fig.3). Taken together, stimuli such as stepping V_m to positive voltage or increasing $[Ca^{2+}]_i$ (binding of calmodulin to CL; further discussed in section 4.3) are necessary to promote a conformational change at the L2 domain, exposing the receptor site for the subsequent CT-CL interaction. The fact that Gap19 readily blocked Cx43 hemichannels prior to channel activation follows the idea that Gap19 stabilizes the closed channel conformation by preventing a CT-CL interaction. Assuming a cooperative binding, the hill coefficient estimates that two CT subunits upon peptide binding would suffice the entry to the closed state.

Importantly, three point-mutations identified in ODDD syndrome, a Cx43-linked genetic disease reside in the L2 region and are associated with aberrant connexin channel functions. I130T impairs both Cx43 hemichannel and gap junction functions (Kalcheva *et al.*, 2007;Lai *et al.*, 2006) whereas G138R and G143S produce leaky hemichannels and deficient junctional coupling (Dobrowolski *et al.*, 2008;Dobrowolski *et al.*, 2007). The dominant negative effect of I130T strengthens its indispensible role in the structural organization of both hemi- and gap junction channels. On the other hand, G138R and G143S mutations are anticipated to promote a conformation change at L2 domain in favor for the CT-CL binding. In fact, the typically reduced phosphorylation status observed in Cx43G138R and G143S could be ascribed to the enhanced CT-CL interaction that masks phosphorylation sites at the CT tail. Surface plasmon resonance and electrophysiological studies will help to further verify whether these mutants indeed promote tbinding to the CT and form hemichannels that are constitutively open or that exhibit increased open probability. It is important to note that interdomain interactions are not Cx43 hemichannel-specific. A similar role has been proposed for closure of Cx26 hemichannels in relation to intracellular acidification (Locke *et al.*, 2011). As introduced in section 1.3, the protonated aminosulfonate binds to the CL domain of Cx26, and disrupts an acidification-favored interaction between CT and CL, resulting in hemichannel closure.

Last but not the least, the mechanisms proposed above should not be confused with the 'ball-and-chain' model suggested for gap junction gating. Despite the identical binding sites delineated *in vitro*, the functional consequences of a CT-CL interaction are distinct between

two types of Cx43 channels: upon binding, gap junctions are gated either to complete closure or residual state whereas hemichannels are driven to the fully open state. The reason for this differential regulation is not clear. Of note, connexin hemichannels are located in 'lipid rafts', which are membrane microdomains enriched in sphingolipids and cholesterol, while gap junction plaques are not in lipid rafts (Locke *et al.*, 2005). Being distributed over membrane domains with slightly different physiochemical properties, connexin hemichannels and gap junctions would interact with distinct connexin hemichannels and gap junctions which on their turn affect structures and functions of the channels (Locke and Harris, 2009).

4.3 CT-CL interaction underlies the biphasic effect of $[Ca^{2+}]_i$ on Cx43 hemichannel opening

As mentioned preceedingly, intracellular $[Ca^{2+}]_i$ is a potent modulator of Cx43 hemichannels. Previous work of our group has outlined a bell-shaped response profile with a moderate $[Ca^{2+}]_i$ elevation (~500 nM) promoting hemichannel opening and higher $[Ca^{2+}]_i$ preventing hemichannel opening. Functional data available so far argues that the activation phase requires an intracellular binding of Cx43 CT to CL possibly acting via an intermediate signaling cascade including Ca^{2+}/CaM, Ca^{2+}/CaM-dependent protein kinase II (CaMKII) and p38 mitogen-activated protein kinase (MAPK) (De Vuyst *et al.*, 2009;Ponsaerts *et al.*, 2010). The inactivation mechanisms have been reported to occur due to high $[Ca^{2+}]$ activation of the actomyosin contractile system which in turn dislodges the CT from the CL.

In the present work, we sought to study the effect of $[Ca^{2+}]_i$ on voltage-dependent Cx43 hemichannel gating and found a similar bimodal effect of Ca^{2+} on Cx43 hemichannel unitary currents: elevating $[Ca^{2+}]_i$ from 50 to 200-500 nM potentiated the single-channel activities while this potentiation disappeared at 1 µM (Chapter III, Fig.6). By including peptides that intervene with a CT-CL interaction in the whole-cell recording pipette, we have further demonstrated that L2 peptide suppressed Ca^{2+}-promoted unitary currents while CT9 peptide containing the last 9 amino acids of the Cx43 CT prevented the hemichannel closure at high $[Ca^{2+}]_i$ (Fig. 3). Collectively, our electrophysiological data confirm the interesting cross-talk between $[Ca^{2+}]_i$ signaling and the intramolecular binding of the CT to CL. In fact, the rapid onset of the potentiation observed in our study suggests that Ca^{2+}-enhanced hemichannel openings are mediated by a direct interaction of Ca^{2+}/CaM with Cx43 rather than being mediated via a CaMKII-involved complex pathway. The Ca^{2+}/CaM complex was previously reported to directly interact with the cytoplasmic side of at least 3 connexins, Cx32, Cx44 and

Cx50 and in turn to modulate the gap junction gating. More recently, a Ca^{2+}/CaM binding site at the CL domain of Cx43 has been identified (K136-S158) (Zhou *et al.*, 2007). As demonstrated by dual-patch clamp recordings of N2A-Cx43 cell pairs, both the CaM inhibitor calmidazolium and a peptide mimicking the sequence of the Ca^{2+}/CaM binding site ($Cx43CL_{136-158}$) could successfully alleviate junctional uncoupling in response to a sub-micromolar increase in $[Ca^{2+}]_i$ (400-800 nM). Furthermore, structural analysis using nuclear magnetic resonance detected conformational changes of both $Cx43CL_{136-158}$ peptide and Ca^{2+}/CaM following the complex formation. It is important to note that the CaM-binding locus is contiguous to the Gap19 domain and spans through part of the L2 region (Fig. 4). Gap19, preventing CT-CL interaction shifts the voltage-sensitivity of Cx43 hemichannels towards more positive voltages, i.e. in opposite direction of the effect of $[Ca^{2+}]_i$ elevation that lowers the voltage threshold for activation. This fact brings up the possibility that Ca^{2+}-triggered signaling pathways (the activation phase) converge on the Cx43 CL domain. Direct binding of Ca^{2+}/CaM to Cx43 could promote a structural rearrangement of the second half of the CL, which is likely to expose the target site for the CT binding. Follow-up studies will be necessary to investigate a direct role of Ca^{2+}/CaM on hemichannel gating and its tight link to the CT-CL interaction.

Figure 3. Effect of L2 and CT9 peptides on unitary current activity of Cx43 3 hemichannels. **A.** Representative whole-cell patch clamp traces recorded in HeLa Cx43 cells, illustrating unitary currents induced by Vm steps to +60 mV. The $[Ca^{2+}]_i$ in the recording pipette was 50 nM. The all-point histogram (right of the traces) illustrates a ~220 pS unitary conductance typical for Cx43 hemichannels. **B.** Increasing $[Ca^{2+}]_i$ to 500 nM strongly promoted current activity and this effect disappeared upon increasing $[Ca^{2+}]_i$ to 1 μM. L2 (100 μM added via recording pipette) removed current-promotion by 500 nM $[Ca^{2+}]_i$ and CT9 (100 μM) prevented current inhibition by 1 μM $[Ca^{2+}]_i$. **C.** All-point histograms illustrating the effect of L2 and CT9 on unitary conductance distribution. **D.** Bar chart summarizing L2 and CT9 effect on unitary current-associated charge transfer (Q_m) at different $[Ca^{2+}]_i$ levels. **E.** Graph illustrating the biphasic effect of $[Ca^{2+}]_i$ on hemichannel opening and the effect of L2 and CT9. *** $p<0.001$ compared to 50 nM [Ca2+]i; $$$ $p<0.001$ compared to 500 nM $[Ca^{2+}]_i$ without L2; ### $p<0.001$ for compared 1 μM $[Ca^{2+}]_i$ without CT9.

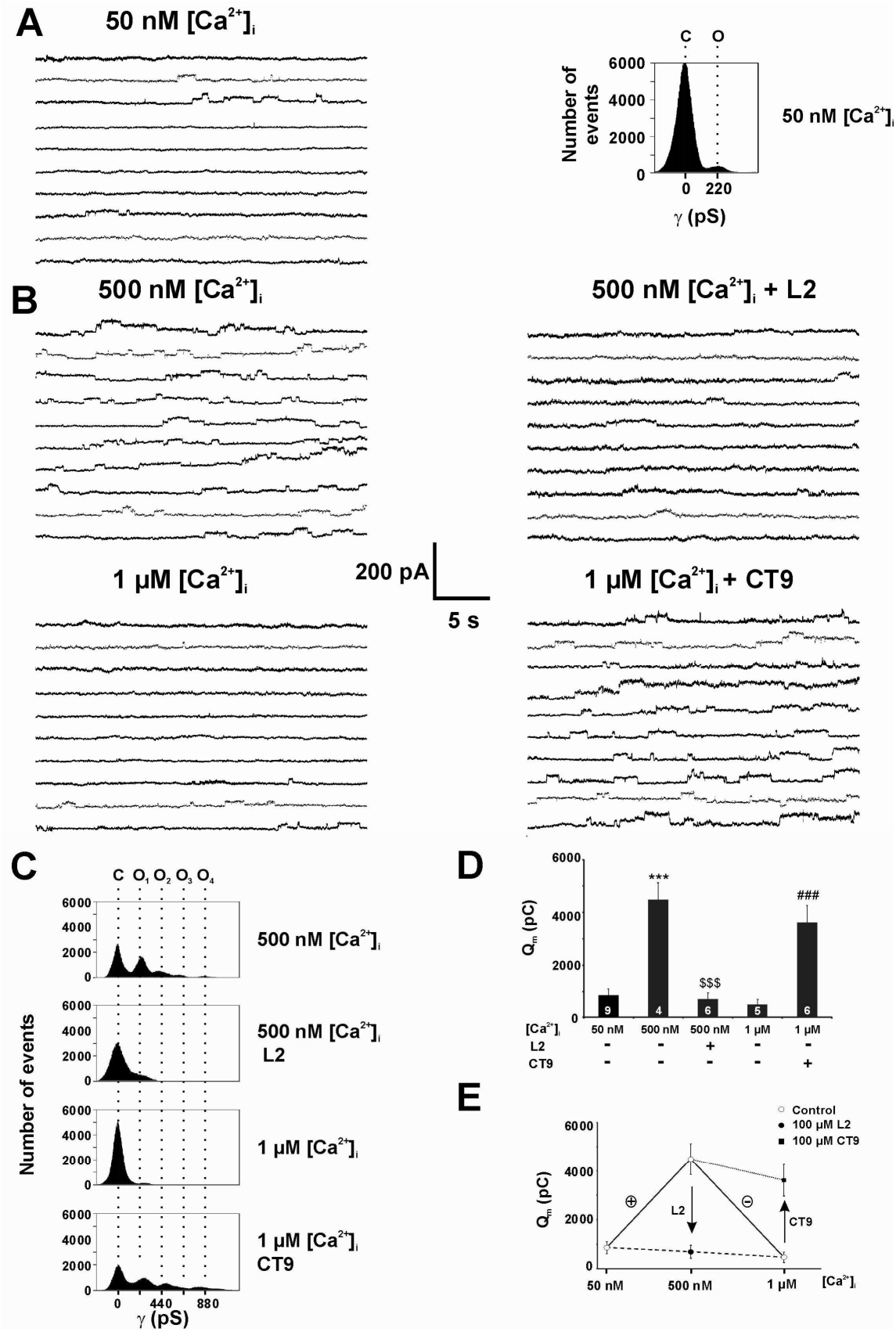
A
50 nM [Ca2+]i
C O
Number of events
6000
4000
2000
0
0 220
γ (pS)
50 nM [Ca2+]i
B
500 nM [Ca2+]i
500 nM [Ca2+]i + L2
1 µM [Ca2+]i
200 pA
5 s
1 µM [Ca2+]i + CT9
C
C O1 O2 O3 O4
500 nM [Ca2+]i
500 nM [Ca2+]i L2
1 µM [Ca2+]i
1 µM [Ca2+]i CT9
Number of events
0 440 880
γ (pS)
D
Qm (pC)
***
###
$$$
9
4
6
5
6
[Ca2+]i 50 nM 500 nM 500 nM 1 µM 1 µM
L2 - - + - -
CT9 - - - - +
E
Control
100 µM L2
100 µM CT9
Qm (pC)
L2
CT9
50 nM
500 nM
1 µM
[Ca2+]i

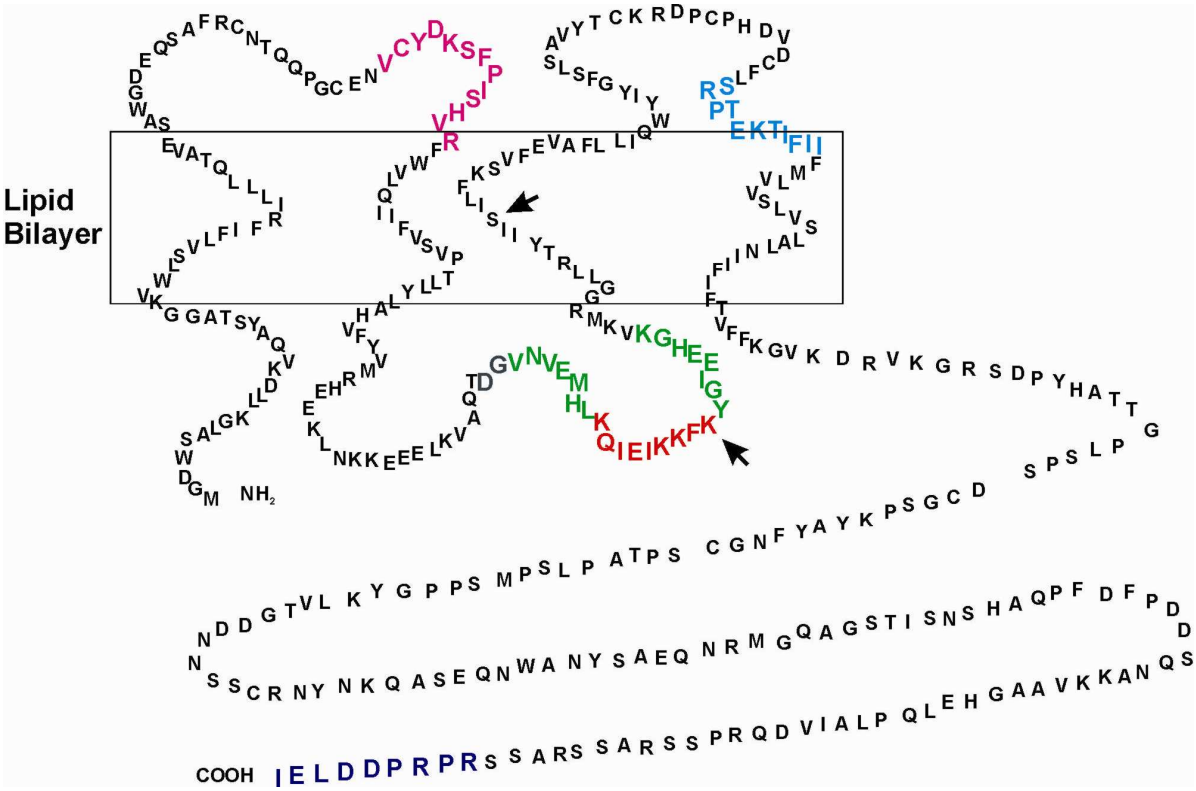

Figure 4. An overview of the domains of domains of Cx43 to which the targeting peptides correspond. Pink, Gap26 sequence; Blue, Gap27 sequence; Purple, CT9 sequence, Red, Gap19 sequence; Green, L2 sequence. The arrows indicate the Ca^{2+}/CaM binding domain.

4.4 Roles of Cx43 hemichannels in ischemia/reperfusion injury

In acutely isolated ventricular cardiomyocytes, Cx43 hemichannels unitary current activities appeared only in response to membrane polarization to strong positive membrane potentials (> +60 mV). This voltage threshold for activation can be hardly attained under physiological conditions, suggesting that unapposed hemichannels residing at the perinexus are typically closed in healthy myocardium. However, slightly elevating $[Ca^{2+}]_i$ to a steady state of ~500 nM effectively shifts the voltage threshold for hemichannel activation to less positive V_m which can realistically be reached in the electrically excitable cardiomyocytes. Based on this finding, we anticipated that cytoplasmic Ca^{2+}-overload, a hallmark of ischemia/reperfusion could promote Cx43 hemichannel activities. Indeed, cardiomyocytes subject to metabolic inhibition exhibited a substantial increase in Cx43 hemichannels unitary current activities. More importantly, Gap19 peptide recued cell death and limited the infarct size after *in vitro* and *in vivo* cardiac ischemia/reperfusion respectively. The contribution of Cx43 hemichannels to myocardial injury may be ascribed to its non-selective nature. An open Cx43 hemichannel provides a non-selective, large-conductance conduit between the cytoplasm and extracellular

fluid, promoting entry of $Na^+/Ca^{2+}/Cl^-$ and liberating essential metabolites such as ATP from the cell. The resulting collapse in ionic homeostasis would eventually lead to myocardial edema following unregulated water uptake through aquaporin. A close functional link of Aquaporin-4 to Cx43 has been recently reported in mouse astrocytes (Nicchia *et al.*, 2005), but little is known about any cross-talk between water channels and Cx43 in cardiomyocytes. As exemplified from the cell volume measurement performed by us and others (Schulz *et al.*, 2007), interfering Cx43 hemichannels indeed attenuated cell volume increases of isolated cardiomyocytes subject to simulated ischemia/reperfusion. A second possible mechanism consists of Na^+ and Ca^{2+} overload secondary to Cx43 hemichannels openings. The process would intensify the Ca^{2+}-dependent cell death including hypercontracure and mitochondria permeability transition (reviewed in (Garcia-Dorado *et al.*, 2012). Finally, extensive loss of intracellular ATP through Cx43 hemichannels could result in rapid development of secondary necrosis and membrane permeabilization (Kalvelyte *et al.*, 2003).

Of note, excessive hemichannel openings may aggravate arrhythmogenesis of reperfused heart beyond its impact on infarct size. There is ample evidence that open hemichannels decrease the space constant and slow the conduction velocity (Kreuzberg *et al.*, 2006a;Kreuzberg *et al.*, 2006b). Opening of hemichannels would also create a non-selective 'sink' that attracts V_m towards 0 mV thereby entirely changing the set-point of plasma membrane excitability. In a conditional mouse model carrying G138R mutation, spontaneous ventricular arrhythmia is caused by a concerted action of impaired junctional coupling and leaky connexin hemichannels (Dobrowolski *et al.*, 2008). Ventricular arrhythmias usually arise from premature ectopic heartbeats that may trigger re-entrant mechanisms which are important for sustaining the arrhythmia. A common triggering event is associated with increased Ca^{2+} loading of the cell, which promotes Ca^{2+} release from the sarcoplasmic reticulum outside the normal cardiac cycle, as observed in reperfused heart following ischemia. Spontaneous release activates an inward current causing a delayed afterdepolarization (DAD). We anticipate that there are several ways through which hemichannel opening could contribute to arrhythmogenesis during ischemia/reperfusion. (i) Enhanced hemichannel activity at resting V_m in response to spontaneous Ca^{2+} release would produce an inward current facilitating DADs and triggered activity. (ii) Adrenergic stimulation upon ischemic insults also increases systolic Ca^{2+} release and subsequent hemichannel opening during the action potential plateau phase would generate net outward current, shortening the action potential duration and thus reducing refractoriness of cardiac

tissue (iii) Increased hemichannel opening forms a leakage pathway that may decrease the spatial constant of current spread in ventricular cardiomyocytes that may further promote re-entry by reducing the conduction velocity. To verify these possibilities, we will use Gap19 as a valuable tool for further studies aiming at investigating the role of Cx43 hemichannels in myocardial injury associated with ischemia/reperfusion.

References

Abrams CK, Islam M, Mahmoud R, Kwon T, Bargiello TA, and Freidin MM (2013) Functional requirement for a highly conserved charged residue at position 75 in the gap junction protein connexin 32. *J Biol Chem,* **288,** 3609-3619.

Bennett MV (2011) Not what you thought: how H+ ions combine with taurine or other aminosulfonates to close Cx26 channels. *J Gen Physiol,* **138,** 377-380.

Bouvier D, Spagnol G, Chenavas S, Kieken F, Vitrac H, Brownell S, Kellezi A, Forge V, and Sorgen PL (2009) Characterization of the structure and intermolecular interactions between the connexin40 and connexin43 carboxyl-terminal and cytoplasmic loop domains. *J Biol Chem,* **284,** 34257-34271.

Braet K, Vandamme W, Martin PE, Evans WH, and Leybaert L (2003) Photoliberating inositol-1,4,5-trisphosphate triggers ATP release that is blocked by the connexin mimetic peptide gap 26. *Cell Calcium,* **33,** 37-48.

D'hondt C, Iyyathurai J, Wang N, Gourdie R, Himpens B, Leybaert L, and Bultynck G (2013) Negatively charged residues (Asp278 and Asp279) in the last ten amino acids of the C-terminal tail of Cx43 hemichannels are essential for loop/tail interactions. *Biochem Biophys Res Commun*, **432,** 707-712.

Danesh-Meyer HV, Kerr NM, Zhang J, Eady EK, O'Carroll SJ, Nicholson LF, Johnson CS, and Green CR (2012) Connexin43 mimetic peptide reduces vascular leak and retinal ganglion cell death following retinal ischaemia. *Brain,* **135,** 506-520.

De Bock M, Culot M, Wang N, Bol M, Decrock E, De Vuyst E, da Costa A, Dauwe I, Vinken M, Simon AM, Rogiers V, De LG, Evans WH, Bultynck G, Dupont G, Cecchelli R, and Leybaert L (2011) Connexin channels provide a target to manipulate brain endothelial calcium dynamics and blood-brain barrier permeability. *J Cereb Blood Flow Metab,* **31,** 1942-1957.

De Vuyst E, Wang N, Decrock E, De Bock M, Vinken M, Van Moorhem M, Lai C, Culot M, Rogiers V, Cecchelli R, Naus CC, Evans WH, and Leybaert L (2009) Ca(2+) regulation of connexin 43 hemichannels in C6 glioma and glial cells. *Cell Calcium,* **46,** 176-187.

Decrock E, De Vuyst E, Vinken M, Van Moorhem M, Vranckx K, Wang N, Van Laeken L, De Bock M., D'Herde K, Lai CP, Rogiers V, Evans WH, Naus CC, and Leybaert L (2009) Connexin 43 hemichannels contribute to the propagation of apoptotic cell death in a rat C6 glioma cell model. *Cell Death Differ,* **16,** 151-163.

Delmar M, Coombs W, Sorgen P, Duffy HS, and Taffet SM (2004) Structural bases for the chemical regulation of Connexin43 channels. *Cardiovasc Res,* **62,** 268-275.

Dobrowolski R, Sasse P, Schrickel JW, Watkins M, Kim JS, Rackauskas M, Troatz C, Ghanem A, Tiemann K, Degen J, Bukauskas FF, Civitelli R, Lewalter T, Fleischmann BK, and Willecke K (2008) The conditional connexin43G138R mouse mutant represents a new model of hereditary oculodentodigital dysplasia in humans. *Hum Mol Genet,* **17,** 539-554.

Dobrowolski R, Sommershof A, and Willecke K (2007) Some oculodentodigital dysplasia-associated Cx43 mutations cause increased hemichannel activity in addition to deficient gap junction channels. *J Membr Biol,* **219,** 9-17.

Duffy HS, Sorgen PL, Girvin ME, O'Donnell P, Coombs W, Taffet SM, Delmar M, and Spray DC (2002) pH-dependent intramolecular binding and structure involving Cx43 cytoplasmic domains. *J Biol Chem,* **277,** 36706-36714.

Ek-Vitorin JF, Calero G, Morley GE, Coombs W, Taffet SM, and Delmar M (1996) PH regulation of connexin43: molecular analysis of the gating particle. *Biophys J,* **71,** 1273-1284.

Evans WH, Bultynck G, and Leybaert L (2012) Manipulating connexin communication channels: use of peptidomimetics and the translational outputs. *J Membr Biol,* **245,** 437-449.

Garcia-Dorado D, Ruiz-Meana M, Inserte J, Rodriguez-Sinovas A, and Piper HM (2012) Calcium-mediated cell death during myocardial reperfusion. *Cardiovasc Res,* **94,** 168-180.

Hawat G, Helie P, and Baroudi G (2012) Single intravenous low-dose injections of connexin 43 mimetic peptides protect ischemic heart in vivo against myocardial infarction. *J Mol Cell Cardiol,* **53,** 559-566.

Hirst-Jensen BJ, Sahoo P, Kieken F, Delmar M, and Sorgen PL (2007) Characterization of the pH-dependent interaction between the gap junction protein connexin43 carboxyl terminus and cytoplasmic loop domains. *J Biol Chem,* **282,** 5801-5813.

Hurst RS, Latorre R, Toro L, and Stefani E (1995) External barium block of Shaker potassium channels: evidence for two binding sites. *J Gen Physiol,* **106,** 1069-1087.

Jackson MB (2010) Open channel block and beyond. *J Physiol,* **588,** 553-554.

Kalcheva N, Qu J, Sandeep N, Garcia L, Zhang J, Wang Z, Lampe PD, Suadicani SO, Spray DC, and Fishman GI (2007) Gap junction remodeling and cardiac arrhythmogenesis in a murine model of oculodentodigital dysplasia. *Proc Natl Acad Sci U S A,* **104,** 20512-20516.

Kalvelyte A, Imbrasaite A, Bukauskiene A, Verselis VK, and Bukauskas FF (2003) Connexins and apoptotic transformation. *Biochem Pharmacol,* **66,** 1661-1672.

Kang J, Kang N, Lovatt D, Torres A, Zhao Z, Lin J, and Nedergaard M (2008) Connexin 43 hemichannels are permeable to ATP. *J Neurosci,* **28,** 4702-4711.

Kreuzberg MM, Schrickel JW, Ghanem A, Kim JS, Degen J, Janssen-Bienhold U, Lewalter T, Tiemann K, and Willecke K (2006a) Connexin30.2 containing gap junction channels decelerate impulse propagation through the atrioventricular node. *Proc Natl Acad Sci U S A,* **103,** 5959-5964.

Kreuzberg MM, Willecke K, and Bukauskas FF (2006b) Connexin-mediated cardiac impulse propagation: connexin 30.2 slows atrioventricular conduction in mouse heart. *Trends Cardiovasc Med,* **16,** 266-272.

Kronengold J, Trexler EB, Bukauskas FF, Bargiello TA, and Verselis VK (2003a) Pore-lining residues identified by single channel SCAM studies in Cx46 hemichannels. *Cell Commun Adhes,* **10,** 193-199.

Kronengold J, Trexler EB, Bukauskas FF, Bargiello TA, and Verselis VK (2003b) Single-channel SCAM identifies pore-lining residues in the first extracellular loop and first transmembrane domains of Cx46 hemichannels. *J Gen Physiol,* **122,** 389-405.

Kwon T, Roux B, Jo S, Klauda JB, Harris AL, and Bargiello TA (2012) Molecular dynamics simulations of the Cx26 hemichannel: insights into voltage-dependent loop-gating. *Biophys J,* **102,** 1341-1351.

Lai A, Le DN, Paznekas WA, Gifford WD, Jabs EW, and Charles AC (2006) Oculodentodigital dysplasia connexin43 mutations result in non-functional connexin hemichannels and gap junctions in C6 glioma cells. *J Cell Sci,* **119,** 532-541.

Liu F, Arce FT, Ramachandran S, and Lal R (2006) Nanomechanics of hemichannel conformations: connexin flexibility underlying channel opening and closing. *J Biol Chem,* **281,** 23207-23217.

Locke D and Harris AL (2009) Connexin channels and phospholipids: association and modulation. *BMC Biol,* **7,** 52.

Locke D, Kieken F, Tao L, Sorgen PL, and Harris AL (2011) Mechanism for modulation of gating of connexin26-containing channels by taurine. *J Gen Physiol,* **138,** 321-339.

Locke D, Liu J, and Harris AL (2005) Lipid rafts prepared by different methods contain different connexin channels, but gap junctions are not lipid rafts. *Biochemistry,* **44,** 13027-13042.

Maeda S, Nakagawa S, Suga M, Yamashita E, Oshima A, Fujiyoshi Y, and Tsukihara T (2009) Structure of the connexin 26 gap junction channel at 3.5 A resolution. *Nature,* **458,** 597-602.

Nicchia GP, Srinivas M, Li W, Brosnan CF, Frigeri A, and Spray DC (2005) New possible roles for aquaporin-4 in astrocytes: cell cytoskeleton and functional relationship with connexin43. *FASEB J,* **19,** 1674-1676.

O'Carroll SJ, Gorrie CA, Velamoor S, Green CR, and Nicholson LF (2013) Connexin43 mimetic peptide is neuroprotective and improves function following spinal cord injury. *Neurosci Res*.

Oviedo-Orta E, Errington RJ, and Evans WH (2002) Gap junction intercellular communication during lymphocyte transendothelial migration. *Cell Biol Int,* **26,** 253-263.

Pearson RA, Dale N, Llaudet E, and Mobbs P (2005) ATP released via gap junction hemichannels from the pigment epithelium regulates neural retinal progenitor proliferation. *Neuron,* **46,** 731-744.

Ponsaerts R, De VE, Retamal M, D'hondt C, Vermeire D, Wang N, De SH, Zimmermann P, Himpens B, Vereecke J, Leybaert L, and Bultynck G (2010) Intramolecular loop/tail interactions are essential for connexin 43-hemichannel activity. *FASEB J,* **24,** 4378-4395.

Retamal MA, Froger N, Palacios-Prado N, Ezan P, Saez PJ, Saez JC, and Giaume C (2007a) Cx43 hemichannels and gap junction channels in astrocytes are regulated oppositely by proinflammatory cytokines released from activated microglia. *J Neurosci,* **27,** 13781-13792.

Retamal MA, Schalper KA, Shoji KF, Bennett MV, and Saez JC (2007b) Opening of connexin 43 hemichannels is increased by lowering intracellular redox potential. *Proc Natl Acad Sci U S A,* **104,** 8322-8327.

Rhett JM, Jourdan J, and Gourdie RG (2011) Connexin 43 connexon to gap junction transition is regulated by zonula occludens-1. *Mol Biol Cell,* **22,** 1516-1528.

Romanov RA, Rogachevskaja OA, Bystrova MF, Jiang P, Margolskee RF, and Kolesnikov SS (2007) Afferent neurotransmission mediated by hemichannels in mammalian taste cells. *EMBO J,* **26,** 657-667.

Romanov RA, Rogachevskaja OA, Khokhlov AA, and Kolesnikov SS (2008) Voltage dependence of ATP secretion in mammalian taste cells. *J Gen Physiol,* **132,** 731-744.

Schulz R, Boengler K, Totzeck A, Luo Y, Garcia-Dorado D, and Heusch G (2007) Connexin 43 in ischemic pre- and postconditioning. *Heart Fail Rev,* **12,** 261-266.

Seki A, Duffy HS, Coombs W, Spray DC, Taffet SM, and Delmar M (2004) Modifications in the biophysical properties of connexin43 channels by a peptide of the cytoplasmic loop region. *Circ Res,* **95,** e22-e28.

Swartz KJ (2007) Tarantula toxins interacting with voltage sensors in potassium channels. *Toxicon,* **49,** 213-230.

Tang Q, Dowd TL, Verselis VK, and Bargiello TA (2009) Conformational changes in a pore-forming region underlie voltage-dependent "loop gating" of an unapposed connexin hemichannel. *J Gen Physiol,* **133,** 555-570.

Verselis VK, Trelles MP, Rubinos C, Bargiello TA, and Srinivas M (2009) Loop gating of connexin hemichannels involves movement of pore-lining residues in the first extracellular loop domain. *J Biol Chem,* **284,** 4484-4493.

Wang J, Ma M, Locovei S, Keane RW, and Dahl G (2007) Modulation of membrane channel currents by gap junction protein mimetic peptides: size matters. *Am J Physiol Cell Physiol,* **293,** C1112-C1119.

Wright CS, van Steensel MA, Hodgins MB, and Martin PE (2009) Connexin mimetic peptides improve cell migration rates of human epidermal keratinocytes and dermal fibroblasts in vitro. *Wound Repair Regen,* **17,** 240-249.

Zhou Y, Yang W, Lurtz MM, Ye Y, Huang Y, Lee HW, Chen Y, Louis CF, and Yang JJ (2007) Identification of the calmodulin binding domain of connexin 43. *J Biol Chem,* **282,** 35005-35017.

Part

V
Summary

In vertebrates, connexin hemichannels in the plasma membrane dock head-to-head with their counterparts in adjacent cells to form gap junction channels, allowing direct cell-cell transfer of electric and chemical/metabolic signals. Each hemichannel comprises a hexamer of connexin proteins which consist of four membrane-spanning domains, two extracellular loops, a cytoplasmic loop (CL) and flanking N- (NT) and C-termini (CT) in the cytoplasmic side of the cell. Accumulating evidence has suggested novel functions of connexin hemichannels beyond gap junction communication. These unapposed hemichannels can open and form a conduit between the intracellular compartment and the extracellular milieu, allowing Na^+ and Ca^{2+} to enter the cell and K^+ and paracrine messengers like ATP, glutamate and others to leave the cell. A frequently applied pharmacological tool to explore new functions of the connexin hemichannel signaling pathway consists of connexin targeting peptides like Gap26 and Gap27, which are identical to sequences located respectively on the first and second extracellular loop regions of Cx43. Intriguingly, despite the growing interest and wide use of connexin mimetic peptides in hemichannel studies, no conclusive data and arguments are available to support a direct action of these substances on hemichannels. In chapter III, we aimed to investigate the effect of Gap26/27 on Cx43 hemichannels at the single channel level. Such an approach allows unequivocal identification of hemichannel currents by their single channel conductance that is typically ~220 pS for Cx43. In HeLa cells stably transfected with Cx43 (HeLa-Cx43), Gap26/27 peptides inhibited Cx43 hemichannels unitary currents over minutes at concentrations in the 100-200 µM range and increased the voltage threshold for hemichannel opening. By contrast, an elevation of intracellular calcium ($[Ca^{2+}]_i$) to 200-500 nM potentiated the unitary hemichannel current activity and lowered the voltage threshold for hemichannel activation. Interestingly, Gap26/27 inhibited the Ca^{2+}-potentiated hemichannel currents and prevented lowering of the voltage threshold for hemichannel activation. Experiments on isolated pig ventricular cardiomyocytes, which display strong endogenous Cx43 expression, demonstrated voltage-activated unitary currents with biophysical properties of Cx43 hemichannels that were inhibited by small interfering RNA targeting Cx43. As observed in HeLa-Cx43 cells, hemichannel current activity in ventricular cardiomyocytes was potentiated by $[Ca^{2+}]_i$ elevation to 500 nM and was inhibited by Gap26/27. Our results indicate that under pathological conditions, when $[Ca^{2+}]_i$ is elevated, Cx43 hemichannel opening is promoted in cardiomyocytes and Gap26/27 counteracts this effect.

In the mammalian heart, Cx43 is the primary connexin expressed in the working ventricular myocardium. Emerging evidence has suggested novel roles of Cx43 hemichannels in cardiac homeostasis. Residing in the periphery of gap junction plaques termed 'perinexus', these unapposed hemichannels are typically closed under control conditions, but may open in response to ischemic insults. Uncontrolled activation of hemichannels provides a non-selective conduit between the cytoplasm and extracellular fluid, introducing a current leakage pathway and liberating essential metabolites from the cell. Thus, excessive openings of Cx43 hemichannels may be deleterious for the myocardium. Currently, there is no pharmacological tool available that allows selective targeting of hemichannels without inhibiting junctional coupling. Thus, in chapter IV, we aimed to characterize a nonapeptide derived from the CL of Cx43 (further called 'Gap19'), which inhibits Cx43 hemichannels without blocking gap junctions or Cx40/pannexin-1 hemichannels. As exemplified by surface plasmon resonance, the selective effect on hemichannels is due to direct binding of Gap19 to the end of CT thereby preventing intramolecular CT-CL interactions which are essential for Cx43 hemichannel activation. The peptide inhibited Cx43 hemichannel unitary currents in both HeLa cells exogenously expressing Cx43 and acutely isolated pig ventricular cardiomyocytes. Treatment with Gap19 counteracted the effect of metabolic inhibition on hemichannel openings, protected cardiomyocytes against volume overload and cell death following ischemia/reperfusion *in vitro* and reduced the infarct size after myocardial ischemia/reperfusion in mice *in vivo*. Collectively, preventing Cx43 hemichannel activation by Gap19 confers protective effects against myocardial ischemia/reperfusion injury.

In summary, the present doctoral work addresses the effect of several Cx43 targeting peptides and intracellular $[Ca^{2+}]_i$ on Cx43 hemichannels at the single-channel level. The understanding towards the mechanistic basis of these hemichannel modulators provides novel insights into the functional regulation of connexin hemichannels. Additionally, Gap19 which selectively targets connexin hemichannels without inhibiting gap junctions emerges as a valuable tool for further studies aiming at investigating the role of Cx43 hemichannels in cardiac injury.

List of publications

Lentacker I., Wang N., Vandenbroucke R.E., Demeester J., De Smedt S.C., Sanders N.N. Ultrasound exposure of lipoplex loaded microbubbles facilitates direct cytoplasmic entry of the lipoplexes. Mol Pharm 6, 457-467 (2009).

De Vuyst E., Wang N., Decrock E., De Bock M., Vinken M., Van Moorhem M., Lai C., Culot M., Rogiers V., Cecchelli R., Naus C.C., Evans W.H. & Leybaert L. Ca(2+) regulation of connexin 43 hemichannels in C6 glioma and glial cells. Cell Calcium 46, 176-187 (2009).

Decrock E., De Vuyst E., Vinken M., Van Moorhem M., Vranckx K., Wang, N., Van Laeken L., De Bock M., D'Herde K., Lai C.P., Rogiers V., Evans W.H., Naus C.C. & Leybaert, L. Connexin 43 hemichannels contribute to the propagation of apoptotic cell death in a rat C6 glioma cell model. Cell Death Differ 16, 151-163 (2009).

Van Moorhem M., Decrock E., Coussee E., Faes L., De Vuyst E., Vranckx K., De Bock M., Wang N., Lambein F., Callewaert G. & Leybaert L. β-ODAP alters mitochondrial Ca2+ handling as an early event in excitotoxicity. Cell Calcium 47, 287–296 (2010).

Ponsaerts R., De Vuyst E., Retamal M., D'hondt C., Vermeire D., Wang N., De Smedt H., Zimmermann P., Himpens B., Vereecke J., Leybaert L. & Bultynck G. Intramolecular loop/tail interactions are essential for connexin 43 -hemichannel activity. FASEB J 24, 4378-4395 (2010).

D'hondt C., Ponsaerts R., De Smedt H., Vinken M., De Vuyst E., De Bock M., Wang N., Rogiers V., Leybaert L., Himpens B. & Bultynck G. Pannexin channels in ATP release and beyond: An unexpected rendezvous at the endoplasmic reticulum. Cell Signal 23, 305-316 (2011).

Van Moorhem M., Decrock E., De Vuyst E., De Bock M., Wang N., Lambein F, Van Den Bosch L & Leybaert L. Involvement of Ca2+ and oxidative stress in L-β-N-oxalyl-α,β-diaminoprop-ionic acid and L-glutamate induced toxicity in motor neurons. Neuroreport 22, 131-135 (2011).

De Bock M., Culot M., Wang N., Bol M., Decrock E., De Vuyst E., da Costa A., Dauwe I., Vinken M., Simon A., Rogiers V., De Ley G., Evans W.H., Bultynck G., Dupont G., Cecchelli R. & Leybaert L. Connexin channels provide a target to manipulate brain endothelial calcium dynamics and blood brain barrier permeability. J Cereb Blood Flow Metab 31, 1942-1957 (2011).

De Bock M., Wang N., Bol M., Decrock E., Ponsaerts R., Bultynck G., Dupont G. & Leybaert L. Connexin-43 hemichannels contribute to cytoplasmic Ca2+ oscillations by providing a bimodal Ca2+-dependent Ca2+-entry pathway. J Biol Chem 287, 12250-12266 (2012).

Ponsaerts R., Wang N., Himpens B., Leybaert L. & Bultynck G. The contractile system as a negative regulator of the connexin 43 hemichannel. Biol Cel 104l, 367-377 (2012).

Decrock E., Krysko D.V., Vinken M., Kaczmarek A., Crispino G., Bol M., Wang N., De Bock M., De Vuyst E., Naus C.C., Rogiers V., Vandenabeele P., Erneux C., Mammano F., Bultynck G. & Leybaert L. Transfer of IP3 is necessary, but not sufficient, for the spread of apoptosis. Cell Death Differ 19,947-957 (2012).

De Bock M., Culot M., Wang N., da Costa A., Decrock E., Bol M., Bultynck G., Cecchelli R. & Leybaert L. Low extracellular Ca(2+) conditions induce an increase in brain endothelial permeability that involves intercellular Ca(2+) waves. Brain Res 148, 78-87 (2012).

Wang N., De Bock M., Decrock E., Bol M., Vinken M., Bultynck G. & Leybaert L. Paracrine signaling through plasma membrane hemichannels. Biochim Biophys Acta - Biomembr, 1828, 35-50 (2012).

Bond S.R., Wang N., Leybaert L. & Naus C.C. Pannexin 1 ohnologs in the teleost lineage. J Membr Biol 245, 483-493 (2012).

Wang N., De Bock M., Antoons G., Gadicherla A.K., Bol M., Decrock E., Evans W.H., Sipido K.R., Bukauskas F.F., Leybaert L. Connexin mimetic peptides inhibit Cx43 hemichannel opening triggered by voltage and intracellular Ca^{2+} elevation. Basic Res Cardiol 107, 304 (2012).

Wang N.*, De Vuyst E.*, Ponsaerts R.*, Boengler K., Palacios-Prado N., Wauman J., Lai C.P., De Bock M., Decrock E., Bol M., Vinken M., Rogiers V., Tavernier J., Evans W.H., Naus C.C., Bukauskas F.F., Sipido K.R., Heusch G., Schulz R., Bultynck G. & Leybaert L. Selective inhibition of Cx43 hemichannels by Gap19 and its impact on myocardial ischemia/reperfusion injury. Basic Res Cardiol 108, 309 (2013). **equal contribution*

Decrock E., Bock M.D., Wang N., Gadicherla A.K., Bol M., Delvaeye T., Vandenabeele P., Vinken M., Bultynck G., Krysko D.V., Leybaert L. IP(3), a small molecule with a powerful message. Biochim Biophys Acta - Mol Cell Res, in press (2013).

Bol M., Van Geyt C., Baert S., Decrock E., Wang N., De Bock M., Gadicherla A.K., Randon C., Evans W.H., Beele H., Cornelissen R., Leybaert L. Inhibiting Connexin Channels Protects Against Cryopreservation-induced Cell Death in Human Blood Vessels. Eur J Vasc Endovasc Surg. (2013) Epub ahead of print.

D'hondt C, Iyyathurai J, Wang N, Gourdie RG, Himpens B, Leybaert L, Bultynck G. Negatively charged residues (Asp378 and Asp379) in the last ten amino acids of the C-terminal tail of Cx43 hemichannels are essential for loop/tail interactions. Biochem Biophys Res Commun 432, 707-712 (2013).

Iyyathurai J., D'hondt C., Wang N, De Bock M., Himpens B., Retamal M.A., Stehberg J., Leybaert L., Bultynck G.. Peptides and peptide-derived molecules targeting the intracellular domains of Cx43: Gap junctions versus hemichannels. Neuropharmacology. (2013)) Epub ahead of print

Posters and Oral presentations

Wang N. (2008) Mechanism of high intracellular calcium induced suppression of connexin 43 hemichannel responses.La communication jonctionelle intercellulaire 'etas des lieux' IV. Poitiers, France. July 3-4, 2008. **Oral communication**

Wang N., De Vuyst E., De Bock M, Decrock E. and Leybaert L. Inhibition of connexin 43 hemichannel responses with high cytoplasmic Ca^{2+} concentrations is mediated by mechanisms different from Ca^{2+} activation of hemichannel responses. (2008). 10^{th} Meeting of the European calcium society. Leuven, Belgium. September 17-20, 2008. **Poster presentation**

Wang N., De Vuyst E., De Bock M., Decrock E., Van Moorhem M.and Leybaert L. Inhibition of connexin 43 hemichannel responses with high cytoplasmic calcium concentrations is mediated by mechanisms different from Ca^{2+} activation of hemichannel responses. (2009). 9th European Meeting on glial cells in health and disease. Paris, France. September 8-12, 2009. **Poster presentation**

Wang N., De Bock M., Bol M., De Vuyst E., Decrock E., Bukauskas F.F. and Leybaert L. (2011). The connexin-mimetic-peptides Gap26 and Gap27 inhibit connexin-hemichannel unitary-current-activities. 55^{th} Annual metting-Biophyscial Society. Baltimore, M.D., U.S.A. March 5-8, 2011. **Poster presentation**

Wang N., Antoons G., De Bock M., Bol M., De Vuyst E., Decrock E., Willecke K., Sipido K.R., Bukauskas F.F.4 and Leybaert L. (2011). The connexin-mimetic-peptides Gap26 and Gap27 inhibit connexin-hemichannel unitary current activities. International gap junction conference. Ghent, Belgium. August 6-11, 2011. **Oral communication**.

Wang N., Sipido K.R., Bukauskas F.F., Leybaert, L. (2011). The connexin mimetic peptides Gap26 and Gap27 inhibit connexin hemichannel unitary current activities. Antwerp, Belgium. October 22, 2011. **Oral communication**.

Wang N., De Bock M., Antoons G., Bol M., Decrock E., Leurs K., Gadicherla A., Evans W.H., Sipido K.R., Bukauskas F.F. and Leybaert L. (2012) Connexin mimetic peptides inhibit Cx43 hemichannel opening triggered by voltage and intracellular Ca^{2+} elevation. 12^{th} European Calcium society Symposium. Toulouse, France. September 9-12, 2012. **Poster presentation**.